THE UNIVERSITY of ADELAIDE

Faculty of Engineering, Computer and Mathematical Sciences
School of Mechanical Engineering

Towards Understanding the Injury Mechanics and Clinical Outcomes of Traumatic Subaxial Cervical Facet Dislocation and Fracture-Dislocation

Ryan David Quarrington

A thesis submitted in fulfilment of the requirements for the degree of Doctor of Philosophy

December 2018

Declaration

I certify that this work contains no material which has been accepted for the award of any other degree or diploma in my name, in any university or other tertiary institution and, to the best of my knowledge and belief, contains no material previously published or written by another person, except where due reference has been made in the text. In addition, I certify that no part of this work will, in the future, be used in a submission in my name, for any other degree or diploma in any university or other tertiary institution without the prior approval of the University of Adelaide and where applicable, any partner institution responsible for the joint-award of this degree.

I acknowledge that copyright of published works contained within this thesis resides with the copyright holder(s) of those works.

I also give permission for the digital version of my thesis to be made available on the web, via the University's digital research repository, the Library Search and also through web search engines, unless permission has been granted by the University to restrict access for a period of time.

I acknowledge the support I have received for my research through the provision of an Australian Government Research Training Program Scholarship.

_____	_____	06/12/2018
Signed		Dated

Acknowledgements

The work presented in this thesis was financially aided by AOSpine Australia and New Zealand, and the Royal Adelaide Hospital Research Foundation. I would like to thank the following people for their support over the last four years.

To Dr. Claire Jones, thank you for igniting my interest in biomechanics and for introducing me to the fantastic world of spinal research. Most of all, thank you for your unwavering support and guidance throughout this journey. You have been a shining example of an effective researcher, a diligent engineer, and a motivating and empathetic supervisor – I will take these lessons with me for the rest of my career. Thank you to Professor Brian Freeman for your ongoing encouragement and support, your invaluable clinical insight, and for affording me the opportunity to present my work all around the world. Associate Professor John Costi, your mentorship and guidance has been integral to this thesis and my professional development.

I am grateful to the Adelaide Spinal Research Group, our collaborators, and our numerous honours and summer students who have contributed to this thesis in one way or another, particularly: Adnan Mulaibrahimovic, Dr. Jillian Clark, Petar Tcherveniakov, Shabnam Torabiardakani, Dr. Simon Sandler, Dr. Yu Chao Lee, Matthew Beard, Dr. David Hall, Dr. Nigel Jones, Dr. Noyel "Namal" Thibbotuwawa, Ioane "Wani" Vakaci, Dr. Will Robertson, Professor Peter Cripton, Alex Martin, Hannah Andrews, Rachael Killian, and Fraser Darcy. Thanks to Garry Clarke, Pascal Symons, and Stephen Kloeden at the Mechanical Workshop, and Phil Schmidt and Derek Franklin at the Processes & Controls Lab, for assisting with the design and build of our often small, fiddly, and frustrating testing components. To Mishelle at RAH Radiology/Dr. Jones & Partners, thank you for squeezing in our early-morning scanning sessions and for the motivating chats during long testing weeks. Many thanks to Suzanne Edwards and Dr. Lynne Giles for their guidance, and for indulging my interest in statistics.

To the biomechanics PhD crew who made this experience far more enjoyable: Erica “Ric” Beaucage-Gauvreau, Sam Sobey, and Dave Haydon. Thank you for Friday lunches, Journal Club, ISB 2017 (honourable mentions to Dr. Vonne van Heeswijk, Sean Patterson, Amy Lewis, and Jas Bahl), and forgetting to eat dinner at The Elephant. Special thanks to Erica for the many hours spent troubleshooting, proofreading, giving feedback on presentations, discussing life, and providing perspective and motivation in times of need. I am indebted to my friends, housemates, and bandmates for providing me with endless good-times and distractions, particularly D & Z, Jarrad & Liv, Ty, and Pagey.

Finally, and most importantly, thank you to my family and my partner Melanie who have endured this journey from the start – I could not have done this without your love and support.

Abstract

Despite potentially devastating outcomes, the injury mechanisms of traumatic subaxial cervical facet dislocation (CFD) and fracture-dislocation (CFD+Fx) are not well understood and have not been reliably produced in biomechanical testing. In particular, bilateral CFD (BFD) with concomitant facet fracture (BFD+Fx) has not been produced experimentally, possibly due to a lack of neck muscle replication. Muscle activation may impose intervertebral compression and anterior shear during injury, increasing loading of the facets and preventing isolated dislocation via intervertebral separation – such separation has been observed during inertially-produced CFD. The mechanical behaviour of the facets during these scenarios, and the effect of axial distraction on the risk of facet fracture or dislocation, have not been investigated. The aim of this thesis was to improve understanding of the epidemiology, clinical outcomes, and injury mechanisms of CFD and CFD+Fx, and to investigate the biomechanics underlying the injury.

In Study 1, a large-cohort medical record and radiographic review of subaxial cervical subluxations, dislocations, and fracture-dislocations presenting at an Australian tertiary hospital over the decade to 2014 was performed. Two primary injury causations were identified: motor vehicle accidents in younger adults, and falls in the elderly. BFD frequently caused spinal cord injury (SCI) and concomitant facet fracture was common. The C6/C7 vertebral level was most commonly involved, and injury to this level most often caused SCI.

In Study 2, the bilateral inferior facets of 31 isolated human cadaver subaxial cervical vertebrae (6×C3, C4, C5, and C7, 7×C6) were loaded quasi-statically in simulated supraphysiologic anterior shear and compressive-flexion directions using a materials testing machine – these motions are thought to be associated with BFD. Facet stiffness and failure load were significantly greater in the simulated compressive-flexion loading direction, and sub-failure deflection and surface strains were higher in anterior shear. Facet tip fractures occurred during anterior shear loading, while failure through the pedicles was most common in compressive-flexion.

In Study 3, the effect of intervertebral axial separation on human cadaver C6 inferior facet biomechanics during non-destructive anterior shear, axial rotation, flexion, and lateral bending motions of twelve C6/C7 functional spinal units (FSUs) was investigated. Axial compression generally increased facet deflection and strains, when compared to intervertebral distraction.

In Study 4, a method was developed to reliably apply 20 mm of constrained anterior shear motion with superimposed intervertebral axial compression or distraction to twelve human cadaver cervical FSUs in a materials testing machine. The effect of superimposed axial compression vs distraction on the type of fractures observed was assessed for the subset of specimens that successfully achieved 20 mm of anterior shear. BFD+Fx was produced in five of 12 specimens, of which three had axial compression superimposed. The mechanical behaviour of the C6 inferior facets at the point of initial anatomical failure did not appear to be affected by intervertebral axial separation.

This thesis presents the first large-cohort clinical investigation of CFD and provides quantitative information about the biomechanical response of the subaxial cervical facets to simulated traumatic loading. Axial compression generally increased facet surface strains and deflections when superimposed on intervertebral motions, and constrained intervertebral anterior shear can produce BFD+Fx. It is anticipated that this thesis will inform the development of improved preventative measures and provide data for the validation of models of cervical trauma.

Table of Contents

List of Tables

List of Figures

List of Abbreviations

2D	Two-dimensional
3D	Three-dimensional
A&FCS	Allen and Ferguson Mechanistic Classification of Subaxial Cervical Injury
AIC	Aikaike information criterion
AIS	Abbreviated Injury Scale
AP	Antero-posterior
AS	Anterior shear
AS	Anterior shear
ASIA	American Spinal Injury Association
ASIA AIS	American Spinal Injury Association Impairment Scale
ATD	Anthropomorphic test device
AUROC	Area Under the Receiver Operating Characteristic
B-A	Bland-Altman
BFD	Bilateral facet dislocation
BFD+Fx	Bilateral facet dislocation with concomitant facet fracture
BFD±Fx	Bilateral facet dislocation with or without concomitant facet fracture
BFD-Fx	Bilateral facet dislocation without concomitant facet fracture
CFD	Cervical facet dislocation
CFD+Fx	Cervical facet dislocation with concomitant facet fracture
CFD±Fx	Cervical facet dislocation with or without concomitant facet fracture
CFD-Fx	Cervical facet dislocation without concomitant facet fracture
CI	Confidence interval
CoR	Centre of rotation
CT	Computed tomography
DFI	Distractive-flexion injury
EMM	Estimated marginal mean
EPV	Events per variable
FOV	Field of view
FSU	Functional spinal unit
Fx	Fracture
GCS	Glasgow Coma Scale
H&L	Hosmer and Lemeshow
ICC	Intra-class correlation coefficient
IQR	Interquartile range
ISNCSCI	International Standards for Neurological Classification of Spinal Cord Injury
ISS	Injury Severity Scale
IVD	Intervertebral disc
LMM	Linear mixed-effects model
LOBI	Level of bony injury
LVDT	Linear variable differential transducer
MBA	Motorbike accident
MC	Marker carrier
MRI	Magnetic resonance imaging
MVA	Motor vehicle accident
MVC	Motor vehicle collision
NHTSA	National Highway Traffic Safety Administration

N_{ij}	Neck injury criterion
NS	Not specified
NZ	Neutral zone
OR	Odds ratio
PMHS	Postmortem human subject
PMMA	Polymethylmethacrylate
PTA	Posterior tangent angle
ROM	Range of motion
SCI	Spinal cord injury
SE	Standard error
SLIC	Subaxial Injury Classification
UFD	Unilateral facet dislocation
UFD+Fx	Unilateral facet dislocation with concomitant facet fracture
UFD±Fx	Unilateral facet dislocation with or without concomitant facet fracture
UFD-Fx	Unilateral facet dislocation without concomitant facet fracture
VB	Vertebral body
vBMD	Volumetric bone mineral density

Publications

A version of Chapter 2 was published in The Spine Journal: Quarrington, R.D., Jones, C.F., Tcherveniakov, P., Clark, J.M., Sandler, S.J.I., Lee, Y.C., Torabiardakani, S., Costi, J.J., Freeman, B.J.C., 2018, **18**(3), 387-398. *Traumatic subaxial cervical facet subluxation and dislocation: epidemiology, radiographic analyses, and risk factors for spinal cord injury*. Ethical approval was granted by the Royal Adelaide Hospital Research Ethics Committee under Protocol No. 140404.

A version of Chapter 3 was published in Journal of Biomechanics: Quarrington, R.D., Costi, J.J., Freeman, B.J.C., Jones, C.F., 2018, **72**, 116-124. *Quantitative evaluation of facet deflection, stiffness, strain and failure load during simulated cervical spine trauma*. Ethical approval was granted by the Royal Adelaide Hospital Research Ethics Committee under Protocol No. 141203.

A version of Chapter 4 has been accepted for publication in Journal of Biomechanics. Quarrington, R.D., Costi, J.J., Freeman, B.J.C., Jones, C.F. *The effect of axial compression and distraction on cervical facet mechanics during anterior shear, flexion, axial rotation, and lateral bending motions*. Ethical approval was granted by the Royal Adelaide Hospital Research Ethics Committee under Protocol No. 141203.

Chapter 1 Introduction

1.1 Overview

Traumatic subaxial cervical facet dislocation (CFD) and fracture-dislocation (CFD+Fx) are often associated with devastating spinal cord injury (SCI), resulting in tetraplegia in up to 87% of cases (Hadley et al., 1992; Lintner et al., 1993; O'Brien et al., 1982; Payer and Schmidt, 2005; Wolf et al., 1991). In 2014-15, the Australian incidence of traumatic SCI was 12.8 cases per million population (Tovell, 2018), amounting to annual personal care costs of approximately AUD$14.6 million (Access Economics Pty Limited, 2009). Despite potentially devastating outcomes, the injury mechanisms of CFD with or without concomitant facet fracture (CFD±Fx) have not been replicated in biomechanical testing (Bambach et al., 2013; Foster et al., 2012). In particular, CFD+Fx has not been reliably produced experimentally. Small-cohort reviews of CFD report that it is often a result of motor vehicle accidents (MVAs), falls, sporting accidents and direct head loading, during which the external loading can be complex and highly variable (Argenson et al., 1988; Brady et al., 1999; Clayton et al., 2012; Cotler et al., 1990; Davidson and Birdsell, 1989; Dvorak et al., 2007; Hasler et al., 2012; Ivancic et al., 2007; Scher, 1977; Sellin et al., 2014; Stathoulis and Govender, 1997; Thompson et al., 2009; Yang et al., 2013). Improved understanding of the complex injury mechanisms leading to CFD is crucial to the development of preventative measures and improved approaches to treatment.

The importance of further research into the occurrence and prevention of cervical spine injuries has been highlighted by The United States Department of Transportation's National Highway Traffic Safety Administration (NHTSA). The 2011-2015 NHTSA priority plan for biomechanical research (National Highway Traffic Safety Administration, 2011) identified the development of anthropomorphic test device (ATD) technology and injury criteria for the subaxial cervical spine, particularly for dynamic rollover and offset/oblique accident events which can cause CFD (Foster et al., 2012). Quantitative information about the biomechanical response of the lower cervical spine to traumatic injury is required to develop improved neck injury criteria.

This thesis aims to improve our understanding of the epidemiology and injury mechanisms of CFD±Fx, and to investigate the biomechanics underlying the injury. A thorough review of literature identified that patient demographics, injury causation and risk factors specific to CFD have not previously been reported. Furthermore, the mechanical behaviour of the cervical articular facets, and the effect of axial distraction on the risk of facet fracture or dislocation, have not been investigated. It is anticipated that the new knowledge documented in this thesis will improve injury classification methods to assist with early CFD detection and will provide data for validation of computational and dynamic experimental models of cervical trauma. This information may assist with the development of better neck injury criteria and ATD design, leading to improved automotive safety design for reducing the risk of cervical trauma.

This chapter begins with an introduction to cervical spine anatomy and injury classification. The clinical literature pertaining to CFD is discussed, including epidemiology reports from small-cohort studies, the association of CFD with SCI, and radiographic features of this injury. This is followed by a review of the experimental methods that have produced CFD, and the measurement techniques that have been used to investigate injury mechanisms. Finally, the specific objectives of the four studies that comprise this thesis are stated. Chapters 2 through 5 report the methods and results of these studies, and the implications of this research are discussed in Chapter 6.

1.2 Anatomy and functions of the spinal column and spinal cord

This section provides a summary of the anatomy and functions of the cervical spine with a particular focus on the subaxial cervical facet joints.

1.2.1 Anatomical orientations and terms

Anatomical features and directions of motion and loading of the human body are described using anatomical planes (Figure 1.1a). The sagittal plane divides the body into left and right halves, and motions within this plane are described by flexion (forward rotation) and extension (backward rotation). The coronal plane is perpendicular to the sagittal plane and bisects

the body into ventral (anterior or front) and dorsal (posterior or back) parts (Figure 1.1b). Left and right lateral bending motions describe movement in the coronal plane. Lastly, the transverse plane is perpendicular to both the sagittal and coronal planes, in which the motions of axial rotation (left and right) occur.

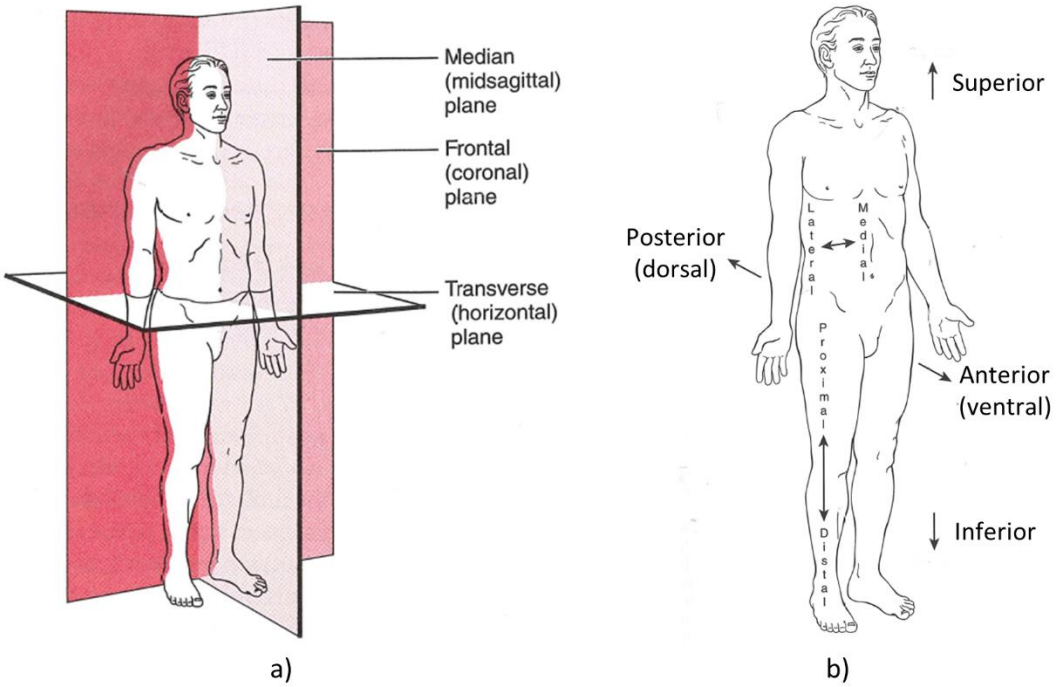

Figure 1.1: Anatomical (a) planes, and (b) positions and terms of the human body.Image adapted from Jenkins *et al.* (2009).[1]

The terms proximal and distal are used to describe features nearer to and further from the attachment of a limb or structure, respectively. Superior (or cranial) describes structures closer to the head, and inferior (or caudal) those nearer the feet. Medial and lateral refer to structures closer to and further, respectively, from the midline of the body in the coronal plane.

[1] Awaiting copyright permissions.

1.2.2 The spinal column

The spinal column spans the length of the human torso, from the base of the skull to the coccyx. It supports the weight of the body and protects the spinal cord, whilst also allowing movement and flexibility to assist with locomotion. There are 33 vertebrae in the spinal column which are classified into five regions (Figure 1.2):

- Cervical (neck) – contains 7 vertebrae;
- Thoracic – contains 12 vertebrae;
- Lumbar – contains 5 vertebrae;
- Sacral – contains 5 fused vertebrae; and,
- Coccygeal – contains 4 fused vertebrae.

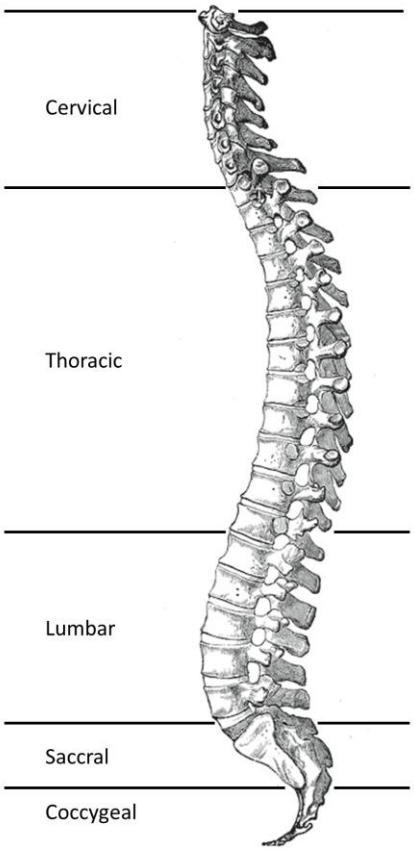

Figure 1.2: The human spinal column. Image adapted from Gray (1918).[1]

Standard anatomical convention dictates that vertebrae are referenced by the first letter of their region followed by their numeric position in that region, from superior to inferior (i.e. C3

[1] Copyright expired.

= third vertebrae of the cervical region). The vertebrae in each region present with specific anatomical and ligamentous structures that act to provide particular functions of the spine.

1.2.3 The cervical spine

The primary role of the cervical spine is to provide a stable and mobile support platform for the head. Although the movements of the head are executed by muscles of the neck, its kinematics are determined by the anatomy of the cervical spine vertebrae and the adjacent joints. The cervical spine can be sub-divided into four regions: the atlas (C1), the axis (C2), the C2-C3 junction, and the subaxial cervical spine (C3-C7) (Bogduk and Mercer, 2000). The morphology of the vertebrae differ in each region to provide unique contributions to the functions of the neck. Traumatic injury of the cervical spine occurs most frequently in the subaxial region (Argenson et al., 1988; Bambach et al., 2013; Burns et al., 2010; Cotler et al., 1990; Du et al., 2014; Goldberg et al., 2001; Payer and Schmidt, 2005; Piccirilli et al., 2013; Shanmuganathan et al., 1994; Wang et al., 2013; Wilson et al., 2013; Yoganandan et al., 1989); therefore, the subaxial cervical spine is the focus of this work.

1.2.4 The subaxial cervical spine

This section describes the skeletal anatomy of a typical subaxial cervical vertebra (Figure 1.3). Anteriorly, the vertebral body (VB) is comprised of a core of trabecular bone with a dense cortical shell. The anterior column acts as the principal axial load bearing component of the spine. In the subaxial cervical region the superior and inferior surfaces of the vertebral bodies (known as ‘endplates’) are angled inferiorly and anteriorly and are slightly concave. The posterior region of the inferior endplate is slightly convex in the transverse plane and articulates with a complimentary concavity and the uncinate processes of the adjacent inferior vertebra to form a saddle-like joint (Bogduk and Mercer, 2000; Penning and Wilmink, 1987).

The pedicles protrude posteriorly from the vertebral body and connect to the laminae to form the vertebral arch. The vertebral arch and the posterior surface of the vertebral body form the spinal canal, through which the spinal cord passes. The spinous process projects posteriorly

from the vertebral arch and transverse processes project bilaterally from the pedicles and vertebral body. Paired superior and paired inferior articular processes (zygapophyses) extend from the vertebral arch and are angled at approximately 40° to the vertical (Nowitzke et al., 1994); however, this angle varies by over 10° between levels (Panjabi et al., 1993). They feature smooth, flat facets which articulate with the corresponding superior and inferior processes of the adjacent vertebrae, forming the facet (or zygapophysial) joints (Jenkins and Hollinshead, 2009).

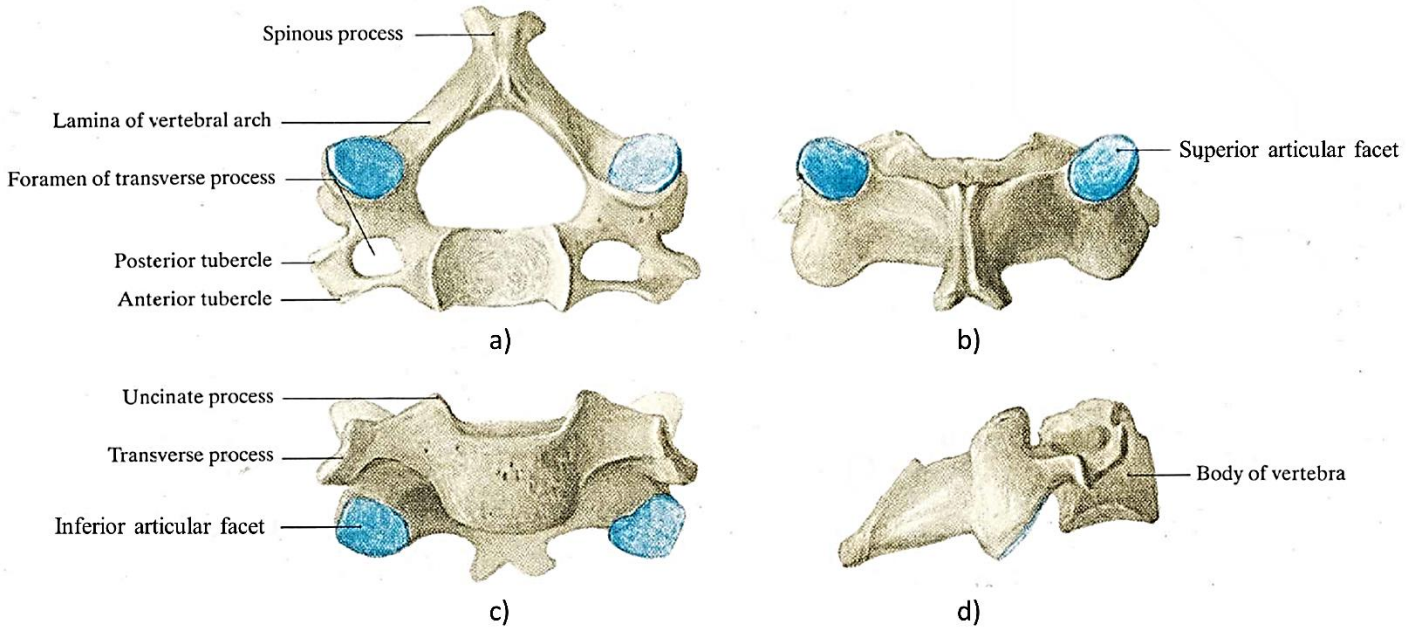

Figure 1.3: (a) Superior; (b) posterior; (c) anterior; and, (d) right lateral views of a human subaxial cervical spine vertebra. Image adapted from Rickenbacher *et al* (2013).[1]

Each pair of adjacent vertebra are stacked together to form a motion segment, or functional spinal unit (FSU), with two articulating joints: an intervertebral disc (IVD); and, the bilateral facet joints (Figure 1.4). The IVD is a fibrocartilaginous joint which transmits the majority of loads in six degrees of freedom between the vertebral bodies whilst also permitting a small amount of motion. In the subaxial cervical spine the disc is substantially thicker anteriorly than it is posteriorly (Mercer and Bogduk, 1999). The bilateral facet joints are an important stabilizing structure of the subaxial cervical spine that resist compression, anterior shear, torsion and flexion of motion segments (Nowitzke et al., 1994; White and Panjabi, 1990). The articular

[1] Image adapted by permission from Springer Nature Customer Service Centre GmbH: Springer Nature, *Applied Anatomy of the Back* by Rickenbacher, J., *et al*. ©1985.

facets are surrounded by a joint capsule (or capsular ligament) comprised of ligamentous connective tissue. In the normal spine the inferior facet (*f1*) of the superior vertebra lies posterior to the superior facet (*f2*) of the inferior vertebra (Figure 1.4).

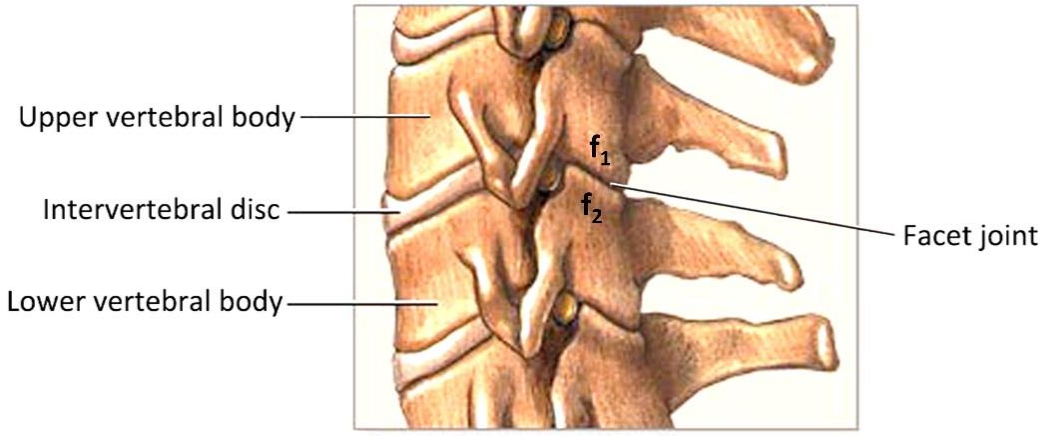

Figure 1.4: Lateral view of a typical cervical functional spinal unit, consisting of two vertebrae, an intervertebral disc and the bilateral facet (or zygapophysial) joints. Adapted from MedlinePlus (2011).[1]

In addition to the capsular ligament, the cervical column is stabilised by five other ligaments (Figure 1.5). The anterior and posterior longitudinal ligaments run vertically anterior and posterior to the vertebral bodies. The ligamentum flavum and interspinous ligaments connect the laminae and spinous processes of adjacent vertebrae, respectively (Gilroy et al., 2012). The ligamentum nuchae (or nuchal ligament) attaches to the spinous process tips and extends superficially to partition the lateral muscles of the neck. All these ligaments stabilise and restrict motion by providing tensile resistance to external loads.

[1] Awaiting copyright permissions.

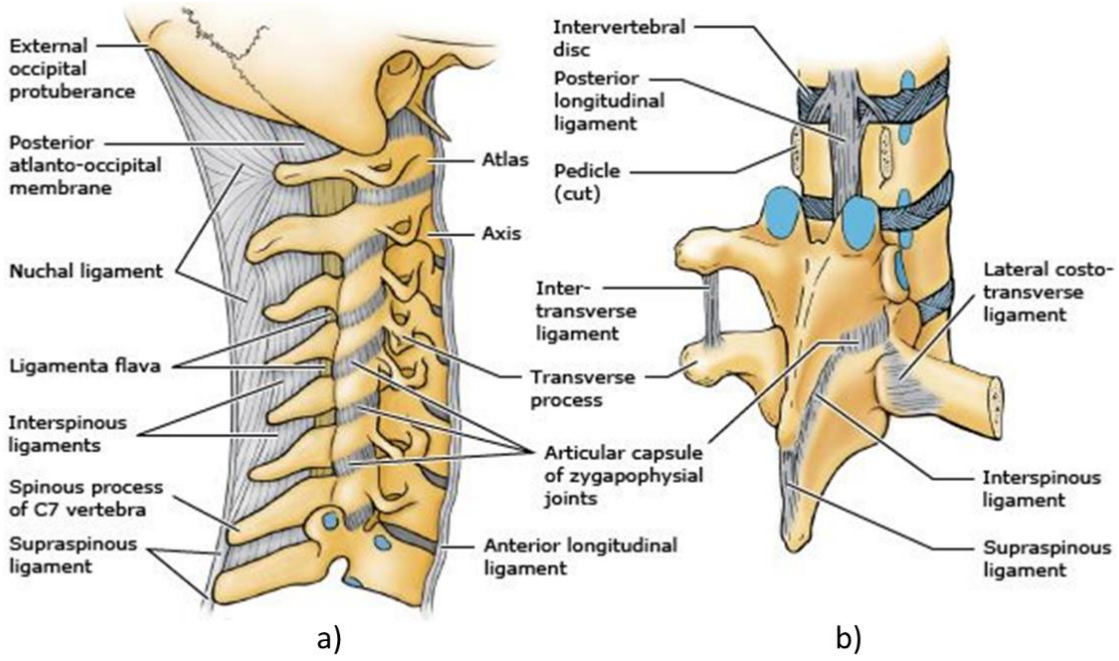

Figure 1.5: a) Lateral and b) postero-lateral views of the cervico-thoracic spine, illustrating ligaments and osseous features. Adapted from Moore *et al.* (2006).[1]

1.2.5 The spinal cord

The spinal cord is an extension of the central nervous system and lies within the spinal canal. It commences at the foramen magnum and terminates opposite the L1 vertebral body in the adult. Its primary function is to transmit and receive nerve signals between the brain and the peripheral nervous system. The spinal cord has an oval cross-section that is largest in the cervical and lumbar regions (~13×9 mm vs. 10×8 mm in the thoracic region), as they contain additional cells and fibres for innervating the limbs. The spinal meninges (dura mater, arachnoid mater, and pia mater) surround the spinal cord to protect it from the osseous and ligamentous features of the canal (Figure 1.6). Cerebrospinal fluid fills the cavity between the arachnoid mater and the pia mater, known as the subarachnoid space (Figure 1.6b), to provide additional protection to the brain and spinal cord. The meninges also carry blood vessels to the spinal cord.

Transverse sectioning of the cord reveals a central, butterfly shaped column of gray matter surrounded by peripheral white matter (Figure 1.6b). Gray matter consists of nerve cell bodies and is divided into three columns: the anterior, posterior, and lateral 'horns'. White matter

[1] Image adapted by permission from Wolters Kluwer Health: *Clinically Oriented Anatomy* by Moore, K.L., *et al*. © 2006.

is also separated into anterior, posterior and lateral compartments, termed ‘funiculi’, each containing bundles of motor and sensory nerve fibres.

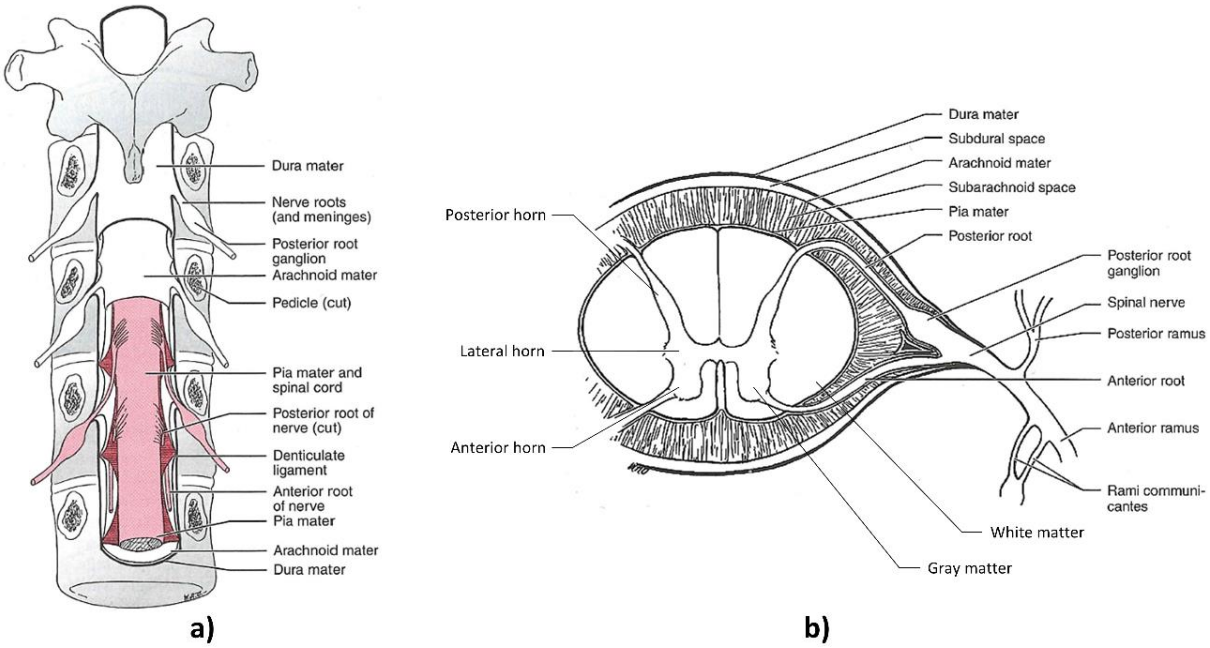

Figure 1.6: a) Coronal illustration of the spinal cord and its protective features; and, b) transverse cross-section of the spinal cord and meninges. Images adapted from Jenkins *et al.* (2009).[1]

Roots and branches of the spinal nerves exit between adjacent vertebrae (predominately through the intervertebral foramina) to connect the spinal cord to a majority of the body (Rickenbacher et al., 2013). Eight paired spinal nerves arise from cervical region of the cord (C1-C8), each of which has two roots: the posterior (or dorsal) root contains the afferent nerve fibres that provide sensory function, and the anterior (or ventral) root contains the fibres that conduct motor function (Chaffee and Greisheimer, 1974). Each paired nerve splits into two primary branches as they emerge from the intervertebral foramen (Figure 1.6b): the posterior rami contains the motor and sensory fibres that supply the skin and the longitudinal back muscles, while the anterior rami form the cervical plexus (C1-C4) and brachial plexus (C5-C8). The cervical plexus supplies the muscles and skin of the neck and posterior scalp, skin on the anterior thoracic wall, and (most importantly) the diaphragm (via the phrenic nerve). The brachial plexus innervates numerous neck and shoulder muscles, and the entire upper limb.

[1] Awaiting copyright permissions.

1.3 Traumatic injuries of the subaxial cervical spine

This section provides an overview of traumatic spinal cord and spinal column injuries that are observed in the subaxial cervical region.

1.3.1 Injury classification systems

Clinically, cervical spine injuries are traditionally categorised based on subjective, qualitative evaluation of their radiographic appearance. As a result, inconsistencies in injury classification between (and even within) institutions occur, causing difficulties in communication and education within the medical community (Vaccaro et al., 2007). This section describes the standardised injury classification systems that have been developed to establish a uniform method of communicating the mechanisms and severity of a traumatic spinal column and spinal cord injury.

The Abbreviated Injury Scale (AIS) is a commonly used anatomically-based system that was created by the Association for the Advancement of Automotive Medicine with specific codes relating to cervical trauma, including CFD (Greenspan et al., 1985). AIS scores are used to categorise injury severity according to body region. Scores range from 1 to 6, where 1 is a minor injury and 6 is considered "incompatible with life" (Copes et al., 1988). The Injury Severity Scale (ISS) was developed to quantify injury to the patient as a whole. A single ISS value is calculated from "the sum of the squares of the highest AIS grade in each of the three most severely injured areas" (Baker et al., 1974). An ISS of 75 is automatically assigned if any region is assigned an AIS score of 6, whilst an ISS >15 is considered major trauma. The AIS and ISS classification systems describe only the anatomical location of traumatic injuries, and their perceived risk of mortality, and do not provide information about the injury mechanism.

Injury classification systems specific to the subaxial cervical spine have been developed, and there is some debate about the importance of considering injury *mechanism* when classifying these injuries. Comprehensive mechanistic subaxial cervical injury classification systems have

been developed, but the suggested terminology has rarely been used clinically (Vaccaro et al., 2007). In the Allen and Ferguson Mechanistic Classification of Subaxial Cervical Injury (A&FCS) (Allen et al., 1982) injury mechanisms were inferred from a retrospective review of medical records and radiography of 165 patients who suffered traumatic subaxial cervical fractures and dislocations. Detailed information regarding neurological injury and injury mechanism (head-neck posture, and location and direction of external injury vector) was available for each patient, and radiographs and records were investigated separately to mitigate bias. Cases that presented with similar radiographic features were grouped and six categories were proposed. The spectrum of injuries described by each category was termed a "phylogeny", and each phylogeny was labelled according to the apparent dominant external injury vector and the posture of the cervical spine at the time of injury: vertical compression, compressive flexion, lateral flexion, compressive extension, distractive extension, and distractive flexion. Each category was sub-divided into 'stages' of injury severity that were ordered from least severe to most severe amount of anatomical damage. For each stage of each phylogeny, bony and soft-tissue injuries (inferred from radiographs), patient demographics, associated neurological impairment, and proposed injury mechanisms were described. The A&FCS was the first to attempt to classify subaxial cervical spinal trauma according to injury mechanism; however, the proposed injury vectors (especially those that describe CFD) have not yet been validated experimentally. Low reliability and non-intuitive clinical relevance have led to sparse clinical use of this classification system (Aarabi et al., 2013; Vaccaro et al., 2007).

In 2007 the Spine Trauma Study Group (Vaccaro et al., 2007) developed the Subaxial Injury Classification (SLIC) and Severity Scale. The SLIC is a point-based system which combines assessment of injury morphology, disco-ligamentous injury, and neurological status of the patient to provide an overall score to guide the treatment of the injury. This classification system completely disregards injury mechanism and anatomy, placing greater emphasis on injury morphology. While the reliability of SLIC was reported to be better than the A&FCS (although the Kappa statistic reported for 'Total SLIC' was lower than for A&FCS; 0.39 vs. 0.63) (Vaccaro

et al., 2007), disagreements on definitions of injury morphology motivated the AOSpine Knowledge Forum Trauma (which shared several members with the Spine Trauma Study Group) to develop their own classification system (Schnake et al., 2017; Vaccaro et al., 2016). The AOSpine Subaxial Cervical Spine Injury Classification System comprised the same assessment of injury and fracture morphology, disco-ligamentous injury, and neurological status as SLIC, but the principal indicator of injury severity was categorised mechanistically similarly to the A&FCS (Schnake et al., 2017). Reliability of the AOSpine System was better than SLIC (Kappa: 0.64 vs. 0.39) but was essentially equivalent to reliability of the A&FCS (Vaccaro et al., 2016).

A reliable, intuitive, and clinically functional system for classifying subaxial cervical injuries is yet to be developed. This section demonstrates that mechanism of injury is likely an important clinical consideration when evaluating injury severity, and illustrates that the relationship between subaxial cervical spine injury mechanism, injury morphology, and injury severity is ambiguous. Controlled, biofidelic, human cadaver biomechanical testing is required to improve our understanding of this relationship, and to develop more accurate injury classification systems.

1.3.2 Spinal column injuries

This section describes the traumatic spinal column injuries commonly observed in the subaxial cervical spine and their associated injury mechanisms. These injuries include fractures of the anterior and posterior vertebral columns, and a particular focus on CFD. The described injuries have been categorised using the naming convention consistent with most modern medical textbooks (Rickenbacher et al., 2013).

1.3.2.1 Burst fracture

A burst fracture describes multiple fractures of the vertebral body, commonly characterised by an outward ‘bursting’ appearance of the cortical shell (Figure 1.7). Fractures of the posterior elements may occur, and the intervertebral disc may migrate through the fractured endplate into the vertebral body. Retropulsed bony fragments may cause compression of the

spinal cord resulting in SCI. These injuries are traditionally attributed to pure axial compression, or combined compressive-flexion injury mechanisms, produced by head-first contact with the neck in a flexed position. These external force vectors cause excessive loading to be transmitted through the vertebral bodies, while accompanying distraction of the posterior elements can lead to disruption of the posterior soft-tissues (Allen et al., 1982; Kwon et al., 2006; Rickenbacher et al., 2013).

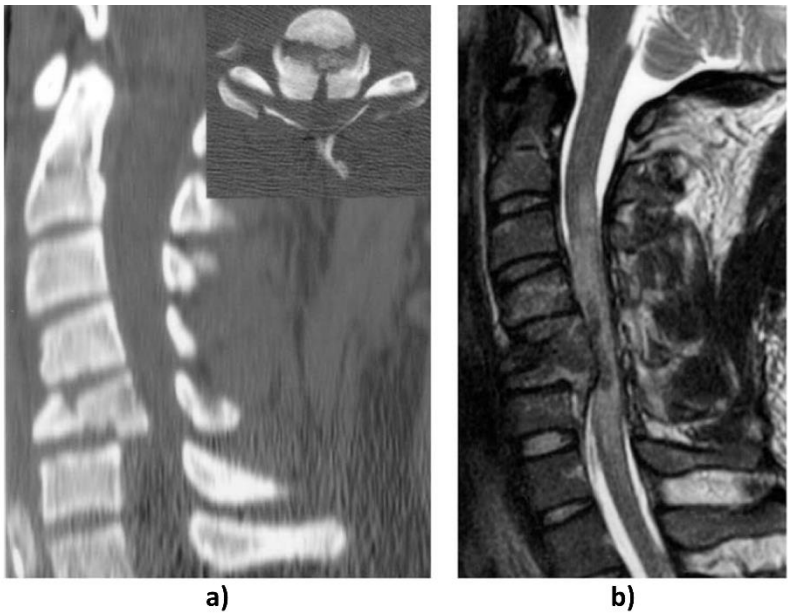

Figure 1.7: a) CT scan of a C5 burst fracture causing substantial canal compromise. b) The corresponding T2-weighted MRI image shows severe cord compression. Image adapted from Kwon *et al.* (2006).[1]

Hyperextension injuries

Fractures of the vertebral arch, the articular pillars, and/or the spinous process are most likely a result of traumatic hyperextension of the head, especially if accompanied by disruption of the disc and anterior longitudinal ligament. These injuries are most common in the cervical region but only account for 8% of subaxial cervical trauma (Rickenbacher et al., 2013; Torretti and Sengupta, 2007). The consequences of extension injuries are most extreme in the upper cervical spine (superior to C3) and are usually a result of hanging, or head-to-windshield contact during a frontal MVA (Figure 1.8). Extension injury in the subaxial cervical region is more

[1] Image adapted by permission from Wolters Kluwer Health: Kwon, B.K., *et al*., 2006. *Subaxial Cervical Spine Trauma*. Journal of the American Academy of Orthopaedic Surgeons **14**(2), 78-89 (https://journals.lww.com/jaaos/Fulltext/2006/02000/Subaxial_Cervical_Spine_Trauma.3.aspx).

commonly a result of low-energy mechanisms, such as head-ground contact during a same-level fall (Torretti and Sengupta, 2007).

Figure 1.8: Illustrations of typical hyperextension injury causation. Image adapted from Rickenbacher *et al.* (2013)[1].

1.3.2.3 Facet subluxation, dislocation and fracture-dislocation

The A&FCS classified the spectrum of subaxial cervical facet subluxation and CFD injuries as 'distractive-flexion injuries' (DFIs) (Allen et al., 1982). During CFD, the inferior facet of the superior vertebra *(f1)* is forced anterior of the adjacent facet *(f2)* into the spinal canal, creating a 'perched' or 'locked' facet (Figure 1.9). Unilateral facet dislocation (UFD) describes a dislocation of one facet only, whereas bilateral facet dislocation (BFD) involves both facets. On lateral radiographs, anterior translation of 25% of the antero-posterior (AP) vertebral body width is indicative of UFD, while greater than 50% translation is commonly used to define BFD (Allen et al., 1982; Beatson, 1963; Dailey et al., 2009). Translation of *f1* relative to *f2*, prior to dislocation, is termed facet subluxation.

[1] Image adapted by permission from Springer Nature Customer Service Centre GmbH: Springer Nature, *Applied Anatomy of the Back* by Rickenbacher, J., *et al*. ©1985.

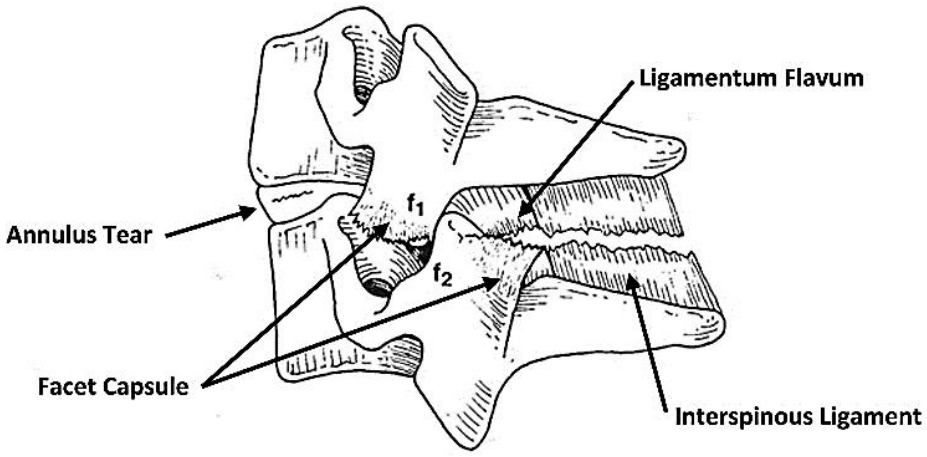

Figure 1.9: Lateral view of a facet dislocation creating a "locked" facet and disruption of surrounding soft-tissue structures. Image adapted from White and Panjabi *et al.* (1990).[1]

CFDs are commonly observed following MVA rollovers, falls and sporting accidents, during which the external loading applied to the neck can be complex and variable. There exists some debate about the aetiology of these injuries, and they are rarely replicated experimentally (Foster et al., 2012). It has been proposed that eccentric axial compressive forces applied to the head (Allen et al., 1982; Cusick and Yoganandan, 2002; Huelke and Nusholtz, 1986; White and Panjabi, 1990), or inertial motion of the head during high deceleration events (Huelke and Nusholtz, 1986) may produce BFD, and that loading and anatomical asymmetry likely superimposes axial rotation and lateral bending onto the injury vector, causing UFD (Allen et al., 1982; Hodgson and Thomas, 1980; Maiman et al., 1983; Roaf, 1960). As part of their DFI classification, Allen *et al.* (1982) stated that intervertebral shear and compressive injury vectors may be produced at the level of injury, and these observations have been supported by subsequent biomechanical testing (Hodgson and Thomas, 1980; Ivancic, 2012b; Maiman et al., 1983; Panjabi et al., 2007; Roaf, 1960). The presence of these intervertebral injury vectors is consistent with the extent of surrounding soft-tissue injury observed after CFD, resulting in instability of the neck.

During BFD, all ligamentous structures that cross the level of injury are disrupted (Beatson, 1963; Vaccaro et al., 2001). In the laboratory, compromise of only the ipsilateral facet capsule, ligamentum flavum and approximately half of the annulus fibrosus are required to

[1] Image adapted for print version by permission from Wolters Kluwer Health: *Clinical Biomechanics of the Spine* by White, A.A., and Panjabi, M.M. ©1990 by J.B. Lippincott Company.

produce UFD (Beatson, 1963; Ebraheim et al., 2009; Nadeau et al., 2012; Sim et al., 2001). Injury to both facet capsules following UFD has been observed in some cases (Nadeau et al., 2012; Vaccaro et al., 2001), suggesting that tissue disruption may occur bilaterally.

Severe vertebral body fractures rarely accompany CFD, but concomitant fracture of the posterior elements is common (Allen et al., 1982). Fracture of the facet tip of *f1* or *f2* (Figure 1.9) is often observed upon clinical presentation (Foster et al., 2012; Piccirilli et al., 2013), suggesting that high loads are transmitted through the facet joint during the injurious motion. The presence of a facet fracture may indicate a larger *shear* component of the injury vector, or an additional *compressive* force that restricts *f1* from 'jumping' over *f2*. Interestingly, these concomitant fractures have not been observed during experimentally produced CFDs (Foster et al., 2012), suggesting that *in vivo* traumatic loading conditions are not adequately being represented in these experiments.

1.3.3 Spinal cord injury (SCI)

SCI is often devastating, with sequelae that cause substantial individual and economic burden. A better understanding of the mechanisms leading to SCI is crucial to developing improved preventative measures. Traumatic SCI is most often caused by intrusion of vertebrae, bone fragments, or herniated disc material into the spinal canal, resulting in compression and spinal cord injury. Spinal cord contusion (or bruising), swelling, partial tearing, or complete transection (rare) may occur, resulting in partial or complete loss of motor and/or sensory function below the level of injury. The segmental region of injury and the magnitude of the lesion contribute to the severity of SCI (Rickenbacher et al., 2013).

1.3.3.1 Neurological grading

The 'gold standard' for assessing the functional impairment of a person after spinal cord injury is the American Spinal Injury Association (ASIA) International Standards for Neurological Classification of Spinal Cord Injury (ISNCSCI) (Marino et al., 2003). This assessment is commonly performed before and after spinal cord decompression surgery to assess the restoration

of neurological function. The motor and sensory response of key myotomes and dermatomes are rated to determine the ASIA Impairment Scale (ASIA AIS) Grade of the individual, ranging from Grade A (complete sensory and motor loss) to Grade E (normal neurological function). The neurological level of injury is defined as the most caudal segment of the cord demonstrating normal motor and sensory function.

1.3.3.2 Relationship with cervical column injury

Although the incidence of cervical column injury is relatively low amongst trauma patients (Torretti and Sengupta, 2007) it is most commonly associated with SCI and has a high rate of early mortality (Hasler et al., 2012). Only one third of traumatic SCIs present with concomitant bone fracture (Rickenbacher et al., 2013) and there is some evidence that CFD-Fx is more likely to cause SCI than CFD+Fx, as associated fractures may maintain patency of the spinal canal (Chakravarthy et al., 2014; Piccirilli et al., 2013); however, this association has not been confirmed statistically in a large-cohort investigation. In animal models, shear SCI caused by vertebral dislocation is associated with more severe primary and secondary pathology than contusion or distraction injuries (Choo et al., 2008; Choo et al., 2007; Fiford et al., 2004), and there is some epidemiological evidence that dislocations and fracture-dislocations are at higher risk of causing complete SCI than other vertebral column injuries (Marar, 1974; Sekhon and Fehlings, 2001; Tator, 1983). The relationship between traumatic cervical column injury and the severity of associated neurological involvement remains unclear, especially within the context of CFD.

1.4 Cervical trauma in the clinical setting

This section provides a review of current clinical cervical trauma literature pertaining to CFD.

1.4.1 Epidemiology of cervical trauma

Epidemiology studies of cervical trauma frequently consider both spinal column and cord injury. Literature concerning SCI is most common, probably due to the long-term consequences

and high associated costs (Burns et al., 2010); however, column injury without SCI can result in significant medical expenses due to long hospital stays (Wang et al., 2009). In the developed world, the annual incidence of column injury is estimated at 190-880 per million population while the incidence of SCI is 35-53 per million population per year (Hasler et al., 2012). In Australia, 264 new cases of traumatic SCI were reported in 2014-15, with an estimated 12.8 cases per million population (Tovell, 2018). A large-cohort study of cervical injury in major trauma patients reported that males aged 35 years or older are most at risk (Hasler et al., 2012). This is consistent with the demographics reported within small-cohort studies of traumatic CFD (Doran et al., 1993; Dvorak et al., 2007; Piccirilli et al., 2013; Rorabeck et al., 1987).

CFD is only observed in a small percentage of patients undergoing radiography for suspected column injury; however, this proportion rises significantly amongst those presenting with SCI or admitted after MVA. Studies of medium-to-large cohorts of blunt trauma patients have reported incidence of cervical spinal injuries from 1.3% to 2.8% (Cadoux et al., 1987; Davidson and Birdsell, 1989; Hoffman et al., 1992) and an incidence of facet subluxation or dislocation of between 0.7% (Goldberg et al., 2001) and 2.9% (Brady et al., 1999). In patients admitted with traumatic cervical SCI, the incidence of CFD increases to between 16% (Scher, 1977) and 32.1% (Wilson et al., 2013). Other studies have observed a rise in the prevalence of cervical spine injury in trauma patients from 1.3% to 5.5% (Davidson and Birdsell, 1989), and from 6.7% to 9% (Clayton et al., 2012) amongst those caused by MVAs. These results demonstrate the high association between CFD and SCI, and the vulnerability of the neck during car accidents.

Vehicle occupants appear to be at elevated risk of cervical column injury, and specifically CFD, during rollovers. Studies of United States crash investigation databases report incidence of cervical spine injury in 12.7% of pure rollovers (Bambach et al., 2013) and 6.5% of cases (of which CFDs account for 8%) where rollover is the most harmful event (Funk et al., 2012). In 46 pure rollover cases, 50% of occupants had AIS 2 or AIS 3+ cervical fractures (not further specified) – 9 out of these 23 (39.1%) suffered CFD (Foster et al., 2012). Of the 23 cases with

cervical column injury, 20 (87.0%) had evidence of loading applied to the head during the injury event, while 100% of CFDs presented with head/facial injuries. This suggests that cervical spine injury during MVA rollovers are most often caused by head-contact injury, and that these scenarios frequently cause CFD.

While high-energy MVAs are the most common cause of cervical trauma in the young, low-velocity injury mechanisms (particularly head-contact injury during falls) are more common in the elderly (Clark and White, 1985; Kato et al., 2008; Thesleff et al., 2015). An increase in SCI associated with falls in the elderly has been observed and is thought to be due (in part) to age-related spondylosis (Kato et al., 2008; Thesleff et al., 2015) which causes narrowing of the spinal canal and may increase the likelihood of neurological involvement in subaxial cervical spine trauma (Eismont et al., 1984; Fehlings et al., 1999; Kang et al., 1994; Song et al., 2009). MVAs and falls are the most common causes of injury in small-cohort reports of CFD (Allen et al., 1982; Anissipour et al., 2017; Argenson et al., 1988; Cotler et al., 1990; Eranki et al., 2016; Hadley et al., 1992; Key, 1975; Rorabeck et al., 1987; Scher, 1977; Shanmuganathan et al., 1994; Vaccaro et al., 1999; Wilson et al., 2013), but there have been no large-cohort investigations (>135 patients) of the epidemiology of DFIs and CFD, or the factors predictive of SCI in this cohort. Such an investigation is necessary to elucidate the mechanisms and features that are associated with the severity of these injuries.

1.4.2 Relationship between features of CFD and SCI

Despite relatively low prevalence across all trauma patients, cervical UFD and BFD result in neurological impairment in over 69% and 89% of cases, respectively (Argenson et al., 1988; Cotler et al., 1990; O'Brien et al., 1982; Shanmuganathan et al., 1994; Wilson et al., 2013; Wolf et al., 1991). BFD results in significantly worse neurological outcome, has a diminished potential for recovery, and results in longer periods of acute hospital stay, than UFD (Cotler et al., 1990; Hadley et al., 1992; Lintner et al., 1993; Wilson et al., 2013). BFD is also associated with greater injury severity and higher probability of complications (Cotler et al., 1990; Foster et al., 2012).

CFD-Fx may have greater potential to injure the spinal cord and may be more difficult to reduce, compared to CFD+Fx (Piccirilli et al., 2013). In a recent case review, neurological integrity was preserved in four cases of BFD due to the substantial concomitant vertebral fractures at the level of injury which effectively maintained canal patency (Chakravarthy et al., 2014). Of 40 patients with rotational facet injuries, patients presenting with UFD were significantly more likely to have neurological involvement than patients with subluxation or UFD with concomitant facet fracture (Shanmuganathan et al., 1994). This supports the findings of Argenson *et al.* (1988), who reported a 70% occurrence of neurological impairment in cases of UFD-Fx from traumatic rotational injury, compared to 30% and 40% in patients with unilateral facet fracture and UFD+Fx, respectively.

1.4.3 Radiographic features of cervical trauma

Radiographs, computed tomography (CT) and/or magnetic resonance imaging (MRI) are routinely used to assess the presence and extent of bony and soft-tissue injury in the spine. Qualitative and quantitative assessments obtained from medical images provide an indication of the clinical stability of the spine, and the likelihood of associated neurological involvement. This is particularly important in patients with suspected subaxial cervical spinal column injury for which rapid intervention is crucial to optimizing patient outcomes (Wilson et al., 2013), and neurological examination is often complicated by reduced levels of consciousness (Hasler et al., 2012; Hills and Deane, 1993).

The Spine Trauma Study Group made recommendations (summarised in Table 1.1) for the most clinically useful radiographic measurements of subaxial cervical trauma by reviewing all available relevant literature (Bono et al., 2006). In a follow-up investigation of inter-observer reliability, intervertebral AP translation, kyphosis, and VB height loss (as measured on x-ray) measurements demonstrated at least moderate reliability (Bono et al., 2011); similar findings were reported by van Middendorp *et al.* (2015). Facet apposition measurements were less reproducible (Bono et al., 2011), while CT-measured spinal canal occlusion (Furlan et al., 2007) and T2-weighted MRI spinal cord compression measurements (Fehlings et al., 2006) have

demonstrated moderate to high inter-observer agreement and intra-observer repeatability. However, these studies performed measurements on medical images from small patient cohorts with a broad spectrum of cervical trauma. The reliability and repeatability of these measurements when applied to CFD has not previously been reported.

Table 1.1: A summary of the radiographic measurements of subaxial cervical injury severity suggested by the Spine Trauma Study Group (Bono et al., 2006).

Measurement method:	Description:	Modality:
Cobb angle or posterior VB tangent angle	Sagittal plane intervertebral kyphosis	Lateral x-ray
VB AP translation	Sagittal plane AP intervertebral translation	Lateral x-ray or mid-sagittal CT slice
VB height loss	Change in sagittal height of fractured VB	Lateral x-ray or mid-sagittal CT slice
Facet apposition	Articular apposition of subluxed or fractured facet	Lateral x-ray or para-sagittal CT slice
Spinal canal occlusion	Change in AP diameter of spinal canal	Mid-sagittal CT slice
Spinal cord compression	Change in AP diameter of spinal cord	Mid-sagittal MRI slice

VB, vertebral body; AP, antero-posterior; CT, computed-tomography; MRI, magnetic resonance imaging

Although cervical vertebral alignment is routinely assessed radiographically to indicate injury severity, it is not known which (if any) of the proposed radiographic measurements are predictive of neurological deficit when applied to CFD. Measurements of spinal canal occlusion (Fehlings et al., 1999; Furlan et al., 2011; Kang et al., 1994; Miyanji et al., 2007) and spinal cord compression (Fehlings et al., 1999; Furlan et al., 2011; Hayashi et al., 1995; Miyanji et al., 2007; Rao and Fehlings, 1999) on CT or MRI correlate with the presence and severity of neurological deficit in subaxial cervical trauma; however, such associations have not been investigated for the other suggested measurements, or in the context of DFI and CFD.

1.5 Biomechanical testing of the subaxial cervical spine

This section presents a review of the experimental models reported in the current cervical spine literature, specifically those relating to CFD and subaxial cervical facet biomechanics. This review is restricted to biomechanical experiments performed using human full-body cadavers (referred to as postmortem human subjects, PMHS) or spinal segments from human cadavers.

1.5.1 Experimental production of CFD and CFD+Fx

CFD and CFD+Fx have been experimentally produced to investigate the biomechanical response of the subaxial cervical spine before, during, and following, the injury event. This section describes the methods that were used to create these injuries in PMHS, full cervical spines, and motion segments, and summarises the key findings of these studies.

1.5.1.1 Quasi-static and dynamic mechanical tests

Experimental methodologies within the current biomechanical literature utilise static, quasi-static and dynamic mechanical tests. Quasi-static testing is conducted at low speed to permit measurement of the mechanical response of specimens under complex applied loading, in a controlled environment. These tests assess the contribution of osseoligamentous structures to resisting applied loads, elucidating the role of these structures during traumatic injury. Dynamic mechanical testing uses drop-towers, impactors, and acceleration/deceleration sleds to simulate real-life traumatic injury. This high-rate testing is commonly used to investigate the progression of tissue failure during an injury event, and to assess the relationship between testing parameters (loading rate, direction, boundary conditions etc.) on injury type and severity.

Static loading has been used to investigate the mechanics of specific disco-ligamentous structures in providing stability, mobility and resisting traumatic injury (Ebraheim et al., 2009; Hedtmann et al., 1989; Sim et al., 2001), as well as the load-bearing role of the facets (Hakim and King, 1976). While the results of these studies may provide important information about the progression of CFD and concomitant injuries, the methodologies are outside the scope of this project and will not be discussed in detail.

1.5.1.2 Motion segment testing

Short spinal segments reduce a specimen to one or two sets of intervertebral joints, allowing for easier interpretation of the effects of intervertebral loads and motions during simulated cervical trauma. Several studies have produced CFD by quasi-static and dynamic loading of motion segments. The earliest of these applied ‘slow’ (rate not specified) compression,

flexion, extension, lateral bending, and shear loading to cervical FSUs and reported the injuries associated with each loading direction (Roaf, 1960). Compression was applied using a materials testing machine, but the methods for applying shear and bending motions were not specified. The author stated that flexion and extension were applied "about the normal axis of rotation", suggesting that constrained intervertebral motions were used. Hyperflexion did not produce clinically-relevant injuries in these motion segments. A combination of anterior shear, axial rotation, and flexion loading produced UFD and BFD, and superimposing these motions with axial compression caused vertebral body and/or facet fractures. UFD has also been produced in cervical FSUs by applying a lateral bending force and gradually increasing axial rotation until dislocation occurs, using a mechanical testing machine (Crawford et al., 2002; Nadeau et al., 2012). Crawford *et al.* (2002) observed no concomitant facet fractures but Nadeau *et al.* (2012) produced UFD+Fx in 3/9 specimens – the authors did not hypothesise why fracture occurred for some specimens and not others. Although these quasi-static methods reproducibly achieved CFD, the rate at which they were created is substantially slower than that observed during real-life trauma.

The only studies to specifically investigate the experimental production of traumatic BFD used a dynamic sled apparatus (Panjabi et al., 1998a) (Figure 1.10). Incrementally-increasing, sagittal decelerations were applied to subaxial cervical FSUs until BFD occurred – the accelerations required to cause BFD ranged between 74.5 and 113.8 $\frac{m}{s^2}$ (Ivancic et al., 2007, 2008; Panjabi et al., 2007). The head was simulated with a 3.3 kg mass attached to the upper mount, which was stabilised by passive, bilateral muscle-simulation cables – the weight of the head and tension in the cables provided an intervertebral compressive preload of 180 N. This model produced BFD in 10 of 12 FSU's, and intervertebral kinematics, canal occlusion, and estimated neck loads during the injury event were reported; however, no BFD+Fx was observed. The absence of concomitant facet fracture may be an artefact of the incremental injury mechanism, as rupture of the posterior ligaments during the impacts prior to achieving BFD was observed in all cases (Panjabi et al., 2007). Compromise of these structures may have permitted excessive

separation of the facet joints during the final inertial loading, allowing the joint to dislocate with minimal facet contact. It is unlikely that this inertial injury mechanism is observed clinically, but a large-cohort investigation of CFD is required to confirm this. Nevertheless, these studies provide important information about intervertebral kinematics and neck loading that may occur during inertially-produced, traumatic BFD-Fx.

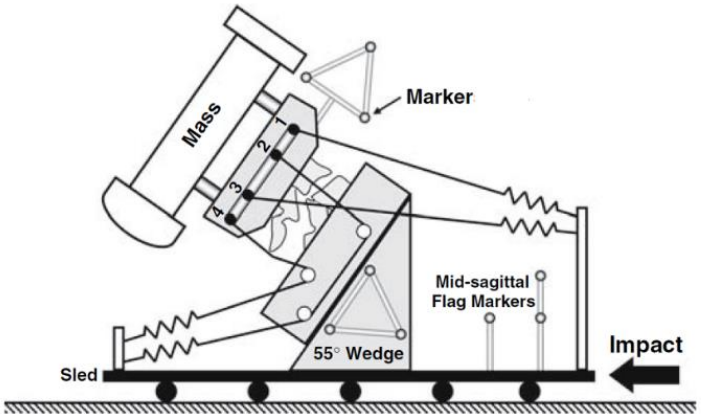

Figure 1.10: Sled apparatus for producing bilateral facet dislocation through incremental trauma.Image adapted from Panjabi *et al.* (2007).[1]

1.5.1.3 Complete cervical spine and PMHS testing

Quasi-static and dynamic testing of motion segments provides information about the intervertebral loads/motions that lead to cervical trauma, but these experimental methods are unable to elucidate the *global* loading scenarios that result in neck injuries. The numerous and intricate joints that comprise the head and neck create complexity when surmising the subaxial intervertebral loads and motions that result from an external loading vector. Therefore, complete cadaveric cervical spines and PMHS have been used to investigate the effects of global loading characteristics (speed, magnitude, direction), head constraints, and spinal posture on the injuries produced. This section provides a critical summary of the quasi-static and dynamic biomechanical experiments that have produced CFD in full cervical spines and PHMS.

Bauze and Ardran (1978) applied quasi-static axial compression loads to cervical spines (without heads) in a 'natural' posture (Figure 1.11a) and produced CFD in the lower subaxial

[1] Image adapted by permission from Springer Nature: Panjabi, M.M., *et al.*, 2007. *Cervical facet joint kinematics during bilateral facet dislocation*. European Spine Journal **16**(10), 1680-1688.

region of 10/12 specimens. The spines were fully constrained at the level of interest by inserting a steel spindle through the spinal canal, up to the level to be dislocated. The cranial portion of the spine was permitted to translate in the transverse plane at the interface with the loading plate. Vertebral kinematics and axial (vertical) load at injury were reported. Compression loading caused extension of the upper cervical region and flexion of the mid-lower region, creating intervertebral compression, flexion and anterior shear motions at the level of CFD. The authors noted that considerable axial rotation and bending motions were occasionally observed, resulting in UFD. The boundary conditions applied in the lower cervical region were clearly non-physiological and most likely influenced injury mechanisms, but this was the first study to experimentally investigate the intervertebral kinematics associated with CFD using a full cervical spine model.

Maiman *et al.* (1983) applied quasi-static axial loading (with varying amounts of anterior eccentricity) to PMHS and cervical spines (partial skull-T3) at rates up to 1.52 m/s using a materials testing machine. Loading was applied by rigidly fixing the actuator to the partial skull and driving the skull-piston assembly vertically (with the upper thoracic region embedded and attached to the base of the test machine), or by impacting the top of the skull of PMHS (with torso supported) using a platen attached to the piston. BFD occurred at C4/C5 in one PMHS when impact loading was applied with 2.5 cm anterior eccentricity. Flexion-compression was identified as the mode of failure; however, the lateral x-ray provided in the manuscript demonstrated a *posterior* dislocation, and superior *and* inferior vertebral body fractures were observed at the level of dislocation suggesting that this was an uncommon injury mechanism.

In a similar study, quasi-static axial compression loading produced BFD at the C5/C6 level of a complete cadaveric cervical spine tested in a ‘straightened neck’ posture (Pintar et al., 1989). Loading was applied via an aluminium rod rigidly attached to the skull (Figure 1.11b). Six-axis loads were measured cranial and caudal to the specimen throughout testing. Interestingly, a compression-extension injury mechanism was reported for this specimen and the axial load at injury was higher than for most other non-dislocated specimens; however, similar

studies have reported that CFD occurs at a lower axial load than other cervical trauma (Nightingale et al., 1991; Pintar et al., 1998). An accompanying C2/C3 fracture-dislocation was reported for this specimen, but injury to multiple cervical levels is not commonly associated with clinical or experimentally produced CFD (Pintar et al., 1998; Yoganandan et al., 1989). These results are inconsistent with other similar studies, possibly due to the initial straightened spinal posture and the axially-aligned compression loading (no anterior eccentricity). This study produced a unique CFD and demonstrates the effect of external loading direction and spinal posture on the features of cervical trauma.

Nightingale *et al.* (1991) demonstrated the influence of head-constraints and torso trajectory on injury mechanisms during cervical trauma. Quasi-static axial compression loading reliably produced lower cervical BFD-Fx when head flexion was restricted, but sagittal anterior translation was permitted (6/6 specimens) (Figure 1.11c). Dislocation was most commonly observed at C7/T1 and exhibited a substantially lower axial load to failure than specimens with vertebral body fractures. The final posture of these specimens demonstrated a first-order buckling mode with an inflection point in the lower cervical region, where dislocation occurred. Intervertebral kinematics were not reported but it is likely that large anterior shear motions occurred at this inflection point (Nightingale et al., 2016). Performing these tests at high-speed with appropriate neck-muscle replication may prevent the cranial region from escaping the weight of the torso, superimposing a larger axial compression force onto the intervertebral anterior shear motion and causing BFD+Fx. This proposed injury mechanism is yet to be verified experimentally.

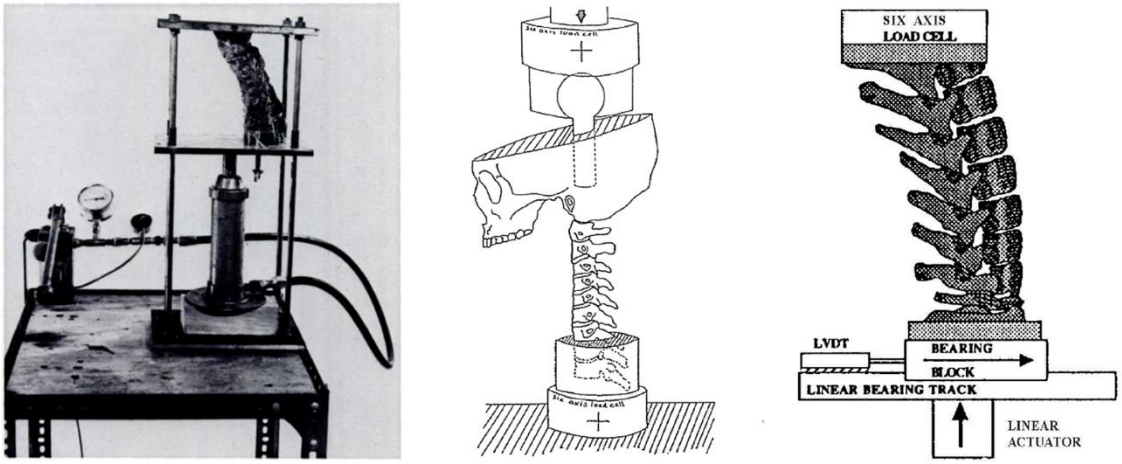

Figure 1.11: The test methods that produced cervical facet dislocation by applying quasi-static loading to full cervical spines. Images adapted from: (a) Bauze and Ardran (1978); (b) Pintar *et al.* (1989); and, (c) Nightingale *et al.* (1991).[1]

In biomechanical testing, dynamic trauma to the cervical spine following head-first impact is most often investigated using a drop-test or pendulum apparatus (Huelke and Nusholtz, 1986) (Figure 1.12). Although producing CFD has not been the focus of these studies, subaxial dislocations are sometimes observed during drop-testing of subaxial or complete cervical spines. Hodgson and Thomas (1980) applied dynamic head loading to 16 PHMS to investigate the effect of impact surface, head-torso alignment, and loading direction, on vertebral body and articular process surface strains, and resultant injuries. Their results suggested that distributed loading on the top of the head tended to prevent head-flexion, creating lower cervical flexion and causing BFD±Fx due to intervertebral compression, flexion, and shear. The authors stated that these intervertebral motions were also produced by *global* cervical flexion due to concentrated axial loading with anterior eccentricity, and that loading asymmetry created an additional axial rotation component, producing subaxial UFD in one specimen.

[1] Awaiting copyright permissions.

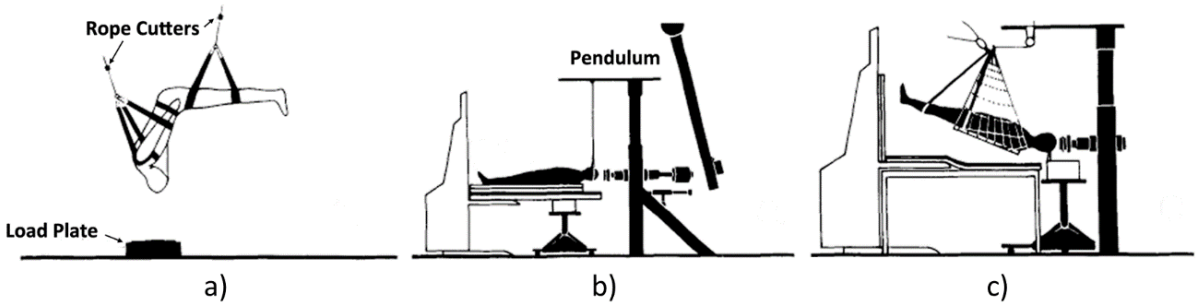

Figure 1.12: (a) drop-test, (b) pendulum; and, (c) combined dynamic impact tests. Image adapted from Huelke and Nusholtz (1986).[1]

UFD±Fx was produced in 6 subaxial cervical spines by applying high-speed, catastrophic constrained axial rotation (Myers et al., 1991). Destructive torsional loading was initially applied to the base of the skull of each specimen, creating atlantoaxial dislocation in all 6 cases and leaving the subaxial region uninjured. Each subaxial spine (C2-T1) was then re-tested using the same loading regime, producing CFD+Fx in five specimens and CFD-Fx in one. These results demonstrated that pure head rotation is not responsible for subaxial spinal injury, but global injury vectors that create constrained intervertebral axial rotation likely produce UFD+Fx.

The only BFD reported during drop-testing of full cadaver cervical spines was described by Nightingale *et al.* (1996). Eleven head-neck complexes were attached to a drop-carriage (including a six-axis load cell) in an inverted posture, with a following "torso" mass of 16 kg. Specimens impacted a flat steel plate with varied sagittal angle (-15 to +30°) and surface texture (low friction or padded). The resting lordosis of each specimen was preserved by orienting the C7/T1 disc at +25° to the transverse plane during embedding of T1-T3, but neither passive nor active neck muscle replication was applied. A C6/C7 BFD-Fx was produced when the low-friction impact platen was angled at 15° to the horizontal. This configuration caused 'pocketing' of the head (restricting head motion) and high-order buckling occurred initially, followed by first order buckling that produced BFD. The vertical load at the time of dislocation injury was not reported, although a time lag between head impact and peak lower cervical loading occurred. The authors described predominantly extension of the head upon impact, and intervertebral distraction

[1] Image adapted by permission from Wiley Materials: Huelke, D.F. and Nusholtz, G.S., 1986. *Cervical spine biomechanics: A review of the literature*. Journal of Orthopaedic Research **4**(2), 232-245.

and flexion (without shear) were thought to be the primary injury mechanisms in the lower cervical spine. However, during computational simulations of these experiments, Nightingale *et al.* (2016) described intervertebral anterior shear, compression, and flexion as the dominant loads in the subaxial region. These simulations also demonstrated that active neck muscle forces substantially increased intervertebral compression and shear forces in the lower cervical spine, compared to simulations without muscle forces – this may explain why BFD+Fx did not occur in the *in vitro* experiments. Subaxial intervertebral loading and kinematics during BFD produced by head-impact testing are yet to be reported.

BFD-Fx was produced in an un-specified number of specimens by applying axial impact loading to the anterior skull of 13 head-neck complexes (C1-T2) (Pintar et al., 1998). Dynamic global cervical flexion was created and local, intervertebral anterior shear, flexion, and axial compression motions were observed during the injury event. The authors proposed that either a global flexion-*distraction* or a flexion-*compression* injury mechanism may cause BFD if intervertebral flexion is produced in the lower cervical spine. They also suggested that the lack of BFD+Fx and/or 'locked facets' after the injury event may be due to an absence of muscle contraction during the experiments, and that the intervertebral axial compression force imposed by muscle tone may cause additional shear load at the level of injury. This hypothesis was supported by the results of computational simulations of subaxial cervical trauma with and without active neck muscle forces (Nightingale et al., 2016). The effect of intervertebral anterior shear and imposed axial compression on the risk of facet fracture during BFD has not previously been investigated.

1.5.1.4 Summary

CFD has been produced during quasi-static and dynamic biomechanical testing of subaxial cervical motion segments and full cervical spines. The *external* axial loads and displacements necessary to produce CFD, and intervertebral kinematics during the injury event have been reported. Intervertebral anterior shear, flexion, compression, *and* distraction motions have all been observed during the experimental production of BFD, while an additional axial

rotation and/or lateral bending component can produce UFD (Table 1.2). Concomitant facet fracture during CFD is commonly observed clinically but rarely occurs experimentally, perhaps due to a lack of neck muscle replication. Such muscle activation increases shear and compression loading in the subaxial cervical spine, which may increase loading through the facet joints and heighten the likelihood of CFD+Fx. Further experimental work is required to investigate this.

Table 1.2: Loading modes and intervertebral motions identified likely to cause cervical facet dislocation and fracture-dislocation.

Author(s)	Year	Investigation type	Loads/motions identified to cause injury
Roaf	1960	Quasi-static mechanical tests, FSU	BFD: Anterior shear, axial rotation, flexion UFD: Axial rotation, flexion Fx: Imposed compression
Bauze & Ardran	1978	Quasi-static mechanical tests, full cervical spine	BFD: Flexion, anterior-shear UFD: Flexion, axial-rotation, lateral bending
Hodgson & Thomas	1980	Dynamic mechanical tests, full cervical spine	BFD: Anterior shear, compression, flexion UFD: Anterior shear, axial rotation, compression, flexion
Allen *et al.*	1982	Retrospective medical record and radiographic review	BFD: Global flexion-distraction
Maiman *et al.*	1983	Quasi-static mechanical tests, full cervical spine	BFD: Global flexion-compression
Argenson *et al.*	1988	Retrospective medical record and radiographic review	UFD: Axial rotation, lateral bending
Pintar *et al.*	1989	Quasi-static mechanical tests, full cervical spine	BFD: Global compression-extension
Myers *et al.*	1991	Dynamic mechanical tests, subaxial cervical spine	UFD+Fx: Constrained axial rotation
Nightingale *et al.*	1991	Quasi-static mechanical tests, full cervical spine	BFD: Flexion
Nightingale *et al.*	1996	Dynamic mechanical tests, full cervical spine	BFD: Axial distraction, flexion
Pintar *et al.*	1998	Dynamic mechanical tests, full cervical spine	BFD: Anterior shear, compression, flexion
Crawford *et al.*	2002	Quasi-static mechanical tests, FSU	UFD: Axial rotation, lateral-bending
Ivancic *et al.* Panjabi *et al.* Ivancic *et al.*	2007 2007 2008	Dynamic mechanical tests, FSU	BFD: Anterior shear, axial distraction, flexion,
Nadeau *et al.*	2012	Quasi-static mechanical tests, FSU	UFD: Axial rotation, flexion, lateral-bending
Nightingale *et al.*	2016	Computer simulations of dynamic mechanical testing of full cervical spines (Nightingale et al., 1996)	BFD: Anterior shear, compression, flexion

FSU, functional spinal unit; BFD, bilateral facet dislocation; UFD, unilateral facet dislocation; Fx, fracture

1.5.2 Measuring vertebral kinematics during cervical trauma

Several different methods are used in biomechanical testing to explore vertebral kinematics during the experimental production of cervical trauma. These techniques provide qualitative and/or quantitative information about the intervertebral motions that are associated with cervical injuries, how these injuries affect normal spinal kinematics, and the extent to which the spinal canal is compromised. This section discusses the benefits and limitations of each technique, specifically regarding measurement accuracy and frame rate.

1.5.2.1 High-speed video cameras and cineradiographs

High-speed cameras have been used to investigate vertebral kinematics and injury progression during dynamic loading and quasi-static axial compression of cadaveric cervical spine specimens (Hodgson and Thomas, 1980; Maiman et al., 1983; Nightingale et al., 1991; Nightingale et al., 1996; Pintar et al., 1989; Pintar et al., 1995; Pintar et al., 1998; Van Toen et al., 2014). A single camera can provide information in a single plane (two-dimensional, 2D), while two or more cameras can be synchronised to obtain three-dimensional (3D) data. These cameras are most commonly employed during dynamic impact testing due to the high frame rates possible (up to 1 million frames per second; i-Speed 726, iX Cameras Ltd., Essex, UK). Nightingale *et al.* (1996) demonstrated that the cervical spine may transition between several complex poses during the first 6 ms following axial head-impact, each of which has the potential to cause traumatic injury. Therefore, it is important that the kinematics of the spine are adequately captured during this short period of time, although accurate quantification of these kinematics is limited by the accuracy of positional measurements derived from high-speed cameras.

High-speed video can also provide qualitative information about changes in spinal pose and progression of injury during traumatic loading (Maiman et al., 1983; Van Toen et al., 2014). In the first study to report high-speed video of CFD, embalmed PMHS with protective helmets were impacted with horizontally propelled masses and the features of cervical trauma were observed (Hodgson and Thomas, 1980). Resection of the lateral aspects of the specimens was

required to directly observe the motion of the vertebrae and facet joints, and it is likely that this altered the injury mechanics.

Intervertebral kinematics can be measured less-intrusively using high-speed video by tracking reflective markers attached to each vertebrae (Pintar et al., 1989; Pintar et al., 1995; Pintar et al., 1998), but this technique is limited by the relatively poor measurement accuracy and resolution of high-speed cameras. Measurement accuracy using high-speed cameras is influenced by the marker tracking and distance calibration method, out-of-plane motion (during 2D analysis), lighting, the distance of the camera(s) from the marker(s), the camera resolution, among other factors. The *measurement resolution* is inversely related to the field of view (FOV), where a larger FOV results in a larger pixel size and, therefore, lower measurement resolution. In the context of tracking spinal motion with an exceptional camera and assuming ideal conditions, a FOV of 180x135 mm, frame rate of 5000 frames per second, and camera resolution of 2048x1536 pixels, optimum measurement resolution would be approximately 0.09 mm. However, camera resolution is inversely related to frame rate (due to data storage and transfer limitations) so this measurement resolution would decrease substantially at higher frame rates for the same FOV.

In one series of experiments, high-speed cameras and lateral radiographs were used to develop “rigid body” kinematic models of FSUs to quantify facet joint kinematics and spinal canal occlusion during dynamic BFD (Ivancic et al., 2007, 2008; Panjabi et al., 2007). Rigid marker carriers were secured to the upper and lower mounts of an acceleration sled (Figure 1.10). Footage from two high-speed digital cameras were used to determine the 3D intervertebral translations and rotations of each FSU. Geometric relationships between anatomical landmarks and the markers were measured, both physically and from neutral lateral radiographs, to develop a 3D model of the FSU. This model was then superimposed onto the first frame of the recording. From this, dynamic translations of the vertebrae were calculated, and facet joint kinematics and canal occlusion were determined. Flexion, facet separation and anterior translation were the primary sagittal motions observed during dislocation. Significant non-sagittal motions also occurred, indicating that bilateral dislocation may be preceded by unilateral dislocation (Ivancic

et al., 2008; Panjabi et al., 2007). Peak canal occlusion was significantly greater than the occlusion observed post-trauma, suggesting that post-injury imaging may underestimate the maximum spinal cord compression experienced (Ivancic et al., 2007) – this result is consistent with other experimental investigations of traumatic spinal canal occlusion (Jones and Clarke, 2018). This methodology could be applied to any anatomy of the vertebra which cannot be tracked directly. However, it is anticipated that deflection of the facets and other posterior elements (relative to the vertebral bodies) may occur during traumatic dislocation which would violate the rigid body assumptions.

Cineradiography and fluoroscopy incorporate the techniques of cinematography and radiography to create a "video x-ray", allowing for direct visualization of cervical vertebral motion during mechanical testing. Bauze and Ardran (1978) and Nightingale *et al.* (1991) used lateral cineradiography and fluoroscopy, respectively, to qualitatively analyse vertebral kinematics during quasi-static axial compression loading that produced subaxial CFD in complete cervical spine specimens. However, the low frame-rates (4 Hz for cineradiography in 1978) and low image quality did not permit accurate quantitative kinematic analysis using these methods. High-speed cineradiography (1000 Hz) has been used to measure deformation of a radiodense surrogate spinal cord during dynamic cervical trauma (Saari et al., 2011), but accurate kinematic analysis of these images is unlikely due to the low camera resolution (256x240 pixels) and bone contrast.

1.5.2.2 Infrared motion-capture systems

Active motion tracking systems such as Optotrak (Northern Digital Inc., Canada) have been used to investigate the kinematics of subaxial cervical spine motion segments during low-velocity trauma (Van Toen et al., 2014) and to compare stability and mobility before and after experimental UFD (Crawford et al., 2002; Duggal et al., 2005; Nadeau et al., 2012; Riesenburger et al., 2012). In these studies, clusters of three or more infrared emitting markers are rigidly attached to each vertebra, usually by inserting a pin into the vertebral body. The location of each marker of each cluster is tracked during testing, from which translations and rotations of the

vertebrae can be calculated using rigid body kinematics principles. This information has been used to quantify range of motion (ROM) and neutral zone (NZ) before and after cervical trauma (Crawford et al., 2002; Nadeau et al., 2012; Riesenburger et al., 2012) and after spinal instrumentation (Duggal et al., 2005; Riesenburger et al., 2012), where ROM is the translation difference between peak applied moments, and NZ is the translation from the neutral position to the first instance of spinal resistance (White and Panjabi, 1990). These techniques have not been used to investigate 3D intervertebral motion *during* CFD.

In the lumbar spine, motion capture data has been combined with 3D models of spine segments (generated from high-resolution medical images) to derive the motion of anatomy that isn't directly observable due to superficial tissues, such as facet joint articulation (Cook and Cheng, 2010). The kinematic response to quasi-static loading of a lumbar spine segment (L1-L5) was recorded using infrared motion capture and the marker locations were registered with computer models generated from CT scans of the vertebrae. The contact area of each facet joint was then calculated throughout the ROM of the segment. This technique assumed that the vertebral body and posterior elements act as a rigid body; however, substantial bending of the lumbar facets (relative to the vertebral body) has been reported during physiological lumbar motion (Green et al., 1994) and it is likely that this would affect the facet apposition calculations. These techniques have not been applied to the cervical spine and do not consider deflection of the posterior elements that likely occurs during physiological and traumatic cervical motion.

Infrared motion capture systems are highly accurate and reliable (Maletsky et al., 2007), and provide a 'simple' method for measuring 3D spinal kinematics, but are limited by their maximum frame rate. The manufacturers of the Optotrak 3020 system (Northern Digital Inc., Ontario, Canada), which is commonly used in biomechanics laboratories, report root-mean-square in-plane and out-of-plane accuracies of 0.1 and 0.15 mm, respectively, and measurement precision of 0.01 mm; however, errors as low as 0.03 mm and 0.04° have been reported during reliability analysis of this system (Maletsky et al., 2007). The maximum frame rate is inversely related to the number of infrared markers included in the system, as each marker transmits a pulse

to the cameras during the acquisition cycle. For example, the Optotrak Certus system, when tracking two rigid bodies (6 markers, the minimum necessary to measure 3D intervertebral motion), has a maximum frame rate of approximately 630 Hz. This is substantially lower than the maximum capable by high-speed cameras and is likely inadequate to capture dynamic injury kinematics; however, these systems are capable of highly accurate kinematic measurements during quasi-static loading.

1.5.3 Intervertebral loads and displacements during CFD

The tolerance of the spine to traumatic injury can be described by the loads and displacements observed at the level of injury (Shea et al., 1991). Failure load is commonly reported as the forces and moments measured (usually via six-axis load cells) at the most inferior and/or superior vertebra of the tested spinal segment at the time of injury. During drop tests, head impact forces are also measured with load-cells positioned under the impact platform (Nightingale et al., 1996; Pintar et al., 1995; Saari et al., 2011). Loads at specific vertebral levels have been reported using an intervertebral load cell in the lumbar spine (Hakim and King, 1976; King et al., 1975), but a similar analysis has not been performed during experimentally produced CFD.

Previous studies that have measured the loads and displacements resulting in CFD are mostly limited to investigations of the gross biomechanical response of the cadaveric head-neck complex under dynamic axial loading (Nightingale et al., 1996; Pintar et al., 1995; Pintar et al., 1998), dynamic axial torsion (Myers et al., 1991), or quasi-static vertical loading (Bauze and Ardran, 1978; Hodgson and Thomas, 1980; Nightingale et al., 1991; Pintar et al., 1989). In general, these studies found that CFD-Fx occurs at lower *global* loads and with larger head-neck motions than other cervical trauma; however, these studies did not provide information about the *intervertebral* (local) load-displacement response at the level of injury.

The only study to report subaxial cervical intervertebral loads during the experimental production of BFD-Fx used inverse dynamics to estimate inter-facet loading during the injury

event (Ivancic et al., 2008). Intervertebral kinematic data, Newton-Euler equations, and force-moment data from a six-axis load cell positioned below the FSU were used to estimate inter-facet six-axis loads during inertially-produced BFD-Fx. An average peak axial compression force of 233.6 N preceded peak anterior shear force of 73.1 N, and flexion moment of 30.7 Nm. Intervertebral motion was also reported for these specimens – axial distraction, flexion, and anterior shear were observed during the injury event, followed significantly later by axial compression after locking of the facets occurred. A similar analysis is required for the injury vectors that cause BFD+Fx.

One study has reported the axial moments and rotations necessary to reliably produce UFD-Fx in nine subaxial cervical FSUs (one C4/C5, and eight C5/C6) (Crawford et al., 2002). The authors maintained a small lateral bending force (magnitude not specified) whilst applying 22.4±4.5° of axial rotation. This combined loading produced UFD-Fx at an average axial torque of 10.2±2.7 Nm. Similar load-displacement responses during UFD+Fx and BFD±Fx have not been reported.

The literature reviewed in this section demonstrates that there is a lack of information regarding the intervertebral loads and displacements that cause CFD, and specifically CFD+Fx. Mechanical testing of PMHS, full cervical spines, and subaxial cervical FSUs have shown that local anterior shear, flexion, compression, and distraction motions occur during subaxial CFD, but there exists little quantitative information regarding the tolerance of the subaxial cervical spine to these loads and displacements. Such information is crucial for developing improved neck injury criteria (see Section 1.5.5).

1.5.4 Mechanical behaviour of the facets during inter-facet loading

The facets are important loadbearing structures of the subaxial cervical spine, and inter-facet contact contributes to intervertebral kinematics observed in this region (Bogduk and Mercer, 2000). Furthermore, CFD often presents with associated facet fracture (Allen et al., 1982; Brady et al., 1999; Piccirilli et al., 2013; Shanmuganathan et al., 1994) suggesting high joint-reaction

forces through the facet during trauma (White and Panjabi, 1990). Despite this, quantitative measures of subaxial cervical facet stiffness, failure load, and fracture location during mechanical testing have not been reported. These are important parameters for validation of computational models of cervical trauma and may inform the design of advanced ATD necks and associated injury criteria. Kinematic measures of cervical vertebrae often assume that the vertebrae act as rigid bodies; however, bending of the facets may not be negligible during trauma (Green et al., 1994). Facet deflection has not been measured in the cervical region during sub-injurious loading, or during CFD.

The mechanical response of the *lumbar* posterior elements to simulated physiologic and traumatic loading scenarios has been reported, but the biomechanics of the cervical facets are understudied. The strain response of the cervical facet capsule during whiplash has been reported (Cholewicki et al., 1997; Panjabi et al., 1998b; Siegmund et al., 2008; Siegmund et al., 2001); however, limited strain data is available for the bony cervical facets. Strain gauges have been used to quantify surface strain of the articular facets during dynamic (Hodgson and Thomas, 1980) and quasi-static (Chang et al., 2007) loading of the cervical spine (Figure 1.13), but these studies did not investigate the loading directions associated with CFD.

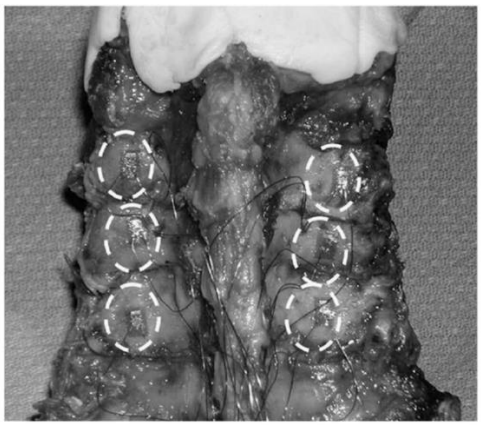

Figure 1.13: Strain gauges applied to the C5-C7 facet joints, indicated by white circles. Image adapted from Chang *et al.* (2007).[1]

The mechanical behaviour of the posterior elements of *lumbar* vertebrae has been quantified during loading of the inferior facets in defined, clinically-relevant directions, but this has not been investigated in the subaxial cervical spine. In the 1970s, Cyron *et al.* applied quasi-static loading to the inferior facets of isolated lumbar vertebrae using a materials testing machine (Figure 1.14a) and measured cyclic fatigue strength (1978) and fracture failure load (1976) of the neural arch. The vertebral bodies were fixed to a support apparatus that facets were loaded to simulate *in vivo* walking (Cyron and Hutton, 1978). Suezawa *et al.* (1980) instrumented the pedicles and pars interarticularis of isolated L5 vertebrae with 15 uniaxial strain gauges and applied forces to the bilateral articular facet surfaces at varying angles (Figure 1.14b). From this they determined the mode of loading that produced the largest strains in the pars interarticularis. A similar investigation is required to investigate the intervertebral loading directions that distinguish CFD-Fx from CFD+Fx.

[1] Image reprinted by permission from the JNS Publishing Group: Chang, U.K., *et al.*, 2007. *Changes in adjacent-level disc pressure and facet joint force after cervical arthroplasty compared with cervical discectomy and fusion*. Journal of Neurosurgery: Spine **7**(1), 33-39.

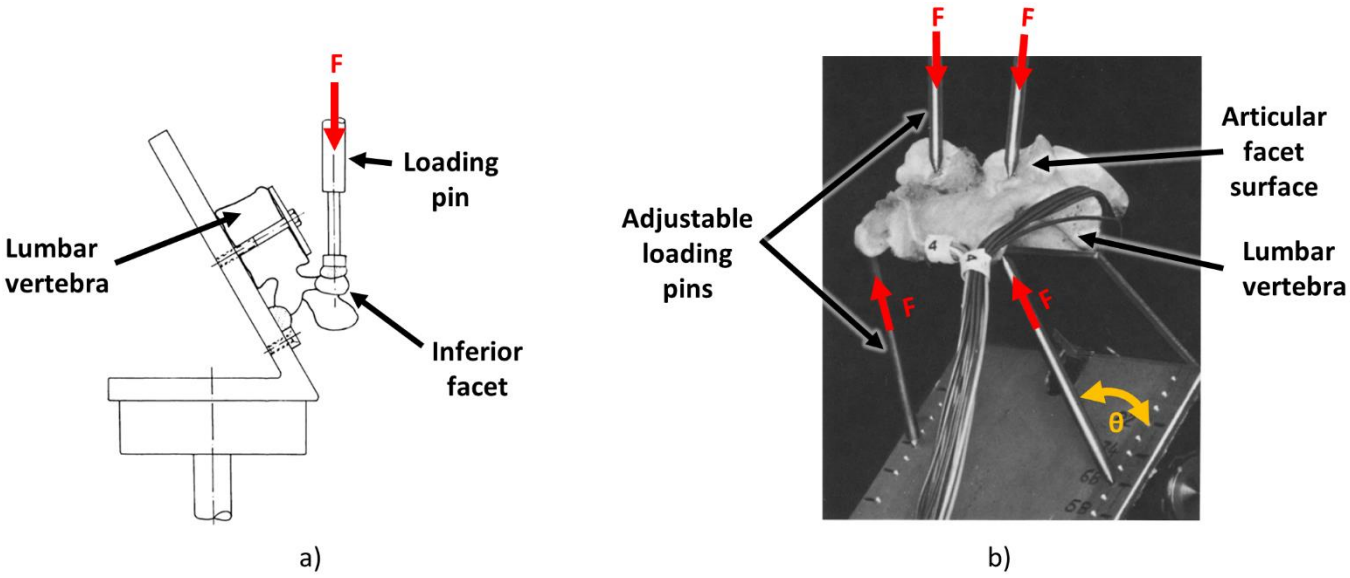

Figure 1.14: Measuring the mechanical response of isolated lumbar facets to simulated *in vivo* loading. F = applied force; θ = angle of applied force. Images adapted from: a) Cyron *et al. (1978; 1976)* and b) Suezawa *et al.* (1980).[1]

It is likely that the cervical facets and other posterior elements deflect (relative to the vertebral body) during traumatic and non-traumatic intervertebral motion, but this has not been investigated experimentally. During destructive loading of the *lumbar* facets, Cyron *et al.* reported linear displacement of the actuator/facets in excess of 12 mm, indicating substantial 'bending' of the posterior elements prior to failure (Cyron et al., 1976). Green *et al.* (1994) quantified sagittal bending of the inferior articular processes during physiological flexion and extension of lumbar FSUs, with and without a 2000 N imposed axial compression. Reflective markers were fixed to the vertebral bodies, the pars interarticularis, and the facet tips, and angular deflections of the posterior elements were measured using a two-dimensional motion-capture system; non-sagittal deflections were not measured. Sagittal deflections of the posterior elements (relative to the vertebral bodies) in excess of 14° were observed during simulated physiological intervertebral flexion (Green et al., 1994). One would expect that similar facet deflection to occur during physiological subaxial cervical intervertebral motion, and prior to CFD+Fx, which would invalidate the rigid-body assumptions of current models of cervical motion. Quantitative

[1] Image adapted by permission from Springer Nature: Suezawa, Y., *et al.*, 1980. *The mechanical response of the neural arch of the lumbosacral vertebra and its clinical significance*. International Orthopaedics **4**(3), 205-209.

information about deflection of the subaxial cervical facets relative to the vertebral body is required.

Other studies have estimated facet and neural arch load-bearing capacity during dynamic acceleration (Hakim and King, 1976; King et al., 1975) and compressive loading (Pollintine et al., 2004); however, these tests were conducted on lumbar spine segments and did not simulate facet dislocation. The *in* vivo flexion and extension bending resistance provided by the bilateral facet joints and capsular ligaments of 19 cervical FSUs (6×C2/C3, 2×C3/C4, 4×C5/C6, 7×C7/T1) was measured (Przybyla et al., 2007) – this study did not apply shear or non-sagittal bending motions, and did not measure the inter-facet contact forces. Lumbar facet contact force has been estimated using extra-articular strain measurements (Zhu et al., 2008) and from finite element analysis (Schmidt et al., 2009), and facet joint pressure has been measured directly (el-Bohy et al., 1989; Jaumard et al., 2011a; Jaumard et al., 2011b); however, these methods do not provide information about the direction or location of facet contact force, and were applied to the lumbar spine. Further investigation of the mechanical response of the cervical facets during loading is required. This data could be used to develop CFD+Fx risk curves for anthropomorphic test devices with instrumented posterior elements.

1.5.5 Anthropomorphic test devices and neck injury criteria

ATDs (or crash-test dummies) simulate the size, proportions and articulations of the human body and contain instrumentation to measure occupant ATD response to simulated motor vehicle collisions and biomechanical experiments. The Hybrid III ATD (Humanetics, USA) is often used to investigate neck injury resulting from MVA rollovers, frontal crashes and drop tests (Bahling et al., 1995; Herbst et al., 1998; Nyquist et al., 1980), and its response has been compared to cadavers via mechanical testing (McElhaney et al., 1988; Nightingale et al., 1991). The Hybrid III neck is rigidly attached to the torso and six-axis load cells can be fixed at the superior and inferior ends, while the head can be instrumented with up to 15 accelerometers (Humanetics Innovative Solutions, 2014). The measurements from these load cells and accelerometers during

simulated neck trauma are used to estimate the likelihood of neck injury for accident scenarios using neck injury criteria.

Injury criteria for the cervical spine, such as the neck injury criterion (N_{ij}), describe the association between physical parameters measured during simulated trauma and the occurrence of a resultant injury, using a mathematical relationship. To develop the N_{ij}, force and moment injury tolerances (Table 1.3) were derived from sagittal impact loading of porcine specimens and ATDs with airbags. The authors of this initial study stated that axial tension and extension moments at the upper neck load cell should be linearly combined to form an indicator of neck injury (Prasad and Daniel, 1984) (Equation 1.1). In Equation 1.1, 'i' refers to the axial injury mechanism (compression [C] or tension [T]) and 'j' indicates the sagittal bending injury mechanism (flexion [F] or extension [E]). F_Z and M_Y are the measured axial force and sagittal moment, respectively, and F_{int} and M_{int} are the critical force and moment values.

$$N_{ij} = \frac{F_Z}{F_{int}} + \frac{M_Y}{M_{int}} \qquad \textbf{Equation 1.1}$$

Similarly, peak tension and peak compression N_{ij} limits for the Hybrid III ATD (Table 1.3) were derived from simulated frontal-impact MVAs containing ATDs (Nyquist et al., 1980). This study attempted to "calibrate" the ATD to replicate specific injuries in well-defined traumatic environments and provide better interpretation of test results; however, these tests were limited to low-energy, frontal impact collisions and did not consider non-sagittal loading. A number of revisions of the N_{ij} criterion have been published, although it is still limited to loading in the sagittal plane (Eppinger et al., 2000).

Table 1.3: Summary of the limits and critical values for the 50th percentile male Hybrid III ATD (Eppinger et al., 2000; NHTSA, 2005).

Nij Criteria	Limit
Critical Intercept Values:	
Tension (N)	6806
Compression (N)	6160
Flexion (Nm)	310
Extension (Nm)	135
Peak Tension (N)	4170
Peak Compression (N)	4000

The results of the experimental work discussed in Section 1.5.1, particularly Nightingale *et al.* (1991), demonstrate that CFD can occur at peak axial loads that are substantially lower than the N_{ij} limits for the Hybrid III ATD, and that the relationship between a cadaver neck response to loading versus the ATD depends considerably on external loading factors (i.e. head constraints) – these factors are not considered when estimating injury risk using the N_{ij}. In addition, the *global* injury vector (measured at the cranial and/or caudal neck load cells of the Hybrid III) likely does not correspond with *intervertebral* or *local* injury vectors observed at the subaxial cervical spine, especially when first-order or higher-order buckling would occur in vivo. It is these intervertebral loads and motions that are indicative of injury risk. Finally, non-sagittal motions likely cause UFD yet these are not considered in the N_{ij}. In summary, a more biofidelic ATD neck with 'intervertebral' instrumentation and improved injury criteria are crucial to developing more effective injury prevention devices. Further research into the intervertebral injury mechanisms that lead to CDF±Fx is required, and this information may be used to inform better injury criteria.

1.6 Motivation, aims and hypotheses

The primary aim of this work is to improve understanding of the biomechanics underlying subaxial cervical facet dislocation and fracture-dislocation. This thesis addresses the following areas that are understudied in the current cervical spine trauma literature:

1) There have been no large-cohort investigations of cervical facet subluxation, dislocation, and fracture-dislocation injuries, and it is unknown which epidemiological or radiographic features of these injuries are predictive of SCI. Such an investigation will

elucidate the causative factors of CFD±Fx (in the Australian context), and may assist with associating global and local injury mechanisms with injury severity;

2) The mechanical response of the subaxial cervical facets during intervertebral motion is understudied. In particular, there exists no published data regarding the effect of superimposed intervertebral axial compression and distraction (intervertebral separation) on the mechanical response of the facets during intervertebral shear, bending, and rotation motions. An improved fundamental understanding of how the facets respond to loading may elucidate the injury mechanisms that differentiate CFD-Fx from CFD+Fx. This information is necessary to validate computational and experimental models of cervical trauma, and may lead to design of better ATD necks and improved neck injury criteria;
3) A method to reliably produce BFD+Fx in *ex vivo* cervical spines in the laboratory has not previously been developed, and the role of constrained anterior shear during the injury event has not been reported. A substantial anterior shear component of the local injury vector has been proposed as a likely cause of concomitant facet fracture during BFD, but this has not been investigated experimentally;
4) The effect of imposed compression and distraction on the mechanical response of the facets during supraphysiologic anterior shear (leading to BFD) has not been reported. Local compression *and* distraction forces at the level of injury have been reported during experimentally produced CFD in whole cervical spines, and the direction of this imposed intervertebral axial force may dictate the occurrence of concomitant facet fracture.

Four studies were undertaken to address the gaps identified in the literature. The aims and hypotheses of these studies are provided below.

1.6.1 Study 1 (Chapter 2)

The aim of Study 1 was to describe the epidemiology and radiographic features of subaxial cervical facet subluxation, dislocation, and fracture-dislocation cases (DFIs) admitted to a single institution over a decade, and to identify which of these parameters were associated with SCI. Current literature pertaining to DFIs is limited to small-cohort reports of the radiographic features or clinical outcomes of treatment methods. It was anticipated that this large-cohort review would provide important information about the injury mechanisms most commonly associated with CFD±Fx, and would have sufficient statistical power to identify which of these variables are risk factors for SCI. Furthermore, observer agreement and repeatability of the proposed quantitative radiographic measures of subaxial spine trauma in the context of DFI were reported for the first time.

Hypothesis: No hypotheses were proposed for this study due to its exploratory nature.

1.6.2 Study 2 (Chapter 3)

The aim of Study 2 was to measure the biomechanical response of cadaveric subaxial cervical inferior facets to loading that simulated traumatic in vivo intervertebral compressive-flexion and anterior shear motions. These motions are thought to occur during BFD±Fx, but the associated inter-facet loading that is most likely to cause concomitant facet fracture had not previously been investigated. A novel method of quantifying the mechanical response of isolated subaxial cervical inferior facets when loaded non-destructively and to failure in these directions, and the results of these tests, are presented in Chapter 3.

Hypothesis: The biomechanical response of the subaxial cervical inferior facets will differ between the simulated *in vivo* intervertebral compressive-flexion and anterior shear loading directions.

1.6.3 Study 3 (Chapter 4)

The aim of Study 3 was to measure the biomechanical response of the C6 inferior facets when intervertebral axial compression and distraction were superimposed on non-destructive

shear, bending, and rotation motions of C6/C7 FSUs. The subaxial cervical facets are important structures during spinal kinematics and load-bearing, but the *in vivo* biomechanical response of the facets during intervertebral motion has not been measured. This response may differ when intervertebral axial compression (due to neck muscle activation) or distraction (due to head inertia or eccentric head contact) is superimposed on these motions. The results of this investigation are reported in Chapter 4.

Hypothesis: Intervertebral axial compression will increase loading of the C6 inferior facets (when compared to axial distraction, and as measured by deflection and surface strain) when superimposed on non-destructive anterior shear, axial rotation, flexion, and lateral bending motions.

1.6.4 Study 4 (Chapter 5)

The aim of Study 4 was to develop a methodology to reliably apply 20 mm of constrained, destructive anterior shear motion to C6/C7 FSUs, with imposed intervertebral axial compression or distraction, and to quantify the biomechanical response of the FSU, and particularly the C6 inferior facets, to this combined loading scenario. Intervertebral anterior shear motions occur during the experimental production of BFD, yet the role of this loading direction during cervical trauma has not been thoroughly investigated. Superimposing axial compression or distraction on traumatic anterior shear motion may dictate the occurrence of concomitant facet fracture. Chapter 5 describes an iterative approach to developing this testing methodology and reports preliminary data regarding the mechanical response of the facets during these tests.

Hypothesis: Intervertebral axial compression will increase failure loads, and loading of the C6 inferior facets (when compared to axial distraction, and as measured by deflection and surface strain), and will produce CFD+Fx when superimposed on 20 mm of constrained anterior shear motion.

Statement of Authorship – Chapter 2

Title of Paper	Traumatic subaxial cervical facet subluxation and dislocation: Epidemiology, radiographic analyses, and risk factors for spinal cord injury
Publication Status	☑ Published ☐ Accepted for Publication ☐ Submitted for Publication ☐ Unpublished and Unsubmitted work written in manuscript style
Publication Details	Quarrington, R.D., Jones, C.F., Tcherveniakov, P., Clark, J.M., Sandler, S.J.I., Lee, Y.C., Torabiardakani, S., Costi, J.J., Freeman, B.J.C., 2018. Traumatic subaxial cervical facet subluxation and dislocation: epidemiology, radiographic analyses, and risk factors for spinal cord injury. The Spine Journal 18, 387-398.

Principal Author

Name of Principal Author (Candidate)	Ryan Quarrington		
Contribution to the Paper	Performed all data analysis, interpreted data, wrote manuscript and acted as corresponding author.		
Overall percentage (%)	70%		
Certification:	This paper reports on original research I conducted during the period of my Higher Degree by Research candidature and is not subject to any obligations or contractual agreements with a third party that would constrain its inclusion in this thesis. I am the primary author of this paper.		
Signature		Date	01/06/2018

Co-Author Contributions

By signing the Statement of Authorship, each author certifies that:

i. the candidate's stated contribution to the publication is accurate (as detailed above);

ii. permission is granted for the candidate in include the publication in the thesis; and

iii. the sum of all co-author contributions is equal to 100% less the candidate's stated contribution.

Name of Co-Author	Claire Jones		
Contribution to the Paper	Supervised study design and development of work, assisted with data collection and interpretation, and reviewed manuscript.		
Signature		Date	05/06/18

Name of Co-Author	Petar Tcherveniakov		
Contribution to the Paper	Assisted with data collection and reviewed manuscript.		
Signature		Date	14/06/18

Name of Co-Author	Jillian Clark		
Contribution to the Paper	Assisted with data collection and reviewed manuscript.		
Signature		Date	18/09/2018

Name of Co-Author	Simon Sandler		
Contribution to the Paper	Performed radiographic analysis and reviewed manuscript.		
Signature		Date	17/09/2018

Name of Co-Author	Yu Chao Lee		
Contribution to the Paper	Performed radiographic analysis and reviewed manuscript.		
Signature		Date	06/06/2018

Name of Co-Author	Shabnam Torabiardakani		
Contribution to the Paper	Assisted with data collection and reviewed manuscript.		
Signature		Date	17/06/2018

Name of Co-Author	John Costi		
Contribution to the Paper	Supervised development of work and reviewed manuscript.		
Signature		Date	14/06/2018

Name of Co-Author	Brain Freeman		
Contribution to the Paper	Supervised development of work, assisted with data interpretation, and reviewed manuscript.		
Signature		Date	14/06/2018

Chapter 2 Traumatic subaxial cervical facet subluxation and dislocation: Epidemiology, radiographic analyses, and risk factors for spinal cord injury[1]

2.1 Introduction

Subaxial cervical spinal cord injury (SCI) is one of the most devastating injuries in medicine (Wiseman et al., 2003). In Australia, 50% of traumatic SCIs reported in a 2008 cohort resulted in 136 cases of tetraplegia, amounting to annual personal care costs of approximately AUD$14.6 million (Access Economics Pty Limited, 2009). In cases of subaxial cervical trauma, patients with facet dislocation present with the most severe neurological deficit (Wilson et al., 2013), resulting in tetraplegia in up to 87% of cases (Hadley et al., 1992; Lintner et al., 1993; O'Brien et al., 1982; Payer and Schmidt, 2005; Wolf et al., 1991). Rapid reduction is crucial, particularly in patients with bilateral facet dislocation and significant neurological deterioration (Wilson et al., 2013). Despite potentially devastating consequences, the spectrum of traumatic subaxial cervical facet subluxation and dislocation — herein termed Distractive Flexion Injuries [DFIs], as described by Allen and Ferguson (1982) — is significantly understudied.

Allen and Ferguson describe four radiological stages of DFI: Stage 1 flexion sprain, Stage 2 unilateral facet dislocation; Stage 3 bilateral facet dislocation with up to 50% translation; and, Stage 4 bilateral facet dislocation with up to 100% translation (Allen et al., 1982). Complete neurologic injury occurs more frequently following bilateral facet dislocation (Allen et al., 1982), but by no means is this certain. Newton *et al.* advocates reduction of cervical facet dislocation within four hours of injury to prevent permanent neurological damage following low velocity trauma (Newton et al., 2011). Whilst there is no consensus on the optimal surgical management of low or high velocity trauma (Arnold et al., 2009; Duggal et al., 2005; Harrington and Park, 2007; Henriques et al., 2004; Kwon et al., 2007; Nassr et al., 2008; Piccirilli et al., 2013; Ramnarain and Govender, 2008; Razack et al., 2000; Wiseman et al., 2003), in the case of SCI

[1] A version of Chapter 2 was published in The Spine Journal: Quarrington, R.D., Jones, C.F., Tcherveniakov, P., Clark, J.M., Sandler, S.J.I., Lee, Y.C., Torabiardakani, S., Costi, J.J., Freeman, B.J.C., 2018, **18**(3), 387-398. *Traumatic subaxial cervical facet subluxation and dislocation: epidemiology, radiographic analyses, and risk factors for spinal cord injury*.

prompt assessment and early intervention is crucial to optimise patient outcome (Hadley, 2002; Hadley et al., 1992; Lee et al., 1994; Newton et al., 2011).

The literature pertaining to DFI comprises only small cohort studies reporting radiographic features (Allen et al., 1982; Argenson et al., 1988; Doran et al., 1993; Lintner et al., 1993; Scher, 1977; Shanmuganathan et al., 1994; Vaccaro et al., 1999; Vaccaro et al., 2001), or the clinical outcomes of surgical or non-surgical treatment methods (Cotler et al., 1990; Dvorak et al., 2007; Eranki et al., 2016; Grant et al., 1999; Hadley et al., 1992; Key, 1975; Piccirilli et al., 2013; Rorabeck et al., 1987; Savini et al., 1987; Wilson et al., 2013). Notably, there have been no large-scale cohort investigations of DFI, with or without concomitant neurological deterioration, reported. In relation to clinical assessment, the neurological examination of patients with subaxial cervical injury is often difficult, as patients commonly present with reduced levels of consciousness (Hasler et al., 2012; Hills and Deane, 1993). Therefore, it is important to establish potential associations between injury epidemiology and radiographic features, and neurological involvement. Furthermore, although qualitative radiographic analysis of cervical vertebral alignment is routinely used to provide an indication of injury severity, it is not known which (if any) of the proposed quantitative radiographic measures of subaxial spine trauma (Bono et al., 2006) are predictive of neurological deficit. The inter-observer agreement and intra-observer repeatability of quantitative radiographic measures has not been reported for DFI.

The primary aims of this study were to describe the epidemiology and radiographic features of DFI in patients presenting to a major Australian tertiary hospital over a decade, and to identify which of these variables are risk factors for SCI. A secondary aim was to investigate the agreement and repeatability of several quantitative radiographic measurements of subaxial cervical trauma severity in the context of DFI.

2.2 Methods

Ethics approval was granted for this study. All patients aged 15 years and over who were admitted to the institution with traumatic subaxial cervical facet dislocation or subluxation

between January 2003 and December 2013 were identified. Reviews of hard-copy and electronic medical records were performed and the following patient demographic and injury characteristics extracted: age at admission, gender, spinal column injury characteristics (dislocation or subluxation, uni- or bilateral, spinal level of bony injury [LOBI] and incidence of associated facet fracture), injury causation information (motor vehicle speed, fall height etc.), and the presence of SCI (determined by the American Spinal Injury Association Impairment Scale [ASIA AIS] or the International Standards for Neurological Classification of Spinal Cord Injury [ISNCSCI] charts, or the documented neurological status recorded in the medical records). DFI type (dislocation or subluxation) was categorised from inspection of medical images and/or description in the medical records. As suggested in Bono *et al*. (2006), facet dislocation (uni- or bilateral, including perched facets) was defined as "no articular surface apposition" while subluxation described a reduction in apposition, when compared to normal alignment, *without* facet dislocation.

All available medical images (radiographs, computed tomography [CT] and magnetic resonance imaging [MRI]) acquired within 24 hours of admission to the Spinal Injuries Unit were retrieved in DICOM format using eFilm Workstation version 1.5.3 (Merge Healthcare, Illinois, USA). Radiographic measures of injury severity (Bono et al., 2006) were performed by two consultant spinal surgeons using a custom MATLAB (Mathworks, Massachusetts, USA) program, as documented in Table 2.1 and illustrated in Figure 2.1 and Figure 2.2. The medical image analysis program is described in detail in Appendix A. Several weeks following the initial analysis, each observer repeated the process on images from a subset of 29 patients (11% of the cohort) to investigate intra-observer repeatability (Bartlett and Frost, 2008). This subset comprised those patients with complete medical imaging (X-ray, CT and MRI) and their demographics matched the study population, but with a higher proportion of dislocation injuries (75.8% vs. 56.2%).

Table 2.1: Radiographic analysis anatomical landmarks and measurements.

Measurements	Imaging Modality and Orientation	Landmarks
Vertebral translation Cobb angle Posterior tangent angle	Lateral X-ray and midsagittal CT slice, re-orientated into anatomical alignment (if required) and cropped to the subaxial spine	Four corners of adjacent subaxial vertebrae at the LOBI
Spinal canal occlusion	Midsagittal CT (as described above)	Anterior and posterior edges of spinal canal at the LOBI and the nearest superior and inferior uninjured levels
Left/right facet apposition*	Left and right parasagittal CT slices through the mid-line of the facet at the LOBI	Anterior and posterior ends of opposing articular facet surfaces
Spinal cord compression	Midsagittal MRI slice, cropped to the subaxial spine	Anterior and posterior edges of spinal cord at the LOBI and the nearest superior and inferior uninjured levels

LOBI, level of bony injury; CT, computed tomography; MRI, magnetic resonance imaging.
** Absolute facet apposition at the LOBI was defined as the mean of left and right facet apposition.*

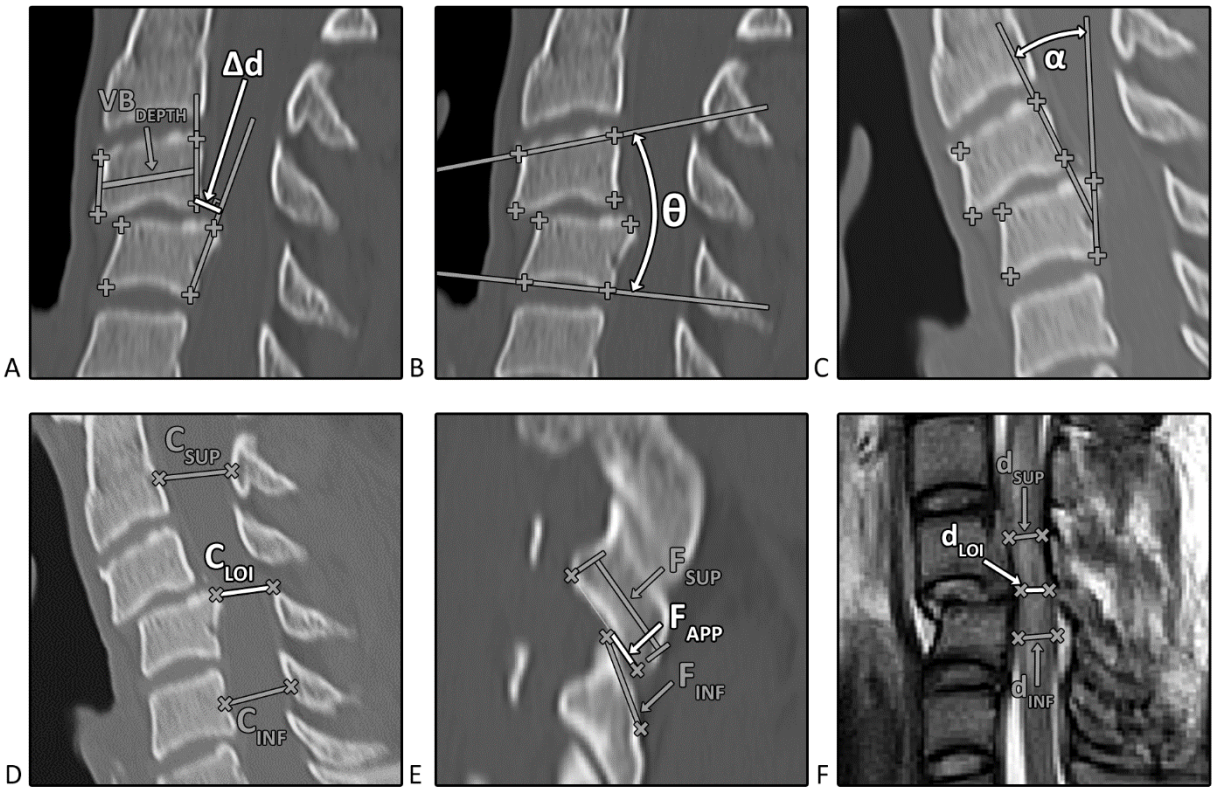

Figure 2.1: Representative diagrams of the radiographic measurements described in Table 1, where black crosses indicate the anatomical landmarks used to calculate each measure: a) Vertebral Translation (% of superior vertebral body depth) = $\frac{\Delta d}{VB_{depth}} \times 100$; b) Cobb Angle (degrees) = θ; c) Posterior Tangent Angle (degrees) = α; d) Spinal Canal Occlusion (% of 'normal' canal depth) = $\frac{C_{LOI}}{(C_{SUP}+C_{INF})\div 2} \times 100$; e) Facet Apposition (% of superior facet surface length) = $\frac{F_{APP}}{F_{SUP}} \times 100$, where FAPP is the length of the overlap of FSUP and FINF; and, f) Spinal Cord Compression (% of 'normal' cord diameter) = $\frac{d_{LOI}}{(d_{SUP}+d_{INF})\div 2} \times 100$.

Statistical analyses were performed using SPSS v22 (IBM, Illinois, USA). Descriptive statistics were applied to epidemiological data. Mann-Whitney U tests and Fisher's exact test of independence analyses ($\alpha = 0.05$) were used to compare continuous and categorical variables, respectively, between SCI and non-SCI populations. Inter-observer agreement and intra-observer repeatability for radiographic measurements were evaluated using Bland-Altman (B-A) plots and intra-class correlation coefficients (ICC) (Bartlett and Frost, 2008; Bland and Altman, 1986, 2003); absolute agreement and consistency ICC measures were obtained. ICC values were interpreted as follows: >0.8 (almost perfect agreement); 0.61-0.8 (substantial agreement); 0.41-0.6 (moderate agreement); 0.21-0.4 (fair agreement); and, 0-0.2 (slight agreement) (Landis and Koch, 1977).

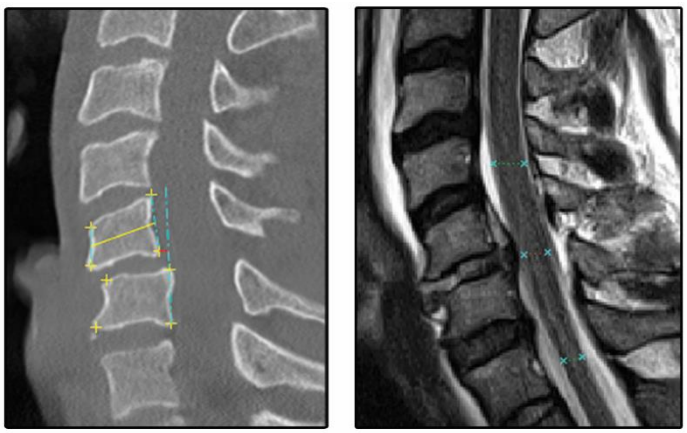

Figure 2.2: Forty-one year old male sustained a C5/C6 unilateral facet fracture-dislocation (DFI Stage 2) without neurological deficit following a motor vehicle accident. Mid-sagittal computed tomography (CT) scans (left) demonstrated 13% vertebral translation at C5/C6. No signal change, and 8% spinal cord compression were identified on T2-weighted magnetic resonance imaging (right).

Where patients had both CT and X-ray images, B-A plots were used to investigate whether measurements from the two modalities were equivalent, and could therefore be assigned to a single variable.

Binary logistic regression models were developed to identify risk factors for SCI. Seven subgroup regression models were developed that included only those patients with complete data for the predictor variables of interest. Two models analysed causation: (1) high-velocity motor vehicle accidents (MVAs), and (2) low velocity falls, respectively. A further five models analysed the radiographic measurements predictive of SCI for (3) MRI and CT; (4) MRI; (5) CT; (6) X-ray and/or CT; and, (7) X-ray.

Each subgroup model was developed as follows. Firstly, univariate modelling (SCI vs. non-SCI) was conducted on each independent variable, and those with $p<0.25$ were included in the initial multivariable regression model (Table 2.9). To avoid complete separation, related classes of categorical variables were combined to eliminate zero cells if they occurred in the contingency table. The multivariate model was then refined using a backward elimination approach (Hosmer and Lemeshow, 2000); the Aikaike information criterion (AIC) assessed model fit at each iterative step. Model refinement was repeated until only significant ($p<0.05$) predictors remained, or the AIC increased by >5 points from the initial or preceding model.

Clinically-plausible two-way main effect interaction variables were sequentially added to the main effects model. The statistical significance of each addition was assessed using a likelihood ratio test, and the term was included in the final model if significant ($p<0.05$).

The Hosmer-Lemeshow goodness-of-fit test assessed the fit of the final model; $p>0.05$ indicated that the fitted model was significantly different from null model. Area Under the Receiver Operating Characteristic (AUROC) curves evaluated the discriminatory power of the model (AUROC>0.5; $\alpha = 0.05$) (Hosmer and Lemeshow, 2000).

2.3 Results

2.3.1 Demographic analyses

Table 2.2 presents the demographic characteristics of the 226 patients admitted with DFI. Facet dislocation (56.2%) was observed more frequently than subluxation, 56.3% of DFIs were bilateral (equivalent to Allen and Ferguson DFI Stage 3 or 4) and concomitant facet fracture was detected in 57.4%.

Table 2.2: Demographics and injury variables distributed by neurologic condition.

Variable	Total (n=226)	SCI (n=75)	Non-SCI (n=150)	p-Value
Age				
Range (years)	16-93	18-88	16-93	
Median (IQR) (years)	40.0 (25.0-59.0)	37.0 (24.0-60.0)	41.5 (30.0-59.0)	0.186
<65 years old	176 (77.9%)	58 (77.3%)	117 (78.0%)	
Gender, n (%)				0.432
Male	163 (72.1%)	57 (76.0%)	106 (70.7%)	
Female	62 (27.6%)	18 (24.0%)	44 (29.3%)	
Injury type, n (%)				<0.001
Dislocation	127 (56.2%)	55 (73.3%)	72 (48.0%)	
Subluxation	99 (43.8%)	20 (26.7%)	78 (52.0%)	
Bilateral/unilateral,* n (%)				<0.001
Bilateral	125 (56.3%)	55 (74.3%)	70 (47.6%)	
Unilateral†	97 (43.7%)	19 (25.7%)	77 (52.4%)	
Spinal level of injury				0.184
C3/C4	22 (9.7%)	7 (9.3%)	15 (10.0%)	
C4/C5	45 (19.9%)	15 (20.0%)	30 (20.0%)	
C5/C6	58 (25.7%)	18 (24.0%)	40 (26.7%)	
C6/C7	87 (38.5%)	34 (45.3%)	52 (34.7%)	
C7/T1	14 (6.2%)	1 (1.3%)	13 (8.7%)	
Associated facet fracture,∨ n (%)	128 (57.4%)	42 (56.0%)	85 (57.4%)	1.000
Glasgow Coma Scale				<0.001
Median (IQR)	15 (15-15)	15 (13-15)	15 (15-15)	

L, left; R, right; NS, not specified; SCI, spinal cord injury; IQR, interquartile range.
** Data not available for 4 patients.*
† Total: 44 L, 46 R, 6 NS; SCI: 6 L, 12 R, 1 NS; Non-SCI: 38 L, 34 R, 5 NS.
∨ *Data not available for 3 patients.*

After the exclusion of one ambiguous case, 75 (33.2%) patients were identified who had sustained SCI. For those patients with neurological deficits, 16 manual ISNCSCI worksheets that had been completed prior to intervention were extracted (16/75 = 21.3%). Of these 81.3% were ASIA AIS A or B classifications, and the remainder were ASIA AIS C (6.3%), or D (12.5%) (Kirshblum et al., 2011). The SCI population had similar demographics to the cohort from which it was drawn (Table 2.2). Facet dislocation and bilateral facet injury were significantly associated with SCI (both $p<0.001$), as was reduced GCS ($p<0.001$) (see Table 2.2). C6/C7 was the most common level of subaxial cervical injury with neurological deficit (45.3%), followed by C5/C6 (24.0%), collectively representing 69.3% of such cases.

There was an equal number of bilateral and unilateral dislocations (62 cases each, Table 2.3). Bilateral dislocations had a substantially higher proportion of associated SCI (61.3%) than unilateral dislocations (27.0%), bilateral subluxations (27.0%), or unilateral subluxations (8.8%). The highest proportion of facet fractures were associated with unilateral subluxations (65.7%)

and dislocations (64.5%), while over 58% of bilateral dislocations had concomitant fracture (Table 2.3).

Table 2.3: Combined injury details.

Combined injury type	Total* (n=222)	SCI†		Facet fracture˅	
		Yes (n=75)	No (n=150)	Yes (n=128)	No (n=95)
Bilateral dislocation	62	38 (61.3%)	24 (38.7%)	36 (58.1%)	26 (41.9%)
Unilateral dislocation	62	17 (27.0%)	46 (73.0%)	40 (64.5%)	22 (35.5%)
Bilateral subluxation	63	17 (27.0%)	46 (73.0%)	28 (44.4%)	35 (55.6%)
Unilateral subluxation	35	3 (8.8%)	31 (91.2%)	23 (65.7%)	12 (34.3%)

**data not available for 4 patients; †data not available for 5 patients; ˅data not available for 4 patients.*

Motor vehicle collisions (MVCs), including motor vehicle/motorcycle accidents and pedestrian injury, were the most common cause of DFI (59.3%), followed by falls (25.7%) (Table 2.4). A shift in predominant injury causation from MVCs (high velocity) in younger persons (<65 years old) to falls (low velocity) in the elderly was observed (Figure 2.3). Rollovers (51.8%) were the most common motor vehicle accident, and most MVAs occurred at high speed (63.6%). Falls were most often from heights of less than two metres (70.7%) (Table 2.4).

Table 2.4: Causal variables distributed by neurologic condition.

	Total (n=226)*	SCI (n=75)	Non-SCI (n=150)	p-Value
Injury cause, n (%)				0.307
MVC	134 (59.3%)	47 (62.7%)	86 (57.3%)	
Fall	58 (25.7%)	15 (20.0%)	43 (28.7%)	
Sporting/cycling accident	17 (7.5%)	6 (8.0%)	11 (7.3%)	
Diving	9 (4.0%)	2 (2.7%)	7 (4.7%)	
Assault	4 (1.8%)	2 (2.7%)	2 (1.3%)	
Other	4 (1.8%)	3 (4.0%)	1 (0.7%)	
MVA details, n (%)				0.326
"Pure" rollover	57 (51.8%)	17 (70.8%)	40 (78.4%)	
Frontal impact	11 (10%)	6 (25.0%)	5 (9.8%)	
Side impact	5 (4.6%)	1 (4.2%)	4 (7.8%)	
Rear impact	2 (1.8%)	0 (0.0%)	2 (3.9%)	
Unknown	35 (31.8%)	-	-	
MVA vehicle speed, n (%)				1.00
Low (≤60 km/h)	16 (14.5%)	5 (18.5%)	11 (18.6%)	
High (>60 km/h)	70 (63.6%)	22 (81.5%)	48 (81.4%)	
Unknown	24 (21.8%)	-	-	
MVA seat position, n (%)				1.00
Driver	68 (61.8%)	23 (63.9%)	44 (65.7%)	
Front seat passenger	17 (15.5%)	6 (16.7%)	11 (16.4%)	
Back seat passenger	19 (17.3%)	7 (19.4%)	12 (17.9%)	
Unknown	6 (5.5%)	-	-	
Seatbelt, n (%)				0.610
Worn	59 (53.6%)	23 (76.7%)	35 (70.0%)	
Not worn	22 (20.0%)	7 (23.3%)	15 (30.0%)	
Unknown	30 (27.3%)	-	-	
Airbag, n (%)				0.262
Deployed	4 (3.6%)	3 (42.9%)	1 (11.1%)	
Not deployed	12 (10.9%)	4 (57.1%)	8 (88.9%)	
Unknown	94 (85.5%)	-	-	
Fall height, n (%)				0.459
<2 metres	41 (70.7%)	9 (69.2%)	32 (80.0%)	
≥2 metres	12 (20.7%)	4 (30.8%)	8 (20.0%)	
Unknown	5 (8.6%)	-	-	

SCI, spinal cord injury; MVA, motor-vehicle accident; MVC, motor-vehicle collision.
** One ambiguous case of neurological deficit was excluded leaving 75 patients with SCI and 150 without SCI.*

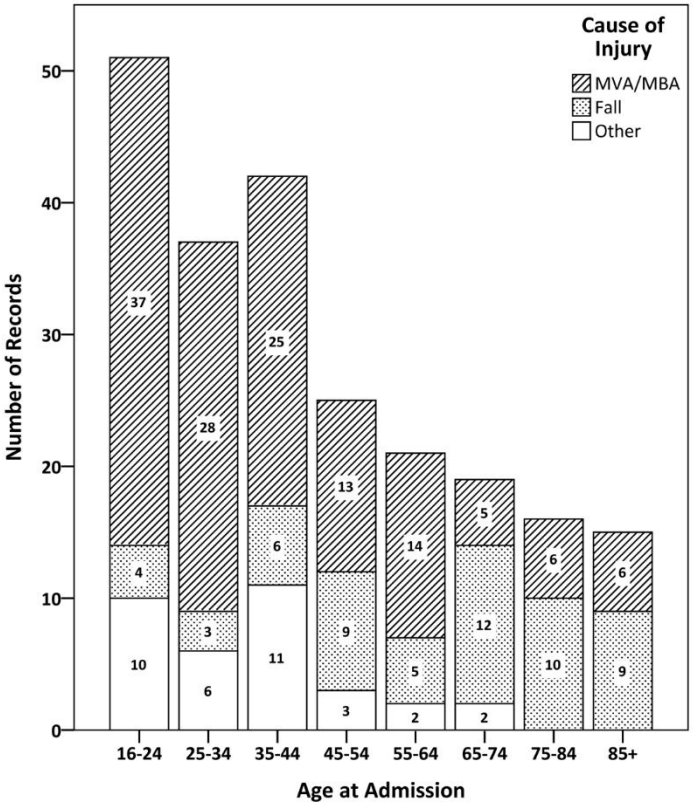

Figure 2.3: Causal variables distributed by admission age. A shift in predominant causality from motor vehicle/motorbike accidents (MVA/MBA) in young adults (<65 years old), to falls in older adults, was observed.

2.3.2 Radiographic analyses

SCI patients had increased spinal canal occlusion (p<0.001) and increased spinal cord compression (p=0.008) (Table 2.5). Mean facet apposition was lower for the SCI (p=0.031) and dislocation (p<0.001) cohorts. Mean vertebral translation was higher (p<0.001) and mean Cobb Angle and Posterior Tangent Angle (PTA) values demonstrated greater flexion (p=0.008; p=0.004, respectively) for those with facet dislocations (Table 2.5). In contrast with the significant negative associations found for facet apposition, other DFI parameters examined did not associate with neurological deficit. Median anterior vertebral translations of 36% and 20% were observed for bilateral and unilateral dislocations, respectively (Table 2.6).

Table 2.5: Radiographic indices distributed by neurologic condition and injury type.

Radiographic indices (median (IQR))	Total	Neurological condition			Injury type		
		SCI	Non-SCI	p-Value	Dislocation	Subluxation	p-Value
Vertebral translation (%)*	13.0 (0.0-34.4)	16.2 (-12.1-57.6)	12.2 (2.3-26.4)	0.646	23.0 (8.3-47.0)	5.1 (-3.6-15.5)	<0.001
Cobb angle (deg)†	-5.2 (-12.3-0.4)	-2.7 (-10.8-0.8)	-6.0 (-13.9- -0.1)	0.174	-7.4 (-15.9- -1.3)	-2.9 (-10.1-3.5)	0.008
PTA(deg)†	-4.2 (-15.7-6.1)	-5.7 (-20.3-6.7)	-4.2 (-14.4-5.7)	0.823	-7.5 (-20.4-2.7)	0.4 (-9.5-10.8)	0.004
Spinal canal occlusion (%)	5.2 (-0.8-14.3)	12.3 (4.4-30.8)	2.0 (-4.2-8.8)	<0.001	5.7 (0.2-16.1)	3.1 (-2.0-11.2)	0.171
Mean facet apposition (%)	56.7 (33.1-76.9)	40.8 (18.8-75.1)	63.5 (37.9-76.7)	0.031	37.9 (20.9-63.8)	74.2 (53.1-84.3)	<0.001
Spinal cord compression (%)	16.9 (8.5-29.5)	22.1 (12.4-44.2)	14.2 (6.8-24.9)	0.008	19.8 (8.4-37.0)	13.2 (7.8-20.7)	0.030

IQR, interquartile range; PTA, posterior tangent angle.
** Positive values indicate anterior translation.*
† Negative values indicate anterior flexion.

Table 2.6: Radiographic measurements for combined injury details.

Measurement variable (median (IQR))	Bilateral dislocation	Unilateral dislocation	Bilateral subluxation	Unilateral subluxation
Vertebral translation (%)	36.0 (-2.7-64.7)	20.0 (10.8-34.9)	6.6 (-4.2-17.3)	1.5 (-3.6-15.1)
Cobb angle (deg)	-7.2 (-14.6-0.8)	-7.5 (-17.4- -7.4)	-2.9 (-10.2-3.7)	-2.8 (-9.3-0.9)
PTA (deg)	-7.2 (-24.5-3.5)	-7.7 (-16.1-1.3)	-1.6 (-15.3-10.7)	3.1 (-4.2-12.4)
Canal occlusion (%)	10.8 (4.2-25.2)	4.6 (-1.0-10.4)	6.1 (-1.1-15.4)	0.8 (-2.7-5.7)
Mean facet apposition (%)	34.9 (1.1-62.8)	43.1 (25.8-64.6)	72.6 (48.1-82.1)	74.2 (59.9-85.7)
Spinal cord compression (%)	25.7 (8.4-50.3)	19.5 (7.9-26.9)	12.8 (8.9-18.7)	17.1 (-0.1-29.4)

IQR, interquartile range; PTA, posterior tangent angle.

Inter-observer agreement and consistency, and intra-observer repeatability, were "moderate" or better (ICC>0.4) for all radiographic measurements, with most demonstrating "almost perfect" reproducibility (Table 2.7 and Table 2.8). Spinal canal occlusion and spinal cord compression demonstrated the lowest levels of inter-observer consistency (ICC = 0.529 and 0.635, respectively) and agreement (ICC = 0.503 and 0.489, respectively) and were the least repeatable for both observers (Observer 1 ICC: 0.788 and 0.677, respectively; Observer 2 ICC: 0.569 and 0.645, respectively). B-A analyses demonstrated adequate agreement and repeatability for all measurements, and no rater or measurement bias was observed (Bland and Altman, 1986, 2003) (Figure 2.4, Figure 2.5, and Figure 2.6 in Section 2.5). B-A analysis also indicated acceptable agreement between corresponding X-ray and CT radiographic measurements of vertebral translation (Figure 2.7 in Section 2.5). Therefore, all measurements were averaged over the two observers and single vertebral translation, Cobb angle and posterior tangent angle values

were assigned for patients who only had one of X-ray or CT images available; where both imaging modalities were available, values from the earliest acquired image were used.

Table 2.7: Intra-observer repeatability of radiographic indices.

Radiographic measure	Observer 1 repeatability	Observer 2 repeatability
CT – Cobb angle	0.914 (0.820-0.960)	0.927 (0.846-0.967)
CT – PTA	0.897 (0.785-0.952)	0.834 (0.666-0.921)
CT – Vertebral translation	0.917 (0.825-0.962)	0.956 (0.906-0.980)
X-ray – Cobb angle	0.856 (0.684-0.939)	0.789 (0.555-0.908)
X-ray – PTA	0.834 (0.641-0.929)	0.749 (0.484-0.889)
X-ray – Vertebral translation	0.912 (0.799-0.963)	0.864 (0.699-0.942)
Facet apposition	0.910 (0.812-0.959)	0.985 (0.967-0.993)
Spinal canal occlusion	0.788 (0.591-0.897)	0.569 (0.245-0.779)
Spinal cord compression	0.677 (0.363-0.854)	0.645 (0.312-0.838)

PTA, posterior tangent angle of kyphosis.

Table 2.8: Inter-observer consistency and agreement of radiographic measurements.

Radiographic measure	Inter-observer consistency	Inter-observer agreement
CT – Cobb angle	0.826 (0.726-0.874)	0.825 (0.760-0.873)
CT – PTA	0.862 (0.810-0.901)	0.863 (0.811-0.901)
CT – Vertebral translation	0.913 (0.879-0.938)	0.913 (0.879-0.938)
X-ray – Cobb angle	0.826 (0.743-0.883)	0.827 (0.745-0.884)
X-ray – PTA	0.735 (0.619-0.820)	0.729 (0.609-0.816)
X-ray – Vertebral translation	0.881 (0.822-0.921)	0.880 (0.821-0.921)
Facet apposition	0.780 (0.702-0.840)	0.776 (0.695-0.837)
Spinal canal occlusion	0.529 (0.393-0.643)	0.503 (0.345-0.629)
Spinal cord compression	0.635 (0.500-0.740)	0.489 (0.042-0.724)

PTA, posterior tangent angle of kyphosis.

The univariate analysis results for the seven subgroups are presented in Table 2.9, and the multivariable logistic regression models are presented in Table 2.10. Each multivariable model was statistically significant and demonstrated acceptable discriminatory power. An example interpretation is as follows: for the subgroup of patients admitted due to falls (Model 2) the association between SCI and age was significant when adjusted for the presence of subluxation or dislocation injury (p=0.026). A one year increase in admission age decreased the odds of SCI by 4.1% (odds ratio (OR) [95% CI]=0.959 [0.925-0.995]). When adjusted for age, patients suffering from facet dislocation were 7.25 times more likely to have SCI than those with subluxation (p=0.027; OR=7.248 [1.255-41.864]).

Table 2.9: Initial univariate analysis of predictor variables for regression models.

Model	Initial predictor variables	p-value	Model	Initial predictor variables	p-value
1. MVA	Vehicle speed	0.604	**2. Fall**	Fall height	0.352
	Seatbelt	0.364		Admission age	0.031
	MVA position	0.654		Sex	0.589
	MVA rollover	0.279		Injury side	0.701
	Admission age	0.215		Injury type	0.031
	Sex	0.964		Facet fracture	0.866
	Injury side	<0.001		Spinal level	0.642
	Injury type	0.005		GCS	0.194
	Facet fracture	0.302			
	Spinal level*	0.041			
	GCS	0.040			
3. MRI+CT	Admission age	0.997	**4. MRI**	Admission age	0.954
	Sex	0.466		Sex	0.960
	Injury side	0.360		Injury side	0.141
	Injury type	0.287		Injury type	0.376
	Facet fracture	1.000		Facet fracture	0.992
	Spinal level	0.816		Spinal level	0.686
	GCS	0.152		GCS	0.065
	Injury causation	0.879		Injury causation	0.686
	MRI cord compression	0.184		Cord compression	0.007
	CT AP displacement	0.820			
	CT cobb angle	0.376			
	CT PTA	0.515			
	Facet apposition	0.248			
	CT canal occlusion	0.022			
5. CT	Admission age	0.951	**6. X-ray±CT**	Admission age	0.982
	Sex	0.845		Sex	0.302
	Injury side	0.011		Injury side	0.005
	Injury type	0.004		Injury type	0.010
	Facet fracture	0.509		Facet fracture	0.482
	Spinal level	0.382		Spinal level	0.873
	GCS	0.012		GCS	0.001
	Injury causation	0.854		Injury causation	0.598
	CT AP displacement	0.052		AP displacement	0.209
	CT cobb angle	0.508		Cobb angle	0.153
	CT PTA	0.632		PTA	0.646
	Facet apposition	0.009			
	CT canal occlusion	<0.001			
7. X-ray	Admission age	0.620			
	Sex	0.106			
	Injury side	0.006			
	Injury type	0.384			
	Facet fracture	0.790			
	Spinal level*	0.553			
	GCS	0.024			
	Injury causation	0.949			
	X-ray AP displacement	0.943			
	X-ray cobb angle	0.090			
	X-ray PTA	0.972			

MVA, motor-vehicle accident; AP, antero-posterior; GCS, Glasgow Coma Scale; MRI, magnetic resonance imaging; CT, computed tomography; PTA, posterior tangent angle.

**Complete separation was observed, so variable was not included in the multivariable regression model.*

Table 2.10: Subgroup multivariable binary logistic regression models.

Variables	p-Value	OR (95% CI)
1. MVA (n=96); H&L = 0.382, AUROC = 0.844 [0.768-0.921], EPV = 11.0		
Injury type:		
Dislocation	0.003	5.760 (1.844-17.995)
Subluxation (reference)	-	-
Injury side:		
Bilateral	0	11.368 (3.445-37.518)
Unilateral (reference)	-	-
GCS	0.024	0.799 (0.658-0.971)
2. Fall (n=52); H&L = 0.228, AUROC = 0.797 [0.662-0.932], EPV = 7.0*		
Admission age	0.026	0.959 (0.925-0.995)
Injury type:		
Dislocation	0.027	7.248 (1.255-41.864)
Subluxation (reference)	-	-
3. MRI+CT (n=56); H&L = 0.805, AUROC = 0.681 [0.541-0.821], EPV = 24.0		
Spinal canal occlusion	0.013	1.041 (1.008-1.074)
4. MRI (n=88); H&L = 0.533, AUROC = 0.644 [0.525-0.763], EPV = 38.0		
Spinal cord compression	0.007	1.035 (1.010-1.062)
5. CT (n=113); H&L = 0.411, AUROC = 0.804 [0.717-0.890], EPV = 12.7		
Injury type:		
Dislocation	0.002	5.110 (1.847–14.140)
Subluxation (reference)	-	-
Injury side:		
Bilateral	0.020	3.236 (1.206–8.681)
Unilateral (reference)	-	-
Spinal canal occlusion	0.001	1.054 (1.021–1.087)
6. X-ray±CT (n=143); H&L = 0.575, AUROC = 0.783 [0.703-0.863], EPV = 15.7		
Injury type:		
Dislocation	0.002	4.045 (1.690–9.682)
Subluxation (reference)	-	-
Injury side:		
Bilateral	0.001	4.697 (1.928–11.441)
Unilateral (reference)	-	-
GCS	0.001	0.696 (0.562–0.862)
7. X-ray (n=78); H&L = 0.142, AUROC = 0.809 [0.708-0.910], EPV = 12.0		
Injury side:		
Bilateral	0.006	7.445 (1.771–31.307)
Unilateral (reference)	-	-
GCS	0.010	0.605 (0.412–0.887)

OR, odds ratio; CI, confidence interval; n, number of observations; H&L, Hosmer and Lemeshow goodness-of-fit p-value; AUROC, area under the receiver operating characteristic; EPV, events per variable; MVA, motor-vehicle accident; GCS, Glasgow Coma Scale; MRI, magnetic resonance imaging; CT, computed tomography. Reference category is indicated for categorical variables.
**This model contained less than 10 EPV, so model is at risk of over-fitting. (Hosmer and Lemeshow, 2000)*

DFI characteristics (facet subluxation vs. dislocation, and unilateral vs. bilateral injury) appeared most frequently across the subgroup models (4 of 7 models) as significant predictors of SCI. In these models, facet dislocation and bilateral injury increased the risk of SCI at least 4.0- and 3.2-fold, respectively, when adjusting for all other variables. GCS was a significant predictor in three models, and a one unit increase in GCS decreased the odds of SCI by more than 20% when adjusting for other variables (Table 2.10). Spinal canal occlusion associated with SCI in the subgroups with CT imaging (p=0.001; OR: 1.054 [1.021-1.087]) when adjusted for DFI characteristics, and in the subgroup with both MRI and CT imaging (p=0.013; OR: 1.041 [1.008-1.074]). For patients with MRI imaging, a 1% increase in spinal cord compression increased risk of SCI by 3.5% (p=0.007; OR: 1.035 [1.010-1.062]). No causal characteristic factors (i.e. MVA Vehicle Speed, Fall Height) were significant predictors for SCI in the subgroup models for patients admitted due to MVAs (Model 1) or falls (Model 2).

2.4 Discussion

Despite the potential for severe neurological impairment, there have been few large-scale cohort investigations of subaxial cervical DFIs. Notably, accurate SCI diagnosis through standardised physical examination is often problematic in DFI cases due to concomitant brain injury (Hasler et al., 2012; Hills and Deane, 1993). This study addresses an unmet need for harnessing the predictive value of DFI radiographic data to assess neurological risk. The major findings indicate that quantitative analyses of routine radiographic data alone, or together with statistical modelling, show potential for the discrimination of subaxial cervical DFI patients with neurological involvement.

The patient population studied had similar demographics and injury mechanisms to those reported in small-cohort investigations of DFI radiographic features (Allen et al., 1982; Argenson et al., 1988; Doran et al., 1993; Lintner et al., 1993; Scher, 1977; Shanmuganathan et al., 1994; Vaccaro et al., 1999; Vaccaro et al., 2001), treatment options (Cotler et al., 1990; Dvorak et al., 2007; Grant et al., 1999; Hadley et al., 1992; Rorabeck et al., 1987; Savini et al., 1987), and clinical outcomes (Eranki et al., 2016; Key, 1975; Piccirilli et al., 2013; Wilson et al., 2013).

Although younger (<65 years old; 75.6%) and older (>65 years old; 60%) male patients were over-represented in this DFI cohort, the proportion of females increased with age (24.4% <65 years old vs. 40% >65 years old). MVCs and falls have been associated with an increased risk of cervical spine injury (Clayton et al., 2012; Hasler et al., 2012; Thompson et al., 2009) and were the two most common causes of injury in this cohort. There was a shift from high-velocity to low-velocity injury mechanisms observed in the young and elderly, respectively; similar has been reported for cervical spine injuries (Clark and White, 1985; Kato et al., 2008; Thesleff et al., 2015) and spinal column fractures in general (Hu et al., 1996). It has been proposed that the increase in SCI due to low-velocity cervical trauma in the elderly may be attributed, at least in part, to age-related spondylosis (Kato et al., 2008; Thesleff et al., 2015). Such changes cause narrowing of the canal and may converge with all-cause falls risk to increase the likelihood of neurological deterioration consequent to subaxial cervical spine trauma (Eismont et al., 1984; Fehlings et al., 1999; Kang et al., 1994; Song et al., 2009). Our findings (Model 2) of significant associations between SCI due to falls when age adjusted for DFI characteristics (dislocation vs. subluxation; unilateral vs. bilateral) are consistent with, and support the validity of, the conclusion that radiographic analysis combined with statistical modelling may provide more information than falls risk analysis, or radiographic analysis, alone.

Anterior vertebral translation of greater than 50% of the antero-posterior vertebral body width (as measured on lateral radiographs) has been reported as indicative of bilateral dislocation (Allen et al., 1982; Beatson, 1963; Dailey et al., 2009), while 25% translation is commonly used to define unilateral dislocation (Dailey et al., 2009). In our study, facet dislocations were observed in 127 cases, of which 51.2% were unilateral injuries (DFI Stage 2). Our findings of median vertebral translation of 36.0% (IQR: -2.7-64.7) and 20.0% (IQR: 10.8-34.9) for cases of bilateral and unilateral dislocation, respectively (Table 2.6) are consistent with previous reports (Allen et al., 1982; Beatson, 1963; Dailey et al., 2009). In the present study, B-A analysis indicated acceptable agreement between corresponding X-ray and CT radiographic measurements of vertebral translation. From this we surmise that radiographic analyses, based upon either imaging

modality, may provide valuable information about DFI and facet dislocation associated with neurological involvement (Beatson, 1963).

Neurological deterioration resulting from subaxial cervical injury was recorded at acute admission in 75 of our 226 DFI cases. Univariate analysis identified significant associations between increased spinal canal occlusion and spinal cord compression and SCI, and between decreased facet apposition and SCI (Table 2.5). Multivariable regression analysis confirmed that facet dislocation (uni- or bilateral) was at least four times more likely to result in neurological involvement than subluxation. Notably, bilateral facet injury was a significant predictor for SCI, increasing such risk by over 320% when compared to unilateral facet injury. SCI was observed in 61.3% of bilateral facet dislocation cases, contrasting markedly with the 25.8% frequency observed for unilateral facet dislocation (Table 2.3). These values are lower than those previously reported in smaller case series, with prevalence of SCI resulting from bilateral and unilateral facet dislocations varying between 87.5% to 100% (Allen et al., 1982; Doran et al., 1993; Hadley et al., 1992; Lintner et al., 1993; Vaccaro et al., 1999) and 37% to 100% (Allen et al., 1982; Argenson et al., 1988; Doran et al., 1993; Hadley et al., 1992; Key, 1975; Piccirilli et al., 2013; Rorabeck et al., 1987; Scher, 1977; Vaccaro et al., 1999). However, these previously reported data mostly relate to patients identified as potential surgical candidates and may be biased towards more severe cases. To our knowledge, only two papers have described the frequency of concomitant SCI in DFI Stage 1 patient-cohorts: 33.3% (Allen et al., 1982) and 81.8% (Lintner et al., 1993). The cited values again are higher than the 26.7% observed in our large-scale retrospective study.

It has been suggested that concomitant fracture of the posterior elements at the level of dislocation may reduce the risk of spinal cord injury by increasing the space available for the spinal cord (Chakravarthy et al., 2014; Piccirilli et al., 2013). Argenson *et al.* (1988) and Shanmuganthan *et al.* (1994), identified greater neurological involvement in unilateral facet dislocations *without* associated fracture. However, "facet fracture" was not identified as a predictive variable in any of the final regression models in our study; its conspicuous absence in

our statistical models suggest that relationships between concomitant fracture and spinal canal dimensions are not predictive of SCI across the spectrum of subaxial cervical DFIs.

Facet fracture was more commonly associated with unilateral than bilateral DFIs, and 65% of unilateral dislocations had a concomitant fracture (Table 2.3). This is consistent with small cohort clinical reviews of DFIs (Allen et al., 1982; Argenson et al., 1988; Beyer et al., 1991; Shanmuganathan et al., 1994). The larger proportion of concomitant facet fracture in cases of unilateral dislocation may be due to less severe injury of the surrounding soft tissue compared to bilateral dislocation (Allen et al., 1982), which would act to restrict intervertebral separation during trauma. This may cause increased loading to be transmitted through the facet joint, resulting in fracture. This proposed mechanism of facet fracture is yet to be experimentally verified.

DFI is thought to result from a biomechanical insult involving compressive head-contact sustained during neck flexion (Allen et al., 1982); however, inference remains a major limitation to meaningful discussion (Table 2.2). Because direct investigation of the association between concomitant head and facial injuries, and SCI was not possible in our retrospective study, the GCS was taken as a surrogate marker for head-contact injury. With the caveat that diffuse axonal injury, and subaxial cervical spine injury, may occur in the absence of head trauma, this clinician-administered scale has been validated as a tool to monitor patients following head-contact injury (Jennett, 1994). Admission GCS scores are routinely recorded in tertiary facilities, allowing for comparisons with other single-centre cohorts and large-scale multi-centre studies. Our finding that GCS demonstrated sensitivity to predict risk for neurological involvement in a single-centre DFI cohort implies a mechanistic relationship between head-contact with DFI and concomitant SCI. GCS consistently has been identified as a risk factor for cervical spinal column (Clayton et al., 2012; Hasler et al., 2012; Hills and Deane, 1993; Williams et al., 1992) and cord (Hasler et al., 2012; Williams et al., 1992) injury in major trauma patients; however, investigations of the correlation between head and/or face trauma and cervical spine injury have produced conflicting results. Some studies identified only head injury (Hills and Deane, 1993), facial injury (Hasler et

al., 2012), or neither (Clayton et al., 2012; Davidson and Birdsell, 1989; Williams et al., 1992) as predictors of cervical trauma, and the reasons for these disparities remain unclear. Although the current literature is inconclusive, the association of reduced GCS with the presence of SCI in our DFI population points towards heightened risk of complex neurology following head-contact injury, and underscores the importance of harnessing the predictive value of quantitative radiographic data for neurological risk assessment.

Direct radiographic measurements of spinal canal occlusion and spinal cord compression were the only spine parameters predictive of SCI in our cohort (Table 2.10). This finding supports previous reports that increased spinal canal compromise (Fehlings et al., 1999; Furlan et al., 2011; Kang et al., 1994; Miyanji et al., 2007) and spinal cord compression (Fehlings et al., 1999; Furlan et al., 2011; Hayashi et al., 1995; Miyanji et al., 2007; Rao and Fehlings, 1999), correlate with the presence or severity of neurological deficit in subaxial cervical trauma. While vertebral translation and kyphosis measurements can predict the stability of an injured spinal segment, and are used clinically as indicators for surgery (Bono et al., 2006; Vaccaro et al., 2007; White and Panjabi, 1990), it is intriguing that these indices of segmental stability were not predictive of neurological involvement in our cohort. Quantitative measures of facet joint apposition have limited clinical utility (Bono et al., 2011) and were not represented in our final CT subgroup regression model (Model 5, Table 2.10). Collectively, these results indicate that vertebral translations observed on medical images are *not* predictors of SCI; this has been anecdotally reported (Barnes, 1948; Durbin, 1957). Given that reliable measurement of spinal canal occlusion and spinal cord compression are not possible on lateral radiographs (Prasad et al., 2003), our results also suggest that this image modality is not an appropriate screening tool for SCI in DFI patients. Spinal canal occlusion measurements obtained from CT are as reliable and repeatable as those from T1-weighted MRI (Fehlings et al., 2006; Fehlings et al., 1999), and strongly correlate with T2-weighted MRI measurements of spinal cord compression in patients with acute cervical SCI (Fehlings et al., 1999). CT spinal canal occlusion measurements alone can indicate the likelihood of SCI in cases of DFI (Model 5, Table 2.10) and may have an adjunctive role in pre-

surgical hospitals; however, MRI is the gold standard for assessing acute injury to the spinal cord, intervertebral discs, ligaments, and surrounding soft tissues (Gold, 2015), all of which are important in planning appropriate surgical intervention.

Inter-observer agreement of the radiographic measurements in this study, and intra-observer repeatability of vertebral translation, spinal canal occlusion (as measured on CT) and T2-weighted MRI spinal cord compression measurements, have been reported for subaxial cervical trauma (Bono et al., 2011; Fehlings et al., 2006; Furlan et al., 2007; van Middendorp et al., 2015). To our knowledge, this is the first report of the repeatability of kyphosis angle and facet apposition for the assessment of DFI. In this study, vertebral translation and kyphosis measurements from CT and X-ray demonstrated almost perfect agreement and repeatability (ICC>0.8). Similar to van Middendorp *et al*. (2015), almost perfect repeatability was observed for X-ray and CT measurements of vertebral translation, while facet apposition measurements were over twice as reliable as those previously reported (ICC = 0.78 vs. 0.33) (Bono et al., 2011). In our study, B-A analysis demonstrated acceptable agreement between corresponding X-ray and CT radiographic measurements of vertebral translation (Figure 2.7 in Section 2.5). This suggests that single vertebral translation, Cobb angle and posterior tangent angle values can be assigned for patients who only had one of X-ray or CT images available, and values from the earliest acquired image modality can be used (Table 2.8). It is intuitively obvious that early imaging offers predictive advantage allowing for the planning of appropriate surgical intervention, with the caveat that our inter-observer agreement data are incongruent with those of Bono *et al*. (2011) who reported ICC values of agreement as low as 0.44 and 0.2 for Cobb angle and posterior tangent angle, respectively.

For CT-measured spinal canal occlusion and T2-weighted MRI spinal cord compression measurements, ICC values for inter-observer consistency and agreement, and intra-observer repeatability, obtained from our study were similar to those reported by Furlan *et al.* (2007); however, repeatability in our study was lower than reported by Fehlings *et al.* (2006). It has been suggested that spinal canal occlusion measurements from mid-sagittal CT images provide

inconsistent results, precluding mid-sagittal imaging from use in the clinical assessment of cervical trauma (Furlan et al., 2011); however, the findings of the present study showed moderate to substantial agreement and repeatability, indicating that CT may be appropriate for predicting risk of neurological compromise.

Overall, ICC values of inter-observer agreement and intra-observer repeatability were greater than, or comparable to, published values for corresponding measurements. This could be due to the use of only two observers in this study, compared to 28 in one previous study (Fehlings et al., 2006). However, our investigation had larger image databases than the previous studies that assessed inter-observer agreement and as such was adequately powered for analysis. Improved inter- and intra-observer agreement could also be attributed to the use of the custom analysis program that was developed for our study. In this program the user was prompted to identify key anatomical landmarks on each image, and the measurements of interest were automatically and systematically calculated from these points. This methodology may have lower associated error than drawing lines to identify anatomy and measure geometry, as is required on medical workstation software such as eFilm. Also, DFIs may permit more accurate identification of anatomical landmarks than other cervical trauma, due to the lower incidence of associated vertebral body fractures, resulting in greater observer agreement.

The inherent limitations of retrospective analyses applied to this study. These were overcome by developing numerous multivariable subgroup regression models containing only patients with complete data for the predictors of interest to identify risk factors for SCI. Due to insufficient documentation (e.g. missing ISNCSCI/AIS charts), together with evidence for systematic inaccuracies in manually completed ISNCSCI worksheets (Armstrong et al., 2017), we were unable to reliably stratify neurological condition, so a binary variable for presence of SCI (neurological deficit vs. no neurological deficit) was assigned to each patient. Dichotomisation of these data allows for the assessment of the spectrum of neurological involvement, but introduces assumptions in relation to injury heterogeneity. Thus, further work will be required to assess the appropriateness of radiographic indices alone, or together with

statistical modelling, to stratify risk in relation to ISNCSCI/AIS injury grades, and spinal cord syndromes. Despite thorough interrogation of patient management systems, radiology and operation notes, some cases where DFI was secondary to more severe injury, such as in cases of polytrauma or death, may have been missed. Therefore, this population represents the cohort of traumatic DFIs that required tertiary hospital admission and were a principal cause of patient discomfort and/or neurological impairment. The repeatability analysis subset was selected to ensure complete X-ray, CT and MR imaging, and therefore had a higher proportion of facet dislocations than the study population; however, B-A analyses of inter- and intra-observer agreement (Figure 2.4, Figure 2.5, and Figure 2.6 in Section 2.5) for the radiographic measures demonstrated no bias across their spectrum, suggesting that the ICC outcomes were representative of the study population.

To our knowledge, this is the first large-scale cohort investigation of the epidemiology and radiographic features of traumatic subaxial cervical facet subluxation and dislocation. Patients presenting with facet dislocation (vs. subluxation), or bilateral facet (vs. unilateral) injury and reduced GCS are at high risk of SCI. Spinal canal occlusion (CT) and spinal cord compression (MRI) measurements at the level of bony injury are the radiographic measures most predictive of neurological deficit. Despite “moderate” inter- and intra-observer agreement for spinal cord compression, statistical modelling of indices of spinal canal occlusion alone, or together with spinal cord compression, may allow for appropriate and timely surgical intervention.

2.5 Supplementary material – Bland-Altman plots for radiographic measurements

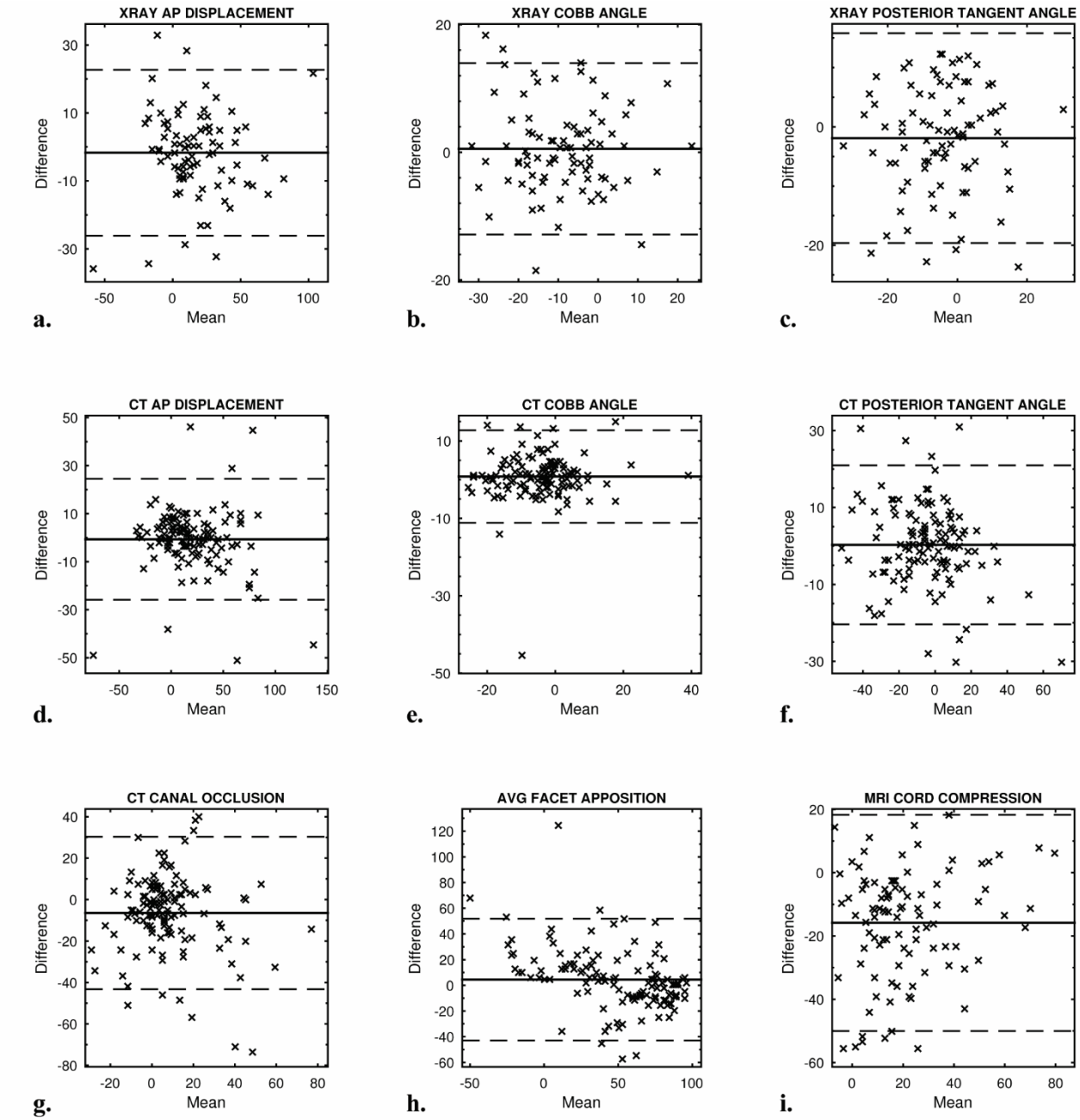

Figure 2.4: Bland-Altman plots for inter-observer agreement of radiographic measurements.

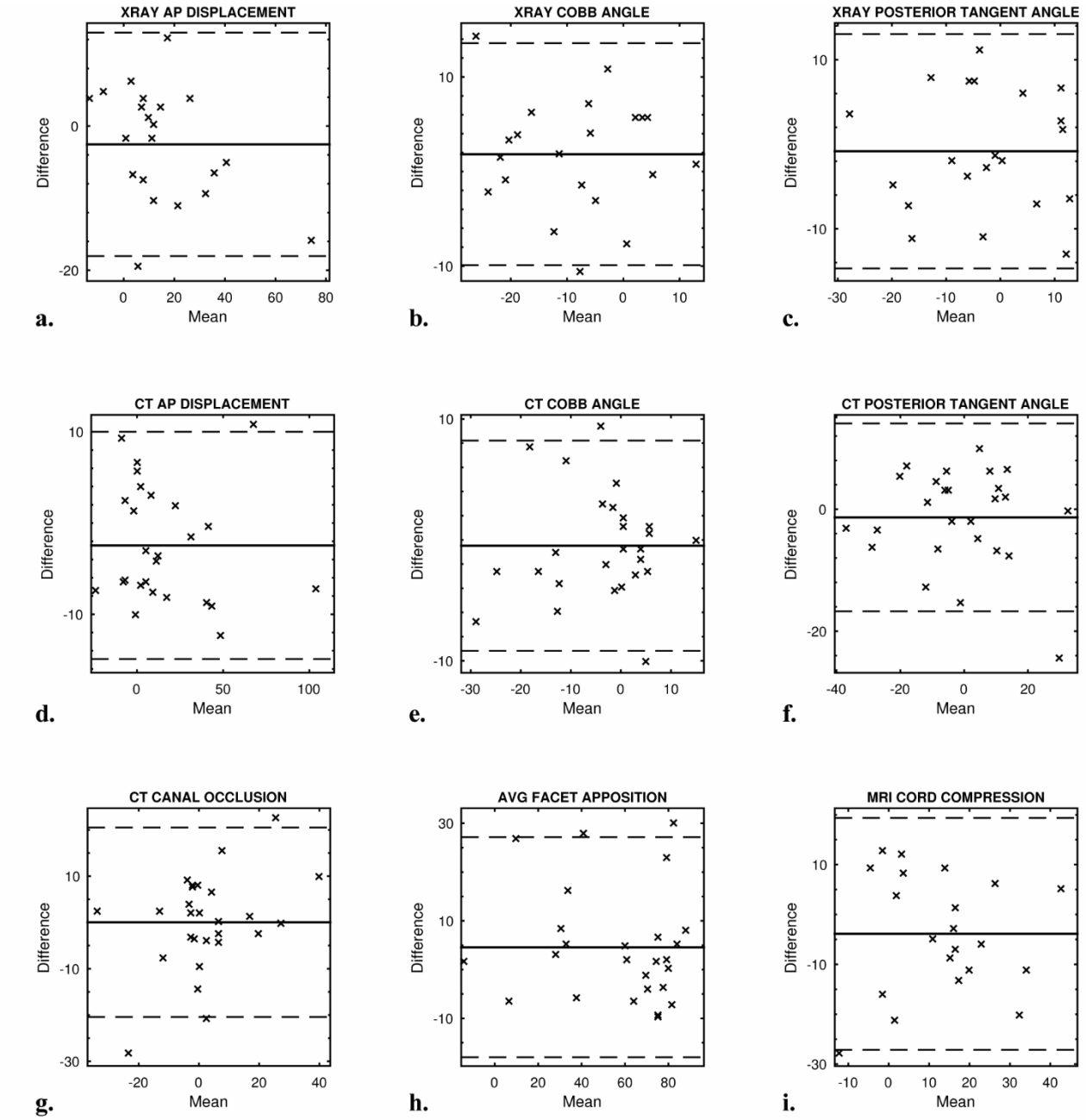

Figure 2.5: Bland-Altman plots for Observer 1 intra-observer repeatability of radiographic measurements.

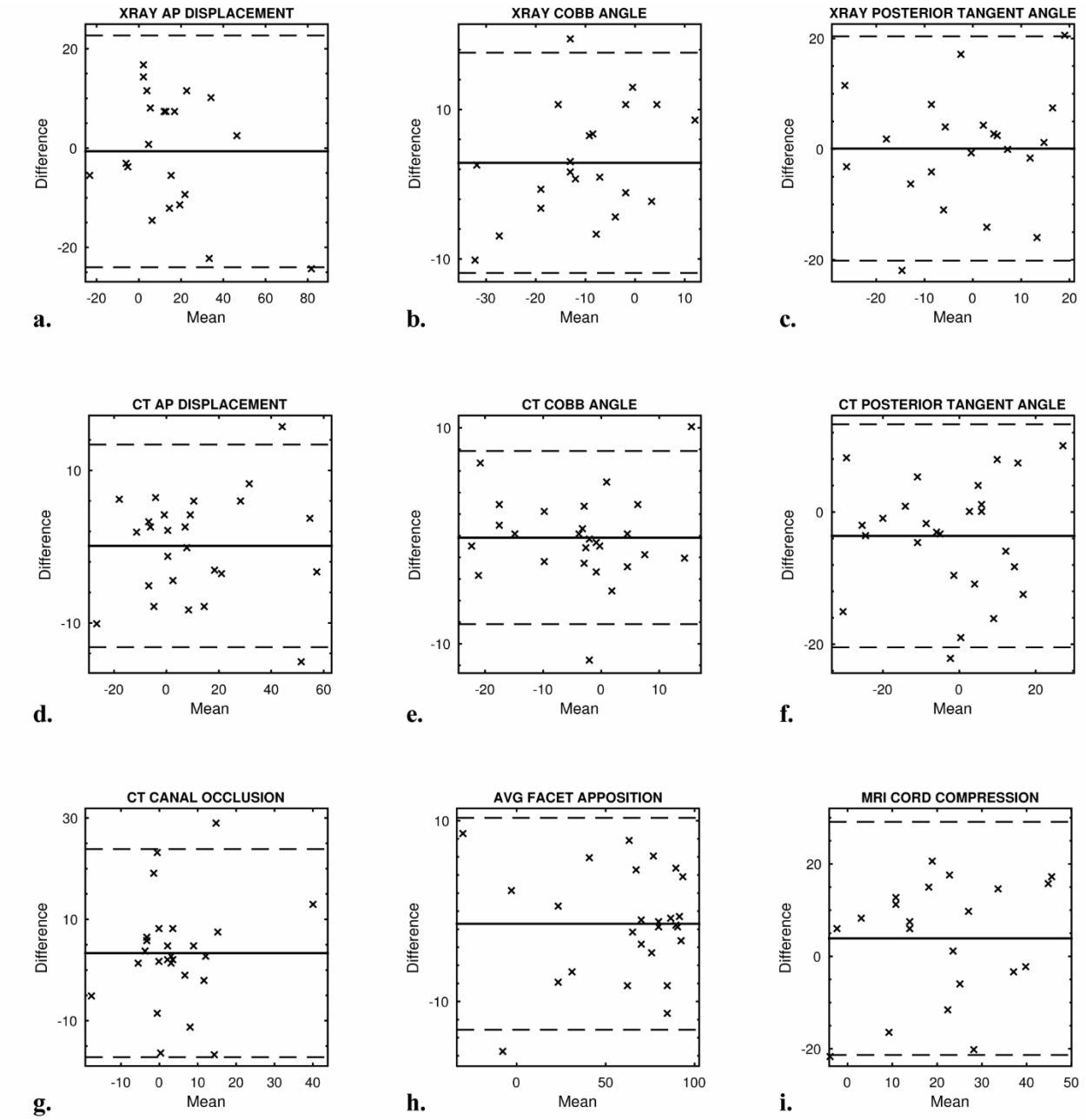

Figure 2.6: Bland-Altman plots for Observer 2 intra-observer repeatability of radiographic measurements.

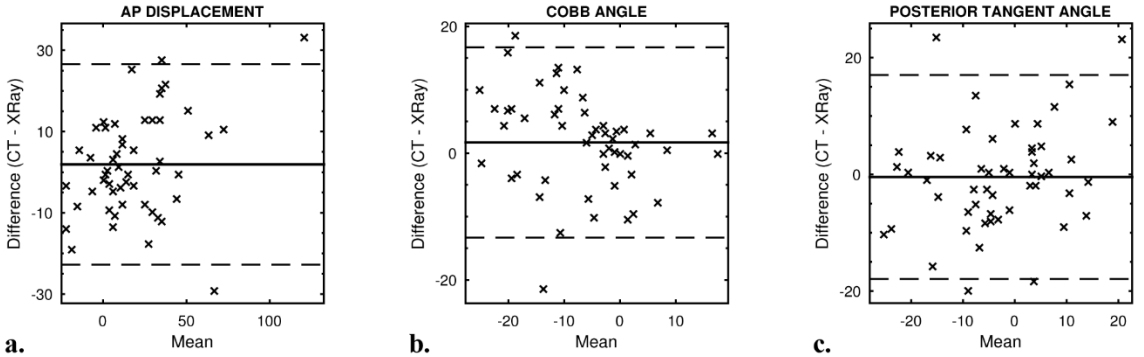

Figure 2.7: Bland-Altman plots for agreement of radiographic measurements from CT and X-ray

Statement of Authorship – Chapter 3

Title of Paper	Quantitative evaluation of facet deflection, stiffness, strain and failure load during simulated cervical spine trauma
Publication Status	☑ Published ☐ Accepted for Publication ☐ Submitted for Publication ☐ Unpublished and Unsubmitted work written in manuscript style
Publication Details	Quarrington, R.D., Costi, J.J., Freeman, B.J.C., Jones, C.F., 2018a. Quantitative evaluation of facet deflection, stiffness, strain and failure load during simulated cervical spine trauma. Journal of Biomechanics 72, 116-124.

Principal Author

Name of Principal Author (Candidate)	Ryan Quarrington		
Contribution to the Paper	Developed testing methods, performed testing of all specimens, performed all data analysis, interpreted data, wrote manuscript and acted as corresponding author.		
Overall percentage (%)	80%		
Certification:	This paper reports on original research I conducted during the period of my Higher Degree by Research candidature and is not subject to any obligations or contractual agreements with a third party that would constrain its inclusion in this thesis. I am the primary author of this paper.		
Signature		Date	01/06/2018

Co-Author Contributions

By signing the Statement of Authorship, each author certifies that:

i. the candidate's stated contribution to the publication is accurate (as detailed above);

ii. permission is granted for the candidate in include the publication in the thesis; and

iii. the sum of all co-author contributions is equal to 100% less the candidate's stated contribution.

Name of Co-Author	John Costi		
Contribution to the Paper	Supervised development of work, assisted with data interpretation, and reviewed manuscript.		
Signature		Date	14/06/2018

Name of Co-Author	Brian Freeman		
Contribution to the Paper	Supervised development of work and reviewed manuscript.		
Signature		Date	14/06/2018

Name of Co-Author	Claire Jones		
Contribution to the Paper	Supervised study design and development of work, assisted with data interpretation, and reviewed manuscript.		
Signature		Date	5/06/2018

Chapter 3 Quantitative evaluation of facet deflection, stiffness, strain and failure load during simulated cervical spine trauma[1]

3.1 Introduction

Traumatic cervical facet dislocation (CFD) is often associated with devastating spinal cord injury, resulting in tetraplegia in up to 87% of cases (Hadley et al., 1992; Payer and Schmidt, 2005). CFD may be unilateral or bilateral, with bilateral facet dislocation (BFD) more often resulting in complete spinal cord injury (Chapter 2) (Allen et al., 1982; Quarrington et al., 2018b). These injuries occur most commonly, and are most often survived, in the subaxial region (C3-T1). They are frequently a result of traffic and sporting accidents, and falls (Chapter 2) (Allen et al., 1982; Quarrington et al., 2018b), during which the external loading applied to the neck can be complex and variable.

BFD is thought to result from a *global, supra-physiologic* flexion moment about the subaxial cervical spine, caused by axial compressive forces applied to the head with large anterior eccentricity (Allen et al., 1982; Cusick and Yoganandan, 2002; Huelke and Nusholtz, 1986; White and Panjabi, 1990), or from inertial motion of the head during high deceleration events (Huelke and Nusholtz, 1986). In head-first impact tests of head-neck specimens, BFDs occurring in the lower cervical spine have been associated with local intervertebral flexion and anterior shear motions (Hodgson and Thomas, 1980; Ivancic, 2012b; Nightingale et al., 2016). The inertial injury mechanism of BFD was validated in one experimental series (Ivancic et al., 2007, 2008; Panjabi et al., 2007) in which incrementally increasing, sagittal decelerations were applied to cervical motion segments (with a head mass surrogate) until dislocation occurred. Large flexion angles and anterior shear displacements were the dominant sagittal *intervertebral* motions observed during the injury event (Panjabi et al., 2007). Interestingly, no cervical facet fracture-dislocations have been produced experimentally, yet facet fractures are associated with up to 88%

[1] A version of Chapter 3 was published in Journal of Biomechanics: Quarrington, R.D., Costi, J.J., Freeman, B.J.C., Jones, C.F., 2018, **72**, 116-124. *Quantitative evaluation of facet deflection, stiffness, strain and failure load during simulated cervical spine trauma*.

of clinical CFD cases (Foster et al., 2012). It has been suggested that concomitant fracture may be due to a large component of anterior shear in the local injury vector (Foster et al., 2012), but this has not been validated experimentally.

Studies that investigated the kinematics of cervical vertebrae during dynamic spinal motion have assumed that the anterior and posterior anatomy act as a rigid body (Ivancic et al., 2007, 2008; Panjabi et al., 2007). However, the high incidence of facet fracture associated with CFD would suggest that large loads are transmitted through this joint during the injurious motions, and one could expect substantial bending of the facets to occur prior to mechanical failure. In addition, sagittal bending of the facets in excess of 14°, relative to the vertebral body, was observed in a *lumbar* specimen during replicated *physiological* intervertebral flexion (Green et al., 1994). The magnitude of facet deflection and the mechanical response of the subaxial cervical facets during loading to simulate supra-physiologic anterior shear and flexion motions have not been reported.

The mechanical response of the cervical facet capsule during simulated trauma has been well characterised, particularly regarding soft-tissue strains during 'whiplash' events (Cholewicki et al., 1997; Panjabi et al., 1998b; Siegmund et al., 2008; Siegmund et al., 2001); however, strain data is not available for the bony facet. Investigations of the load-bearing capacity (Hakim and King, 1976; King et al., 1975; Pollintine et al., 2004), failure mechanisms (Cyron et al., 1976), fatigue strength (Cyron and Hutton, 1978) and surface strain response (Schulitz and Niethard, 1980; Shah et al., 1978; Suezawa et al., 1980) of the *lumbar* facets and neural arch have been performed, but similar analyses have not been reported for the subaxial cervical spine, or during simulated facet dislocation. Quantitative measures of the mechanical response of the cervical facets to simulated traumatic loading may be important for validation of computational models of cervical trauma and to inform design of advanced anthropomorphic test device (ATD) necks and associated injury criteria.

The aim of this study was to quantify the sagittal deflection, apparent stiffness, surface strain and failure load of subaxial cervical inferior facets under loads simulating the proposed injury vectors of supraphysiologic *in vivo* compressive-flexion and anterior shear motions.

3.2 Methods

3.2.1 Specimen preparation

Thirty-one functional spinal units (FSUs); six C2/C3, six C3/C4, six C4/C5, seven C5/C6 and six C6/C7, were dissected from fourteen fresh-frozen human cadaver cervical spines (mean donor age 69 years, range 48-92; eight male). Radiographs and high-resolution computed tomography (CT) scans (Toshiba Aquilion ONE, Otawara, Japan; 0.5 mm slice thickness, 0.3 mm in-plane resolution) were obtained and each specimen was screened for excessive degeneration, injury and disease by a senior spinal surgeon. Average volumetric bone mineral density (vBMD) was quantified from CT using a calibration phantom (Mindways Software Inc., Texas, USA) and 'FIJI' image analysis software (1.51p, ImageJ, Maryland, USA) (Schindelin et al., 2012) (Figure 3.1a). Vertebral endplate depths and sagittal facet angles were measured using FIJI (Figure 3.1b&c).

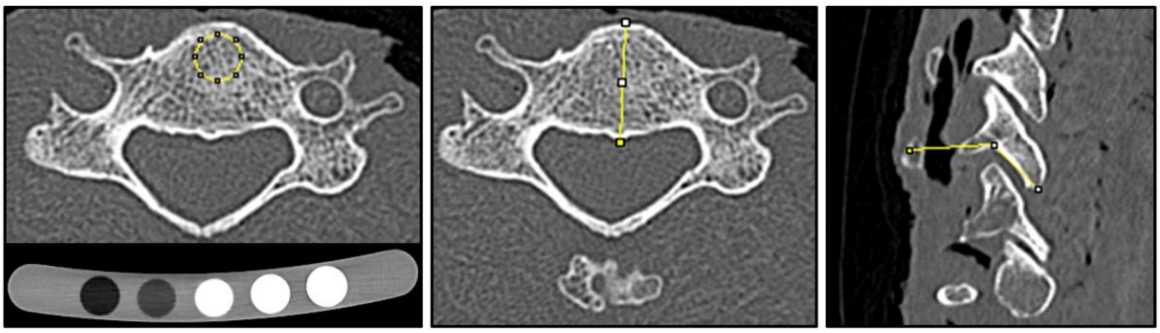

Figure 3.1: Measurements obtained from high-resolution computed tomography images: a) average volumetric bone mineral density; b) vertebral body depth; and, c) sagittal facet angle.

Specimen musculature was removed and the vertebral disc and bilateral facet joint capsules were preserved (Figure 3.2a). The vertebral bodies of each FSU were embedded in polymethylmethacrylate (PMMA; Vertex Dental, Utrecht, Netherlands) using a custom adjustable mold (Figure 3.2b). To assist with fixation a wood screw was inserted through the vertebral bodies and disc, and steel wire was wrapped around the vertebral bodies and through

the transverse foramen (Figure 3.2a); excess wire and the screw-tip protruded from the superior endplate of the superior vertebra into a rectangular embedding cavity approximately 50 mm in length. The FSU was placed in the mold which was then filled with PMMA. A support bar was positioned within the spinal canal along the posterior surfaces of the vertebral bodies and was fixed to the PMMA block (Figure 3.2b and c). Three types of support bars, accommodating variation in specimen geometry, were used to prevent embedding failure: 1) 90x20x1.5 mm aluminum; 2) 90x20x5 mm steel; and, 3) 90x10x5 mm steel.

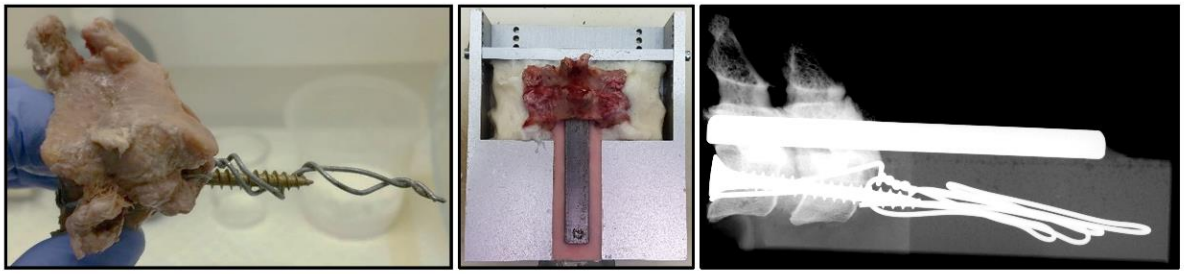

Figure 3.2: Specimen preparation: a) cervical functional spinal unit dissected of soft-tissue, with wood-screw and steel wire attached to the vertebral bodies; b) the specimen was positioned in a custom mold with the spinous processes pointing vertically, perpendicular to the base, such that the posterior surfaces of the vertebral bodies aligned with the top surface. The lateral anatomy was pressed into plasticine to hold the specimen in the desired orientation, and to prevent the facets being embedded. The mold was then filled with PMMA and a support bar was fixed to the posterior surfaces of the vertebral bodies; c) a lateral radiograph of the embedded specimen.

3.2.2 Mechanical loading

Each specimen-PMMA assembly was rigidly mounted to the base of a biaxial materials testing machine (8874, Instron, High Wycombe, UK) via a custom support apparatus attached to a rotary table (VU150, Vertex, Taichung City, Taiwan) (Figure 3.3). Using the rotary table, the inferior articular facet surfaces of the inferior vertebrae were positioned relative to the actuator to simulate the loading vectors applied by the opposing facets during *in vivo*, supraphysiologic compressive-flexion and anterior shear motions (Figure 3.3). A 10 N pre-load, and then three cycles of sub-failure loading to 100 N (a non-destructive load determined from pilot testing), was applied bilaterally to the geometric centre of each articular facet surface at 1 mm/s using 6 mm diameter hemispherical loading pins, in each loading direction. These loading directions were deduced from close inspection of the subaxial cervical facet joint anatomy and their load-bearing

role during intervertebral anterior shear and compressive-flexion motions. Anterior shear motion causes the bilateral facet joints to engage so loading was applied to the bilateral inferior articular facet surfaces in a postero-anterior direction, parallel to the inferior vertebral endplate. During physiological subaxial cervical flexion motion the subaxial cervical facets are unloaded (Jaumard et al., 2011a); however, this study aimed to simulate inter-facet loading during *supraphysiologic* compressive-flexion-compression motion. The centre of rotation of compression-flexion is likely further anterior and inferior than occurs during physiological flexion, causing the facet joints to engage rather than separate. This scenario was simulated by applying loading to the bilateral facets that was directed perpendicular to the articular facet surfaces (Figure 3.3).

The posterior elements of the superior vertebra provided a physiological boundary condition for the loaded inferior facets. Uniaxial strain gauges (FLA-1-23-1L, TML, Tokyo, Japan) were attached to the loading pins to ensure that symmetrical loading was applied to the bilateral facets at the start of each test. Following completion of the sub-failure testing, each specimen was loaded to failure in one of the two directions (randomly assigned) at 10 mm/s. The non-destructive and destructive loading rates chosen were the maximum possible to obtain sufficient motion-capture data.

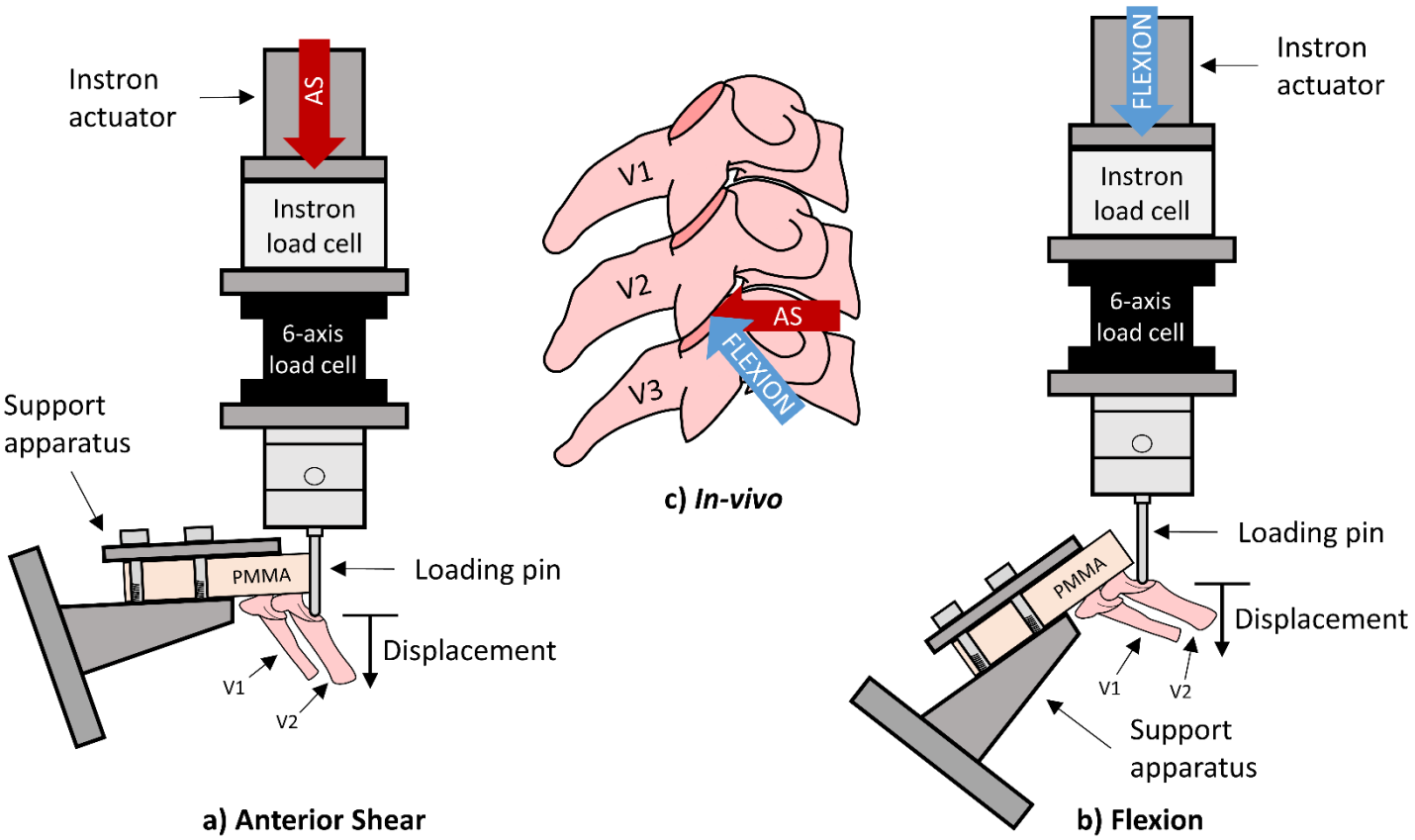

Figure 3.3: Lateral schematic of the mechanical testing setup used to apply the proposed facet loading vectors experienced during supra-physiologic a) anterior shear (AS; red arrow), and b) compressive-flexion (blue arrow) motions. Loading was applied to the inferior facets of V2 via bilateral loading pins which simulated the opposing facets at the level of interest (superior facets of V3 in c). V1 is the superior vertebra adjacent to the level of injury and was included to provide a physiological boundary condition for the posterior elements of V2. Displacement of the loading pin was calculated from the Instron actuator linear variable differential transducer.

3.2.3 Instrumentation and data collection

The inferior vertebra of each specimen was instrumented to measure the mechanical response of the bilateral inferior facets to loading. Tri-axial rosette strain gauges (FRA-1-23-1L, TML, Tokyo, Japan) and custom light-weight motion capture marker-carriers (Optotrak Certus, Northern Digital Inc., Ontario, Canada) were fixed to the bilateral inferior facet bases and tips, respectively (Figure 3.4). A third marker-carrier was attached to the inferior vertebral body via a K-wire (Figure 3.4). Anatomical landmarks were digitised using a 1 mm diameter spherical probe tip (Figure 3.5).

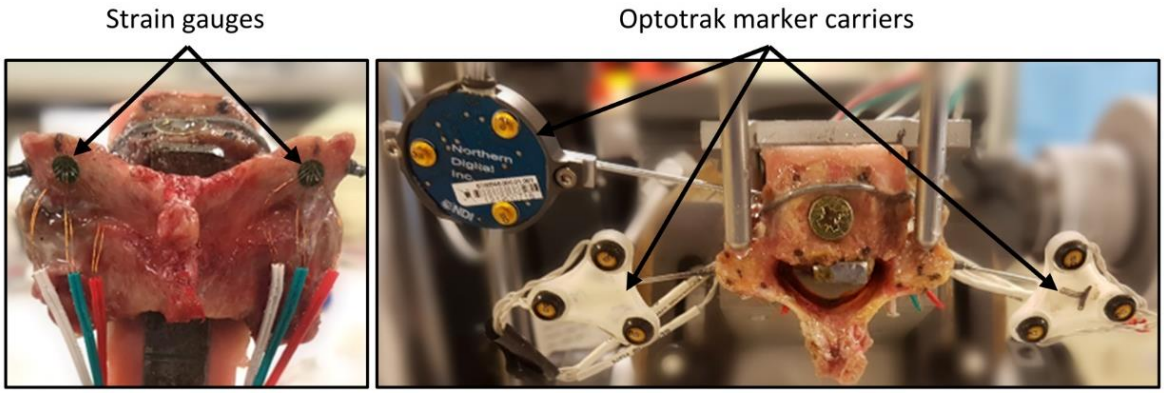

Figure 3.4: Specimens instrumented with tri-axial rosette strain gauges (left) and Optotrak marker-carriers (right).

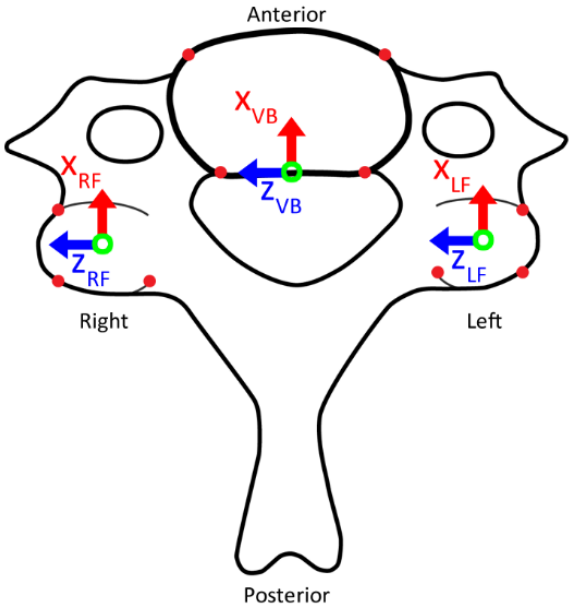

Figure 3.5: A schematic of the inferior view of a cervical vertebra, where the red circles indicate the anatomical landmarks that were digitised. The local coordinate systems are illustrated, with x-axes in red, z-axes in blue, and the origins in green. The origin of the vertebral body was defined as the sagittal midpoint of the posterior edge of the inferior vertebral endplate. The origin of the facets were defined as the geometric centre of the articular surfaces. VB = vertebral body, RF = right facet, LF = left facet.

Loads and actuator position were measured by a biaxial load cell (Dynacell ±25 kN, Instron, High Wycombe, UK) and an internal linear variable differential transducer (LVDT), respectively (Figure 3.3). A six-axis load cell (MC3A-6-1000 ±4.4 kN, AMTI, Massachusetts, USA) was connected in series to measure off-axis loads and moments. Failure tests were recorded at 100 Hz using a high-speed camera (i-Speed TR, Olympus Corporation, Tokyo, Japan).

3.2.4 Data processing

Data were processed using custom MATLAB code (R2015a, Mathworks, Massachusetts, USA). Strain gauge, LVDT, load cell, and motion capture data were filtered using a second-order, two-way Butterworth low-pass filter. A cut-off frequency of 100 Hz was used for all except the motion capture data (30 Hz).

The aforementioned 4.4 kN six-axis load cell was used to monitor the 10 N pre-load, and the 25 kN biaxial load cell controlled the 100 N load-limit for each test; however, a substantial 'shear' load (perpendicular to the direction of the applied load) occurred during the simulated anterior-shear tests, due to the inclined angle of the facets in this specimen orientation. This off-axis load appeared to cause mechanical cross-talk in the biaxial load cell, as 100 N of applied load (through the axis of the loading pins) was not consistently measured by the six-axis load cell during anterior-shear tests. Therefore, to ensure the outcome measures for each specimen were obtained at an equivalent load, values corresponding to an applied load of 47 N (the highest load reached by all specimens), measured by the six-axis load cell, were determined. This load is comparable to physiological cervical facet joint forces (Jaumard et al., 2011a; Kumaresan et al., 2001).

Load-displacement plots were generated for the sub-failure tests, and apparent facet stiffness (N/mm) was determined from the slope of the linear region (Figure 3.6). Maximum principal and shear strains were calculated from the output of each rosette gauge. Local anatomical coordinate systems, consistent with International Society of Biomechanics' recommendations for spinal joints (Wu et al., 2002), were defined for the vertebral body and facets using the anatomical landmark coordinates illustrated in Figure 3.5. Angular deflection of the facets relative to the vertebral body (in degrees) was calculated by solving for Euler angles using a *z-y-x* sequence (Robertson et al., 2013); facet deflections were only appreciable in the sagittal plane (about *z*). For the destructive tests, the instant of initial failure (of either one or both facets, defined as a distinct reduction in load and confirmed using high-speed camera footage) was identified (Figure 3.6), and the applied load, facet deflection and surface strains were

determined at this point. The failure mode of each specimen was determined from viewing the high-speed camera footage and by visual inspection of the specimen.

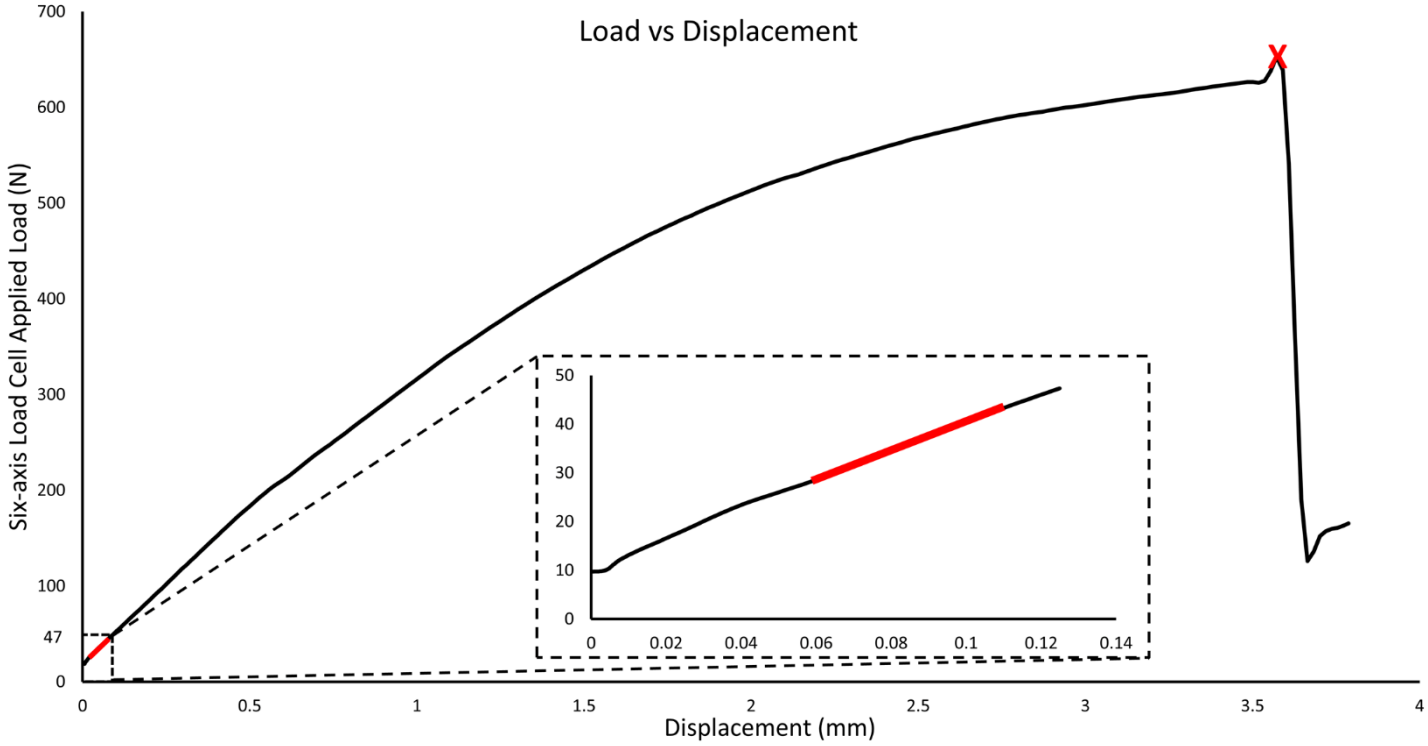

Figure 3.6: An example filtered load-displacement plot for a destructive test in the flexion loading direction with the instant of initial failure indicated (red X). The load-displacement plot for the corresponding non-destructive test is also shown (inset). The red lines represent the linear region, from which the apparent facet stiffness was calculated. Data from the last cycle of each non-destructive test were used for statistical analyses. Where anatomical asymmetry led to loading asymmetry, the larger of the two strain and deflection values were used.

3.2.5 Statistics

Statistical analyses were performed using SPSS v22 (IBM, Illinois, USA). Eight linear mixed-effects models (LMM) were developed to identify if loading direction was significantly associated with the following outcome measures: non-destructive 1) facet stiffness, 2) maximum principal strain, 3) maximum shear strain and 4) sagittal deflection; and, 5) applied load, 6) maximum principal strain, 7) maximum shear strain, and 8) sagittal deflection at failure. Each model was developed as follows. Firstly, Shapiro-Wilk and Levene tests were performed to assess

normality and homogeneity of variance of the dependent variables, respectively. If required, statistically significant outliers were removed and/or data was log-transformed to meet these criteria. The effect of test direction was assessed in all models, and this effect was adjusted for spinal level, the interaction of spinal level with test direction, donor demographics, specimen bone quality and geometry, and the type of support bar. As multiple specimens from the same donor were used in this study, a random effect of spinal level, nested within cadaver ID, was included. Each model was refined using a manual backward step-wise approach until only significant predictors remained (α=0.05).

3.3 Results

Donor and specimen details, and failure outcomes, are provided in Table 3.1. One C3/C4 specimen (Test #1) was omitted from all analyses due to technical difficulties during testing. Failure data was not available for a further six specimens due to: inadequate fixation of the specimen in the embedding material (N=2; #13 and #16); poor bone quality resulting in loading pins puncturing the facets or fracture occurring at the bone-screw interface (N=3; #2, #12 and #17); and, slipping of the rotary table (N=1; #4).

Table 3.1: Donor and specimen details, and failure test outcome measures. vBMD = volumetric K2HPO4 equivalent bone mineral density (mg/cm^3). Dashes indicate that failure data was not available. Test 1 was omitted due to technical difficulties.

Test #	Specimen ID	Spinal level	Sex	Age	Average vBMD	Failure direction	Failure load (N)	Failure location
2	H023	C6	M	92	-27.3	-	-	-
3	H001	C3	M	48	192.2	Anterior shear	226.4	Facet tips
4	H001	C5	M	48	293.5	-	-	-
5	H001	C7	M	48	212.9	Anterior shear	473.6	Facet tips
6	H027	C4	F	64	177.7	Anterior shear	336.3	Facet tips
7	H012	C3	F	67	434.7	Flexion	822.7	Pedicles
8	H027	C6	F	64	142.2	Anterior shear	330.8	Facet tips
9	H012	C5	F	67	140.2	Anterior shear	327.2	Facet tips
10	H012	C7	F	67	118.5	Anterior shear	292.3	Facet tips
11	H017	C5	F	86	27.6	Anterior shear	123.5	Facet tips
12	H017	C3	F	86	34.3	-	-	-
13	H006	C4	M	57	238.5	-	-	-
14	H032	C7	M	65	161.0	Flexion	573.1	Facet tips
15	H032	C3	M	65	161.0	Anterior shear	316.4	Facet tips
16	H006	C6	M	57	207.4	-	-	-
17	H032	C5	M	65	171.9	-	-	-
18	H045	C6	F	74	121.6	Anterior shear	416.6	Facet tips
19	H045	C4	F	74	136.6	Anterior shear	405.9	Facet tips
20	H039	C7	F	86	92.9	Flexion	873.5	Facet bases
21	H039	C5	F	86	156.3	Flexion	1073.1	Facet bases
22	H039	C3	F	86	194.2	Anterior shear	382.5	Facet tips
23	H018	C5	M	84	207.6	Flexion	1109.1	Pedicles
24	H018	C7	M	84	179.1	Anterior shear	562.8	Facet tips
25	H018	C3	M	84	209.2	Flexion	878.6	Pedicles
26	H026	C6	M	74	145.0	Anterior shear	391.5	Facet tips
27	H026	C4	M	74	140.4	Flexion	790.1	Pedicles
28	H021	C4	F	61	216.2	Flexion	658.4	Pedicles
29	H021	C6	F	61	179.6	Flexion	1203.4	Facet bases
30	H044	C7	M	62	118.7	Flexion	743.8	Pedicles
31	H028	C6	M	50	127.2	Flexion	542.1	Facet tips

The eight final multivariable LMMs are presented in Table 3.2 and Table 3.3 in Section 3.5. A significant interaction between test direction and specimen level was associated with apparent facet stiffness (p=0.007), when adjusted for vBMD and support bar type (Table 3.2). Post-hoc analysis demonstrated that specimens were significantly stiffer when loaded in the compressive-flexion direction compared to the anterior shear direction for all spinal levels (Figure 3.7, Table 3.4 in Section 3.5), but this difference was less pronounced in the lower levels (C6 and C7) compared to the upper levels (C3-C5). In the anterior shear loading direction, stiffness was

significantly higher for C6 and C7 vertebrae compared to C5 (Table 3.5: C5 vs. C6, p=0.006; C5 vs. C7, p=0.010), while the inverse relationship tended towards significance for the compressive-flexion loading direction (Table 3.5: C5 vs. C6, p=0.152; C5 vs. C7, p=0.099) (Figure 3.7).

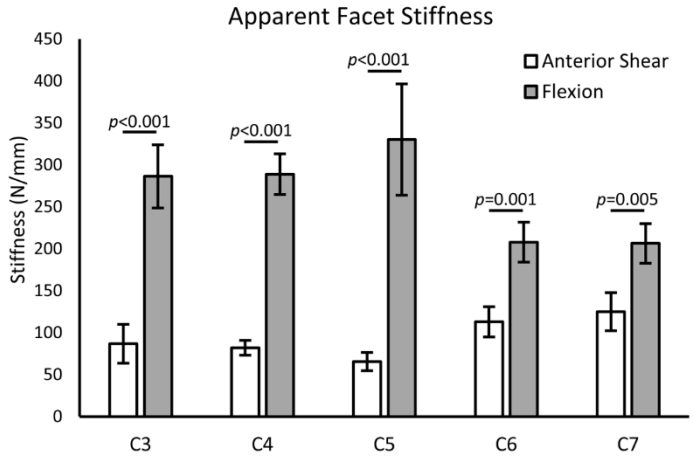

Figure 3.7: Mean measured apparent facet stiffness for the anterior shear and flexion loading directions, grouped by the spinal level of the tested vertebra. p-Values for post-hoc analysis of the final multivariable linear mixed-effects model (α=0.05) are shown.

Lower stiffness measurements for the anterior shear loading direction corresponded with significantly larger maximum principal strains (p<0.001), shear strains (p<0.001), and sagittal facet deflections (p=0.009) compared to specimens loaded under simulated compressive-flexion, when adjusted for gender and vertebral body depth, gender, and vBMD, respectively (Figure 3.8, Table 3.2).

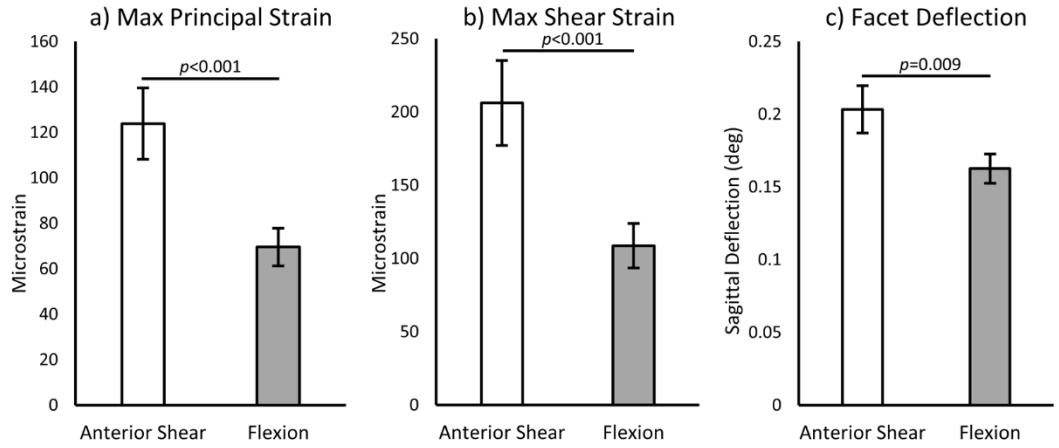

Figure 3.8: Mean measured maximum (a) principal strain, (b) shear strain, and (c) sagittal facet deflection measured at 47 N in the non-destructive tests. p-Values from the respective final multivariable linear mixed-effects models (α=0.05) are shown.

Failure load was significantly higher in simulated compressive-flexion than for specimens failed in anterior shear (p=0.001), when adjusted for vBMD and support bar type (Figure 3.9, Table 3.3). Sagittal facet deflection at initial failure was also larger in compressive-flexion (p=0.001). The highest failure load was 1.2 kN, and deflections ranged from 1.15° to 5.58° (mean = 2.60±0.34°) for anterior shear and from 2.55° to 10.24° (mean = 5.75±0.73°) for compressive-flexion. There was no statistical difference between the maximum principal (p=0.566) and shear strains (p=0.164) observed at failure for the two loading directions (Figure 3.9, Table 3.3). Principal and shear strains ranged from 815 to 7,394 microstrain (με) and 2,676 to 16,897 με for anterior shear, and from 852 to 5,858 με and 739 to 8,545 με for the compressive-flexion loading direction, respectively.

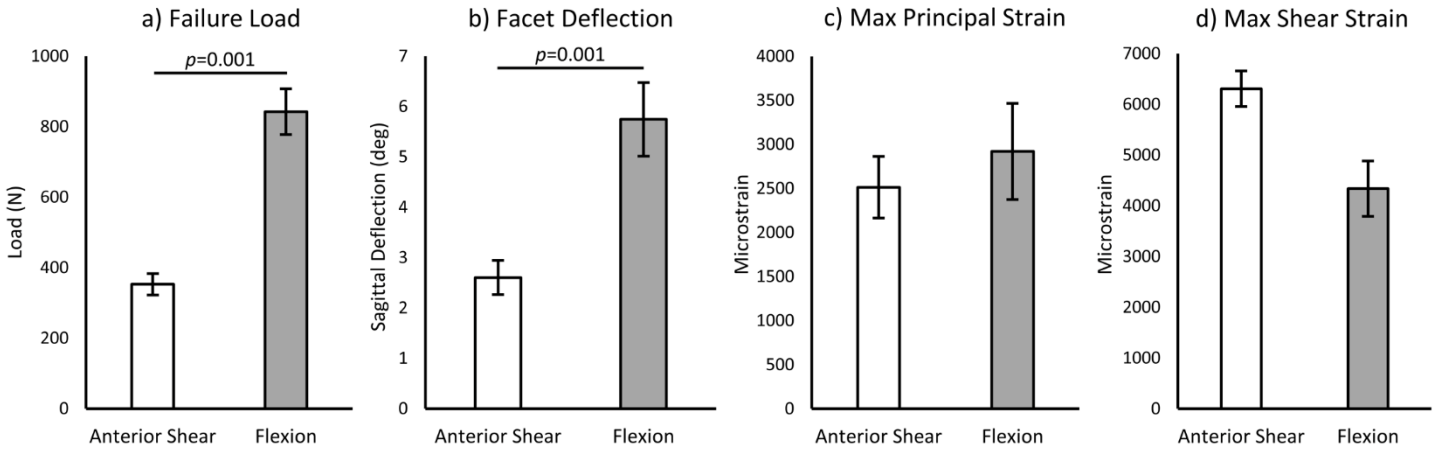

Figure 3.9: Mean measured a) failure load, b) sagittal facet deflection, c) maximum principal strain, and d) maximum shear strain at initial failure for simulated anterior shear and flexion loading. p-Values from the respective final multivariable linear mixed-effects models (α=0.05) are shown.

Two distinct fracture locations were identified (Figure 3.10). All specimens that were loaded destructively in the anterior shear direction failed through the inferior facet tips (13/13 specimens; Table 3.1). Of the eleven specimens tested to failure under simulated compressive-flexion, six fractured through the pedicles, three through the facet bases, and two through the facet tips (Table 3.1).

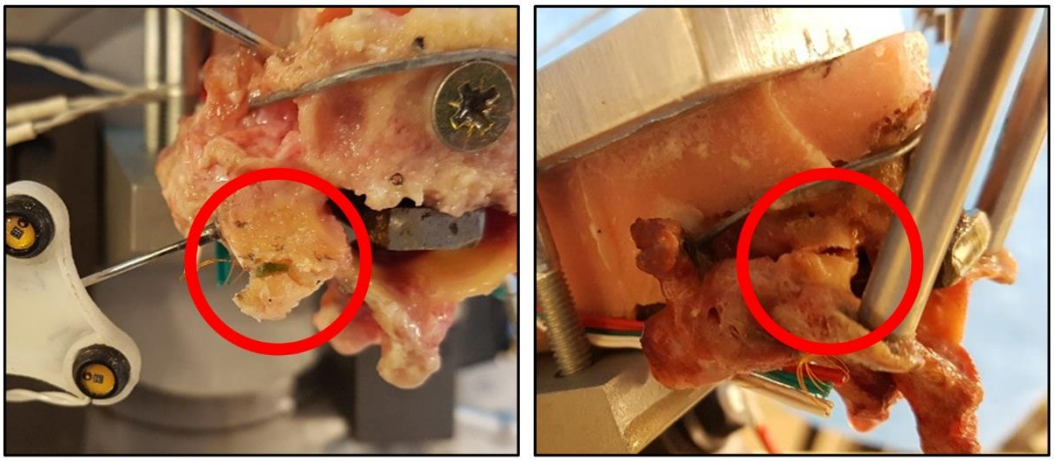

Figure 3.10: Fracture through the facet tip occurred for all specimens tested to failure in the anterior shear direction (left), while specimens failed under simulated compressive-flexion typically fractured through the pedicles (right).

3.4 Discussion

Despite the potentially devastating consequences of CFD, very little published data exists regarding the biomechanics underlying this injury mechanism. The mechanical response of the subaxial facets, which are often fractured during CFD (Allen et al., 1982; Foster et al., 2012), have not previously been investigated. In this present study, bilateral loading was applied to the inferior facets of subaxial cervical vertebrae in directions that replicate traumatic anterior shear and compressive-flexion; these motions are thought to be associated with CFD (Allen et al., 1982; Cusick and Yoganandan, 2002; Hodgson and Thomas, 1980; Ivancic, 2012b; Nightingale et al., 2016; White and Panjabi, 1990). Facet stiffness was higher in compressive-flexion, which corresponded to higher sagittal deflections and sub-failure surface strains when compared to the anterior shear loading direction. The strain and stiffness responses differed between the upper and lower cervical regions. Failure load was higher in compressive-flexion, and distinct failure locations were observed for the two loading directions in most cases.

There is little published data regarding cervical facet biomechanics with which to compare our results. Wang *et al*. (2012) measured average C3 and C4 inferior facet uniaxial strains of 42 and 38 microstrain (με), respectively, at 20° of flexion applied to four-vertebrae FSUs from sheep; they did not apply anterior shear. These values are lower than, but comparable to, the maximum principal strains measured during non-destructive compressive-flexion testing in the present study (69±8 με, Figure 3.8a).

Maximum principal and shear strains were both significantly larger (at 47 N of applied load) during non-destructive simulated anterior shear motion than for simulated compressive-flexion motion (Figure 3.8). The strain response and apparent stiffness of the facets were significantly different in the upper and lower regions of the subaxial cervical spine. Maximum shear strains were significantly higher at the lower spinal levels than at C3 and C4, for both loading directions ($p=0.001$, Table 3.2). Interestingly, no significant differences in strains were observed at failure between loading directions or between spinal levels (Figure 3.9, Table 3.3). This was unexpected, given that the failure locations were distinctly different between loading

direction groups; however, strain measurements of bone are highly dependent on the anatomical location of the gauge, which was remote to the fracture sites. A difference in strain response may have been observed if gauges were positioned on the pedicles and facet tips.

Apparent facet stiffness was significantly higher in the simulated compressive-flexion loading direction than anterior shear at all spinal levels, but this difference was less pronounced for the C6 and C7 vertebrae (Figure 3.7, Table 3.4). We hypothesise that this is due to the change in facet and pedicle orientation observed at the lower cervical levels (Panjabi et al., 1991; Panjabi et al., 1993), although facet angle was not a significant predictor in the final multivariable model. 'Facet stiffness' is a difficult parameter to interpret as the axis about which the facet deflects will be different for the two tested orientations. This will alter the contributions from the other posterior elements in resisting the applied loads – the term 'apparent facet stiffness' was used to reflect this. It is likely that larger stiffness values observed in the compressive-flexion testing orientation are, in part, due to increased contributions from the pars interarticularis and the pedicles.

Sagittal angular deflections of the cervical facets (relative to the vertebral body) at the time of failure were significantly larger in compressive-flexion than for anterior shear loading (Figure 3.9), with one specimen demonstrating facet deflection in excess of 10°. Our results indicate that the vertebral body and posterior elements are unlikely to be well represented as a single rigid body during simulated cervical trauma. This should be considered during kinematic analyses of motion segment injury involving the posterior elements by modelling the anterior and posterior anatomy of each vertebrae as separate rigid bodies and measuring their motions independently.

The mechanism of failure was generally different for the two simulated loading modes, and this difference was associated with significantly different failure loads (Figure 3.9). Bending of the facets during simulated anterior shear loading caused the point of load application to translate inferiorly towards the facet tip. We hypothesise that this may be representative of the

change in facet articulation contact during *in vivo* anterior shear motion (Figure 3.11). As this translation occurred, the volume of bone beneath the loading pin decreased until fracture occurred through the facet tip (13/13 specimens) (Figure 3.11). This fracture location is consistent with that described in radiographic reports of CFD (Allen et al., 1982). In contrast, for most specimens (6/11) that were failed in the simulated compressive-flexion orientation, the point of contact of the loading pin remained constant, and failure occurred through the pedicles or the facet base (Figure 3.11, Table 3.1). In the two specimens that fractured through the facet tip in the compressive-flexion loading direction, substantial translation of the loading pin was observed (similar to that observed for the anterior-shear loading mode), and the corresponding failure loads were lower than the other compressive-flexion specimens. The failure loads for pedicle fractures observed in the present study were considerably lower than those recorded for the lumbar spine (Cyron et al., 1976), likely due to the smaller size of the cervical vertebrae. No similar data exists for the cervical posterior elements, or for facet tip fractures. Facet tip, and facet base and pedicle fractures are commonly observed clinically, and correspond to AOSpine subaxial cervical spine facet injury classifications F2 and F3, respectively (Vaccaro et al., 2016).

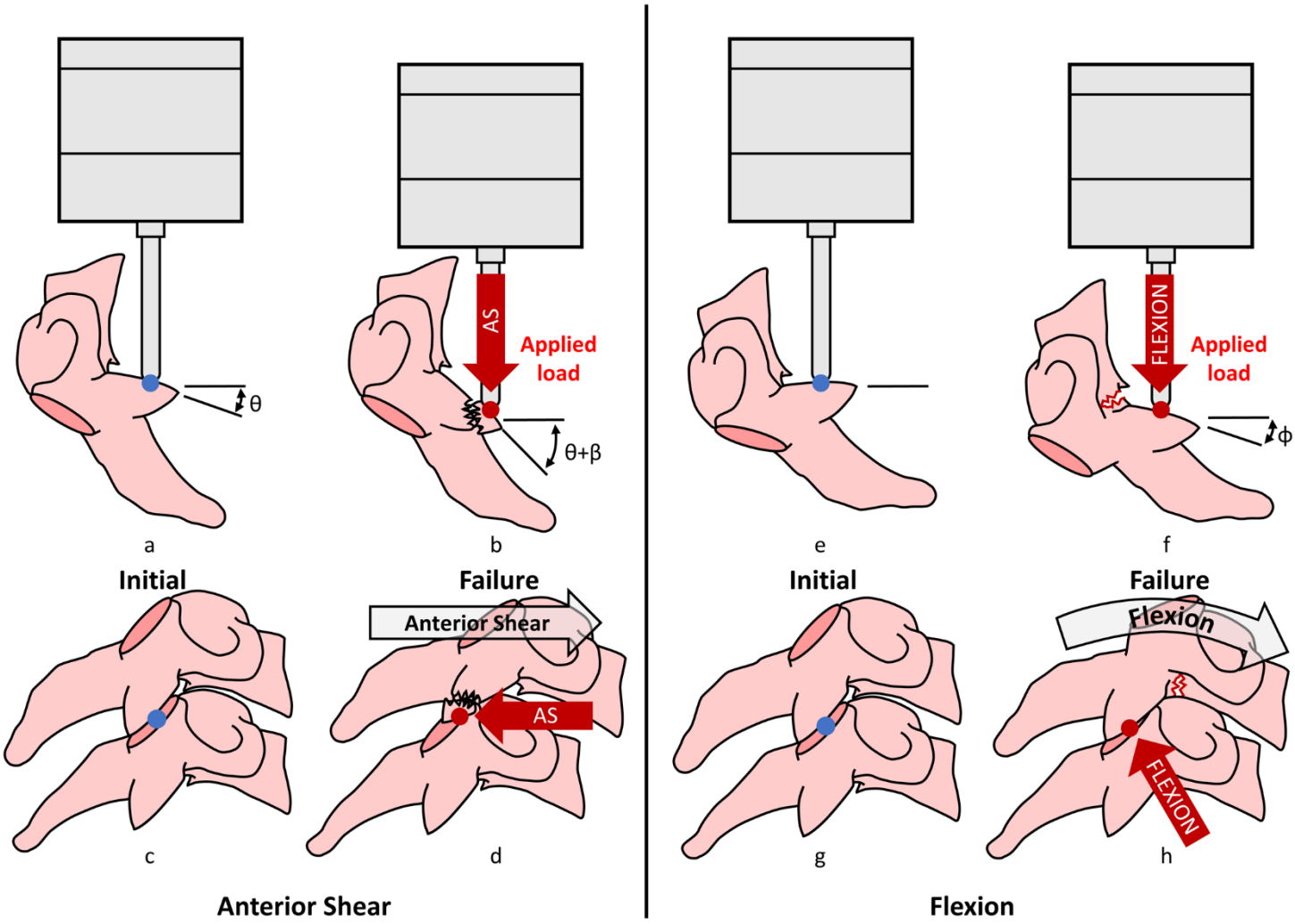

Figure 3.11: Illustrations of the failure mechanisms observed for the anterior shear (a & b) and flexion (e & f) test directions, and the proposed equivalent *in vivo* loading environments (c & d, and g & h, respectively). In both testing orientations, the initial point of contact was the geometric centre of the articular surface, to replicate the centre of pressure in the normal facet joint (blue dots; a, c, e & g). During testing in the simulated anterior shear direction the facets deflected away from the load vector (angle β, b) and the point of contact translated inferiorly towards the facet tip (red dots, b & d) until fracture occurred. In contrast, the contact location remained constant for a majority of specimens tested to failure under simulated compressive-flexion, causing bending to occur about the pedicles (angle φ, f) through which fracture occurred for 6 specimens (f & h). AS = anterior shear.

The information presented in the current study may assist with developing improved computational models of cervical spinal motion and trauma. The non-destructive results suggest that the stiffness and strain responses of the posterior elements in the upper and lower subaxial regions should be considered independently when modelling the cervical spine. For example, the final multivariable LMM (Table 3.2) indicates that maximum principal strains observed at the C6 and C7 facet bases during sub-failure loading will be significantly larger than those experienced in the upper cervical spine. Gender, vertebral size, or vBMD were significant variables in six of

the eight LMMs (Table 3.2 and Table 3.3), indicating that these specimen-specific parameters are important to consider when developing and validating computational models concerned with the cervical facets.

Substantial off-axis shear loads were observed during the anterior shear tests, due to the inclined angle of the facets in this specimen orientation. We chose to define outcome measures for each loading direction at an equivalent applied load (disregarding the off-axis loads), as this may be most useful for validation of computational models; however, the presence of these shear loads may be important to describe the dynamic facet loads experienced during cervical trauma. The off-axis loads recorded at the non-destructive analysis time-point, and at the point of initial failure, are reported in Table 3.6 in Section 3.6. Additionally, the non-destructive analysis was repeated using outcome measures determined at an equivalent resultant sagittal load ($\sqrt{[\text{axial load}^2 + \text{shear load}^2]}$) of 60 N (the highest resultant load reached by all specimens). The results of this analysis were the same for all outcome measures except maximum principal strain, in which the test direction*spinal level interaction was significant (Table 3.8 in Section 3.6).

Physiological boundary conditions are an important consideration of biomechanical testing. 'Support bar type' was significant in 50% of the final LMMs and was associated with three of the four destructive outcome measures (Table 3.2 and Table 3.3), demonstrating that minor variations in boundary conditions significantly influenced the measured facet response. This *ex vivo* model included the superior adjacent vertebra to provide a boundary condition for the loaded posterior elements. Pilot testing demonstrated that facets were stiffer, and deflections were smaller, when the superior adjacent facets were present, rather than resected. However, we did not apply a boundary condition to the inferior vertebral endplate to replicate the opposing vertebral body at the level of injury. We believe that such a boundary condition may influence the failure mechanisms, as the vertebral body and intervertebral disc may restrict large flexion motions (Allen et al., 1982).

To permit the same loading method for both test directions, hemispherical loading pins were used to apply quasi-static point loads to the facets; however, this may not be not representative of *in vivo* facet loading conditions. Point loading may have induced higher stresses at the point of application leading to the 'punctured' facets that occurred in three specimens (these specimens were excluded from failure analysis), although two of these specimens also had the lowest vBMD values. The quasi-static loading rates applied in this study are lower than the 3 m/s thought necessary to cause cervical injury due to head-impact loading (McElhaney et al., 1979; Nightingale et al., 1996; Van Toen et al., 2014); however, these rates permitted accurate control of the test machine during non-destructive testing, and ensured that sufficient motion capture data was acquired during the failure tests. Importantly, clinically relevant fractures were observed for most specimens.

This study provides information about the mechanical response of the subaxial cervical inferior facets when loaded in directions that simulate the injury mechanisms of bilateral facet dislocation. When loaded in compressive-flexion, apparent stiffness and failure load of the cervical facets were greater, which corresponded to larger sagittal angular deflections and higher sub-failure surface strains when compared to the anterior shear loading direction. The stiffness and strain responses differed between the upper and lower subaxial cervical regions, and most outcome measures were significantly associated with donor gender, specimen size or bone quality. Facet fractures occurred in all specimens that were loaded to failure in anterior shear, while fractures through the pedicles were most common for the destructive compressive-flexion tests. The data reported may be used to validate and inform computational models of cervical trauma, and could assist with developing cervical injury tolerances for ATDs with instrumented posterior elements.

3.5 Supplementary material – Final linear mixed-effects models and post-hoc analysis results

Table 3.2: Final multivariable linear mixed-effects models for non-destructive test outcomes.

Log-transformed apparent facet stiffness (N/mm):				
	Estimated Marginal Means (95% CI)			
Variable	*Anterior shear*	*Flexion*	*p-Value*	*Exp. estimate (Exp. 95% CI)*
Test Direction[a] * Spinal level			**0.007**	
C3	83.68 (60.70, 115.24)	304.60 (221.19, 419.47)	0.134	0.51 (0.29, 0.91)
C4	82.76 (58.56, 116.98)	293.54 (207.68, 414.88)	0.204	0.52 (0.28, 0.96)
C5	66.35 (48.91, 89.92)	312.00 (230.21, 422.84)	0.099	0.39 (0.22, 0.70)
C6	119.70 (89.84, 159.33)	231.13 (173.64, 307.97)	0.773	0.96 (0.55, 1.67)
C7†	117.80 (86.92, 159.49)	217.89 (160.93, 295.30)	-	-
vBMD	α	α	**0.043**	1.0014 (1.0000, 1.0028)
Support bar type			**0.002**	
Type 1	α	α	**0.004**	0.62 (0.46, 0.84)
Type 2	α	α	0.570	0.91 (0.64, 1.29)
Type 3†	α	α	-	-

[a]Reference = flexion; † indicates reference category; α indicates purposely empty Estimated Marginal Mean (EMM) cell. EMMs are only presented for the a priori independent variable 'Test direction' or its interactions.

Log-transformed maximum principal strain (με):				
	Estimated Marginal Means (95% CI)			
Variable	*Anterior shear*	*Flexion*	*p-Value*	*Exp. estimate (Exp. 95% CI)*
Test direction[a]	100 (80, 126)	58 (46, 73)	**<0.001**	1.74 (1.39, 2.16)
Gender[b]	α	α	**0.012**	1.77 (1.15, 2.73)
Vertebral body depth	α	α	**0.017**	1.15 (1.03, 1.28)

[a]Reference = flexion; [b]Reference = Male; α indicates purposely empty Estimated Marginal Mean (EMM) cell. EMMs are only presented for the a priori independent variable 'Test direction' or its interactions.

Log-transformed maximum shear strain (με):				
	Estimated Marginal Means (95% CI)			
Variable	*Anterior shear*	*Flexion*	*p-Value*	*Exp. estimate (Exp. 95% CI)*
Test direction[a]	149 (118, 188)	79 (62, 99)	**<0.001**	1.90 (1.59, 2.26)
Spinal level			**0.001**	
C3	109 (67, 178)	57 (35, 94)	**0.016**	0.42 (0.21, 0.84)
C4	58 (33, 99)	31 (18, 52)	**0.000**	0.22 (0.11, 0.46)
C5	182 (112 297)	96 (59 157)	0.300	0.70 (0.35, 1.40)
C6	248 (157, 391)	131 (83, 206)	0.888	0.96 (0.49, 1.85)
C7†	259 (158, 425)	137 (83, 224)	-	-
Gender[b]	α	α	**0.006**	1.89 (1.22, 2.94)

[a]Reference = flexion; [b]Reference = Male; † indicates reference category; α indicates purposely empty Estimated Marginal Mean (EMM) cell. EMMs are only presented for the a priori independent variable 'Test direction' or its interactions.

Sagittal facet deflection (°):				
	Estimated Marginal Means (95% CI)			
Variable	*Anterior shear*	*Flexion*	*p-Value*	*Estimate (95% CI)*
Test direction[a]	0.203 (0.177, 0.230)	0.163 (0.136, 0.189)	**0.009**	0.041 (0.011, 0.070)
vBMD	α	α	**0.022**	-4.26E-4 (-7.84E-4, 0.000)

[a]Reference = flexion; α indicates purposely empty Estimated Marginal Mean (EMM) cell. EMMs are only presented for the a priori independent variable 'Test direction' or its interactions.

Table 3.3: Final multivariable linear mixed-effects models for failure test outcomes.

Log-transformed failure load (N):				
	Estimated Marginal Means (95% CI)			*Exp. estimate*
Variable	*Anterior shear*	*Flexion*	*p-Value*	*(Exp 95% CI)*
Test direction[a]	415.30 (341.38, 505.22)	735.83 (617.08, 877.43)	**0.001**	0.56 (0.42, 0.75)
vBMD	α	α	**0.009**	1.002 (1.001, 1.004)
Support bar type			**0.011**	
Type 1	α	α	**0.004**	0.57 (0.40, 0.82)
Type 2	α	α	0.147	0.79 (0.57, 1.10)
Type 3[†]	α	α	-	-

[a]Reference = flexion; [†] indicates reference category; α indicates purposely empty Estimated Marginal Mean (EMM) cell. EMMs are only presented for the a priori independent variable 'Test direction' or its interactions.

Maximum principal strain (με):				
	Estimated Marginal Means (95% CI)			
Variable	*Anterior shear*	*Flexion*	*p-Value*	*Estimate (95% CI)*
Test direction[a]	2556 (1522, 3591)	2878 (1928, 3828)	0.566	-321.85 (-1513.64, 869.94)
vBMD	α	α	**0.043**	8.48 (0.30, 16.65)
Support bar type			**0.042**	
Type 1	α	α	0.949	-57.86 (-1925.91, 1810.20)
Type 2	α	α	**0.039**	-1531.88 (-2971.66, -92.10)
Type 3[†]	α	α	-	-

[a]Reference = flexion; [†] indicates reference category; α indicates purposely empty Estimated Marginal Mean (EMM) cell. EMMs are only presented for the a priori independent variable 'Test direction' or its interactions.

Maximum shear strain (με):				
	Estimated Marginal Means (95% CI)			
Variable	*Anterior shear*	*Flexion*	*p-Value*	*Estimate (95% CI)*
Test direction[a]	6041 (4057, 8025)	4632 (2722, 6541)	0.164	1409.07 (-669.13, 3487.27)
Support bar type			**0.007**	
Type 1	α	α	0.560	984.89 (-2496.40, 4466.18)
Type 2	α	α	**0.018**	-3288.13 (-5913.03, -663.24)
Type 3[†]	α	α	-	-

[a]Reference = flexion; [†] indicates reference category; α indicates purposely empty Estimated Marginal Mean (EMM) cell. EMMs are only presented for the a priori independent variable 'Test direction' or its interactions.

Sagittal facet deflection (°):				
	Estimated Marginal Means (95% CI)			
Variable	*Anterior shear*	*Flexion*	*p-Value*	*Estimate (95% CI)*
Test direction[a]	2.961 (1.790, 4.132)	5.260 (4.017, 6.502)	**0.001**	-2.299 (-3.516, -1.082)

[a]Reference = flexion; a indicates purposely empty Estimated Marginal Mean (EMM) cell. EMMs are only presented for the a priori independent variable 'Test direction' or its interactions.

Table 3.4: Post-hoc analysis of the test direction*spinal level interaction identified in the final multivariable linear mixed-effects model for log-transformed apparent facet stiffness – comparison between test directions at each spinal level.

Spinal level	Mean difference, anterior shear-flexion (95% CI)*	p-Value
C3	-1.292 (-1.701, -0.883)	**<0.001**
C4	-1.266 (-1.715, -0.818)	**<0.001**
C5	-1.549 (-1.958, -1.139)	**<0.001**
C6	-0.659 (-1.038, -0.280)	**0.001**
C7	-0.616 (-1.025, -0.206)	**0.005**

**Based on Estimated Marginal Means.*

Table 3.5: Post-hoc analysis of the test direction*spinal level interaction identified in the final multivariable linear mixed-effects model for log-transformed apparent facet stiffness – comparison between spinal levels for each test direction.

Test direction	Spinal level (I)	Spinal level (J)	Mean difference I-J (95% CI)*	p-Value
Anterior shear	C3	C4	0.011 (-0.440, 0.462)	0.961
		C5	0.232 (-0.198, 0.662)	0.283
		C6	-0.358 (-0.787, 0.072)	0.100
		C7	-0.342 (-0.784, 0.100)	0.126
	C4	C3	-0.011 (-0.462, 0.440)	0.961
		C5	0.221 (-0.230, 0.672)	0.329
		C6	-0.369 (-0.822, 0.084)	0.108
		C7	-0.353 (-0.818, 0.112)	0.133
	C5	C3	-0.232 (-0.662, 0.198)	0.283
		C4	-0.221 (-0.672, 0.230)	0.329
		C6	-.590 (-1.005, -0.175)	**0.006**
		C7	-.574 (-1.003, -0.146)	**0.010**
	C6	C3	0.358 (-0.072, 0.787)	0.100
		C4	0.369 (-0.084, 0.822)	0.108
		C5	.590 (0.175, 1.005)	**0.006**
		C7	0.016 (-0.394, 0.426)	0.939
	C7	C3	0.342 (-0.100, 0.784)	0.126
		C4	0.353 (-0.112, 0.818)	0.133
		C5	.574 (0.146, 1.003)	**0.010**
		C6	-0.016 (-0.426, 0.394)	0.939
Flexion	C3	C4	0.037 (-0.414, 0.487)	0.870
		C5	-0.024 (-0.454, 0.406)	0.909
		C6	0.275 (-0.154, 0.705)	0.203
		C7	0.334 (-0.107, 0.776)	0.134
	C4	C3	-0.037 (-0.487, 0.414)	0.870
		C5	-0.061 (-0.512, 0.390)	0.786
		C6	0.239 (-0.214, 0.691)	0.294
		C7	0.298 (-0.167, 0.762)	0.204
	C5	C3	0.024 (-0.406, 0.454)	0.909
		C4	0.061 (-0.390, 0.512)	0.786
		C6	0.300 (-0.115, 0.715)	0.152
		C7	0.359 (-0.070, 0.788)	0.099
	C6	C3	-0.275 (-0.705, 0.154)	0.203
		C4	-0.239 (-0.691, 0.214)	0.294
		C5	-0.300 (-0.715, 0.115)	0.152
		C7	0.059 (-0.351, 0.469)	0.773
	C7	C3	-0.334 (-0.776, 0.107)	0.134
		C4	-0.298 (-0.762, 0.167)	0.204
		C5	-0.359 (-0.788, 0.070)	0.099
		C6	-0.059 (-0.469, 0.351)	0.773

**Based on estimated marginal means.*

3.6 Supplementary material – Off-axis 'shear' loads

Table 3.6: Off-axis 'shear' loads observed at 47 N of nominal applied load during non-destructive tests, and at point of initial failure during destructive tests. Vertebral body (VB) depth, average left and right facet angle measurements, and the type of support bar used are also shown. Dashes indicate that failure data was not available. Test 1 was omitted due to technical difficulties.

Test #	Specimen ID	Spinal level	VB depth (mm)	Mean facet angle (deg)	Support bar	Failure test direction	Off-axis shear load (Non-destructive tests, N)		Fail. shear load (N)
							Anterior shear	Flexion	
2	H023	C6	21.24	138.61	1	-	19.96	-4.84	-
3	H001	C3	18.29	121.90	1	AS	24.03	1.75	-168.93
4	H001	C5	22.62	138.99	1	-	21.55	2.08	-
5	H001	C7	20.15	119.59	1	AS	9.81	-1.89	-139.68
6	H027	C4	15.00	124.54	1	AS	30.17	5.12	-234.25
7	H012	C3	22.67	133.61	1	Flexion	31.08	0.36	-110.43
8	H027	C6	16.60	125.84	1	AS	14.16	1.82	-75.80
9	H012	C5	20.21	134.51	1	AS	21.31	2.13	-129.45
10	H012	C7	19.66	125.88	1	AS	8.53	2.99	-79.88
11	H017	C5	17.38	140.13	1	AS	34.12	7.97	-77.91
12	H017	C3	17.26	138.94	1	-	36.60	2.43	-
13	H006	C4	16.23	137.15	1	-	32.28	4.16	-
14	H032	C7	17.19	137.37	1	Flexion	41.24	4.06	-152.90
15	H032	C3	17.19	133.01	1	AS	27.88	5.29	-215.56
16	H006	C6	17.38	134.08	1	-	18.70	5.82	-
17	H032	C5	17.52	147.97	2	-	41.62	0.74	-
18	H045	C6	16.64	126.87	1	AS	11.53	0.45	-123.37
19	H045	C4	15.61	132.34	2	AS	20.87	1.19	-220.63
20	H039	C7	16.78	134.28	3	Flexion	7.38	-2.29	-25.87
21	H039	C5	15.57	146.56	3	Flexion	23.32	-1.03	-17.15
22	H039	C3	16.02	131.14	2	AS	23.10	2.34	-236.74
23	H018	C5	17.10	145.41	2	Flexion	43.99	1.03	-55.37
24	H018	C7	18.86	122.30	2	AS	12.15	-1.54	-198.51
25	H018	C3	18.52	131.14	2	Flexion	8.29	-1.22	-45.47
26	H026	C6	18.43	132.82	3	AS	12.82	4.44	-61.32
27	H026	C4	18.58	142.66	2	Flexion	23.64	0.09	-91.02
28	H021	C4	17.09	132.65	2	Flexion	17.91	-0.07	-53.61
29	H021	C6	17.85	124.92	3	Flexion	5.59	-1.09	-46.68
30	H044	C7	20.35	133.51	3	Flexion	9.58	-0.32	-28.21
31	H028	C6	19.71	125.17	2	Flexion	24.77	7.34	-101.46

AS = anterior shear.

Table 3.7: Sagittal load angle (relative to direction of nominal applied load) at non-destructive resultant load analysis time-point (60N).

			Sagittal resultant load angle (deg)	
Test #	**Specimen ID**	**Spinal level**	**Anterior shear**	**Flexion**
2	H023	C6	22.0	-4.8
3	H001	C3	27.2	2.5
4	H001	C5	25.1	2.9
5	H001	C7	12.1	-1.8
6	H027	C4	32.1	6.3
7	H012	C3	33.1	0.4
8	H027	C6	16.7	2.2
9	H012	C5	24.2	2.7
10	H012	C7	10.8	3.8
11	H017	C5	35.2	10.1
12	H017	C3	37.8	3.1
13	H006	C4	34.2	5.1
14	H032	C7	40.9	5.4
15	H032	C3	29.9	6.6
16	H006	C6	21.9	7.3
17	H032	C5	42.3	0.9
18	H045	C6	13.9	0.7
19	H045	C4	23.8	1.6
20	H039	C7	8.5	-2.8
21	H039	C5	25.1	-1.1
22	H039	C3	26.2	2.7
23	H018	C5	43.2	1.4
24	H018	C7	15.6	-1.7
25	H018	C3	10.2	-1.6
26	H026	C6	15.8	6.2
27	H026	C4	25.5	0.5
28	H021	C4	21.0	0.0
29	H021	C6	7.8	-1.4
30	H044	C7	11.3	-0.3
31	H028	C6	27.3	8.8

Table 3.8: Final multivariable linear mixed-effects models for outcomes from the non-destructive resultant sagittal load analysis (60N).

Log-transformed apparent facet stiffness (N/mm):				
	Estimated Marginal Means (95% CI)			
Variable	*Anterior shear*	*Flexion*	*p-Value*	*Exp. estimate (Exp. 95% CI)*
Test direction[a] * Spinal level			**0.010**	
C3	80.96 (57.69, 113.64)	300.37 (214.01, 421.58)	**0.021**	0.50 (0.28, 0.89)
C4	90.20 (62.55, 130.06)	292.66 (202.96, 422.00)	0.069	0.57 (0.31, 1.05)
C5	70.25 (50.96, 96.83)	307.97 (223.41, 424.54)	**0.005**	0.42 (0.23, 0.75)
C6	127.61 (94.35, 172.60)	235.57 (173.99, 318.62)	0.994	1.00 (0.57, 1.76)
C7[†]	117.80 (85.54, 162.23)	217.02 (157.43, 298.87)	-	-
vBMD	α	α	**0.042**	1.0015 (1.0001, 1.0030)
Support bar type			**0.002**	
Type 1	α	α	**0.004**	0.59 (0.43, 0.83)
Type 2	α	α	0.455	0.87 (0.60, 1.27)
Type 3[†]	α	α	-	-

[a]Reference = flexion; [†] indicates reference category; α indicates purposely empty Estimated Marginal Mean (EMM) cell. EMMs are only presented for the a priori independent variable 'Test direction' or its interactions.

Log-transformed maximum principal strain (με):				
	Estimated Marginal Means (95% CI)			
Variable	*Anterior shear*	*Flexion*	*p-Value*	*Exp. estimate (Exp. 95% CI)*
Test direction[a] * Spinal level			**0.043**	
C3	63 (40, 102)	77 (48, 124)	**0.031**	0.51 (0.28, 0.94)
C4	97 (56, 167)	64 (37, 110)	0.846	0.94 (0.50, 1.77)
C5	142 (88, 227)	71 (44, 113)	0.458	1.25 (0.68, 2.28)
C6	180 (116, 278)	98 (64, 152)	0.650	1.14 (0.64, 2.04)
C7[†]	145 (90, 234)	90 (56, 145)	-	-
Gender[b]	α	α	**0.003**	1.95 (1.30, 2.93)
Vertebal body depth	α	α	**0.034**	1.13 (1.01, 1.26)

[a]Reference = flexion; [b]Reference = Male; [†] indicates reference category; α indicates purposely empty Estimated Marginal Mean (EMM) cell. EMMs are only presented for the a priori independent variable 'Test direction' or its interactions.

Log-transformed maximum shear strain (με):				
	Estimated Marginal Means (95% CI)			
Variable	*Anterior shear*	*Flexion*	*p-Value*	*Exp. estimate (Exp. 95% CI)*
Test direction[a]	178 (140, 225)	106 (83, 134)	**<0.001**	1.68 (1.40, 2.02)
Spinal level			**0.001**	
C3	α	α	**0.012**	0.39 (0.19, 0.80)
C4	α	α	**<0.001**	0.22 (0.10, 0.46)
C5	α	α	0.236	0.66 (0.33, 1.34)
C6	α	α	0.930	0.97 (0.49, 1.91)
C7[†]	α	α	-	-
Gender[b]	α	α	**0.006**	1.93 (1.23, 3.02)

[a]Reference = flexion; [b]Reference = Male; [†] indicates reference category; α indicates purposely empty Estimated Marginal Mean (EMM) cell. EMMs are only presented for the a priori independent variable 'Test direction' or its interactions.

Sagittal facet deflection (°):

	Estimated Marginal Means (95% CI)			
Variable	*Anterior shear*	*Flexion*	*p-Value*	*Estimate (95% CI)*
Test direction[a]	0.250 (0.219, 0.281)	0.211 (0.180, 0.241)	**0.024**	0.040 (0.006, 0.074)
vBMD	α	α	**0.017**	-5.25E-4 (-9.49E-4, 0.000)

[a]Reference = flexion; α indicates purposely empty Estimated Marginal Mean (EMM) cell. EMMs are only presented for the a priori independent variable 'Test direction' or its interactions.

Statement of Authorship – Chapter 4

Title of Paper	The effect of axial compression and distraction on cervical facet mechanics during anterior shear, flexion, axial rotation, and lateral bending motions
Publication Status	☐ Published ☐ Accepted for Publication ☑ Submitted for Publication ☐ Unpublished and Unsubmitted work written in manuscript style
Publication Details	Quarrington, R.D., Costi, J.J., Freeman, B.J.C., Jones, C.F. The effect of axial compression and distraction on cervical facet mechanics during anterior shear, flexion, axial rotation, and lateral bending motions. Journal of Biomechanics.

Principal Author

Name of Principal Author (Candidate)	Ryan Quarrington		
Contribution to the Paper	Developed testing methods, performed testing of all specimens, performed all data analysis, interpreted data, wrote manuscript and acted as corresponding author.		
Overall percentage (%)	80%		
Certification:	This paper reports on original research I conducted during the period of my Higher Degree by Research candidature and is not subject to any obligations or contractual agreements with a third party that would constrain its inclusion in this thesis. I am the primary author of this paper.		
Signature		Date	01/06/2018

Co-Author Contributions

By signing the Statement of Authorship, each author certifies that:

i. the candidate's stated contribution to the publication is accurate (as detailed above);
ii. permission is granted for the candidate in include the publication in the thesis; and
iii. the sum of all co-author contributions is equal to 100% less the candidate's stated contribution.

Name of Co-Author	John Costi		
Contribution to the Paper	Supervised development of work, assisted with data interpretation, and reviewed manuscript.		
Signature		Date	14/06/2018

Name of Co-Author	Brian Freeman		
Contribution to the Paper	Supervised development of work and reviewed manuscript.		
Signature		Date	14/06/2018

Name of Co-Author	Claire Jones		
Contribution to the Paper	Supervised study design and development of work, assisted with data interpretation, and reviewed manuscript.		
Signature		Date	5/06/2018

Chapter 4 The effect of axial compression and distraction on cervical facet mechanics during anterior shear, flexion, axial rotation, and lateral bending motions[1]

4.1 Introduction

The primary function of the cervical spine is to support and orientate the head. This function is facilitated by the anatomy of the vertebral body and facet joints, and the surrounding ligaments and musculature. In the subaxial cervical spine, intervertebral kinematics are predominantly dictated by the facet joints, where contact between articulating facets prevents excessive axial rotation, lateral bending and anterior shear (Bogduk and Mercer, 2000). The geometry of the cervical facets is responsible for coupled motions in axial rotation and lateral bending, and is related to the instantaneous axes of rotation observed in the subaxial cervical spine (Bogduk and Mercer, 2000; Nowitzke et al., 1994). In addition, the facet joints bear up to 64% of the axial load in the neutral cervical spine (Pal and Sherk, 1988) and this proportion increases during physiological motion (Panzer and Cronin, 2009). Facet fracture is frequently associated with other cervical injuries (Dvorak et al., 2007), suggesting that high loads are transferred through these joints during trauma.

Despite their important role in cervical kinematics and load-bearing, little is known about the mechanical response of the cervical facets during physiological or non-physiological intervertebral motion. Facet surface strains have been measured during non-traumatic anterior shear motion of cervical functional spinal units (FSUs) (Cripton, 1999), but have not been reported for other intervertebral motions. In a recent study, surface strain, deflection, stiffness and failure load of the subaxial inferior facets were quantified during uni-axial loading that simulated *physiologic* intervertebral flexion and anterior shear motions (Quarrington et al., 2018a) (Chapter 3); however, point loads were applied to the articular facet surfaces, which may

[1] A version of Chapter 4 has been accepted for publication in Journal of Biomechanics. Quarrington, R.D., Costi, J.J., Freeman, B.J.C., Jones, C.F. *The effect of axial compression and distraction on cervical facet mechanics during anterior shear, flexion, axial rotation, and lateral bending motions*.

not accurately represent *in vivo* conditions. The response of the cervical facets to *axial rotation* and *lateral bending* has not been investigated. Such measures are required for the validation of computational models of physiological cervical spine motion and to improve fundamental understanding of cervical spine biomechanics.

The biomechanics of the cervical facets during non-physiological cervical motion have not been investigated. Facet fractures are associated with up to 70% of cervical facet dislocations (CFD) (Anissipour et al., 2017; Dvorak et al., 2007); however, facet fracture has not been reported during the experimental production of CFD in cadavers. This may be due to a lack of muscle forces, restricting intervertebral separation (Foster et al., 2012).

CFD was produced in FSUs by applying incrementally increasing sagittal decelerations (Ivancic et al., 2007, 2008; Panjabi et al., 2007). Rupture of the posterior ligaments and facet capsules *prior* to the final impact event was required, which may have permitted excessive separation of the intervertebral joints and allowed the facets to dislocate with minimal contact. A similar mechanism for producing dislocation without facet-fracture is commonly reported, in which *local* intervertebral distraction and flexion of the posterior elements is produced by *global* axial compressive forces with large anterior eccentricity (Allen et al., 1982; Cusick and Yoganandan, 2002; Huelke and Nusholtz, 1986; White and Panjabi, 1990). Such a mechanism would cause early failure of the posterior ligaments, permitting dislocation of the facets without fracture. Non-physiological intervertebral distraction may reduce loading of the facets during the intervertebral motions commonly associated with CFD, reducing the likelihood of concomitant facet fracture, but this is yet to be investigated experimentally.

CFDs have also been produced in the lower cervical spine during head-first impact tests. These injuries were associated with local *compressive,* rather than *distractive,* axial forces (Hodgson and Thomas, 1980; Ivancic, 2012a; Nightingale et al., 1996), but no facet fractures were created. This may be due to an absence of neck muscle replication (Foster et al., 2012; Hu et al., 2008). Neck muscle activation prior to a potentially injurious event (i.e. bracing for impact)

may impose an additional intervertebral compressive load during injury that restricts pathological flexion and intervertebral distraction, causing increased loading of the facets. Such muscle forces increase peak compressive and shear forces in the lower cervical spine, when compared to no muscle activation, in computer simulated head-impact tests (Nightingale et al., 2016). The effect of axial compression versus distraction on loading of the facets during intervertebral motion has not previously been reported.

The aim of this study was to quantify the mechanical response of the C6 inferior facets in C6/C7 FSUs during constrained, non-destructive, quasi-static anterior shear, axial rotation, lateral bending, and flexion motions (within physiological limits), and to determine the effect of intervertebral axial distraction and compression when imposed on these motions. We hypothesise that axial compression will increase loading of the facets (as measured by deflection and surface strain) when superimposed on shear, bending and rotation motions.

4.2 Methods

4.2.1 Specimen preparation

Cervical motion segments (C5-T1 or C6/C7) were dissected from twelve fresh-frozen human cadavers (mean donor age 70±13 years, range 46-88; nine male) and non-osteoligamentous tissue was removed. High-resolution computed tomography (CT) scans (SOMATOM Force, Siemens, Erlangen, Germany; 0.23×0.23×0.4 mm voxel size) were obtained and each specimen was screened for excessive degeneration, injury or disease by a senior spinal surgeon. Mean volumetric bone mineral density (vBMD) of the anterior third of the C6 and C7 vertebral bodies was determined using a calibration phantom (Mindways Software Inc., Texas, USA) and image analysis software (FIJI 1.51p, ImageJ, Maryland, USA) (Schindelin et al., 2012). Vertebral endplate depths, and facet heights and sagittal angles, were also measured using FIJI.

For Tests #1-5, the distal levels of C5-T1 motion segments were augmented with screws/wire to assist with fixation in blocks of polymethylmethacrylate (PMMA; Vertex Dental, Utrecht, Netherlands). For Tests #6-12, the exposed endplates and posterior elements of C6/C7

FSUs were similarly augmented, and the distal third of each vertebra were embedded with the disc orientated horizontally and the centre aligned with the geometric centre of the mold. All C6/C7 joints and disco-ligamentous tissues were maintained. A more detailed description of the embedding methods, and justification for changing these methods, is provided in Section 5.2.1.

A custom alignment jig ensured that specimens were consistently aligned during embedding, with 22 mm of separation between the molds and 8 mm between the inferior mold and the centre of the C6/C7 intervertebral disc (Figure 4.1); this ensured that the centre-of-rotation (CoR) of the flexion-extension axis of the test machine coincided with the CoR of C6/C7 flexion (Penning, 1960), and that the shear force and moment distribution across the intervertebral joints was consistent for all specimens.

4.2.2 Mechanical loading

Each specimen was fixed to a six-axis materials testing machine (8802, Instron, High Wycombe, UK) in an inverted posture (Figure 4.1). The mold containing the inferior vertebra was fixed to the upper flexion-extension actuator, and the superior vertebra was secured to a six-axis load cell (MC3A-6-1000 ±4.4 kN, AMTI, Massachusetts, USA) mounted on a motorised X-Y table on the base of the testing machine.

Each specimen underwent constrained, non-destructive shear and bending motions under three axial loading conditions. The 'neutral' condition replicated physiological *in vivo* loading (due to head-weight only) by applying a 50 N axial compression force (Bell et al., 2016; DiAngelo and Foley, 2004). For the 'compressed' condition, a 300 N compression force was applied to simulate the loading experienced due to neck muscle bracing; muscle activation can produce intervertebral axial compression forces between 100-1400 N (Bell et al., 2016; Chancey et al., 2003; Cripton et al., 2001; Hattori, 1981; Newell et al., 2014; Pospiech et al., 1999). The 300 N load did not produce off-axis loads exceeding the design limits of the test machine. Finally, 2.5 mm of axial distraction (relative to the neutral position) mimicked the largest non-destructive intervertebral separation previously reported for cervical motion segments (Shea et al., 1991).

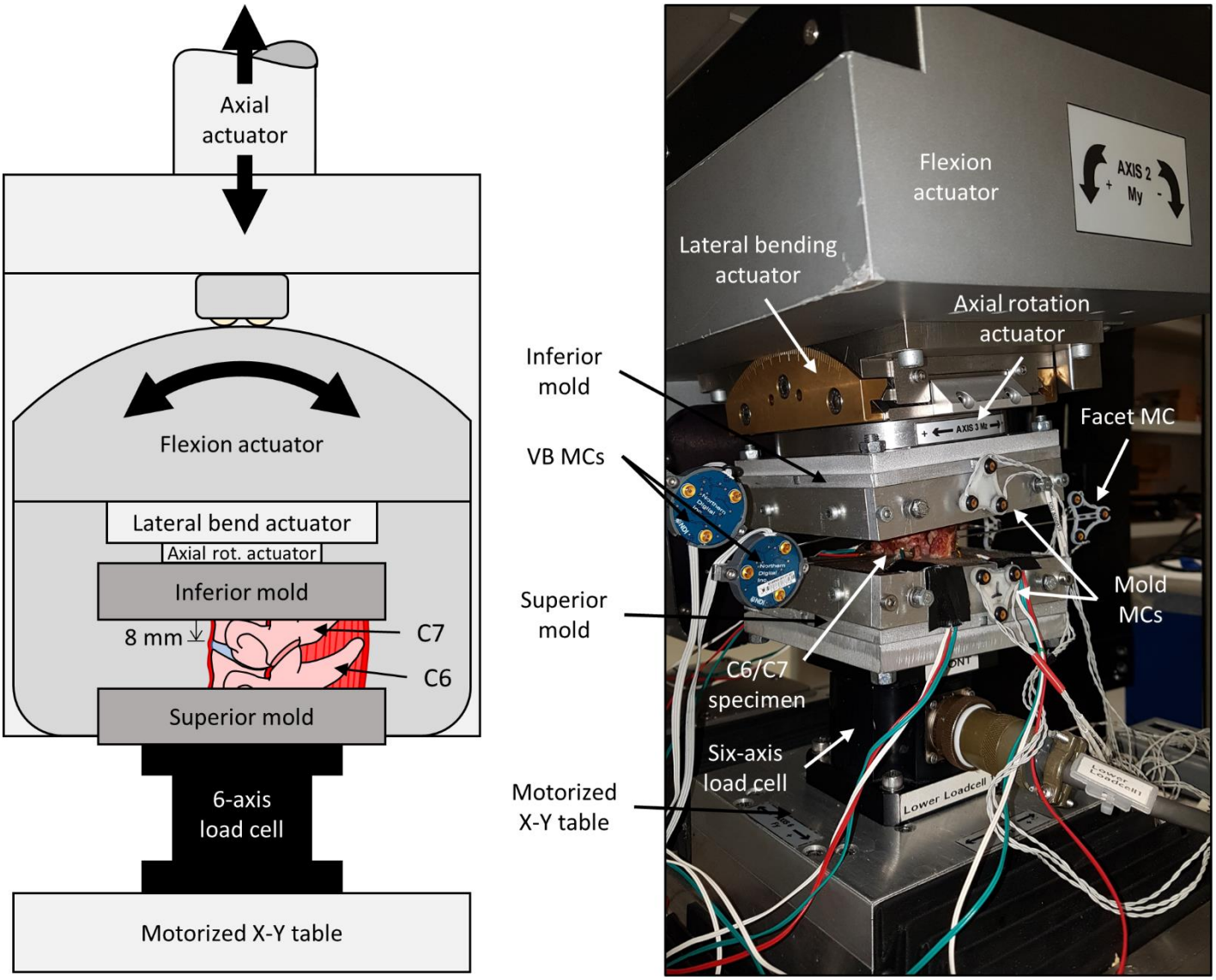

Figure 4.1: Lateral schematic of the embedded specimen attached to the six-axis testing machine in an inverted posture (left) and an oblique photo of the test setup (right). The position of the superior mold was held constant and axial rotation, flexion, and lateral bending motions were individually applied to the inferior mold by their respective rotary motors. Anterior shear motion was applied to the superior mold by the motorised X-Y table. Each motion was combined with either neutral, compressed, or distracted intervertebral separation, which was applied by the axial actuator. Six-axis forces and moments were recorded by the load-cell to which the superior mold was attached. VB = vertebral body, MC = marker carrier.

Prior to testing, the axial actuator *position* corresponding to 10 N of axial load and 0 N or Nm off-axis loads ('unloaded position'), and for each axial condition (50N, 300N, 2.5mm distraction), were recorded. The vertical actuator position of each axial condition was maintained while the specimen underwent three repetitions of constrained anterior shear (1 mm, 0.1 mm/s), flexion (10°, 1 °/s), right axial rotation (4°, 1 °/s) and left lateral bending (5°, 1 °/s); the displacement/rotation limits were based on *in vivo* ranges of motion (Lin et al., 2014; Penning

and Wilmink, 1987; Salem et al., 2013; Wu et al., 2007). The displacement rates were selected to optimise motion-capture frame rate. The order of application of the axial conditions and the motions were block randomised for each specimen. A two-second "hold" was applied at the peak of each rotation/displacement and between each motion. Specimen hydration was maintained using saline-soaked gauze and saline spray. Following completion of this non-destructive testing, each specimen was tested to failure in anterior shear in either the compressed or distracted axial condition (described in Chapter 5).

4.2.3 Instrumentation and data collection

The bases of the bilateral inferior facets of C6 were instrumented with tri-axial strain gauges (FRA-1-23-1L, TML, Tokyo, Japan). The infero-lateral corners of the C6 inferior facets were exposed by resecting a small section of the facet capsule (<3×3 mm) and light-weight motion capture marker-carriers were attached to the bone surface using cyanoacrylate adhesive (Loctite 401, Henkel, Düsseldorf, Germany) (Figure 4.2). Marker-carriers were attached to the C6 and C7 vertebral bodies with K-wires, and to the superior and inferior molds (Figure 4.1). Anatomical landmarks on the vertebral bodies and the C6 inferior facets were digitised (Figure 4.3). Loads, actuator positions, and strain gauge data were collected at 600 Hz using a data acquisition system (PXIe-1073, BNC-2120 & PXIe-4331 (x2), National Instruments, USA). Motion capture data were acquired at 200 Hz (Optotrak Certus, Northern Digital Inc., Ontario, Canada; system bias < 0.09°, precision = 0.006°).

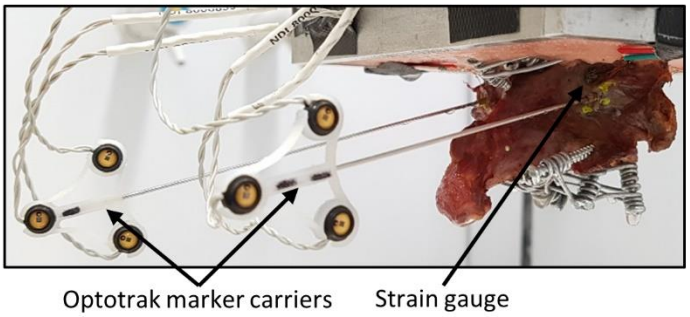

Figure 4.2: The C6 bilateral inferior facets were instrumented with triaxial rosette strain gauges and Optotrak marker-carriers prior to embedding the inferior anatomy and screw/wire constructs.

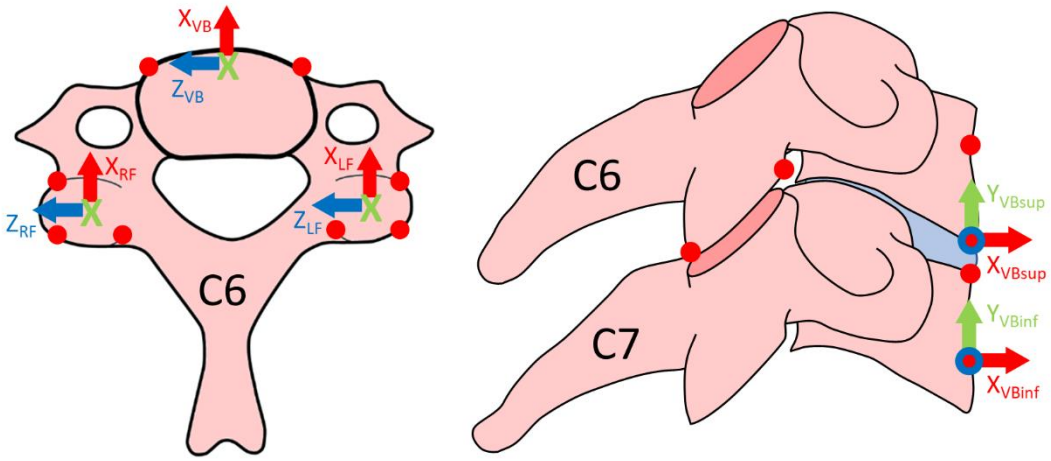

Figure 4.3: Schematics of the inferior (left) and right lateral (right) views of a C6 vertebra and C6/C7 FSU, respectively. The red circles indicate the anatomical landmarks that were digitised. The local coordinate systems are illustrated, with x-axes in red, z-axes in blue, and y-axes in green. The origin of the vertebral body was defined as the sagittal midpoint of the anterior edge of the inferior vertebral endplate. The origins of the facets were defined as the geometric centre of the articular surfaces. X indicates an axis directed into the page, while O indicates an axis directed out of the page. VB = vertebral body, RF = right facet, LF = left facet.

4.2.4 Data processing

Data were processed using custom MATLAB code (R2015a, Mathworks, Massachusetts, USA). Load, position, and strain data were filtered using a second-order, two-way Butterworth low-pass filter with a cut-off frequency of 100 Hz. Motion capture data were filtered similarly, with a cut-off frequency of 30 Hz.

Peak load (force/moment), maximum (tensile) and minimum (compressive) principal strains, shear strains, and angular facet deflections were calculated at the position limit of the last repetition, for each axial condition. Local vertebral body and facet coordinate systems were defined (Figure 4.3) (Wu et al., 2002). Sagittal, transverse, and coronal angular deflection of the

bilateral facets, relative to the vertebral body, were calculated by solving for Euler angles using a *z-y-x* sequence (Robertson et al., 2013).

4.2.5 Statistics

Statistical analyses were performed using SPSS v24 (IBM, Illinois, USA). For each motion, seven linear mixed-effects models (LMMs) were developed to identify if axial condition was significantly associated with the following outcome measures: 1) peak load; 2) maximum principal strain; 3) minimum principal strain; 4) maximum shear strain; 5) sagittal facet deflection; 6) transverse facet deflection; and, 7) coronal facet deflection. The effect of axial condition was assessed in all models, and this effect was adjusted for facet side (left vs. right), donor demographics, specimen bone mineral density, vertebral body size, facet height and angle, order of test condition and imposed axial condition, and the type of specimen (four- vs. two-vertebrae). A random effect of facet side, nested within cadaver ID, was included. Shapiro-Wilk and Levene's tests evaluated normality and homogeneity of variance of the dependent variable for each model, and statistically significant outliers were removed and/or data was log-transformed to meet these criteria. Each model was refined using a manual backward step-wise approach until only significant predictors remained (α=0.05). Bonferroni-adjusted post-hoc comparisons of estimated marginal means (EMMs) were performed for significant categorical predictors. A post-hoc power analysis confirmed that these models were suitably powered (Section 4.6.1).

4.3 Results

Demographic information and geometric measurements for the 12 specimens are provided in Table 4.1, and average load-displacement plots for each axial condition and test direction are illustrated in Figure 4.4. The neutral and compressed conditions corresponded to mean intervertebral axial compressions (relative to the unloaded position) of 0.13±0.01 and 0.62±0.06 mm, respectively, while 2.5 mm of distraction applied a mean tensile force of 456.66±50.54 N. Off-axis loads for each test direction are illustrated in Figure 4.8 to Figure 4.11 in Section 4.5. A summary of the final multivariable LMMs is presented in Table 4.2; the final

number of specimens per group, EMMs and *p*-values from post-hoc comparisons are provided in Table 4.3 to Table 4.6 in Section 4.6.

Table 4.1: Specimen details and geometry. VB = vertebral body. vBMD = volumetric K2HPO4 equivalent bone mineral density.

Test #	Specimen identifier	Sex	Age	Specimen type	Mean VB Depth (mm)	Mean vBMD (mg/cm^3)	Facet Height (mm)		Facet angle (°)	
							Left	Right	Left	Right
1	H010	M	71	Four vertebrae	16.7	138.8	9.1	9.9	114.1	114.0
2	H013	M	58	Four vertebrae	15.6	115.0	7.8	5.1	125.6	131.4
3	H014	M	58	Four vertebrae	17.4	83.6	5.4	9.7	136.0	139.1
4	H003	M	46	Four vertebrae	15.6	142.9	8.0	7.3	138.3	135.6
5	H002	F	62	Four vertebrae	16.1	216.7	8.9	11.2	135.4	133.1
6	H004	F	75	Two vertebrae	16.2	99.0	9.4	11.5	129.1	123.3
7	H036	M	58	Two vertebrae	17.2	125.5	10.3	8.1	130.2	110.3
8	H009	M	85	Two vertebrae	19.1	223.5	9.7	8.5	130.4	131.6
9	H041	M	82	Two vertebrae	15.7	74.1	6.9	8.9	117.5	132.0
10	H020	M	76	Two vertebrae	16.9	105.2	9.0	11.1	126.3	121.4
11	H033	F	88	Two vertebrae	16.6	117.1	8.6	5.7	130.9	128.5
12	H043	M	81	Two vertebrae	17.5	164.4	7.1	7.0	130.5	128.3

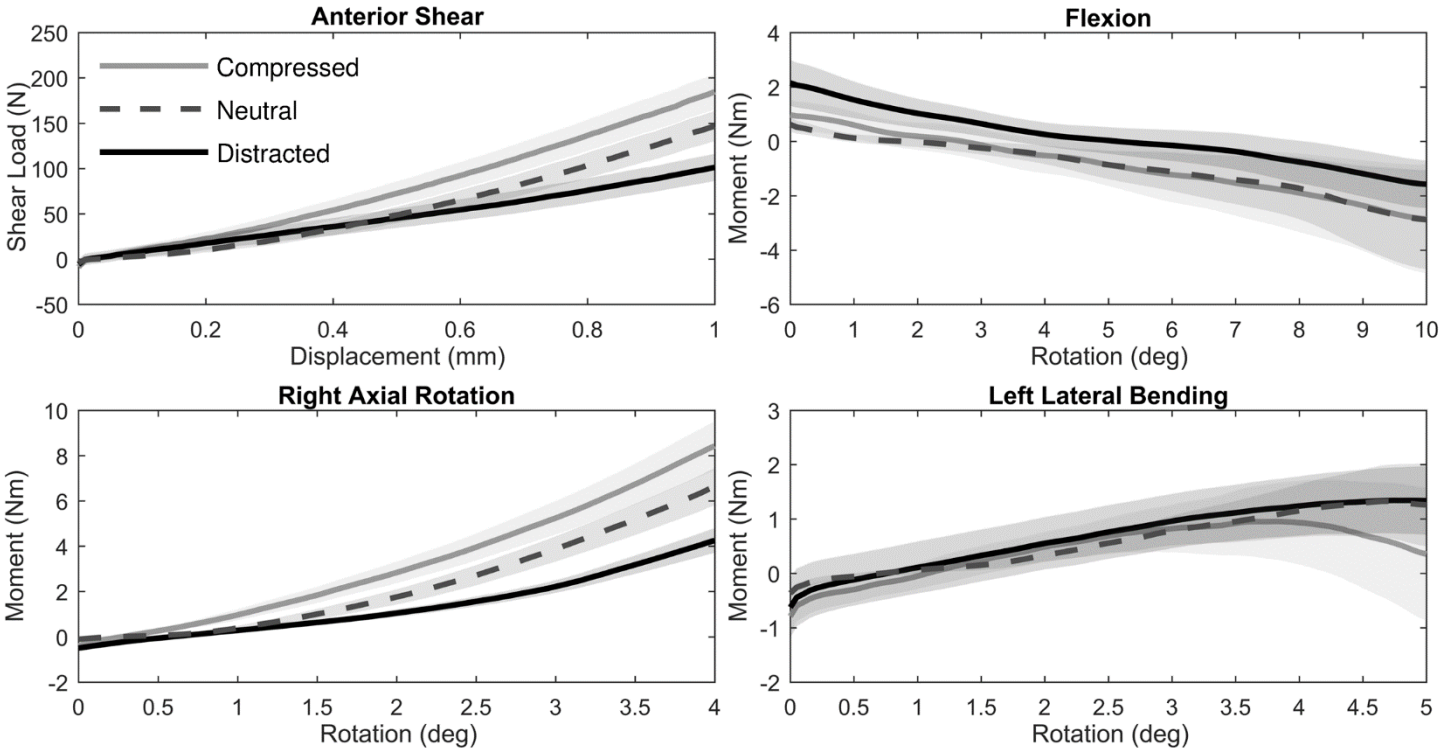

Figure 4.4: Average load-displacement/rotation plots for the loading region of each motion in each axial condition. The shaded regions indicate ±1 standard error. Superimposed axial compression increased anterior shear force and right axial rotation moment but didn't affect flexion or lateral bending moments. This may be because shear and axial rotation motions occur in the transverse plane, so axial separation is constant throughout, whereas flexion and lateral bending (with fixed CoR) inherently cause distraction/compression of the posterior/anterior and contralateral/ipsilateral anatomy, respectively.

Table 4.2: Summary of the final multivariable linear mixed-effects models for each motion. Significant p-values (α=0.05) for the axial condition variable are bolded.

Outcome variable:	Axial condition p-value:	Significant covariates:
Anterior shear		
Peak load	**<0.001**	
Maximum principal strain	0.664	
Minimum principal strain	**0.025**	
Maximum shear strain	**0.004**	Gender, axial condition order
Sagittal facet deflection	**<0.001**	Facet side, age
Transverse facet deflection	0.366	Gender, vBMD, age
Coronal facet deflection	0.742	
Flexion		
Peak load	0.298	
Maximum principal strain	0.529	Axial condition order
Minimum principal strain	**<0.001**	
Maximum shear strain	**0.039**	Facet side, vBMD, axial condition order
Sagittal facet deflection	0.447	vBMD, Facet height
Transverse facet deflection	**0.026**	
Coronal facet deflection	0.168	
Axial rotation		
Peak load	**<0.001**	
Maximum principal strain	0.074	Facet side
Minimum principal strain	0.776	Facet side, gender
Maximum shear strain	**0.002**	Age
Sagittal facet deflection	0.178	Facet side
Transverse facet deflection	0.388	Facet side, gender
Coronal facet deflection	0.868	Facet side
Lateral bending		
Peak load	0.604	
Maximum principal strain	0.277	
Minimum principal strain	**<0.001**	
Maximum shear strain	**0.016**	
Sagittal facet deflection	**0.034**	Facet side, axial condition order
Transverse facet deflection	0.946	
Coronal facet deflection	0.947	

Axial condition was significantly associated with peak load for the anterior shear and axial rotation motions (Table 4.2). During these motions, peak loads were largest for the compressed condition, lower for the neutral condition, and lowest for the distracted condition (Figure 4.5). No significant association was found between axial condition and peak load for flexion and lateral bending.

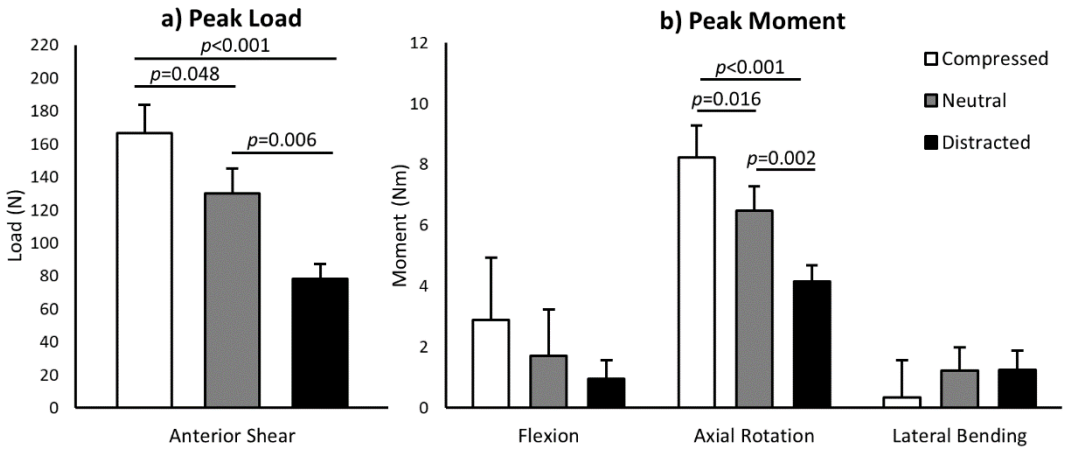

Figure 4.5: Mean (±1 SE) measured peak: a) anterior shear load; and, b) bending moments for the compressed, neutral, and distracted axial conditions. Outliers that were omitted from statistical analysis are not displayed. Significant differences between axial conditions for each motion, as determined by Bonferroni-adjusted post-hoc analysis of the final multivariable linear mixed-effects models (α=0.05), are indicated.

Intervertebral distraction and compression did not significantly affect maximum (tensile) principal facet strains but were associated with a difference in minimum (compressive) principle strains for all motions except axial rotation, when adjusted for gender (Table 4.2). Tensile strains were significantly greater for the 'unloaded' right facet during right axial rotation, while compressive strains were largest for the left facet (Figure 4.6). Shear strains were greatest during the tests with imposed compression for anterior shear (when adjusted for gender and axial order), axial rotation (when adjusted for age) and lateral bending (Table 4.2). This difference was observed during flexion for the left facets only (Figure 4.6).

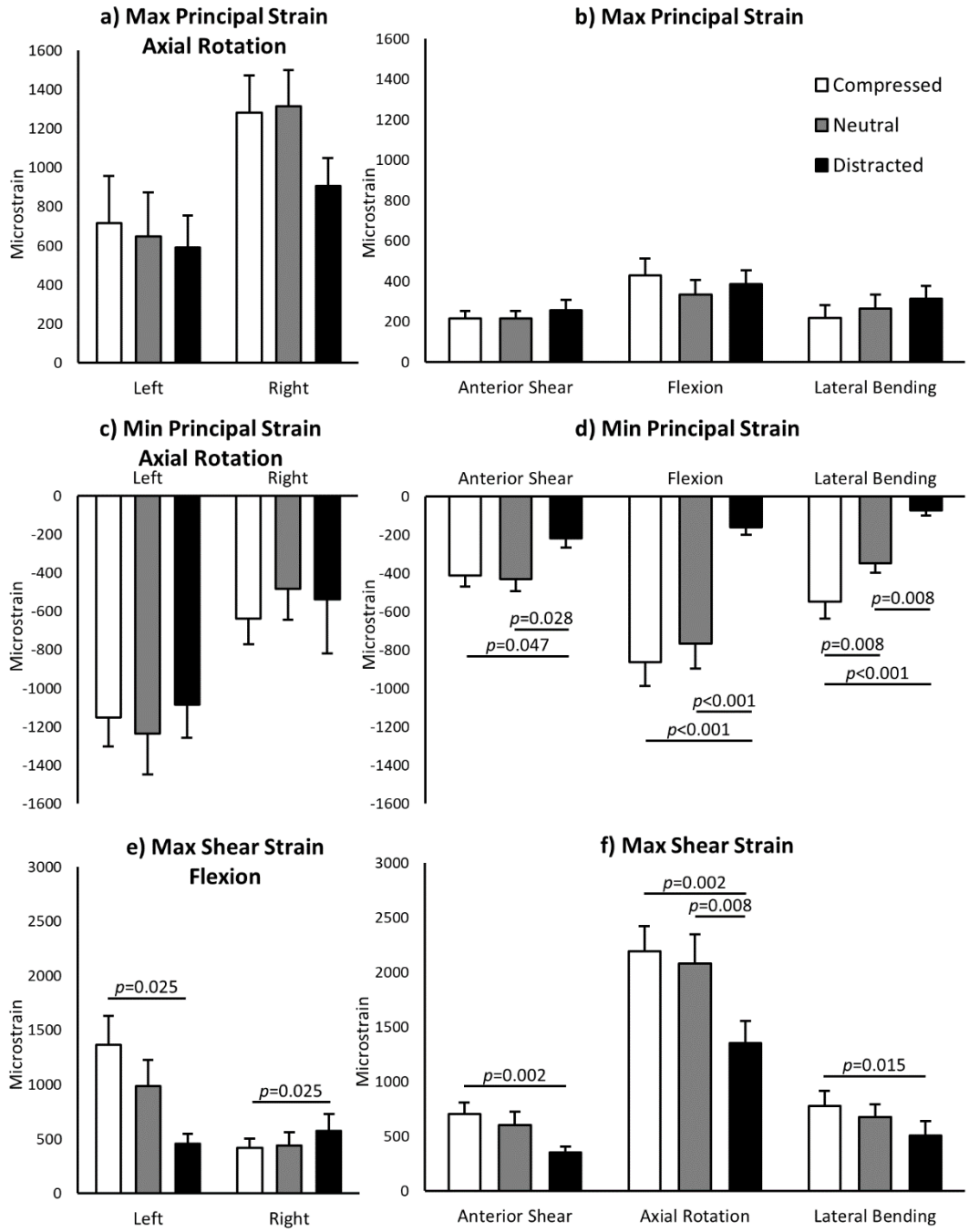

Figure 4.6: Mean (±1 SE) measured: a) & b) maximum principal strains; c) & d) minimum principal strains; and, e) & f) maximum shear strains for the compressed, neutral, and distracted axial conditions. Outliers that were omitted from statistical analysis are not displayed. Left and right facet measurements are grouped for those outcomes with no significant difference between sides. Significant differences between axial conditions for each motion, as determined by Bonferroni-adjusted post-hoc analysis of the final multivariable linear mixed-effects models (α=0.05), are indicated.

Sagittal facet deflections differed significantly between the left and right facets for all motions except flexion (Table 4.2). For anterior shear, the magnitude of negative sagittal deflections (anticlockwise about the z-axis and away from the vertebral body) were significantly larger for the compressed and neutral axial conditions when compared to the distracted state and

adjusted for facet side and age (Figure 4.7). A significant difference in sagittal deflections for the neutral versus distracted conditions was also observed during lateral bending, when adjusted for facet side and loading order. The largest magnitude sagittal facet deflections occurred for the left facets during compressed axial rotation (mean: -1.68±0.23°).

Transverse facet deflections were only appreciable during flexion and axial rotation motions. They were significantly higher when compression and neutral axial loads were imposed on flexion motions, compared to the distracted condition, and were larger for the left facet during axial rotation (when adjusted for gender). Coronal deflections were not appreciable for any load/motion combination.

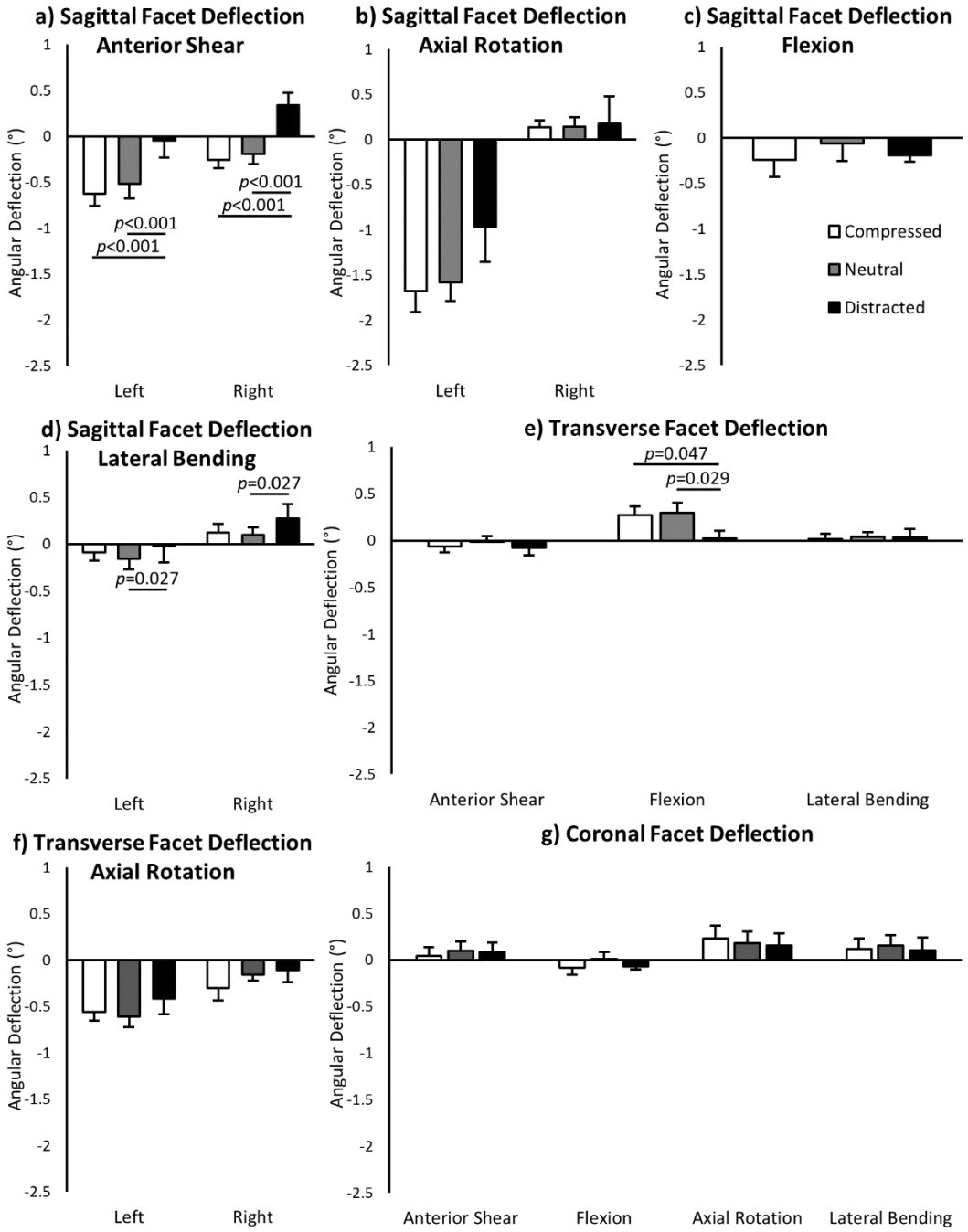

Figure 4.7: Mean (±1 SE) measured: a) – d) sagittal; e) & f) transverse; and, g) coronal facet deflections for the compressed, neutral, and distracted axial conditions, for each motion. Negative angles indicate left transverse and coronal deflections, and sagittal deflections away from the vertebral body. Outliers that were omitted from statistical analysis are not displayed. Left and right facet measurements are grouped for those outcomes with no significant difference between sides. Significant differences between axial conditions for each motion, as determined by Bonferroni-adjusted post-hoc analysis of the final multivariable linear mixed-effects models (α=0.05), are indicated.

4.4 Discussion

The facets are important load-bearing structures of the subaxial cervical spine, yet their mechanical response during physiological motion is understudied. During cervical trauma, axial compression or distraction can be imposed on pathological intervertebral motions. This may alter facet mechanics and influence the occurrence of concomitant facet fracture (Foster et al., 2012). In the present study, axial compressions (50 and 300 N) and distraction (2.5 mm) were superimposed on C6/C7 FSUs during constrained intervertebral motions, and the mechanical response of the C6 bilateral inferior facets was measured. In general, the axial compression conditions caused increased loading of the facets, but this was dependent on test direction.

Peak loads were comparable to those observed at corresponding intervertebral displacement/rotation of subaxial cervical FSUs (King Liu et al., 1982; Moroney et al., 1988; Shea et al., 1991). Cripton *et al.* (1999) observed an increase in overall shear stiffness when a compressive preload of 200 N was imposed on anterior shear motion (111.7±13.6 vs. 90.9±10.9 N/mm without axial preload). This is consistent with the current study, as significantly larger peak anterior shear loads were observed at 1 mm displacement for the compressed compared to neutral condition (166.7±17.2 vs. 130.0±15.3 N, Figure 4.5a).

The magnitude of *minimum* principal strains was significantly larger for the compressed and neutral conditions, compared to the distracted state, for all motions except axial rotation. However, *maximum* principal strains were not significantly affected by axial condition, and their magnitudes were generally lower than the compressive strains (Figure 4.6). The increase in strain magnitude with axial compression is likely a result of greater facet contact, indicating that the posterior inferior facet bases experience predominantly compressive stresses during facet articulation.

Maximum principal and shear facet strains (for the neutral condition) were larger than those observed during loading of isolated subaxial facets that simulated non-destructive anterior shear motions (Maximum: 216±39 vs. 124±16 με; Shear: 602±121 vs. 206±29 με) and

compressive-flexion rotations (Maximum: 336±72 vs. 70±8 με; Shear: 712±144 vs. 109±15 με) (Quarrington et al., 2018a) (Chapter 3). Maximum and minimum principal strains during anterior shear translations were also generally larger for the current study compared to during unconstrained anterior shear (Cripton, 1999), despite larger intervertebral shear displacement (mean 2 mm) in the latter study. In the latter, the lack of constraints permitted flexion of up to 2° which may have transferred load from the facets to the intervertebral disc, reducing strain on the posterior elements. The difference in facet principal strain measurements demonstrates the importance of constrained versus unconstrained intervertebral motion and may provide insight into how facet fractures are associated with dislocation injuries.

The constrained shear motion that was applied in the current study may simulate the mechanisms of bilateral CFD due to first-order buckling caused by compressive forces to the head. During first-order buckling, the flexion rotation that is physiologically coupled with anterior shear motion is restricted by the lordotic posture of the superior cervical levels, which creates a constrained, uncoupled shear motion (Nightingale et al., 1991; Nightingale et al., 1996; Nightingale et al., 2016). In contrast, the unconstrained methodology implemented by Cripton *et al*. (1999) more closely represents intervertebral anterior shear motion that precedes *inertially*-produced CFD (Panjabi et al., 2007). Interestingly, an imposed axial compression force to simulate neck bracing muscle activation did not significantly increase principal strain magnitudes in either the current study (when compared to "neutral") or that reported by Cripton *et al*. (1999). However, the compressive forces imposed in these studies are at the lower end of those estimated for muscle activation.

During left lateral bending, compressive strains were significantly different between each axial condition, and shear strains were significantly larger for the compressed condition compared to the distraction condition (Figure 4.6d&f). Despite being an asymmetric motion, no significant difference between facet sides was observed for any strain measurements. In contrast, the principal strain responses of the left and right facets were significantly different during right axial rotation, and the effect of axial condition was not significant (Figure 4.6a&c). Tensile strains

were larger for the 'unloaded' right facets, presumably due to the facet capsule restricting joint separation, whilst compressive strains were of greater magnitude for the loaded left facets due to bony contact (when adjusting for gender). Adjusting for age, maximum shear strains associated with axial rotation *were* significantly larger for the compressed and neutral conditions, compared to distraction (Figure 4.6f, Table 4.2). This result was independent of facet side, demonstrating that the strains experienced by the 'loaded' facet due to bony contact are comparable to those experienced by the contralateral facet due to the capsule.

Sagittal facet deflections were significantly asymmetric throughout all motions except flexion (Figure 4.7a-d). The left facet deflected more than the right during anterior shear (when adjusting for age), although this significant difference may be an artefact of performing repeated experiments on a small number of specimens. It was hypothesised that this anomaly may be due to sidedness of facet geometry, but these measurements were not significant covariates in the final LMM (Table 4.2). The magnitude of the sagittal deflections during combined compression-flexion were comparable to those reported by Quarrington *et al*. (2018a) (0.25±0.18° vs. 0.17±0.01°) (Chapter 3); however, the sagittal deflections observed during compression-imposed anterior shear were substantially larger (L&R averaged = 0.44±0.11° vs. 0.20±0.02°), probably due to the relatively low load (47 N) applied to the facets in that study. Larger deflections during anterior shear displacement with axial compression are consistent with higher compressive and shear strain magnitudes for these tests, supporting the conclusion that the facets experience greater loading in this condition, compared to the distracted condition.

Right axial rotation produced the largest sagittal deflections; the (loaded) left facets experienced deflections that were greatest during compression, whilst the ipsilateral right facets deflected 0.17±0.30° *towards* the vertebral body when rotation was superimposed with axial distraction. Positive sagittal deflection of the 'unloaded' facet, combined with the large tensile principal strains observed at the facet base, suggests that the capsular ligaments have a substantial impact on cervical facet mechanics during axial rotation.

Axial condition did not significantly affect sagittal or transverse deflections during axial rotation; however, this could be due to the use of Euler angles for calculating deflections. The nature of this method may have caused deflections to be inconsistently distributed between the sagittal and transverse planes for each specimen, due to differences in vertebral geometry. Therefore, a consistent difference in deflections was not associated with axial condition. However, both sagittal and transverse deflections for the compressed and neutral conditions were larger than for the distraction condition, so it is likely that axial compression caused larger *resultant* left facet deflections.

The motions applied in this study were fully constrained, with a fixed CoR. The flexion, lateral bending, and axial rotation motors were aligned with the average physiological CoR of each motion for C6/C7 FSUs (Anderst et al., 2015; Penning, 1960), but the testing machine used in the current study was unable to alter the axis-of-rotation throughout the motion, as occurs *in vivo*. In addition, physiological cervical motions are coupled with off-axis translations and rotations (Lin et al., 2014; Wachowski et al., 2009; Wu et al., 2007). However, motion segments do not exhibit physiological kinematics during cervical trauma (Ivancic et al., 2008; Nightingale et al., 1996; Nightingale et al., 2016; Panjabi et al., 2007), and it is important to obtain quantitative information about the mechanical response of cervical FSUs and the facets during constrained intervertebral motions to develop improved injury tolerance levels.

Approximately one-third of the superior and inferior anatomy of C6 and C7, respectively, were embedded in PMMA. Therefore, the boundary conditions for each vertebra are likely not representative of the *in vivo* environment, and this may have affected the mechanical response of the posterior elements. However, repeated measures analysis was used to determine the effect of axial condition on this response, and great care was taken to ensure that each specimen was prepared in a consistent manner.

This study provides quantitative information about the mechanical response of the C6 inferior facets during constrained shear and bending motions of C6/C7 FSUs under three axial

loading conditions. The response was dependent on test direction, but compressive and shear strains, and sagittal deflections, were generally largest in the compressed conditions. This information may assist when validating computational models of cervical spinal motion and improves our understanding of cervical facet biomechanics.

4.5 Supplementary material – Off-axis load plots

The average load-displacement plots for the six forces and moments associated with the constrained anterior shear, axial rotation, flexion, and lateral bending motions, and for each axial condition, are presented in the following figures.

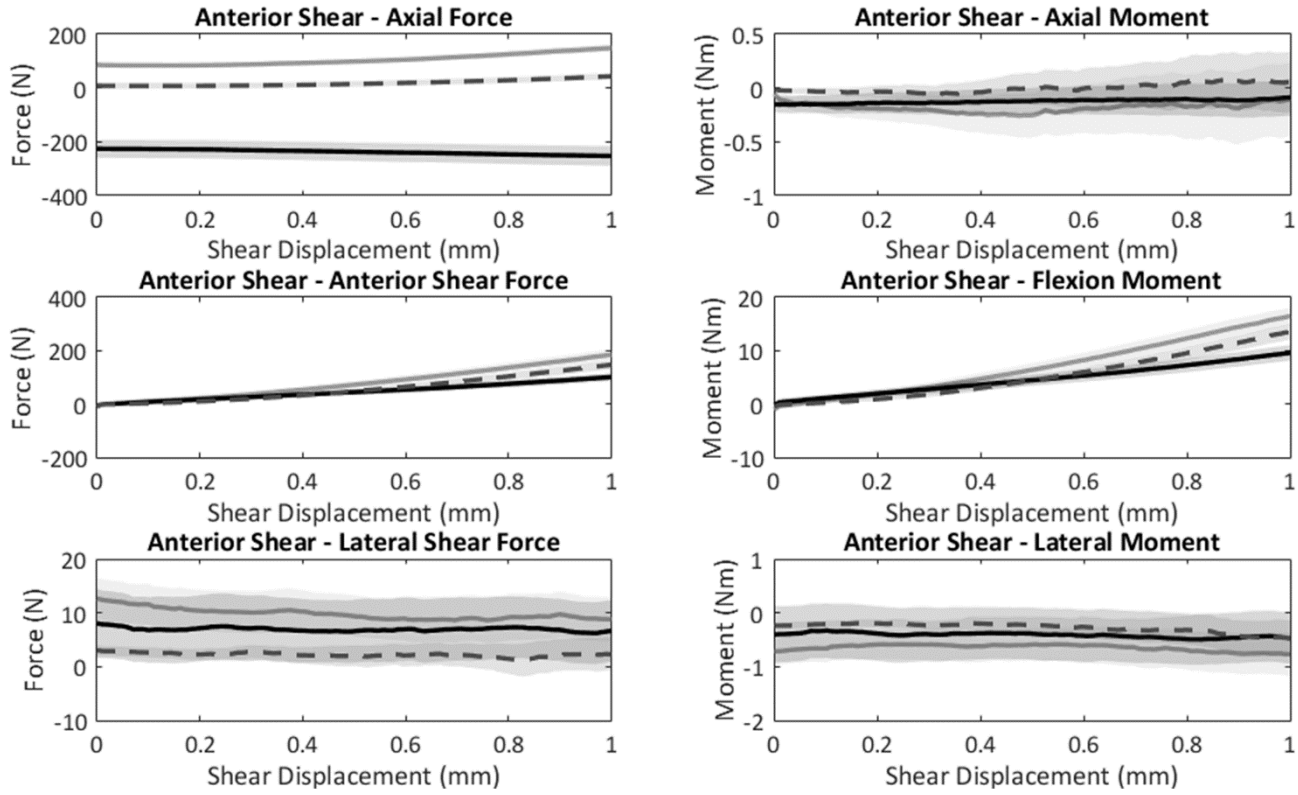

Figure 4.8: Average off-axis load-displacement plots for the loading region of anterior shear motion imposed with each axial condition. The shaded regions indicate ±1 standard error.

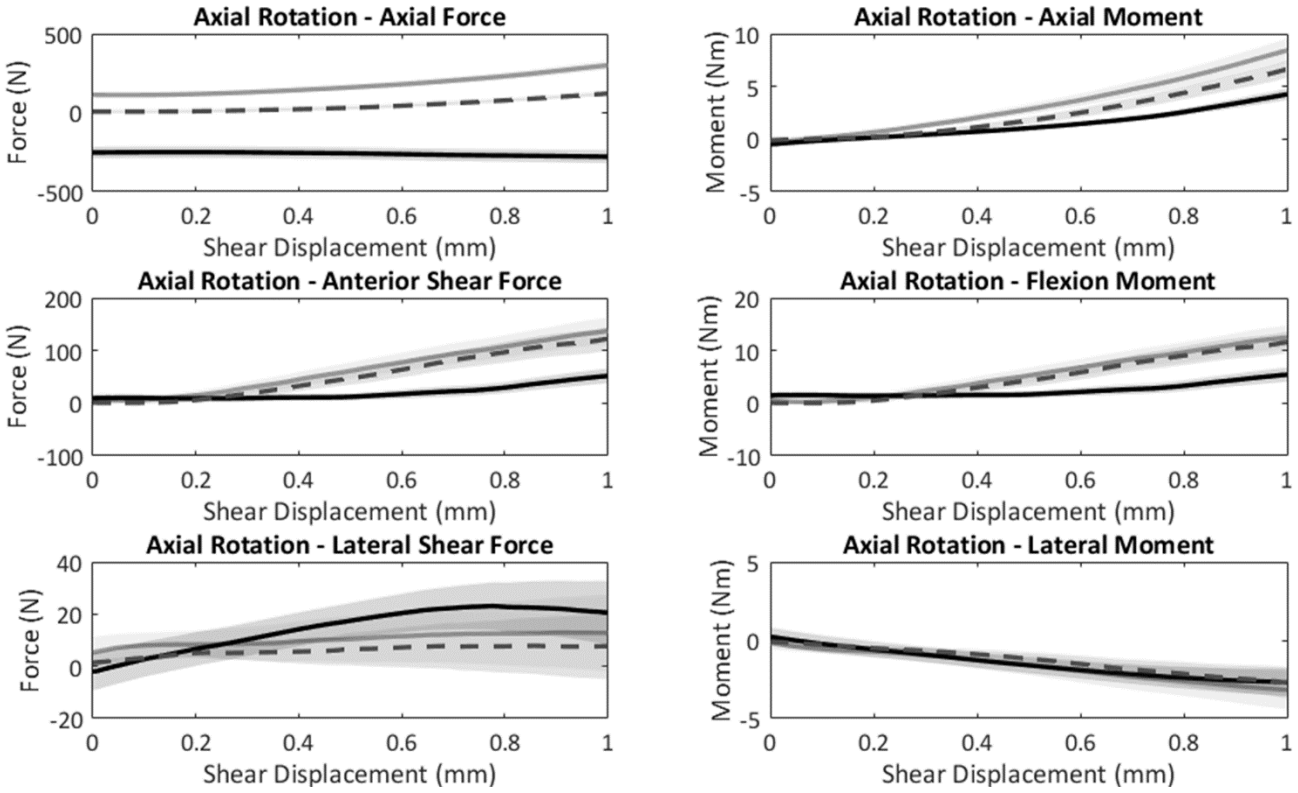

Figure 4.9: Average off-axis load-displacement plots for the loading region of axial rotation motion imposed with each axial condition. The shaded regions indicate ±1 standard error.

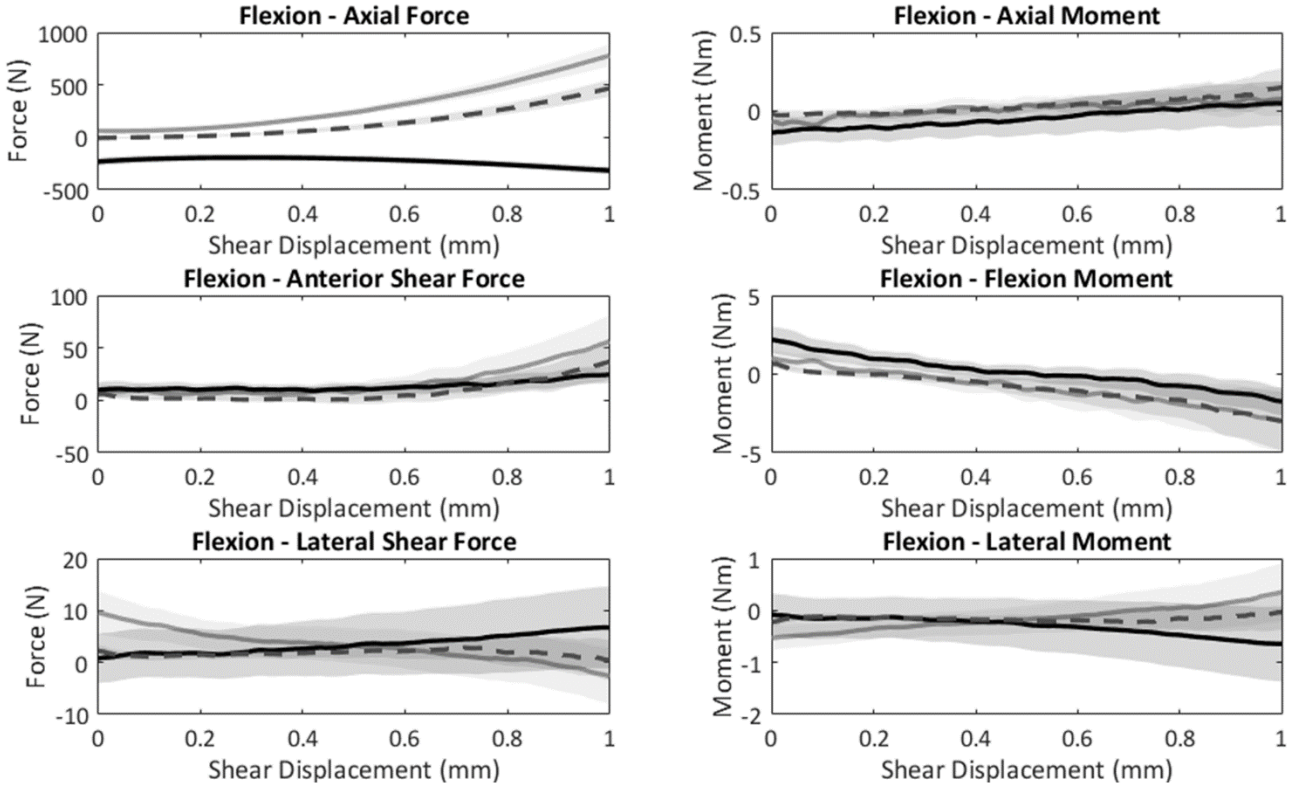

Figure 4.10: Average off-axis load-displacement plots for the loading region of flexion motion imposed with each axial condition. The shaded regions indicate ±1 standard error.

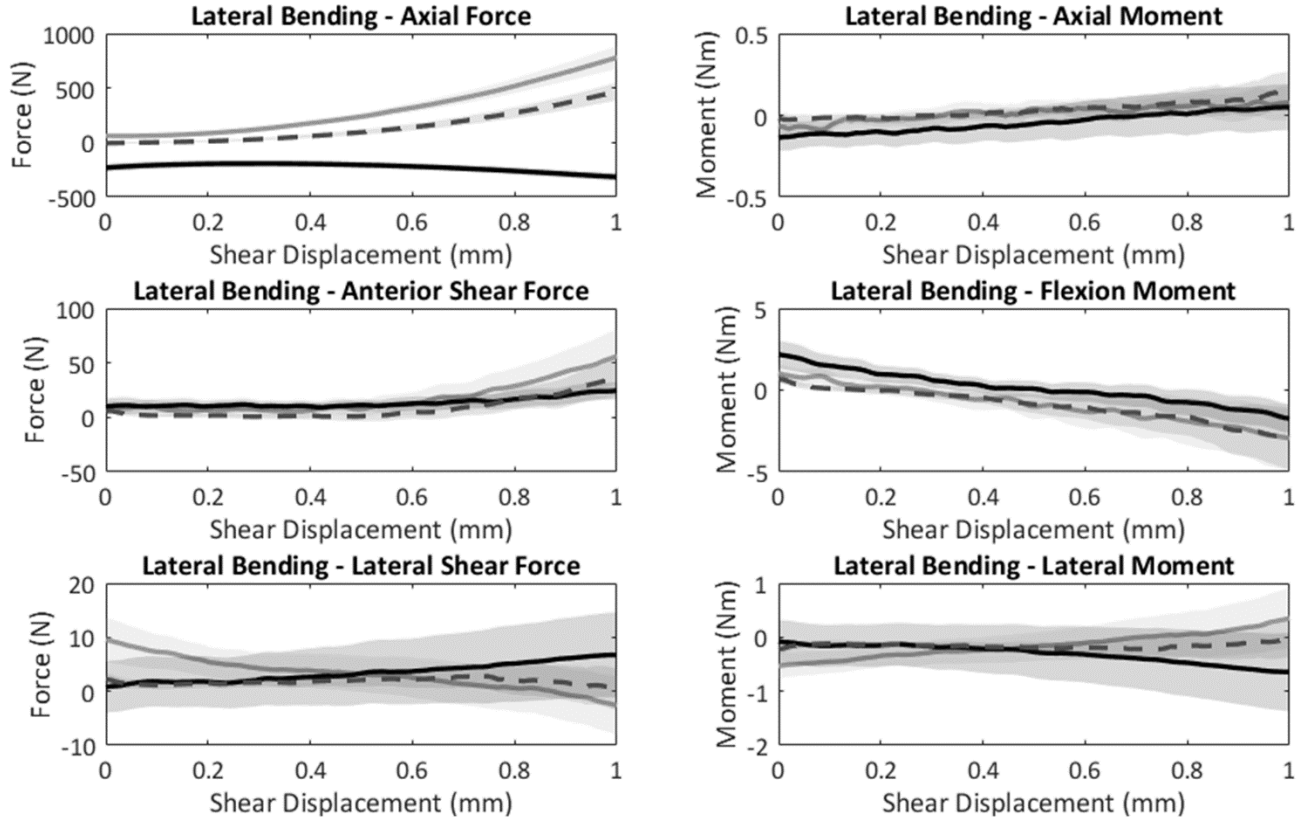

Figure 4.11: Average off-axis load-displacement plots for the loading region of lateral bending motion imposed with each axial condition. The shaded regions indicate ±1 standard error.

4.6 Supplementary material – Final linear mixed-effects models

Table 4.3: Final multivariable linear mixed-effects models for each outcome parameter during the anterior shear tests.

Peak load (N):			
Variable:	*EMMs (95% CI):*	*p-Value:*	*Estimate (95% CI):*
Axial state		**<0.001**	
Compressed	166.67 (136.68, 196.67)	**0.048**	36.65 (5.44, 67.85)
Distracted	78.38 (48.39, 108.38)	**0.006**	-51.65 (-82.85, -20.45)
Neutral*	130.03 (100.03, 160.02)	-	-
** indicates reference category. Sub-category p-values were determined from post-hoc comparison of estimated marginal means, using Bonferonni correction for multiple comparisons. N ≥ 9 per group.*			
Max principal facet strain (με):			
Variable:	*EMMs (95% CI):*	*p-Value:*	*Estimate (95% CI):*
Axial state		0.664	
Compressed	217 (130, 304)	1.000	1.52 (-100.12, 103.16)
Distracted	256 (169, 343)	0.855	40.28 (-61.36, 141.92)
Neutral*	216 (129, 303)	-	-
** indicates reference category. Sub-category p-values were determined from post-hoc comparison of estimated marginal means, using Bonferonni correction for multiple comparisons. N ≥ 10 per group.*			
Min principal facet strain (με):			
Variable:	*EMMs (95% CI):*	*p-Value:*	*Estimate (95% CI):*
Axial state		**0.025**	
Compressed	-398 (-507, -289)	1.000	14.39 (-122.91, 151.68)
Distracted	-236 (-347, -124)	**0.028**	176.76 (37.61, 315.92)
Neutral*	-412 (-521, -304)	-	-
** indicates reference category. Sub-category p-values were determined from post-hoc comparison of estimated marginal means, using Bonferonni correction for multiple comparisons. N ≥ 9 per group.*			
Log-transformed max shear facet strain (με):			
Variable:	*EMMs (95% CI):*	*p-Value:*	*Exponentiated estimate (95% CI):*
Axial state		**0.004**	
Compressed	623(449, 864)	0.335	1.31 (0.89, 1.94)
Distracted	315 (227, 437)	0.078	0.66 (0.45, 0.98)
Neutral*	475 (342, 659)	-	-
Gender		**0.002**	
F	792 (480, 1309)		3.06 (1.59, 5.87)
M*	259 (193, 348)	-	-
Axial order		**0.01**	
** indicates reference category. Sub-category p-values were determined from post-hoc comparison of estimated marginal means, using Bonferonni correction for multiple comparisons. N = 12 per group.*			

Sagittal facet deflection (°):			
Variable:	*EMMs (95% CI):*	*p-Value:*	*Estimate (95% CI):*
Axial state		**<0.001**	
Compressed	-0.441 (-0.627, -0.255)	0.960	-0.09 (-0.33, 0.16)
Distracted	0.146 (-0.040, 0.332)	**<0.001**	0.50 (0.26, 0.74)
Neutral*	-0.356 (-0.541, -0.170)	-	-
Facet side		**0.013**	
L	-0.388 (-0.568, -0.209)		-0.34 (-0.60, -0.08)
R*	-0.045 (-0.234, 0.144)	-	-
Age	-	**0.021**	-0.01 (-0.02, 0.00)

** indicates reference category. Sub-category p-values were determined from post-hoc comparison of estimated marginal means, using Bonferonni correction for multiple comparisons. Negative values indicate a deflection of the facet away from the posterior surface of the vertebral body. EMMs evaluated at age = 71.32. N ≥ 11 per group.*

Transverse facet deflection (°):			
Variable:	*EMMs (95% CI):*	*p-Value:*	*Estimate (95% CI):*
Axial state		0.366	
Compressed	-0.150 (-0.273, -0.027)	0.556	-0.05 (-0.14, 0.04)
Distracted	-0.161 (-0.284, -0.039)	0.371	-0.06 (-0.16, 0.03)
Neutral*	-0.099 (-0.222, 0.024)	-	-
Gender		**0.01**	
F	-0.300 (-0.503, -0.098)		-0.33 (-0.56, -0.09)
M*	0.027 (-0.083, 0.137)	-	-
vBMD	-	**0.027**	0.002 (0.000, 0.004)
Age	-	**0.037**	-0.008 (-0.016, -0.001)

** indicates reference category. Sub-category p-values were determined from post-hoc comparison of estimated marginal means, using Bonferonni correction for multiple comparisons. EMMs evaluated at age = 72.8, vBMD = 144.09. N ≥ 10 per group.*

Coronal facet deflection (°):			
Variable:	*EMMs (95% CI):*	*p-Value:*	*Estimate (95% CI):*
Axial state		0.742	
Compressed	0.039 (-0.163, 0.242)	0.938	-0.06 (-0.22, 0.10)
Distracted	0.086 (-0.117, 0.288)	1.000	-0.01 (-0.17, 0.15)
Neutral*	0.097 (-0.106, 0.300)	-	-

** indicates reference category. Sub-category p-values were determined from post-hoc comparison of estimated marginal means, using Bonferonni correction for multiple comparisons. N = 12 per group.*

Table 4.4: Final multivariable linear mixed-effects models for each outcome parameter during the flexion tests.

Peak load (Nm):			
Variable:	*EMMs (95% CI):*	*p-Value:*	*Estimate (95% CI):*
Axial state		0.298	
Compressed	-2.89 (-6.13, 0.35)	1	-0.58 (-3.67, 2.50)
Distracted	-0.59 (-3.90, 2.73)	0.545	1.72 (-1.46, 4.89)
Neutral*	-2.30 (-5.61, 1.01)	-	-
** indicates reference category. Sub-category p-values were determined from post-hoc comparison of estimated marginal means, using Bonferonni correction for multiple comparisons. N = 12 per group.*			
Log-transform of max principal facet strain (με):			
Variable:	*EMMs (95% CI):*	*p-Value:*	*Exponentiated estimate (95% CI)[β]:*
Axial state		0.529	
Compressed	308 (210, 423)	0.561	1.14 (0.90, 1.44)
Distracted	288 (196, 398)	0.830	1.10 (0.87, 1.39)
Neutral*	234 (149, 337)	-	-
Axial order		**0.024**	
** indicates reference category. [β] To permit log-transformation a constant of 300 was added to each measured value to ensure they were non-negative; therefore, the exponentiated estimates correspond to the transformed data. Sub-category p-values were determined from post-hoc comparison of estimated marginal means, using Bonferonni correction for multiple comparisons. N = 12 per group.*			
Min principal facet strain (με):			
Variable:	*EMMs (95% CI):*	*p-Value:*	*Estimate (95% CI):*
Axial state		**<0.001**	
Compressed	-884 (-1105, -663)	0.669	-117.99 (-361.78, 125.80)
Distracted	-175 (-399, 50)	**<0.001**	591.16 (343.84, 838.47)
Neutral*	-766 (-983, -548)	-	-
** indicates reference category. Sub-category p-values were determined from post-hoc comparison of estimated marginal means, using Bonferonni correction for multiple comparisons. N = 12 per group.*			
Log-transformed max shear facet strain (με):			
Variable:	*EMMs (95% CI):*	*p-Value:*	*Exponentiated estimate (95% CI):*
Axial state		**0.039**	
Compressed	588 (412, 840)	0.2	1.46 (0.93, 2.31)
Distracted	326 (228, 465)	0.721	0.81 (0.51, 1.28)
Neutral*	402 (281, 573)	-	-
Facet side		**0.009**	
L	586 (417, 825)		1.90 (1.20, 3.01)
R*	309 (219, 434)	-	-
vBMD		**0.034**	0.99 (0.98, 1.00)
Axial order		**0.009**	
** indicates reference category. Sub-category p-values were determined from post-hoc comparison of estimated marginal means, using Bonferonni correction for multiple comparisons.EMMs were evaluated at vBMD = 133.81. N = 12 per group.*			

Sagittal facet deflection (°):			
Variable:	*EMMs (95% CI):*	*p-Value:*	*Estimate (95% CI):*
Axial state		0.447	
Compressed	-0.245 (-0.503, 0.012)	0.439	-0.18 (-0.47, 0.11)
Distracted	-0.191 (-0.449, 0.066)	0.775	-0.13 (-0.42, 0.17)
Neutral*	-0.065 (-0.323, 0.192)	-	-
vBMD		**0.002**	-0.007 (-0.011, -0.003)
Facet height		**0.008**	0.19 (0.06, 0.32)

** indicates reference category. Sub-category p-values were determined from post-hoc comparison of estimated marginal means, using Bonferonni correction for multiple comparisons. Negative values indicate a deflection of the facet away from the posterior surface of the vertebral body.EMMs evaluated at vBMD = 135.82, Facet Height = 8.78. N ≥ 11 per group.*

Transverse facet deflection (°):			
Variable:	*EMMs (95% CI):*	*p-Value:*	*Estimate (95% CI):*
Axial state		**0.026**	
Compressed	0.272 (0.081, 0.463)	1	-0.03 (-0.25, 0.20)
Distracted	-0.001 (-0.196, 0.195)	**0.028**	-0.30 (-0.53, -0.07)
Neutral*	0.297 (0.107, 0.488)	-	-

** indicates reference category. Sub-category p-values were determined from post-hoc comparison of estimated marginal means, using Bonferonni correction for multiple comparisons. N ≥ 9 per group.*

Coronal facet deflection (°):			
Variable:	*EMMs (95% CI):*	*p-Value:*	*Estimate (95% CI):*
Axial state		0.168	
Compressed	-0.082 (-0.223, 0.059)	0.131	-0.09 (-0.19, 0.01)
Distracted	-0.052 (-0.196, 0.092)	0.45	-0.06 (-0.17, 0.04)
Neutral*	0.011 (-0.130, 0.152)	-	-

** indicates reference category. Sub-category p-values were determined from post-hoc comparison of estimated marginal means, using Bonferonni correction for multiple comparisons. N = 12 per group.*

Table 4.5: Final multivariable linear mixed-effects models for each outcome parameter during the axial rotation tests.

Peak load (Nm):			
Variable:	*EMMs (95% CI):*	*p-Value:*	*Estimate (95% CI):*
Axial state		**<0.001**	
Compressed	8.228 (6.480, 9.976)	**0.016**	1.75 (0.51, 2.99)
Distracted	4.159 (2.411, 5.907)	**0.002**	-2.32 (-3.56, -1.08)
Neutral*	6.480 (4.732, 8.228)	-	-
** indicates reference category. Sub-category p-values were determined from post-hoc comparison of estimated marginal means, using Bonferonni correction for multiple comparisons. N = 12 per group.*			
Max principal facet strain (με):			
Variable:	*EMMs (95% CI):*	*p-Value:*	*Estimate (95% CI):*
Axial state		0.074	
Compressed	1000 (720, 1280)	1.000	19.03 (-221.97, 260.02)
Distracted	748 (468, 1028)	0.115	-233.23 (-474.23, 7.76)
Neutral*	981 (701, 1261)	-	-
Facet side		**0.042**	
L	652 (301, 1003)		-515.72 (-1011.79, -19.65)
R*	1168 (817, 1518)	-	-
** indicates reference category. Sub-category p-values were determined from post-hoc comparison of estimated marginal means, using Bonferonni correction for multiple comparisons. N = 12 per group.*			
Min principal facet strain (με):			
Variable:	*EMMs (95% CI):*	*p-Value:*	*Estimate (95% CI):*
Axial state		0.776	
Compressed	-1053 (-1357, -749)	1.000	-86.92 (-462.40, 288.57)
Distracted	-926 (-1194, -658)	1.000	39.95 (-316.44, 396.34)
Neutral*	-966 (-1258, -674)	-	-
Facet side		**0.002**	
L	-1296 (-1584, -1009)	-	-458.88 (-868.66, -49.09)
R*	-667 (-925, -410)	-	-
Gender		**0.030**	
F	-1211 (-1570, -853)	-	-629.28 (-984.79, -273.77)
M*	-752 (-956, -549)	-	-
** indicates reference category. Sub-category p-values were determined from post-hoc comparison of estimated marginal means, using Bonferonni correction for multiple comparisons. N ≥ 7 per group.*			
Max shear facet strain (με):			
Variable:	*EMMs (95% CI):*	*p-Value:*	*Estimate (95% CI):*
Axial state		**0.002**	
Compressed	2194 (1736, 2652)	1.000	114.84 (-366.99, 596.68)
Distracted	1353 (895, 1810)	**0.008**	-726.38 (-1208.21, -244.55)
Neutral*	2079 (1622, 2537)	-	-
** indicates reference category. Sub-category p-values were determined from post-hoc comparison of estimated marginal means, using Bonferonni correction for multiple comparisons. N ≥ 10 per group.*			

Sagittal facet deflection (°):			
Variable:	*EMMs (95% CI):*	*p-Value:*	*Estimate (95% CI):*
Axial state		0.178	
Compressed	-0.777 (-1.133, -0.421)	1.000	-0.05 (-0.51, 0.40)
Distracted	-0.385 (-0.741, -0.029)	0.279	0.34 (-0.11, 0.79)
Neutral*	-0.722 (-1.078, -0.366)	-	-
Facet side		**<0.001**	
L	-1.408 (-1.761, -1.055)		-1.56 (-2.07, -1.05)
R*	0.152 (-0.218, 0.522)	-	-

** indicates reference category. Sub-category p-values were determined from post-hoc comparison of estimated marginal means, using Bonferonni correction for multiple comparisons. Negative values indicate a deflection of the facet away from the posterior surface of the vertebral body. N = 12 per group.*

Transverse facet deflection (°):			
Variable:	*EMMs (95% CI):*	*p-Value:*	*Estimate (95% CI):*
Axial state		0.388	
Compressed	-0.503 (-0.659, -0.348)	1	-0.01 (-0.18, 0.16)
Distracted	-0.396 (-0.558, -0.233)	0.521	0.10 (-0.08, 0.27)
Neutral*	-0.493 (-0.653, -0.332)	-	-
Facet side		**0.021**	
L	-0.612 (-0.787, -0.437)	-	-0.30 (-0.54, -0.05)
R*	-0.316 (-0.499, -0.133)	-	-
Gender		**0.002**	
F	-0.705 (-0.925, -0.485)	-	-0.48 (-0.75, -0.22)
M*	-0.223 (-0.369, -0.077)	-	-

** indicates reference category. Sub-category p-values were determined from post-hoc comparison of estimated marginal means, using Bonferonni correction for multiple comparisons. N ≥ 9 per group.*

Coronal facet deflection (°):			
Variable:	*EMMs (95% CI):*	*p-Value:*	*Estimate (95% CI):*
Axial state		0.868	
Compressed	0.222 (-0.026, 0.469)	1.000	0.03 (-0.26, 0.33)
Distracted	0.145 (-0.102, 0.393)	1.000	-0.04 (-0.34, 0.25)
Neutral*	0.190 (-0.063, 0.443)	-	-
Facet side		**0.051**	
L	0.376 (0.111, 0.641)		0.38 (0.00, 0.76)
R*	-0.005 (-0.282, 0.272)	-	-

** indicates reference category. Sub-category p-values were determined from post-hoc comparison of estimated marginal means, using Bonferonni correction for multiple comparisons. N ≥ 10 per group.*

Table 4.6: Final multivariable linear mixed-effects models for each outcome parameter during the lateral bending tests.

Peak load (Nm):			
Variable:	*EMMs (95% CI):*	*p-Value:*	*Estimate (95% CI):*
Axial state		0.604	
Compressed	0.349 (-1.510, 2.208)	0.785	-0.89 (-3.00, 1.22)
Distracted	1.252 (-0.607, 3.111)	1.000	0.01 (-2.10, 2.13)
Neutral*	1.237 (-0.622, 3.096)	-	-
** indicates reference category. Sub-category p-values were determined from post-hoc comparison of estimated marginal means, using Bonferonni correction for multiple comparisons. N = 12 per group.*			
Maximum principal facet strain (με):			
Variable:	*EMMs (95% CI):*	*p-Value:*	*Estimate (95% CI):*
Axial state		0.277	
Compressed	218 (99, 337)	1.000	18.68 (-138.20, 175.57)
Distracted	316 (199, 432)	0.276	116.53 (-38.88, 271.94)
Neutral*	199 (80, 318)	-	-
** indicates reference category. Sub-category p-values were determined from post-hoc comparison of estimated marginal means, using Bonferonni correction for multiple comparisons. N ≥ 11 per group.*			
Log-transformed minimum principal facet strain (με):			
Variable:	*EMMs (95% CI):*	*p-Value:*	*Exponentiated estimate (95% CI)*[β]:
Axial state		**<0.001**	
Compressed	-592 (-715, -457)	**0.008**	0.89 (0.83, 0.96)
Distracted	-76 (-245, 102)	**0.008**	1.13 (1.04, 1.23)
Neutral*	-357 (-498, -208)	-	-
** indicates reference category. [β] To permit log-transformation a constant of 2500 was added to each measured value to ensure they were non-negative; therefore, the exponentiated estimates correspond to the transformed data. Sub-category p-values were determined from post-hoc comparison of estimated marginal means, using Bonferonni correction for multiple comparisons. N ≥ 9 per group.*			
Log-transformed max shear facet strain (με):			
Variable:	*EMMs (95% CI):*	*p-Value:*	*Exponentiated estimate (95% CI):*
Axial state		**0.016**	
Compressed	588 (400, 862)	1	1.15 (0.69, 1.90)
Distracted	294 (205, 420)	0.052	0.57 (0.35, 0.93)
Neutral*	512 (355, 740)	-	-
** indicates reference category. Sub-category p-values were determined from post-hoc comparison of estimated marginal means, using Bonferonni correction for multiple comparisons. N ≥ 10 per group.*			

Sagittal facet deflection (°):			
Variable:	*EMMs (95% CI):*	*p-Value:*	*Estimate (95% CI):*
Axial state		**0.034**	
Compressed	0.139 (-0.050, 0.329)		0.273 (0.023, 0.523)
Distracted	0.156 (-0.021, 0.333)		0.290 (0.063, 0.516)
Neutral*	-0.134 (-0.311, 0.044)	-	-
Facet side		**0.016**	
L	-0.106 (-0.282, 0.070)		-0.320 (-0.571, -0.068)
R*	0.214 (0.029, 0.399)	-	-
Loading order		**0.043**	

** indicates reference category. Sub-category p-values were determined from post-hoc comparison of estimated marginal means, using Bonferonni correction for multiple comparisons. Negative values indicate a deflection of the facet away from the posterior surface of the vertebral body. N ≥ 10 per group.*

Transverse facet deflection (°):			
Variable:	*EMMs (95% CI):*	*p-Value:*	*Estimate (95% CI):*
Axial state		0.946	
Compressed	0.015 (-0.118, 0.149)	1.000	-0.027 (-0.190, 0.137)
Distracted	0.030 (-0.107, 0.166)	1.000	-0.012 (-0.179, 0.154)
Neutral*	0.042 (-0.091, 0.175)	-	-

** indicates reference category. Sub-category p-values were determined from post-hoc comparison of estimated marginal means, using Bonferonni correction for multiple comparisons. N ≥ 9 per group.*

Coronal facet deflection (°):			
Variable:	*EMMs (95% CI):*	*p-Value:*	*Estimate (95% CI):*
Axial state		0.947	
Compressed	0.120 (-0.120, 0.361)	1.000	-0.032 (-0.313, 0.249)
Distracted	0.108 (-0.132, 0.348)	1.000	-0.044 (-0.325, 0.236)
Neutral*	0.152 (-0.088, 0.393)	-	-

** indicates reference category. Sub-category p-values were determined from post-hoc comparison of estimated marginal means, using Bonferonni correction for multiple comparisons. N ≥ 9 per group.*

4.6.1 Post-hoc power analysis

A post-hoc power analysis was performed to ensure that the LMMS were suitably powered. In biomechanical experiments of human cadaver material, 6 specimens per group are generally sufficient to detect significant differences, so great care was taken to ensure that the events-per-variable did not fall below 6 for any model. Model convergence was evaluated at each step to ensure the statistical integrity of each model was acceptable. After consultation with a statistician, a post-hoc power analysis determined that this study was suitably powered (Power = 1.00). A one-way, post-hoc ANOVA power calculation was performed using the G*Power software (Faul et al., 2007), in a deflated sample size was used (to account for variance inflation of LMMs) based on a minimum of 6 specimens per group.

Chapter 5 Towards a methodology to produce cervical bilateral facet dislocation and investigate the roles of axial compression and distraction on failure load and mechanism

5.1 Introduction

Traumatic subaxial cervical bilateral facet dislocation (BFD) and fracture-dislocation (BFD+Fx) often cause tetraplegia (Hadley et al., 1992; Payer and Schmidt, 2005), typically resulting in lifetime personal care costs of approximately US$3 million (DeVivo et al., 2011). BFD±Fx of the subaxial region (C3-T1) occurs most frequently at C6/C7 and is often caused by traffic accidents and falls (Quarrington et al., 2018b) (Chapter 2). During these injury events, eccentric axial compressive forces applied to the head (Allen et al., 1982; Cusick and Yoganandan, 2002; Huelke and Nusholtz, 1986; White and Panjabi, 1990), or inertial motion of the head during high deceleration events (Huelke and Nusholtz, 1986), create an external bending moment about the subaxial cervical spine (Pintar et al., 1998).

It has traditionally been accepted that during BFD±Fx external loading produces a *distractive-flexion* or *compressive-flexion* injury vector at the level of injury (Allen et al., 1982; Beatson, 1963; Pintar et al., 1998). These proposed injury mechanisms were ascertained from retrospective analyses of radiographic images and medical records, and from quasi-static manipulation (to dislocation) of functional spinal units (FSUs). However, *global* flexion moments alone do not cause BFD±Fx when applied to whole cervical spines (Nightingale et al., 1991; Pintar et al., 1998). Intervertebral *anterior shear* motions are also observed in the lower cervical spine during the experimental production of BFD (Hodgson and Thomas, 1980; Ivancic, 2012b; Maiman et al., 1983; Panjabi et al., 2007; Roaf, 1960), yet the role of this loading direction during cervical trauma has not been thoroughly investigated.

In a recent computational study of the response of the cervical spine to axial compression impact loading, intervertebral anterior-shear loads as high as 3000 N were observed in the lower cervical spine due to first-order buckling, causing forward translation of C6 on C7 (Nightingale

et al., 2016). However, these simulations were unable to model failure of anatomical structures so it could not be confirmed that dislocation would have occurred. Cripton (1999) noted that the facet joints of subaxial cervical FSUs were close to dislocation even when applying non-traumatic unconstrained anterior shear loads (200 N), so it is likely that the loads observed by Nightingale *et al.* (2016) would have produced BFD±Fx. Developing a better understanding of the response of cervical FSUs to intervertebral anterior shear is crucial in elucidating the injury mechanisms of BFD and BFD+Fx.

Only one published experimental series has reliably produced dynamic BFD (Ivancic et al., 2007, 2008; Panjabi et al., 2007). In this study, incrementally increasing sagittal decelerations were applied to C3/C4, C5/C6, and C7/T1 FSUs (with a head mass surrogate attached) until dislocation occurred. Intervertebral motion primarily comprised flexion, anterior shear, and distraction, and peak inter-facet separation (perpendicular to the sagittal plane of the inferior facet) of up to 8 mm was observed during the first half of the injurious motion (Panjabi et al., 2007). No BFD+Fx were produced despite the fact that concomitant facet fractures are commonly associated with clinical BFD (Foster et al., 2012). This could be an artefact of the incremental inertial injury mechanism, as rupture of the posterior ligaments was observed during the impact immediately preceding BFD for all specimens. Compromise of these structures may have permitted excessive distraction or unconstrained subluxation of the facet joints, allowing the joint to dislocate without high inter-facet loads.

The occurrence of BFD+Fx has also been absent during head-first impact tests of cadaveric specimens. In these tests, BFDs occurring in the lower cervical spine were preceded by local intervertebral flexion and anterior shear motions, but with associated local *axial compression* rather than *distraction* (Hodgson and Thomas, 1980; Ivancic, 2012; Nightingale et al., 2016). Others have suggested that the lack of BFD+Fx observed during head-impact tests may be due to an absence of muscle force replication, either passive (maintaining normal neck posture) or to simulate neck bracing prior to impact (Foster et al., 2012). Muscle activation may impose an additional intervertebral compression load during injury that restricts pathological

flexion and intervertebral distraction, causing increased loading of the facets and potentially leading to fracture. Nightingale *et al.* (2016) reported that including muscles in head-impact simulations substantially increased intervertebral compressive and shear loads when compared to simulations *without* muscles, especially when first-order buckling occurred. The magnitude of intervertebral distraction or compression that is superimposed on the injury vectors leading to BFD may dictate the loading that is transferred to the cervical facets and is important in determining the risk of BFD+Fx.

The biomechanical response of the subaxial facets during cervical trauma is significantly understudied. In a recent study hemispherical loading pins applied point loading to subaxial inferior cervical facets to simulate destructive intervertebral anterior shear motions, during which facet surface strain, deflection, stiffness and failure load were quantified (Quarrington et al., 2018a) (Chapter 3); however, point loading is unlikely to fully represent *in vivo* conditions, especially when compression or distraction are superimposed on the shear motion. Elucidating the mechanical response of the facets during intervertebral anterior shear motion, with axial compression or distraction, will improve fundamental understanding of how axial loading contributes to BFD and BFD+Fx.

The role of anterior shear during cervical BFD, and the effect of compression/distraction on the mechanical response of the facets and the risk of BFD+Fx, have not previously been investigated. Therefore, the aim of this study was to develop an experimental method to reliably apply constrained, destructive anterior shear motions to C6/C7 FSUs with imposed intervertebral axial compression or distraction, and to investigate the effect of axial condition on the biomechanical response and injury patterns of the facets.

5.2 Methods

5.2.1 Specimen preparation and embedding

Donor information, screening, handling and medical imaging measurement details for the twelve cervical motion segments used in this study are described in Section 4.2.1. Initially,

the distal levels of five C5-T1 motion segments were augmented with screws/wire (Figure 5.1a) to assist with fixation in blocks of polymethylmethacrylate (PMMA; Vertex Dental, Utrecht, Netherlands). The C5 and T1 vertebrae were included to provide a larger surface area to assist with fixation within the PMMA. However, the large coupled flexion moment associated with the applied *supraphysiological* anterior shear motions caused failure of the specimen-PMMA assembly during testing, either due to motion at the embedded levels (Specimens #1 and #3-5) or fracture at the embedded vertebra/screw interface (Specimen #2). Iterative improvements to the augmentation and embedding protocols were made for each specimen, but it became apparent that motion at the C5/C6 and C7/T1 levels, or techniques implemented to restrict this motion, were responsible for the embedding failure. Therefore, C6/C7 FSUs were used for the remaining tests (N=7). Screw/wire constructs were attached to the exposed vertebral endplates and posterior elements were embedded along with the distal third of each vertebra (Figure 5.1b). All C6/C7 joints and disco-ligamentous tissues were maintained. The first specimen embedded in this manner (Specimen #6) fractured through the vertebral body at the specimen/PMMA interface due to poor bone quality (Table 5.1); however, five of the remaining six specimens achieved BFD without embedding failure (embedding failure of C7 occurred for Specimen #12).

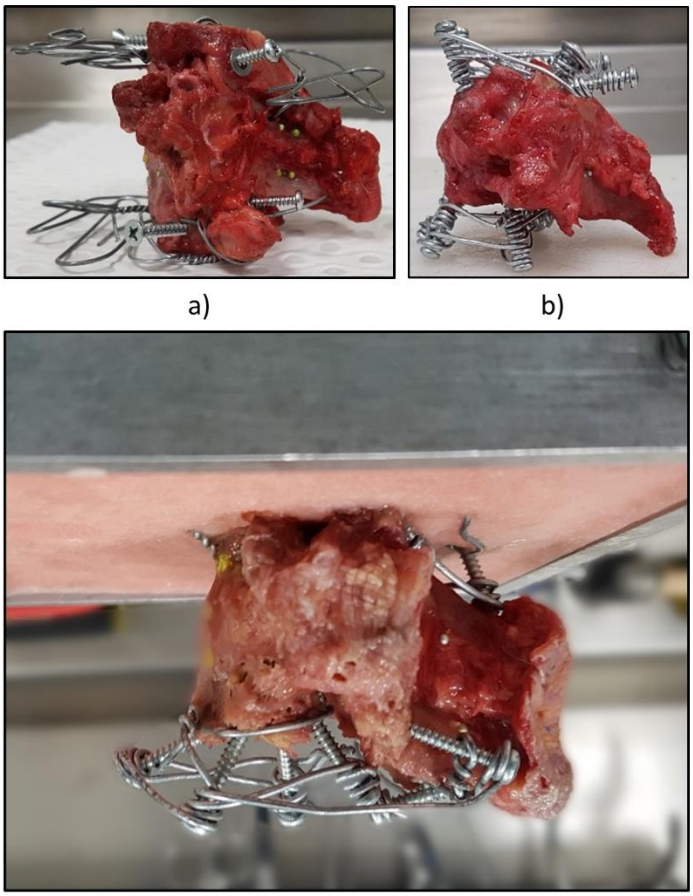

Figure 5.1: Specimen preparation: Screws and wire were used to assist with fixation of a) six C5-T1; and, b) six C6/C7 motion segments in blocks of polymethylmethacrylate. A C6/C7 specimen with the superior anatomy and screw/wire construct embedded is shown in c).

5.2.2 Mechanical loading

Each specimen was mounted on a six-axis load cell (MC3A-6-1000 ±4.4 kN, AMTI, Massachusetts, USA) fixed to the base of a six-axis materials testing machine (8802, Instron, High Wycombe, UK). Either 300 N of axial compression or 2.5 mm of distraction was applied (randomly assigned). As detailed in Chapter 4, the 'compressed' condition simulated the loading experienced due to neck muscle activation (Bell et al., 2016; Chancey et al., 2003; Cripton et al., 2001; Hattori, 1981; Newell et al., 2014; Pospiech et al., 1999), while axial distraction created intervertebral separation of similar magnitude to that observed by Panjabi *et al.* (2007) during inertially induced experimental BFD. Specimens were fixed in the compressed or distracted condition by fastening locking struts to the exterior surface of the molds (Figure 5.2). The specimens were then removed from the six-axis material testing machine and transferred to a

biaxial material testing machine (8874, Instron, High Wycombe, UK) for destructive anterior shear testing.

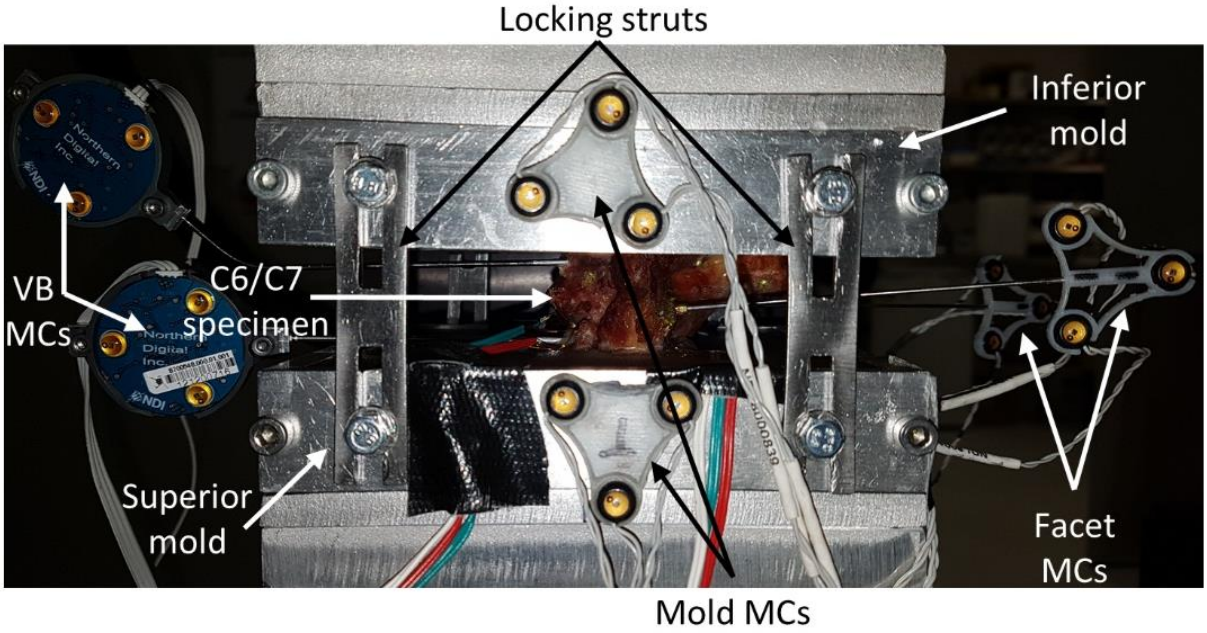

Figure 5.2: Photo of a specimen fixed in the compressed or distracted position by fastening locking struts to the exterior surface of the embedding molds. Motion capture marker carriers (MCs) are also pictured. VB = vertebral body.

The superior vertebra was fixed to the axial actuator of the biaxial test machine such that quasi-static anterior shear (1 mm/s) could be applied (Figure 5.3). The inferior vertebra was secured to the base of the test machine via an adjustable support apparatus intended to maintain the compressed or distracted state of the specimen throughout testing. Forces and moments were recorded by a six-axis load cell (MC3A-6-1000, AMTI, Massachusetts, USA) attached to the actuator as a displacement of 20 mm was applied. This displacement was slightly greater than the average endplate depth of the C6/C7 vertebrae (Panjabi et al., 1991) to ensure that a 'Stage 4' dislocation injury could be achieved (Allen et al., 1982). During testing, large off-axis forces (perpendicular to the axis of the actuator) occurred as the facet joints engaged. This produced some off-axis (axial) deflection of the actuator, causing the molds to separate by an additional 2.05±0.25 mm for the compressed specimens, and 1.64±0.38 mm for the distracted specimens.

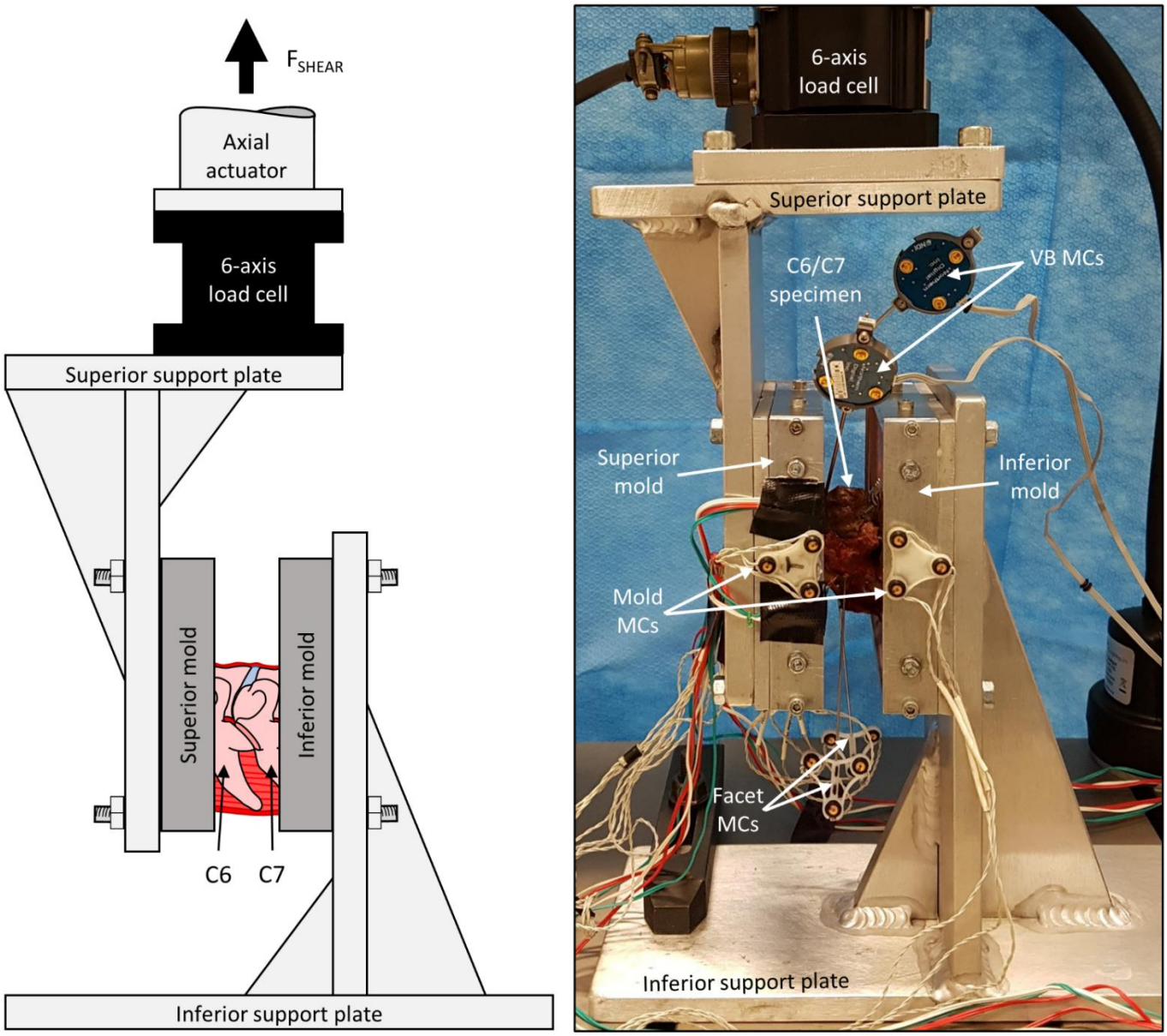

Figure 5.3: Lateral schematic of the embedded specimen attached to the biaxial testing machine (left) and corresponding photograph (right). Anterior shear motion was applied to the superior mold by the actuator and six-axis forces and moments were recorded by the load-cell. Intervertebral separation corresponding to 300 N of compression or 2.5 mm of distraction was imposed throughout the test by the support plates. Motion capture marker carriers (MCs) are pictured. VB = vertebral body.

5.2.3 Instrumentation, data collection and processing

The bilateral inferior facets of C6 were instrumented with rosette strain gauges (FRA-1-23-1L, TML, Tokyo, Japan) and motion capture marker-carriers (Optotrak Certus, Northern Digital Inc., Ontario, Canada), and all data (including load cell and position data) were collected and processed as described in Chapter 4. Each test was video-recorded at 400 Hz using a high-speed camera (i-Speed TR, Olympus Corporation, Tokyo, Japan). Following completion of

testing, Specimens #6-12 were fixed in their final position using locking struts, removed from the testing machine, and attached to a radiolucent support fixture (Figure 5.4). The specimens then underwent high-resolution computed tomography (CT) scans (SOMATOM Force, Siemens, Erlangen, Germany; 0.4 mm slice thickness, 0.23 mm in-plane resolution) and the presence and features of vertebral fractures were determined.

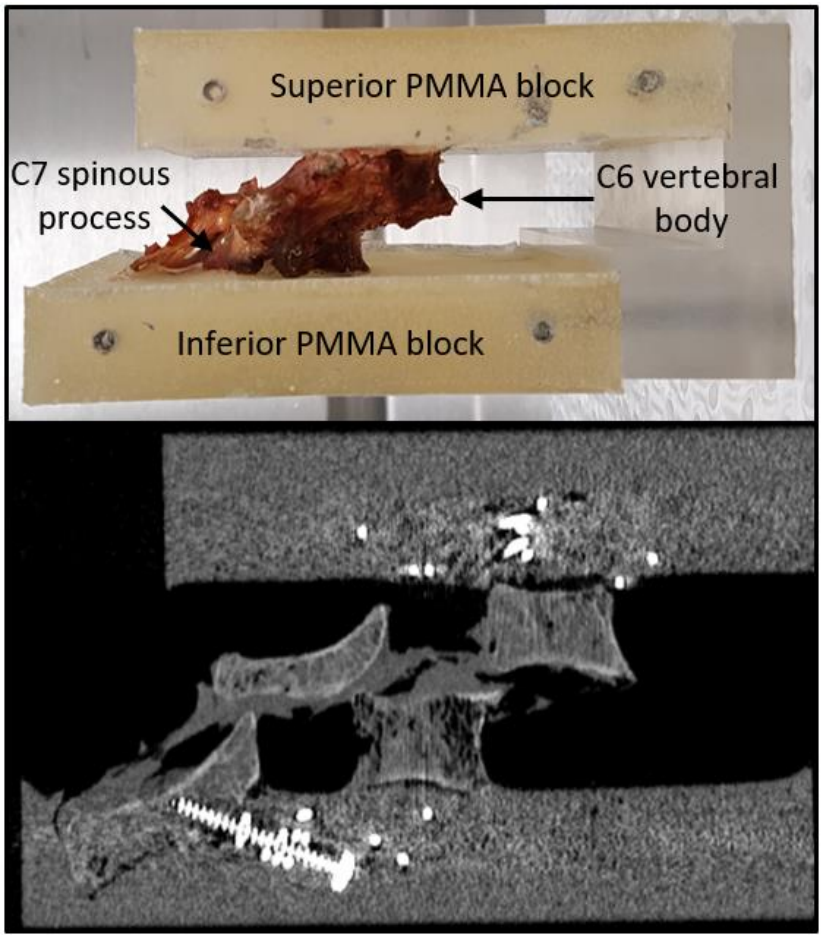

Figure 5.4: A photo of a specimen fixed in the final, post-test position (top) and the corresponding sagittal computed tomography image (bottom).

5.2.4 Supraphysiologic anterior shear analysis point

All twelve specimens achieved at least 2.19 mm of *supraphysiologic* anterior shear prior to exhibiting motion within the PMMA embedding. Therefore, the change (from unloaded) in shear and axial load, maximum (tensile) and minimum (compressive) principal strains, maximum shear strains, and angular facet deflections were calculated at *2.19 mm* of applied anterior shear (Figure 5.5). Linear mixed-effects models (LMMs) were developed to identify if axial condition (compressed vs. distracted) was significantly associated with these outcome measures. Using

SPSS v24 (IBM, Illinois, USA), the normality and homogeneity of variance of each dependent variable was assessed using Shapiro-Wilk and Levene tests, respectively, and statistically significant outliers were removed to meet these criteria if required – this was only necessary in 4/8 models, and at most 2/24 observations were removed. The effect of axial condition was assessed in all models, and this effect was adjusted for facet side (left vs. right), donor demographics, specimen bone mineral density, vertebral body size, facet height and angle, and the type of specimen (four-vertebrae vs. two). Because measurements from the left and right facets of each specimen were included as separate observations, a random effect of cadaver ID was included. Each model was refined using a manual backward step-wise approach until only significant predictors remained (α=0.05).

5.2.5 Initial anatomical failure analysis point

Shear load-displacement plots were generated for the five specimens that achieved 20 mm of shear motion without embedding failure (Figure 5.5). The instant of initial anatomical failure (defined as a distinct reduction in shear load and confirmed using high-speed camera footage) was identified (Figure 5.5), and the aforementioned outcome measures (Section 5.2.4) were determined at this point. This component of the study was underpowered to perform statistical analyses due to the small number of successful tests; descriptive statistics are reported.

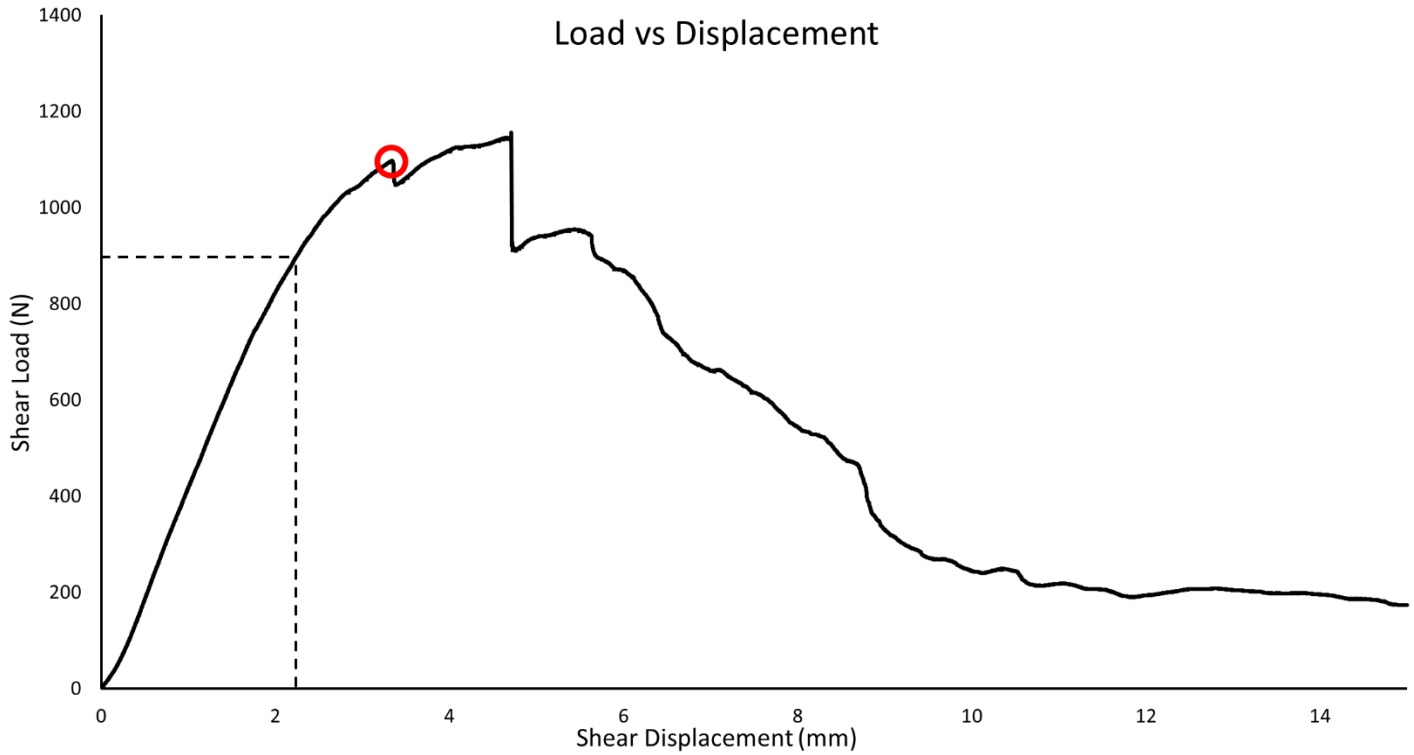

Figure 5.5: A typical filtered anterior shear load-displacement plot. The instant of initial failure (red O) and the position at which the supraphysiologic shear analysis was performed (dashed lines) are indicated.

5.3 Results

Donor and specimen details are provided in Table 5.1. Strain data from the left facet of Specimen #7 was omitted from all analyses as the readings were unreliable due to technical difficulties.

Table 5.1: Donor and specimen details. vBMD = volumetric K2HPO4 equivalent bone mineral density.

Test #	Specimen ID	Sex	Age	Mean vBMD (mg/cm^3)	Specimen type
1	H010	M	71	138.8	Four vertebrae
2	H013	M	58	115.0	Four vertebrae
3	H014	M	58	83.6	Four vertebrae
4	H003	M	46	142.9	Four vertebrae
5	H002	F	62	216.7	Four vertebrae
6	H004	F	75	99.0	Two vertebrae
7	H036	M	58	125.5	Two vertebrae
8	H009	M	85	223.5	Two vertebrae
9	H041	M	82	74.1	Two vertebrae
10	H020	M	76	105.2	Two vertebrae
11	H033	F	88	117.1	Two vertebrae
12	H043	M	81	164.4	Two vertebrae

5.3.1 Supraphysiologic anterior shear

The eight final multivariable LMMs from the supraphysiologic anterior shear (i.e. 2.19 mm) analyses are presented in Table 5.4 in Section 5.5 – a summary of these models is provided in Table 5.2.

Table 5.2: Summary of the final multivariable linear mixed-effects models for supraphysiologic anterior shear motion. Significant p-values (α=0.05) for the axial condition variable are bolded.

Outcome variable:	Axial condition p-value:	Significant covariates:
Shear load	0.200	
Axial load	**0.002**	
Maximum principal strain	0.312	Facet height
Minimum principal strain	0.916	Facet side, facet angle
Maximum shear strain	**0.050**	
Sagittal facet deflection	**0.031**	
Transverse facet deflection	0.642	Facet side, specimen type
Coronal facet deflection	0.213	

For most specimens (3/5), the supraphysiologic anterior shear analysis point was >49% of the displacement that was required to cause initial anatomical failure (Figure 5.5). There was a significantly larger increase in axial load at the supraphysiologic anterior shear analysis point for the compressed specimens, compared to the distracted specimens. No association with shear load was observed (Figure 5.6).

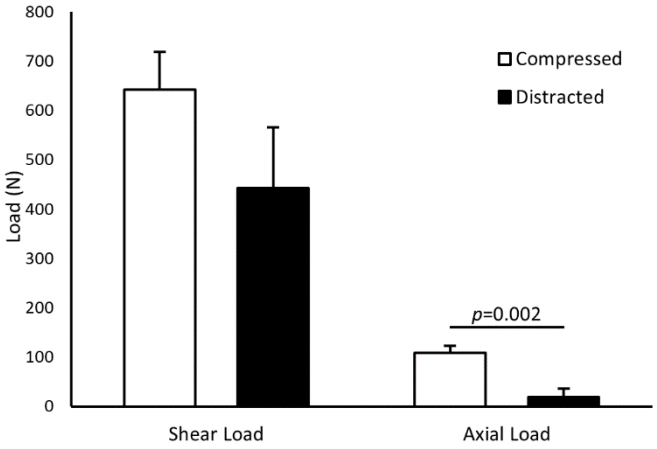

Figure 5.6: Mean (±1 SE) measured anterior shear and axial load for the compressed and distracted axial conditions at the supraphysiologic anterior shear analysis point. Significant differences between the compressed and distracted axial conditions, as determined by the final multivariable linear mixed-effects models (α=0.05), are indicated.

There were no significant differences in maximum (tensile) or minimum (compressive) principal strains between axial conditions (Figure 5.7); however, compressive strains were larger for the left facets than the right across both conditions. Maximum shear strains were significantly larger for the compressed group.

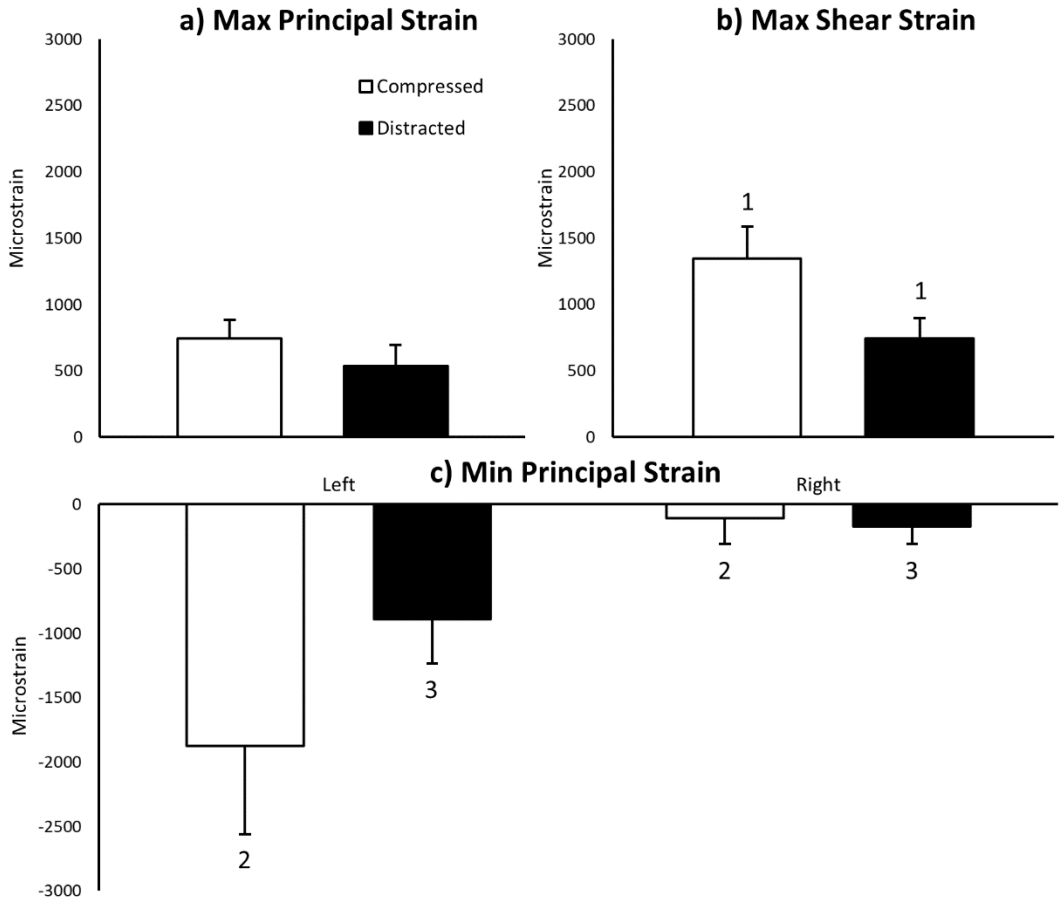

Figure 5.7: Mean (±1 SE) measured: a) maximum principal; b) maximum shear; and, c) minimum principal strains for the compressed and distracted axial conditions at the supraphysiologic anterior shear analysis point. Outliers that were omitted from statistical analysis are not displayed. Left and right facet measurements are grouped for outcomes with no significant difference between sides. Significant differences between the compressed and distracted axial conditions, as determined by the final multivariable linear mixed-effects models (α=0.05), are indicated by numbers 1, 2, and 3.

Facet deflections at 2.19 mm of anterior shear motion were significantly larger for the distracted specimens, compared to the compressed specimens (Figure 5.8). In these plots, negative angles reflect: (a) sagittal deflections *away* from the vertebral body; (b) left coronal deflections (*away* from the vertebral body for the right facet, *towards* for the left); and, (c) left transverse deflections (*away* from the vertebral body for the left facet, *towards* for the right). Transverse deflections were significantly different for the left compared to the right facets (Table 5.2), but there was no effect of axial condition.

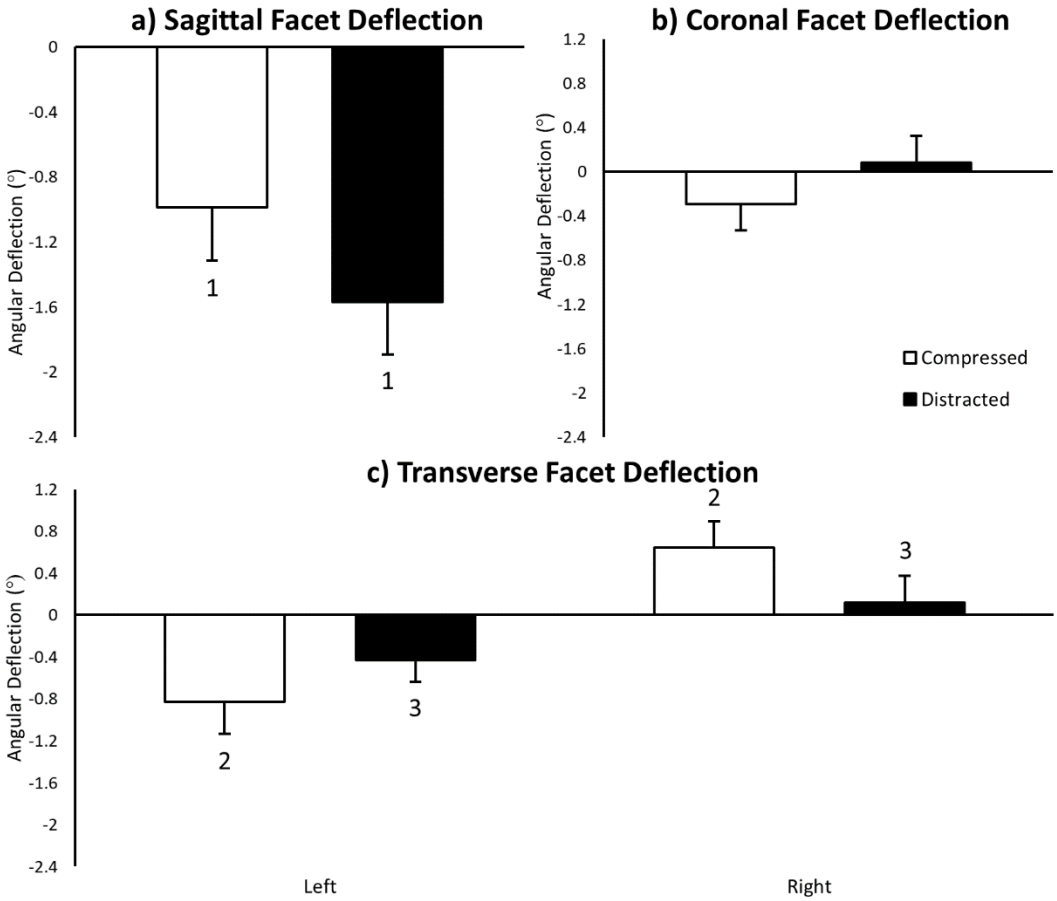

Figure 5.8: Mean (±1 SE) measured: a) sagittal; b) coronal; and, c) transverse facet deflections for the compressed and distracted axial conditions at the supraphysiologic anterior shear analysis point. Outliers that were omitted from statistical analysis are not displayed. Left and right facet measurements are grouped for those outcomes with no significant difference between sides. Significant differences between the compressed and distracted axial conditions, as determined by the final multivariable linear mixed-effects models (α=0.05), are indicated by numbers 1, 2, and 3.

5.3.2 Fracture-dislocation specimens

Five specimens (three compressed, two distracted) successfully underwent 20 mm of constrained anterior shear motion, producing BFD+Fx in all cases. Six-axis load-displacement plots for each successful test are presented in Section 5.5. Fractures of the C6 inferior facet(s) occurred for all specimens, and 4/5 were bilateral; C7 superior facet fractures also occurred for 3 specimens (1 bilateral) (Table 5.3). Fractures through the facet tip (8 occurrences), articular pillar (5 occurrences), spinous process (1 occurrence), and vertebral body (1 occurrence) were observed. There did not appear to be any correlation between axial condition and the type of fractures observed.

Table 5.3: Outcome measures for each test. Dashes indicate that failure data was not available.

Test #	Axial condition	Supra. shear load (N)	BFD+Fx shear load (N)	Initial failure	C6 Fx locations	C7 Fx locations
1	Distracted	461.38	-	-	-	-
2	Compressed	583.24	-	-	-	-
3	Distracted	316.85	-	-	-	-
4	Distracted	149.88	-	-	-	-
5	Compressed	515.99	-	-	-	-
6	Distracted	145.96	-	-	-	-
7	Compressed	771.64	1409.67	Bilateral facets	Bilateral facet tip	None
8	Distracted	882.26	1095.77	Right facet	Bilateral facet tip	None
9	Distracted	700.32	793.80	Right facet	Right articular pillar; Spinous process; Left facet tip	Left facet tip
10	Compressed	939.17	1766.52	Left facet	Left articular pillar; Right facet tip	Bilateral articular pillar
11	Compressed	408.90	571.98	Right facet	Right facet tip	Left articular pillar
12	Compressed	630.50	-	-	-	-

BFD, bilateral facet dislocation; Fx, fracture.

Initial failure was most often unilateral, and forces at this analysis point were generally higher for the compressed specimens. Unilateral facet fracture occurred first for 4/5 specimens, 3 of which involved the right facet; bilateral fracture was observed for one specimen (Table 5.3). Compressed specimens exhibited larger shear displacement (5.57±0.58 vs. 3.11±0.22 mm), shear load (1249.39±354.02 vs. 944.78±150.98 N), and axial load (233.18±15.60 vs. 78.82±30.91 N) at initial failure compared to the two distracted specimens (Figure 5.9a-c). On average, maximum principal (2696±1014 vs. 1119±288 με), minimum principal (-1109±770 vs. -668±484 με), and maximum shear (3805±1117 vs. 1786±639 με) strains were also generally larger for the compressed specimens at the point of initial failure. Minimum principal strains tended to be larger in magnitude for the left facet than the right facet, regardless of which facet failed at this analysis point (Figure 5.9d-f).

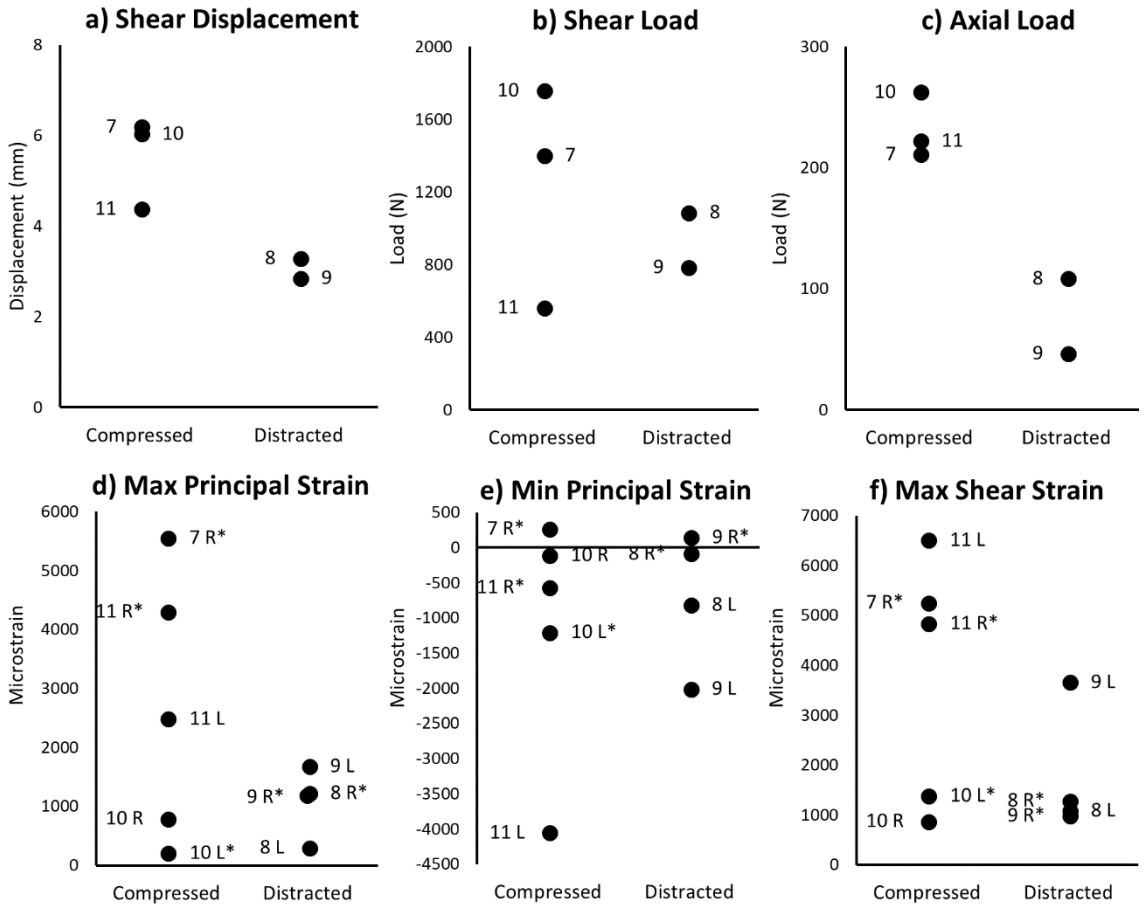

Figure 5.9: The measured (a) shear displacement, (b) shear load, and (c) axial load at the point of initial failure for each specimen (grouped by axial condition) is displayed, along with the measured: (d) maximum principal; (e) minimum principal; and, (f) maximum shear facet strains at this analysis point. Strain data from the left facet of Specimen #7 is omitted due to technical difficulties. * indicates the facet(s) that failed at this instance. L = left; R = right.

Facet deflection data is presented in Figure 5.10; data for Specimen #10 was unavailable due to technical difficulties. The mean change in sagittal deflection was comparable for the compressed and distracted specimens (-3.69±1.57 vs. -3.77±1.17°). However, the *magnitudes* of coronal and transverse deflections away from the vertebral body were generally larger for the compressed specimens.

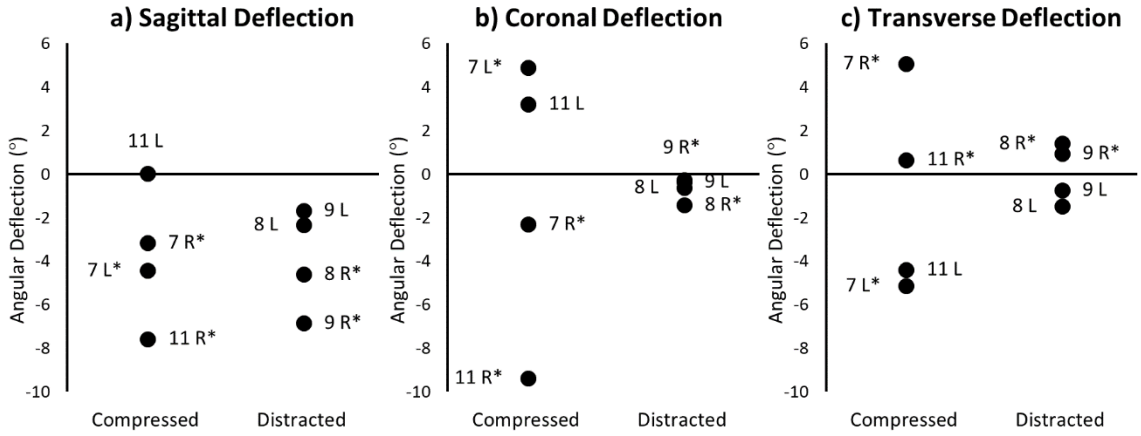

Figure 5.10: Measured: a) sagittal; b) coronal; and, c) transverse facet deflections for the compressed and distracted specimens at the point of initial failure. Data for Specimen #10 was not available due to technical difficulties. * indicates the facet(s) that failed at this instance. L = left; R = right.

5.4 Discussion

Intervertebral anterior shear motion is associated with traumatic subaxial cervical BFD (Hodgson and Thomas, 1980; Ivancic, 2012b; Maiman et al., 1983; Panjabi et al., 2007; Roaf, 1960). It has been proposed that shear motion imposed with axial compression may cause BFD+Fx (Foster et al., 2012), but the mechanical response of the facets during this motion/loading combination has not previously been reported. In the present study, a methodology was developed to reliably apply 20 mm of constrained anterior shear to C6/C7 FSUs combined with imposed axial compression or distraction. Twelve specimens achieved 2.19 mm of *supraphysiologic* intervertebral anterior shear motion, and BFD+Fx was produced in the five specimens that successfully underwent 20 mm shear without embedding failure. Shear and axial forces, and the mechanical responses of the bilateral C6 inferior facets, were determined at 2.19 mm of shear (for all specimens) and at the point of initial failure (for the successful experiments). In general, the compressed specimens experienced higher forces, facet strains and non-sagittal deflections at both analysis points.

Change in shear and axial loads were larger for the compressed specimens at the supraphysiologic shear analysis points, but this was only statistically significant for axial load. A significantly larger change in axial load for the compressed group may support the theory of increased facet engagement for these specimens, as the off-axis forces were likely caused by the

inclined sagittal angle of the subaxial cervical facets. For the successful failure tests, shear and axial loads, and shear displacement at the initial anatomical failure analysis point tended to be larger for the compressed group. Interestingly, the lowest shear failure load occurred for a compressed specimen (#11), probably due to its small vertebral size (Table 4.1). As with the supraphysiological shear results, the differences observed at point of failure were likely due to altered facet engagement caused by the changes in axial separation.

Sagittal facet deflections (away from the vertebral body) at 2.19 mm of anterior shear were significantly larger for the distracted specimens, while transverse deflections tended to be larger for the compressed specimens. For transverse deflections, a significant difference between facet sides was observed because deflections for both facets were calculated in the vertebral body coordinate system. Using the 'right-hand rule', transverse rotations about the y-axis (superior-inferior) directed away from the vertebral body (as would be expected to occur during supraphysiologic anterior shear) were negative for the left facet and positive for the right facet. Transverse deflections were larger in magnitude for the compressed specimens for both facets, but this was not statistically significant (Table 5.2). It is likely that the ~10° angle that the inferior C6 facets make with the coronal plane (Panjabi et al., 1993) would result in large transverse deflections during supraphysiologic anterior shear, and these deflections would be greater for the compressed specimens where the articulating facets are fully engaged.

Sagittal facet deflections up to 7.5° were observed at the point of initial anatomical failure; however, an effect of axial condition was only apparent for non-sagittal deflections. The sagittal deflections for the fractured facets were slightly larger than those reported for isolated C6 inferior facets in Chapter 3 (5.23±0.82° vs. 3.43±0.08°) (Quarrington et al., 2018a), perhaps due to the different facet loading mechanisms. Coronal and transverse deflections away from the vertebral body were generally larger for the compressed group and, as previously suggested, it is likely that the magnitude of non-sagittal deflections would be greater for these specimens due to larger facet articulation compared to the distracted condition.

In general, the larger overall deflections for the compressed specimens corresponded with higher maximum principal and shear strains at the facet bases, compared to the distracted group. Maximum principal strains at point of facet failure (when averaged across all specimens) were comparable to those reported for the simulated anterior shear C6 specimens in Chapter 3 (2517±1030 vs. 2370±1014 με), but shear strains tended to be lower (2782±943 vs. 6595±3157 με) (Quarrington et al., 2018a). This possible difference in shear strains could be due to the different loading methods implemented in the two studies, as the point-loading pins used in Study 2 may have produced more shear deformation than the C7 superior facets.

Large variation in strain values, both between specimens and between facets for the same specimen, were observed. This is common for these types of studies, as surface strain measurements of bone are highly dependent on the quality and structure of the underlying bone, and on the anatomical location of the strain gauge. The use of full-field strain measurement techniques, such as digital image correlation, could be used in future experiments to obtain principal and shear strains at the fracture location (if soft tissue is removed to reveal the bony surface); however, in the current study, visualization of the bony facet tip (where fracture most commonly occurred) was occluded by the capsule.

The facet fractures observed in this study are clinically relevant and correspond to AOSpine subaxial cervical spine facet injury classifications F2 and F3 (Vaccaro et al., 2016). There did not appear to be a difference in the number of fractures between groups, perhaps because the imposed axial compression and distractions were at the low-end of those estimated for neck muscle forces (Bell et al., 2016; Chancey et al., 2003; Cripton et al., 2001; Hattori, 1981; Newell et al., 2014; Pospiech et al., 1999) and inertial intervertebral separation (Panjabi et al., 2007), respectively. The magnitudes of these conditions were restricted by the design limits of the six-axis materials testing machine (distraction) and were consistent with those applied in Study 3 (Chapter 4). Intervertebral axial forces may be much higher during traumatic *in vivo* BFD±Fx – peak compression forces of over 4000 N (due to muscle forces and external loading) were estimated during computer simulations of first-order buckling of the cervical spine

(Nightingale et al., 2016). Combining destructive anterior shear motion with *supraphysiologic* axial compression or distraction may cause different injury patterns between groups and further elucidate the effect of axial separation on the risk of facet fracture. This could be achieved in future experiments by adding an independent, horizontal actuator and load cell to the test setup that can apply substantially larger axial compression and distraction loads to the specimen, while applying constrained, destructive anterior shear motion using the Instron 8874 axial actuator (Figure 5.11).

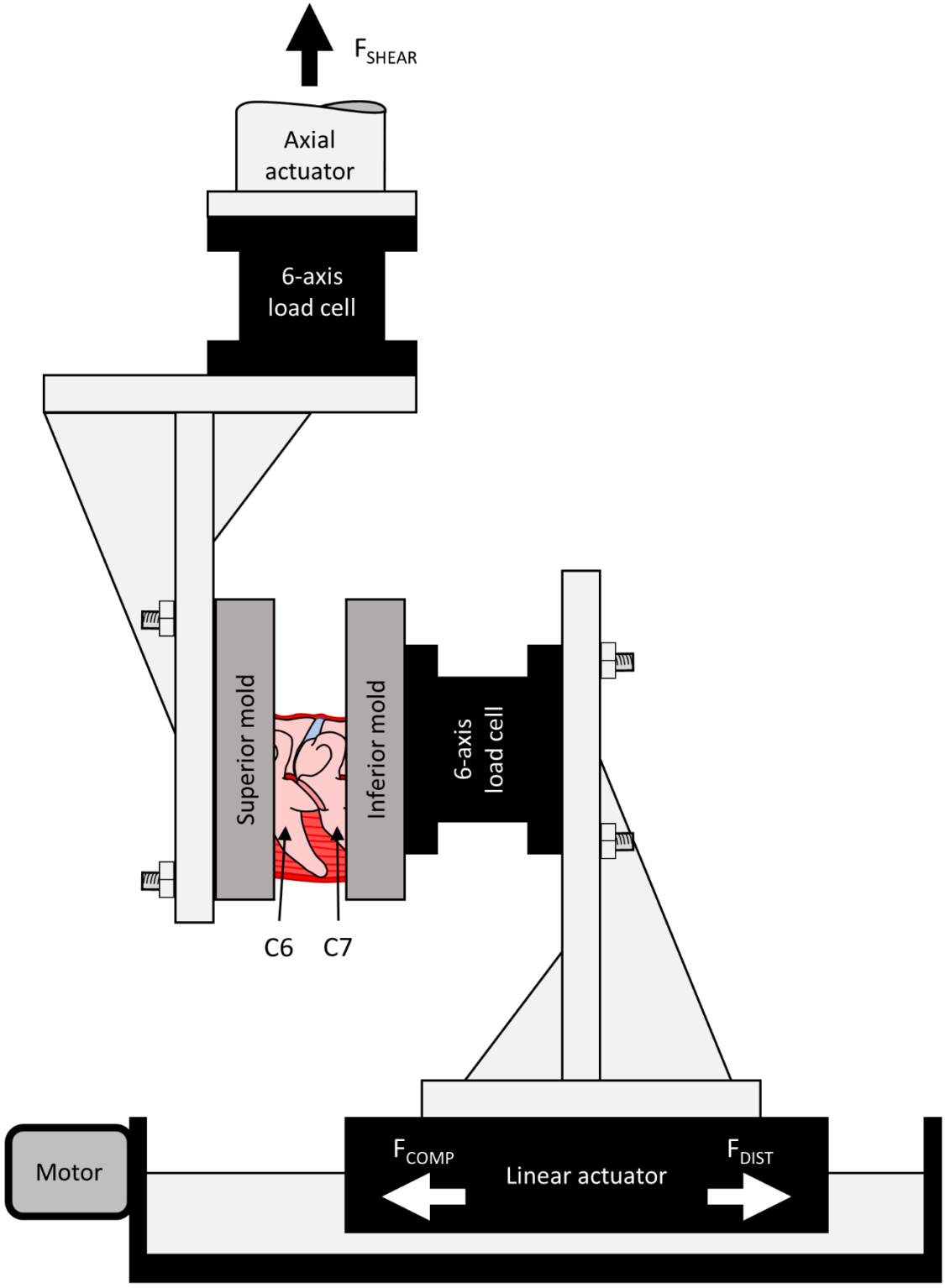

Figure 5.11: Lateral schematic of the proposed modified test setup, which includes a horizontal linear actuator and six-axis load cell to apply supraphysiologic axial compression and distraction during destructive anterior shear testing.

Surrounding muscle tissue was dissected from all specimens, but several of the muscles that span the C6/C7 motion segment (including longissimus and intertransversarii) have origins and insertions at the respective transverse processes (Bakkum and D. Cramer, 2013). Therefore,

the absence of these muscles may influence failure loads and fracture locations. Future experiments could attempt to maintain or simulate these muscles to produce a more biofidelic experimental model of BFD+Fx.

In the subaxial cervical spine, physiological intervertebral anterior shear motion is coupled with flexion rotation (Panjabi et al., 1986), presumably due to the inclined sagittal angle of the facet joints; however, intervertebral kinematics are non-physiologic during cervical trauma (Ivancic et al., 2008; Nightingale et al., 1996; Nightingale et al., 2016; Panjabi et al., 2007). When cervical "buckling" occurs, the flexion rotation that is physiologically coupled with anterior shear motion is restricted by the lordotic posture of the superior cervical levels, which may cause constrained, uncoupled shear motion to occur in the subaxial cervical region (Nightingale et al., 1991; Nightingale et al., 1996; Nightingale et al., 2016). This constrained motion likely prevents "unloading" of the facets via intervertebral separation, or through unrestricted facet subluxation (due to intervertebral flexion), leading to BFD+Fx. Therefore, the magnitude of intervertebral separation (compression or distraction) that is superimposed on constrained anterior shear motion may contribute to the risk of BFD+Fx. To investigate this, a method to apply constrained, supraphysiologic intervertebral anterior shear motion (with superimposed compression or distraction) to C6/C7 FSUs was developed.

The challenges associated with applying constrained, supraphysiologic anterior shear to cervical FSUs highlights the strength of the structures that resist this motion and may indicate why BFD+Fx has not been produced experimentally during drop-testing of whole cervical spines. In this study, large axial forces (Figure 5.6, Figure 5.9c) and flexion moments (see Section 5.5) occurred due to the inclined sagittal orientation of the C6/C7 facets, causing embedding failure in 7/12 specimens. These off-axis loads also caused horizontal deflection of the actuator (perpendicular to the axis of applied motion), permitting unwanted intervertebral distraction (the magnitude of which was similar for both groups). Our results suggest that, for BFD+Fx to occur *in vivo*, the adjacent superior and inferior spinal levels must resist these coupled, off-axis loads, and the local injury vector must have a substantial shear component. This loading scenario may

occur if a compressive preload (such as that provided by passive or active neck muscles) is present during first-order cervical buckling (producing local intervertebral shear). To our knowledge, this has not been replicated experimentally.

This is the first study to investigate supraphysiologic and traumatic constrained intervertebral anterior shear in subaxial cervical FSUs, and the first to experimentally produce BFD+Fx. Change in axial load, and shear strain at the C6 inferior facet base, were both larger for the compressed specimens at the supraphysiologic and failure analysis points, while shear displacement and load also tended to be larger at failure for these specimens. Sagittal facet deflections were significantly larger for the distracted group at 2.19 mm of shear, and were similar to the compressed specimens at failure, but non-sagittal deflections were generally larger for the compressed specimens at both analysis points. Clinically relevant facet fractures were created during the five successful experiments, demonstrating that intervertebral anterior shear motion contributes to BFD+Fx. Increasing the magnitude of superimposed axial compression and distraction to supraphysiologic levels may further elucidate how intervertebral separation contributes to the risk of BFD+Fx during traumatic anterior shear.

5.5 Supplementary material – Six-axis load-displacement plots

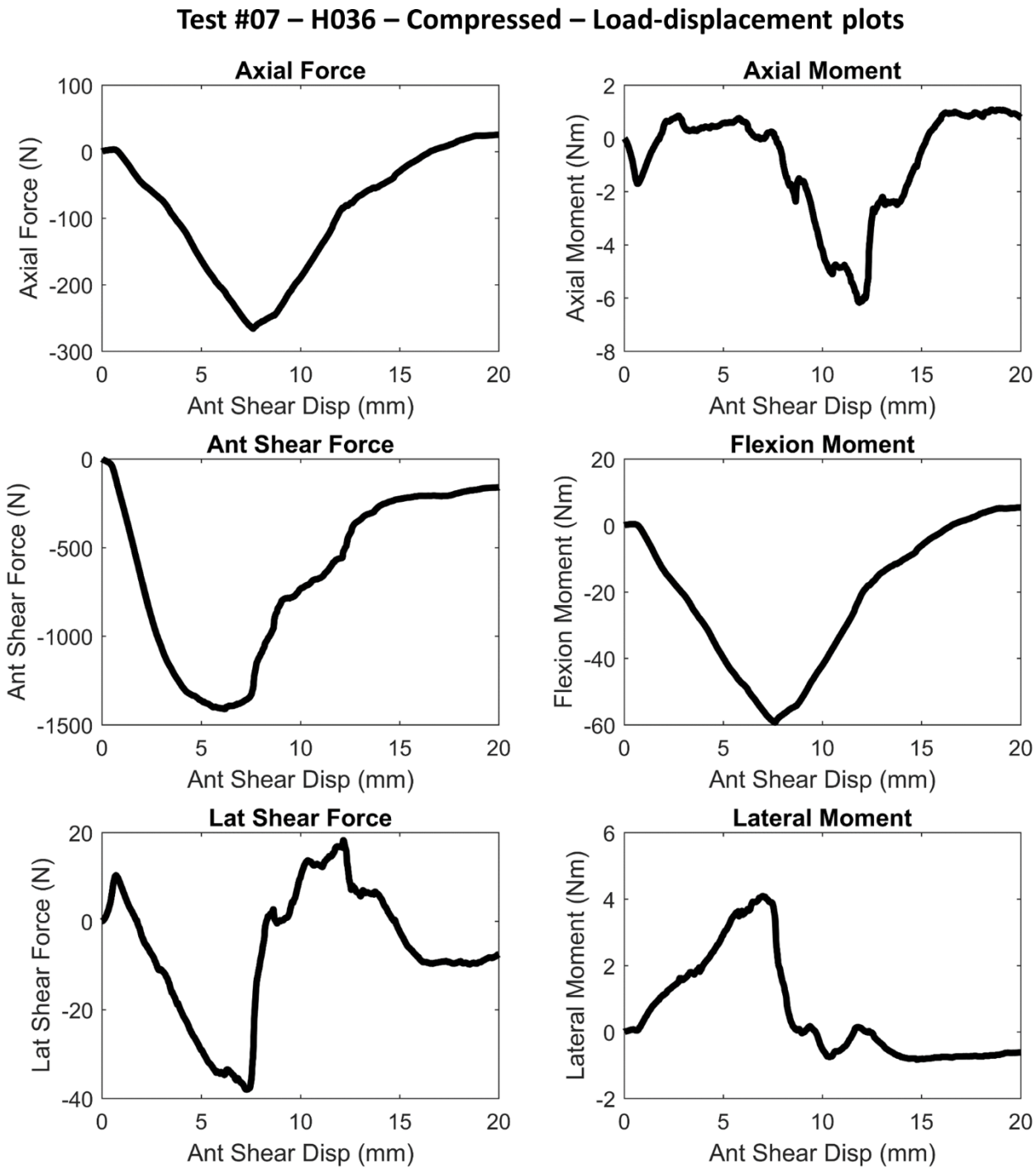

Figure 5.12: Six-axis load-displacement plots for 20 mm anterior shear applied to Specimen #7 with 300 N of imposed compression.

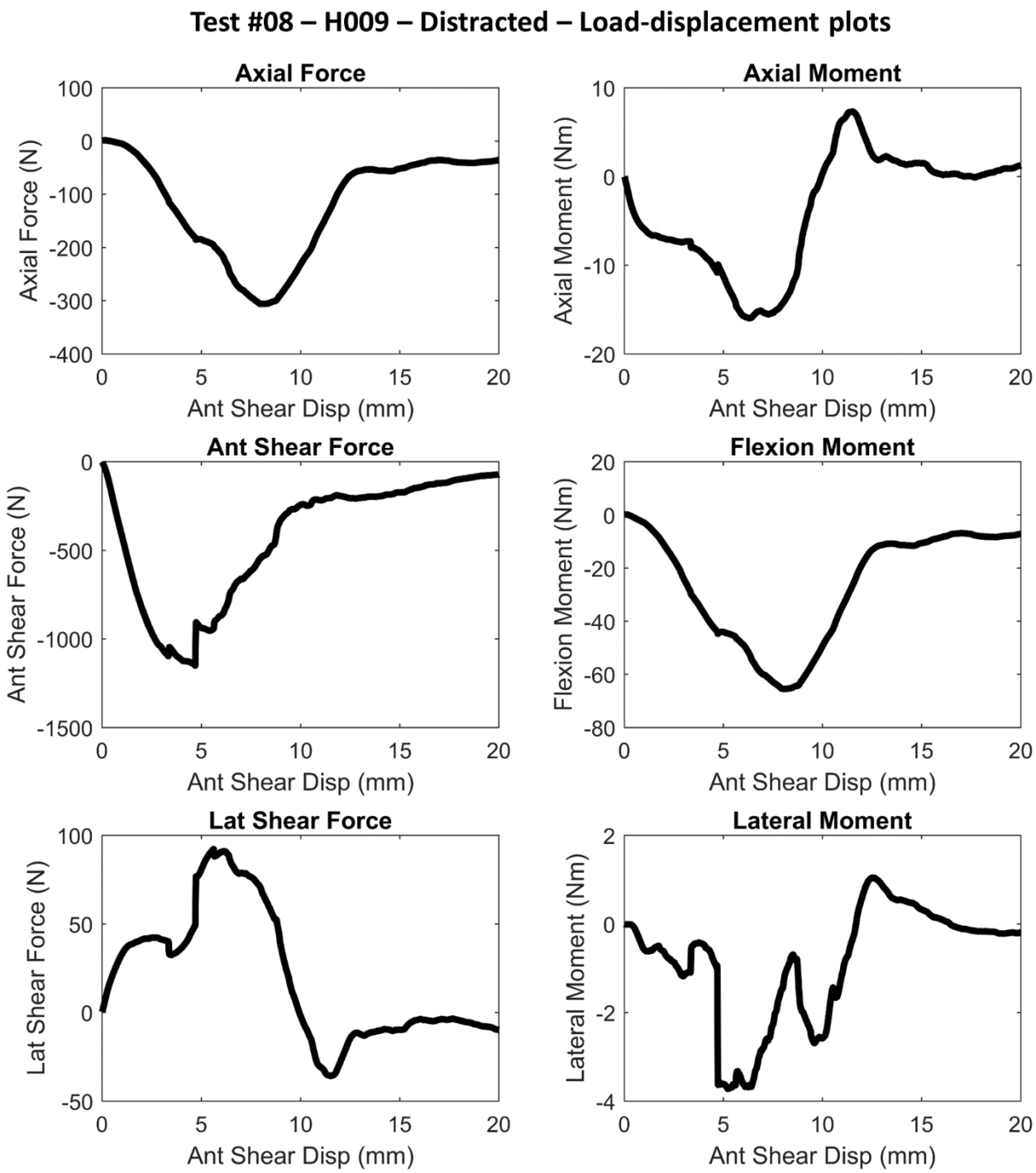

Figure 5.13: Six-axis load-displacement plots for 20 mm anterior shear applied to Specimen #8 with 2.5 mm of imposed distraction.

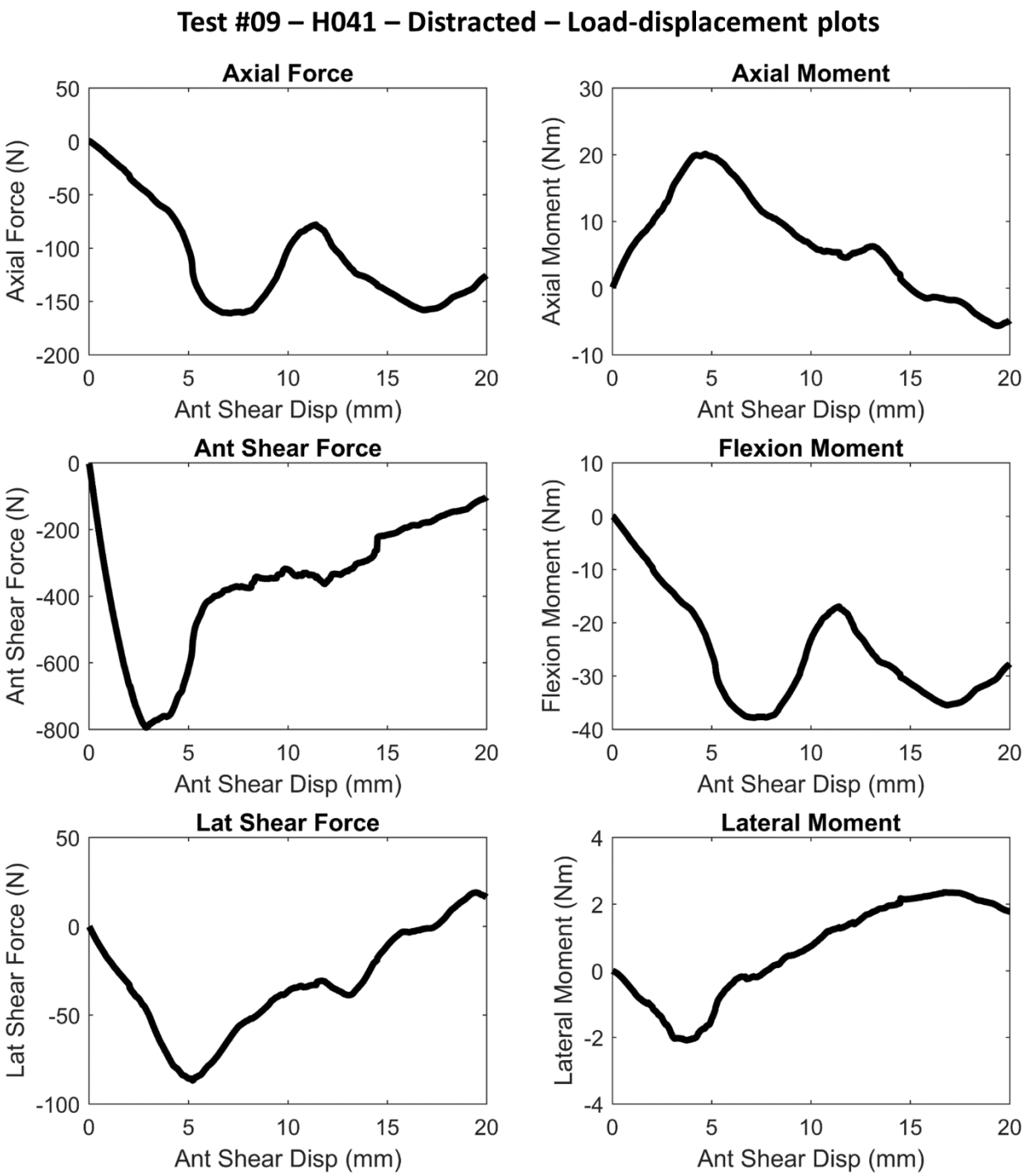

Figure 5.14: Six-axis load-displacement plots for 20 mm anterior shear applied to Specimen #9 with 2.5 mm of imposed distraction.

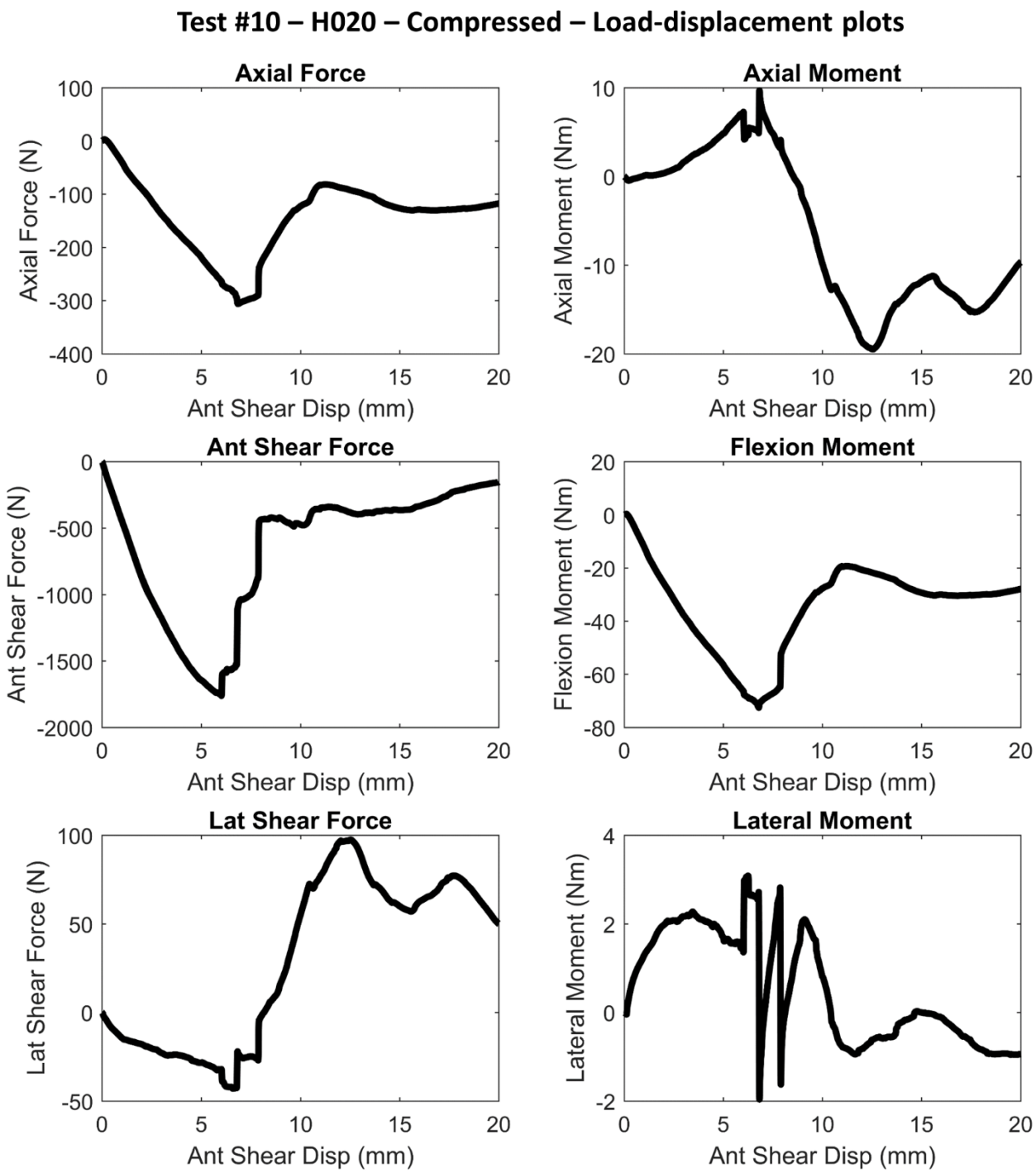

Figure 5.15: Six-axis load-displacement plots for 20 mm anterior shear applied to Specimen #10 with 300 N of imposed compression.

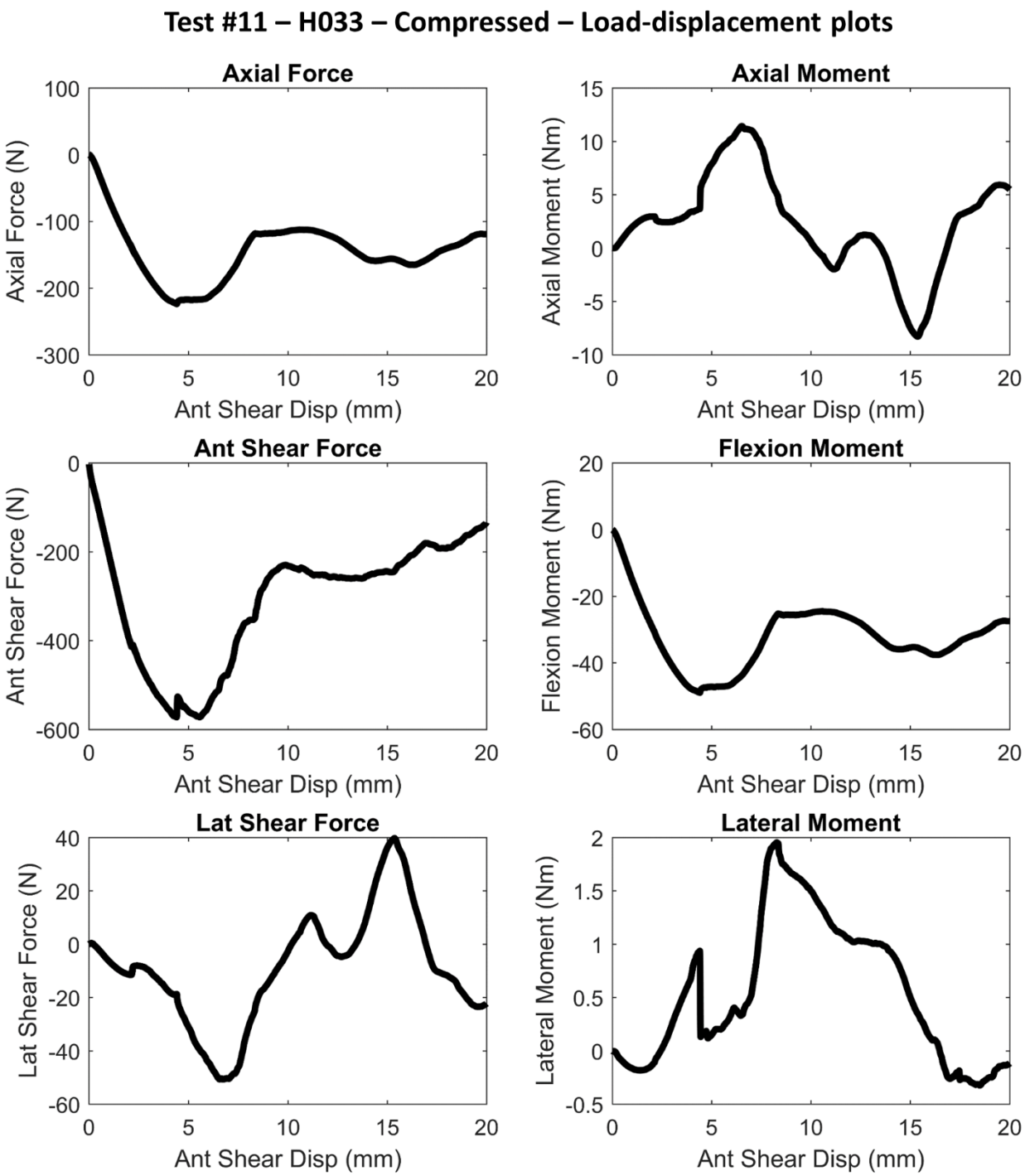

Figure 5.16: Six-axis load-displacement plots for 20 mm anterior shear applied to Specimen #11 with 300 N of imposed compression.

5.6 Supplementary material – Final linear mixed-effects models

Table 5.4: Final multivariable linear mixed-effects models for each outcome parameter at the supraphysiologic anterior shear analysis point.

Shear Load:			
Variable:	*EMMs (95% CI):*	*p-Value:*	*Estimate (95% CI):*
Axial State		0.2	
Compressed	-641.58 (-869.62, -413.53)		-198.80 (-521.30, 123.70)
Distracted*	-442.77 (-670.82, -214.73)		
** indicates reference category; N=12.*			
Axial Load:			
Variable:	*EMMs (95% CI):*	*p-Value:*	*Estimate (95% CI):*
Axial State		**0.002**	
Compressed	-108.26 (-142.89, -73.62)		-88.89 (-137.87, -39.91)
Distracted*	-19.37 (-54.01, 15.26)		
** indicates reference category; N=12.*			
Maximum Principal Strain:			
Variable:	*EMMs (95% CI):*	*p-Value:*	*Estimate (95% CI):*
Axial State		0.312	
Compressed	870 (416, 1324)		307 (-341, 956)
Distracted*	563 (103, 1022)		
Facet Height		**0.031**	93 (11, 174)
** indicates reference category. EMMs evaluated at Facet Height = 8.41 mm; N=23.*			
Minimum Principal Strain:			
Variable:	*EMMs (95% CI):*	*p-Value:*	*Estimate (95% CI):*
Axial State		0.916	
Compressed	-595 (-852, -338)		17 (-340, 375)
Distracted*	-613 (-879, -346)		
Facet Side		**0.001**	-976 (-1400, -551)
L	-1092 (-1447, -736)		
R*	-116 (-342, 110)		
Facet Angle		**0.013**	32 (8, 56)
** indicates reference category. EMMs evaluated at Facet Angle = 128.11 deg; N=23.*			
Maximum Shear Strain:			
Variable:	*EMMs (95% CI):*	*p-Value:*	*Estimate (95% CI):*
Axial State		**0.05**	
Compressed	1334 (928, 1739)		601 (-1, 1202)
Distracted*	733 (287, 1179)		
** indicates reference category; N=22.*			

Sagittal Facet Deflection:			
Variable:	*EMMs (95% CI):*	*p-Value:*	*Estimate (95% CI):*
Axial State		**0.031**	
Compressed	-0.537 (-1.157, 0.084)		0.951 (0.110, 1.791)
Distracted*	-1.487 (-2.054, -0.921)		

** indicates reference category. Negative values indicate a deflection of the facet away from the posterior surface of the vertebral body; N=24.*

Transverse Facet Deflection:			
Variable:	*EMMs (95% CI):*	*p-Value:*	*Estimate (95% CI):*
Axial State		0.642	
Compressed	-0.101 (-0.426, 0.223)		0.091 (-0.343, 0.524)
Distracted*	-0.192 (-0.487, 0.102)		
Facet Side		**0.009**	-0.968 (-1.637, -0.299)
L	-0.631 (-1.080, -0.181)		
R*	0.337 (-0.025, 0.700)		
Specimen Type		**0.041**	-0.459 (-0.892, -0.025)

** indicates reference category; N=24.*

Coronal Facet Deflection:			
Variable:	*EMMs (95% CI):*	*p-Value:*	*Estimate (95% CI):*
Axial State		0.213	
Compressed	-0.356 (-0.886, 0.174)		-0.420 (-1.126, 0.286)
Distracted*	0.064 (-0.404, 0.531)		

** indicates reference category; N=23.*

Chapter 6 Summary and integrated discussion

6.1 Overview

This thesis presents four studies that were undertaken to improve fundamental understanding of the injury mechanisms and biomechanics underlying traumatic subaxial cervical facet dislocation (CFD) and fracture-dislocation (CFD+Fx). In Study 1, a hard-copy medical record review of 'distractive flexion injuries' (DFIs – including subluxations, dislocations, and fracture-dislocations) of the subaxial cervical spine (Allen et al., 1982), admitted to the Royal Adelaide Hospital over a decade was performed to describe the epidemiology and radiographic features of these patients, and to identify which of these variables are risk factors for spinal cord injury (SCI). Custom software was developed to provide surgeons with a systematic method of quantifying subaxial cervical injury severity from radiographic images using recommended measurement techniques, and the inter- and intra-observer agreement of this method was evaluated.

In Study 2, the bilateral inferior facets of isolated subaxial cervical vertebrae were loaded in directions to simulate traumatic *in vivo* compressive-flexion and anterior shear motions, as these motions are thought to be associated with bilateral facet dislocation (BFD) and fracture-dislocation (BFD+Fx). The mechanical response of the facets during non-destructive testing, and at the point of anatomical failure, were quantified.

In Study 3, intervertebral axial compression and distraction were superimposed on non-destructive shear, bending and rotation motions of C6/C7 functional spinal units (FSUs) to investigate how intervertebral axial separation affected the mechanical response of the C6 inferior facets.

The same FSUs were used in Study 4 to develop a methodology to reliably apply 20 mm of constrained anterior shear motion with superimposed intervertebral axial compression or distraction (in the hope of producing BFD±Fx). The effect of axial condition on the biomechanical response of the C6 inferior facets at 2.19 mm of *supraphysiologic* anterior shear

were determined, and preliminary data from the point of initial anatomical failure was obtained. Injury patterns of the facets were investigated.

6.2 Summary of findings

6.2.1 Study 1

Study 1 is the first clinical study of traumatic subaxial cervical facet subluxation and dislocation in a cohort of 226 patients presenting to a single institution over a 10 year period. Epidemiology, radiographic analyses, and risk factors for SCI were reported (Quarrington et al., 2018b). Most patients (56.2%) sustained unilateral (51.2%) or bilateral facet (48.8%) dislocation. Facet fracture was more commonly associated with unilateral than bilateral DFIs, and 65% of unilateral dislocations had a concomitant fracture. The C6/C7 vertebral level was most commonly involved (38.5%) and injury to this level had the highest proportion of neurological involvement (45.3%); this result informed the decision to study the C6/C7 level in Studies 3 and 4. Younger adults (< 65 years) were over-represented amongst motor vehicle accidents, whilst falls contributed to the majority of DFIs sustained by older adults. Greater vertebral translation, together with lower facet apposition, distinguished facet dislocation from subluxation. Patients presenting with facet dislocation (vs. subluxation), bilateral facet (vs. unilateral facet) injury, and reduced GCS, were most likely to have an associated SCI. Spinal canal occlusion (measured on CT) and spinal cord compression (measured on MRI) measurements at the level of bony injury were the radiographic measures most predictive of SCI. All radiographic measurements demonstrated at least "moderate" inter- and intra-observer agreement, with most demonstrating "almost perfect" reproducibility.

6.2.2 Study 2

The mechanical response of the inferior facets of subaxial cervical vertebrae differed significantly between quasi-static loading that simulated non-traumatic anterior shear motion, and that which simulated compressive-flexion. Facet stiffness and failure load were significantly greater in the compressive-flexion loading direction, and deflection and surface strains were higher in anterior shear at the non-destructive analysis point (47 N applied load). The non-

traumatic strains and stiffness responses differed between the upper and lower subaxial cervical regions. Facet deflections greater than 10° were observed at the point of failure, demonstrating that the vertebral body and posterior elements are unlikely to be well represented as a single rigid body during simulations of cervical trauma. Fracture occurred through the facet tip during anterior shear loading, while failure through the pedicles was most common in compressive-flexion. The difference in fracture location occurred due to translation of the loading pins as the facets deflected in the anterior shear testing orientation. In contrast, the point of contact remained constant during the compressive-flexion tests, and this corresponded with significantly larger failure load for the specimens that were failed in the simulated compressive-flexion test direction. Specimen-specific variables such as spinal level, gender, and vertebral size, were significantly associated with most outcome measures, indicating that these parameters are important considerations during the development and validation of computational models involving the cervical facets.

6.2.3 Study 3

Simulated head-weight loading (50 N) and neck muscle bracing (300 N) generally increased loading of the inferior facets of C6 (as measured by deflection and surface strain), compared to 2.5 mm of axial distraction, when imposed on quasi-static, constrained, anterior shear, axial rotation, flexion, and lateral bending motions of C6/C7 FSUs. Minimum principal and maximum shear strains were largest in the compressed condition for all motions, except for minimum principal strains during axial rotation. For right axial rotation, maximum principal strains were significantly larger for the 'unloaded' right facets (presumably caused by the capsule restricting inter-facet separation), and minimum principle strains were larger in magnitude for the left facets (due to bony facet engagement), regardless of axial condition. Sagittal deflections were largest in the compressed conditions during anterior shear and lateral bending motions, when adjusted for facet side.

6.2.4 Study 4

A method to apply constrained, supraphysiologic intervertebral anterior shear with superimposed axial compression or distraction to C6/C7 FSUs was iteratively developed. For the first time, BFD+Fx was experimentally produced in 5/12 specimens – 3 specimens were superimposed with 300 N compression, while 2 were superimposed with 2.5 mm of axial distraction. All 12 specimens achieved 2.19 mm of *supraphysiologic* anterior shear prior to embedding failure. Change in axial load (disregarding the imposed axial compression/distraction forces), and shear strain at the C6 inferior facet base, were both larger for the compressed specimens at the supraphysiologic and failure analysis points, while shear displacement and load were also generally larger at failure for these specimens. Sagittal facet deflections were significantly larger for the distracted group at 2.19 mm of shear and were similar to the compressed specimens at failure. Non-sagittal deflections were generally larger for the compressed specimens at both analysis points, probably due to the inclined angle of the C6/C7 facet joint relative to the coronal plane and the increased facet engagement for the compressed specimens. Clinically relevant facet fractures were created during the five successful experiments, demonstrating that intervertebral anterior shear motion contributes to BFD+Fx.

6.3 Epidemiology and radiographic features of CFD

The demographics and injury mechanisms of the large-scale cohort investigation of subaxial cervical subluxation, dislocation, and fracture-dislocation injuries were consistent with small-cohort studies of DFIs and comparable to reports of cervical trauma as a whole. Young males in high-velocity motor vehicle accidents, and elderly individuals suffering head-contact during falls, were the most common demographics in this cohort. Although it is difficult to confirm without detailed information regarding mechanism of injury, it appears unlikely that any of the CFD±Fx cases occurred *without* contact to the head (i.e. inertial injury mechanism) – CFD cases with concomitant injuries reported in the case-notes generally described associated head/facial injuries, and this sub-cohort had lower mean GCS than other DFIs (13.85±2.98 vs. 14.07±2.38). This agrees with Foster *et al.* (2012) who noted that concomitant head/facial injury

occurred for all cases of CFD reported in the NHTSA Crash Injury Research and Engineering Network (CIREN) database. Collectively, this suggests that CFD±Fx is rarely caused by inertial motion of the head during high deceleration events and is most often due to a compressive force applied to the head.

SCI was most commonly associated with BFD and was present in over 60% of cases, although this is lower than the prevalence reported in the literature (Allen et al., 1982; Doran et al., 1993; Hadley et al., 1992; Lintner et al., 1993; Vaccaro et al., 1999). This discrepancy may be due to selection bias towards more severe cases, as most studies that report the incidence of SCI in cases of BFD relate to surgical candidates. Others have reported an association between concomitant facet fracture and *reduced* neurological involvement (Argenson et al., 1988; Chakravarthy et al., 2014; Piccirilli et al., 2013; Shanmuganathan et al., 1994) but this was not observed in the current study, perhaps because SCI was not stratified by ISNCSCI/AIS score.

Facet fractures were associated with over 60% of CFDs and occurred more frequently in cases of UFD than BFD. This is consistent with previous small-cohort reviews of DFIs (Allen et al., 1982; Argenson et al., 1988; Beyer et al., 1991; Shanmuganathan et al., 1994). This may be due to the primary injury vector associated with UFD±Fx, and less severe soft-tissue damage associated with these injuries. Axial rotation is traditionally thought to be associated with UFD±Fx (Hodgson and Thomas, 1980; Maiman et al., 1983; Roaf, 1960), and UFD-Fx has been created when quasi-static axial rotation, combined with small amounts of flexion and lateral bending, was applied to cervical FSUs (Nadeau et al., 2012). In Study 3, 4° of constrained, non-destructive axial rotation produced the largest deflections of the contralateral 'loaded' facet, and highest surface strains of *both* facets (regardless of imposed axial loading) of all the directions tested. In addition, clinical UFD±Fx cases often present with less severe injury of the surrounding soft tissue compared to BFD±Fx (Allen et al., 1982) – these structures likely restrict intervertebral separation during trauma. Reduced intervertebral axial separation resulted in significantly higher shear strains at the base of the engaged facet, and larger (but not significant) facet deflections, in Study 3. These experimental findings seem to support the theory that maintaining surrounding

soft-tissue structures during UFD will increase the loading transmitted to the facets, possibly resulting in fracture.

6.4 Measuring the mechanical response of the subaxial cervical facets during defined loading

The results of Study 1 support the findings of small-cohort studies that facet fractures are commonly associated with CFD, especially UFD (Allen et al., 1982; Argenson et al., 1988; Beyer et al., 1991; Shanmuganathan et al., 1994). However, facet fractures are rarely created during the experimental production of CFD in human cadaver cervical spines. This may be due to an absence of muscle force replication (either passive or to simulate neck bracing) which may produce a larger component of *anterior shear* in the local injury vector (Foster et al., 2012; Nightingale et al., 2016). For nearly 60 years, biomechanical investigations of cervical trauma have postulated that intervertebral anterior shear loads and motions are likely associated with CFD±Fx (Cripton, 1999; Hodgson and Thomas, 1980; Ivancic, 2012b; Maiman et al., 1983; Nightingale et al., 2016; Panjabi et al., 2007; Roaf, 1960), but the effect of this loading direction on cervical facet mechanics has not been thoroughly investigated. Understanding the biomechanics of the subaxial cervical facets during supraphysiologic and traumatic anterior shear motions is crucial to understanding the mechanisms of CFD+Fx.

The mechanical response of the *lumbar* facets to simulated physiologic and traumatic loading scenarios has been reported, and the strain response of the cervical facet capsule during whiplash is well understood, but this thesis reports the first series of experiments to investigate the biomechanics of the subaxial cervical facets during replicated supraphysiologic and traumatic motions. Most research towards understanding subaxial cervical trauma has involved dynamic, drop/impact testing of whole cervical spines (with or without heads) during which the applied intervertebral loading is relatively uncontrolled. These experiments have not produced clinically relevant CFD+Fx. Therefore, the overall aim of Studies 2, 3, and 4 was to obtain information about the response of individual anatomical units (including the facets) when loaded in the directions traditionally associated with cervical trauma – namely anterior shear, flexion, axial

rotation, and lateral bending. Improving fundamental understanding of how the facets respond to these defined loading directions may elucidate the mechanisms of CFD+Fx, and the quantitative information obtained can be used to validate computational models of cervical trauma.

6.4.1 Testing methods

In Study 2, angular deflections, apparent stiffness, surface strains, and failure load of isolated subaxial cervical bilateral inferior facets were measured during loading that simulated the proposed injury vectors of supraphysiologic *in vivo* compressive-flexion and anterior shear motions. These intervertebral motions have been observed in the lower cervical spine during experimentally produced BFD (Hodgson and Thomas, 1980; Ivancic, 2012b; Nightingale et al., 2016; Panjabi et al., 2007), but the individual contributions to facet loading, and risk of associated facet fracture, of each motion are not well understood. Loading was applied directly to the bilateral articular facet surfaces using custom hemispherical loading pins attached to the actuator of an Instron materials testing machine. Specimens were subjected to non-destructive loading in each direction by orientating the articular facet surfaces relative to the actuator to simulate the loading vectors applied by the opposing facets during each motion (Figure 3.3). This testing methodology was informed by studies that investigated the mechanical response of the posterior elements of isolated *lumbar* vertebrae (Cyron and Hutton, 1978; Cyron et al., 1976; Suezawa et al., 1980).

The loading directions used to simulate each motion were deduced from close inspection of the subaxial cervical facet joint anatomy and their load-bearing role during intervertebral anterior shear and compressive-flexion motions (Figure 3.3). Intervertebral anterior shear motion occurs in the sagittal and transverse planes, with the superior vertebra translating anteriorly relative to the inferior vertebra. This motion causes the bilateral facet joints to engage due to their inclined, overlapping sagittal orientation. Therefore, loading was applied to the bilateral inferior articular facet surfaces in a postero-anterior direction, parallel to the inferior vertebral endplate (Figure 3.3). During *physiological* subaxial cervical flexion motion the subaxial cervical facets are unloaded (Jaumard et al., 2011a); however, this study aimed to simulate inter-facet loading

during supraphysiologic compressive-flexion motion, such as that caused by a global axial compression with large anterior eccentricity – this loading scenario was proposed as a likely cause of BFD±Fx by Allen *et al.* (1982). Such a scenario may force the centre of rotation of intervertebral flexion further anterior and inferior than occurs physiologically, causing the facet joints to engage rather than separate. This scenario was simulated by applying loading to the bilateral facets that was directed perpendicular to the articular facet surfaces.

Axial rotation is commonly associated with UFD±Fx (Hodgson and Thomas, 1980; Maiman et al., 1983; Roaf, 1960), but it was not possible to investigate the mechanical response of the facets to unilateral inter-facet loading using the Study 2 testing methodology. The line of action of the axial rotation 'injury' vector passes through the vertebral body, making it impractical to load the inferior articular facet surface in this direction using a loading pin. However, investigating the mechanical response of the facets during intervertebral axial rotation, as well as anterior shear, flexion, and lateral bending motions, was achieved in Study 3 by using FSUs.

Facet deflection and surface strain measurement methods were developed in Study 2 and were modified as needed for Study 3 and Study 4. Angular deflection (or 'bending') of the facets and posterior elements relative to the vertebral body was first described by Cyron *et al.* (1976) during destructive testing of *lumbar* vertebrae. Green *et al.* (1994) measured sagittal deflections exceeding 14° during physiological flexion of lumbar FSUs using an infrared motion-capture system; however, this two-dimensional system did not measure non-sagittal deflections. A similar analysis had not previously been reported for the cervical spine.

6.4.2 Angular facet deflections

For the first time, 3D deflections of the subaxial cervical facets were measured in Studies 2, 3, and 4 by rigidly fixing custom, light-weight, motion capture marker-carriers to the bilateral facets and to the vertebral body. The three-camera Optotrak Certus HD motion-capture system (Northern Digital Inc., Ontario, Canada) captured the 3D co-ordinates of these marker-carriers during each test, from which sagittal, transverse, and coronal angular deflections of the facets

were calculated by solving for Euler angles. Accuracy and repeatability of this system was deemed adequate to capture these deflections (Appendix B)

Non-sagittal deflections were negligible during non-destructive and destructive simulated anterior shear and compressive-flexion loading in Study 2, but were considerable during axial rotation in Study 3 and at the two supraphysiologic anterior shear analysis points in Study 4 (2.19 mm and initial anatomical failure). It is unsurprising that sagittal deflections were larger than transverse and coronal deflections during non-traumatic anterior shear motion (as reported in Studies 2 and 3) given the largely coronal orientation of the subaxial cervical facet joints. Transverse and coronal C6 inferior facet deflections were negligible at the point of failure in Study 2 (0.45±0.31° and 0.23±0.26°, respectively); however, in Study 4 transverse and coronal deflections were consistently larger for the compressed than the distracted specimens, and their magnitudes were comparable to the sagittal deflections. The discrepancy between the results of Studies 2 and 4 is likely due to the difference in load-application methodology and the anatomical orientation of the C6/C7 facet joints (discussed in detail in Section 6.5.2). The significance of these 'off-axis' deflections demonstrates the importance of obtaining 3D kinematic data during biomechanical experiments, even during 'planar' motions.

Interpreting 3D angular deflections of the facets proved challenging. Solving for Euler angles conveniently compartmentalised the deflections into anatomically-relevant planes, but anatomical differences (both inter- *and* intra-specimen), or small misalignments when assigning co-ordinate systems, may have caused deflections to be distributed inconsistently between these planes, especially during asymmetric motions. This was observed in Study 3, where the difference in sagittal and transverse deflections between the compressed conditions (50 and 300 N), and the distracted condition, was not statistically significant for right axial rotation despite clear evidence of a trend for both the left and right facets. The standard errors for this test direction were larger than the other motions, supporting our theory that the facet deflections observed during axial rotation were primarily 'sagittal' for some specimens but had a larger component in the 'transverse' plane for others. It is likely that 'resultant' facet deflections would have been

significantly different between axial condition groups during axial rotation; however, representing a change in 3D angulation as a single value is difficult, especially for variations that are small in magnitude. Use of the helical axis of motion to characterise the deflection of each facet, relative to the vertebral body, as a translation along and a rotation about this axis was investigated, but this method has large associated errors for angles <5° (Metzger et al., 2010).

6.4.3 Principal and shear surface strains

Tri-axial rosette strain gauges were fixed to the bilateral inferior facet bases, slightly superior to the insertion point of the inferior facet capsule, of each specimen tested in Studies 2-4 to quantify maximum and minimum principal surface strains, and maximum shear surface strains during loading. There is very little published experimental cervical facet strain data with which to compare. Maximum and minimum principal strains during non-destructive, *constrained* anterior shear motions in Study 3 were generally larger than during *unconstrained* anterior shear applied to subaxial cervical FSUs (Cripton, 1999), despite larger shear displacement (mean 2 mm) in the latter study. Maximum principal strains at the point of facet failure during simulated anterior shear loading of the isolated C6 specimens reported in Study 2 were comparable to the successful tests in Study 4, but shear strains were lower. This difference in shear strains may be due to different loading methods in the two studies. In Study 4, the conforming angled C7 superior facets may have produced less shearing deformation at the facet bases than the rigid, point-loading pins used in Study 2.

The principal strain responses of the left and right facets were significantly different during right axial rotation in Study 3. Despite typically being considered 'unloaded' during this motion, *maximum principal* (tensile) strains at the right facet bases were similar in magnitude to the *minimum principal* (compressive) strains measured for the 'loaded' left facets. It is likely that the tensile principal strains observed at the right facets were caused by the facet capsule restricting inter-facet separation, whilst the compressive strains of the left facets were due to bony contact. This hypothesis is supported by the corresponding facet deflection results, which demonstrated large deflections of the left facets *away* from the vertebral body (as would be expected to occur

for the inferior facets during facet joint compression), whilst the right facets demonstrated bending *towards* the vertebral body (and towards the opposing C7 superior facet) which could only be caused by the capsular ligament. These results suggest that the facet capsules have a substantial impact on cervical facet mechanics during axial rotation and should be modelled appropriately during computational simulations of cervical motion.

In Study 3 and 4, strain gauges could not be attached to the bony surface of the facet tip without disrupting the C6/C7 facet capsules, so the strain response at the fracture site was not measured. Full-field strain measurement techniques, such as digital image correlation, could be used to quantify strains over the entire posterior surface of inferior subaxial cervical facets, but this would require resection of the capsule and other surrounding soft-tissue. Compromising these structures may change the biomechanical response of the facets to loading. Further work is required to develop methods that can quantify *in vivo* surface strains of the cervical facets.

Occasionally, large variations in strain magnitudes, both between specimens and between facets for the same specimen, were observed in Studies 2-4. Surface strain measurements of bone are highly dependent on the quality and structure of the underlying bone, and on the anatomical location of the strain gauge. Therefore, intra- and inter-specimen anatomical variability, and difficulties in replicating strain gauge placement, likely contributed to the variation in strain readings. The effect of this variation was mitigated by using linear mixed-effects models (with a random effect of facet side nested within cadaver ID) to evaluate within-specimen differences between groups. In accordance with the assumptions of these statistical models, any significant outliers were omitted from each analysis.

6.4.4 Failure mechanisms

Fractures of the facet tip, articular pillar, spinous process, and laminae (usually of the superior vertebra), and occasionally vertebral body fractures of the inferior vertebra, are associated with CFD (Allen et al., 1982). The mechanisms leading to each of these fracture types are not well understood and had not previously been observed experimentally. In Study 2,

clinically relevant facet fractures (Vaccaro et al., 2016) were produced and the mechanical response of the subaxial cervical facets to simulated traumatic inter-facet loading was directly observed. For all 13 specimens failed under simulated anterior shear, the point of load application translated inferiorly towards the facet tips as the facets deflected away from the line of action of the loading pins. As this translation occurred the volume of bone beneath the loading pins decreased until fracture occurred through the facet tips. In contrast, fracture through the pedicles was observed for most specimens failed in the compressive-flexion direction (6/11). The point of contact of the loading pin did not translate for these specimens, and the axis of rotation of the facet deflections appeared to be about the pedicles (Figure 3.11). Failure through the pedicles was associated with significantly higher failure loads than fracture through the facet tips, probably due to this region having a higher proportion of dense cortical bone.

The fractures observed during constrained, destructive intervertebral anterior shear in Study 4 (due to facet-on-facet contact loading) were generally consistent with those observed during the simulated anterior shear loading in Study 2. C6 inferior facet tip fractures occurred during all five successful tests, regardless of the axial condition imposed. Direct visualization of the exact mechanisms leading to failure were not possible due to the presence of surrounding soft tissue, but the comparable fracture patterns to those of the anterior shear tests of Study 2 suggest a similar response of the C6 inferior facets in the FSU model. A spinous process fracture occurred for one specimen, but no such fractures were observed in Study 2. This fracture was probably caused by the nuchal ligament restricting anterior translation of C6, or interference of the C6 and C7 spinous processes. Neither the nuchal ligament nor the C7 vertebra (including the spinous process) were present in Study 2, and these different boundary conditions should be considered when interpreting the results of these studies.

6.4.5 Specimen-specific parameters

Specimen-specific parameters including spinal level, gender, age, vertebral size, facet geometry, and vBMD were significantly associated with the outcome measures in Studies 2-4. This information may help to develop improved computational models of cervical spinal motion

and trauma, as many simulations use generic cervical-spine segment models. The anatomical geometry and material properties of these models are usually derived from average measurements of numerous cadaveric specimens (such as Panjabi *et al.* (1991) and (1993)), disregarding demographic and individual variation that may significantly alter the mechanical response of the facets during loading.

In Study 2, the interaction of test direction (anterior shear or compressive-flexion) and specimen level was significantly associated with facet stiffness, and specimen level was significantly associated with maximum shear strain (Section 3.5). Post-hoc analysis demonstrated that the stiffness and strain response differed between the upper (C3-C5) and lower (C6-C7) levels of the subaxial cervical spine. Facet stiffness was greater at the lower than the upper levels for anterior shear, but the opposite was true for compressive-flexion. This difference is likely due to the change in facet and pedicle orientation observed at the lower cervical levels (Panjabi et al., 1991; Panjabi et al., 1993) as this angle will alter the contributions from the other posterior elements in resisting the applied loads. Maximum shear strains were significantly higher at the lower levels than at C3 and C4, regardless of test direction. Smaller facet size in the lower cervical spine (Panjabi et al., 1993), and the aforementioned variations in facet angle between the upper and lower regions, probably cause this difference in surface strains. As such, the upper and lower regions of the subaxial cervical spine should be considered independently when modelling cervical motion and trauma.

Gender, vertebral size, and facet geometry, were significantly associated with facet surface strains at non-destructive analysis points in Studies 2-4. As discussed in Section 6.4.3, surface strain measurements from strain gauges are highly dependent on the region of bone on which they are fixed, so anatomical variations (both within and between specimens) are likely to affect these measurements. The significant association between specimen-specific parameters and surface strain measurements in our experiments demonstrate that such parameters should be used (wherever possible) when developing and validating computational models of the cervical spine.

6.5 The effect of imposed axial compression and distraction during intervertebral anterior shear of cervical FSUs

6.5.1 Load-displacement response

Facet contact, intervertebral disc pressure, and elongation of surrounding soft-tissue structures contribute to the load-displacement (or "stiffness") response of cervical FSUs (Cripton, 1999; Hartman et al., 2016; Rasoulinejad et al., 2012), and their relative contribution to this response is likely affected by intervertebral axial separation. In Study 3 and Study 4, the loads at peak anterior shear displacement and at the supraphysiologic shear/failure analysis point, respectively, were used as a surrogate measure for stiffness – the shear load-displacement plots for each axial condition had distinctly different linear regions, so traditional stiffness measurements were not performed.

In Study 3, peak anterior shear loads were comparable to those observed at corresponding intervertebral anterior shear displacement of subaxial cervical FSUs (Cripton, 1999; King Liu et al., 1982; Moroney et al., 1988; Shea et al., 1991). Cripton (1999) observed an increase in overall shear stiffness when a compressive preload of 200 N was imposed on anterior shear motion (111.7±13.6 vs. 90.9±10.9 N/mm without axial preload). This is consistent with those observed in Study 3, as significantly larger peak anterior shear loads were observed at 1 mm displacement for the compressed compared to neutral condition. Axial condition was also associated with peak axial moments in Study 3. Superimposed axial compression caused the largest axial moments, followed by the neutral and then distracted axial conditions, but no such association was observed for the flexion or lateral bending motions. Anterior shear and axial rotation motions occur in the transverse plane, so (in principle) intervertebral axial separation should not change throughout constrained motion, whereas flexion and lateral bending (with fixed CoR) inherently cause distraction/compression of the posterior/anterior and contralateral/ipsilateral anatomy, respectively. This may explain why imposed axial distraction/compression significantly altered the 'stiffness' response in anterior shear and axial rotation, but not in flexion and lateral bending.

In Study 4, the change in axial and shear loads (from unloaded) at 2.19 mm of supraphysiologic anterior shear motion tended to be larger for the compressed specimens, when compared to the distracted specimens. The significant difference in axial force between axial condition groups was expected, as these forces are likely due to facet engagement which is affected by axial separation. The load-bearing proportion of the subaxial cervical facets increases substantially under high axial compression loads (Teo and Ng, 2001), indicating increased facet engagement, whereas intervertebral axial distraction causes separation of the articulating facets (Figure 6.1). Applying 2.19 mm of constrained anterior shear to the compressed specimens caused further engagement (compression) of the facet joints, further increasing the initial inter-facet loads. For the distracted specimens, a region of low-stiffness was observed at the beginning of each axial load-displacement trace (Figure 5.13 and Figure 5.14 in Section 5.5), suggesting that no facet engagement occurred initially. Upon engagement of the facet joints (presumably articulation of the facet tips due to the superimposed distraction, Figure 6.1d), a smaller change (compared to the compressed specimens) in axial and shear forces was produced. This difference was significant for the change in axial force, but not for the difference in shear force. This may suggest that the resistance to shear motion for the distracted specimens, presumably due in part to elongation of the surrounding ligaments, is comparable to the resistance provided predominantly by facet contact for the compressed specimens. The significantly larger change in distractive axial load for the compressed group supports the theory that these specimens experienced greater facet engagement, as the off-axis forces would primarily be caused by the inclined sagittal angle of the subaxial cervical facets – such off-axis forces occurred during the simulated anterior shear loading of isolated facets in Chapter 3.

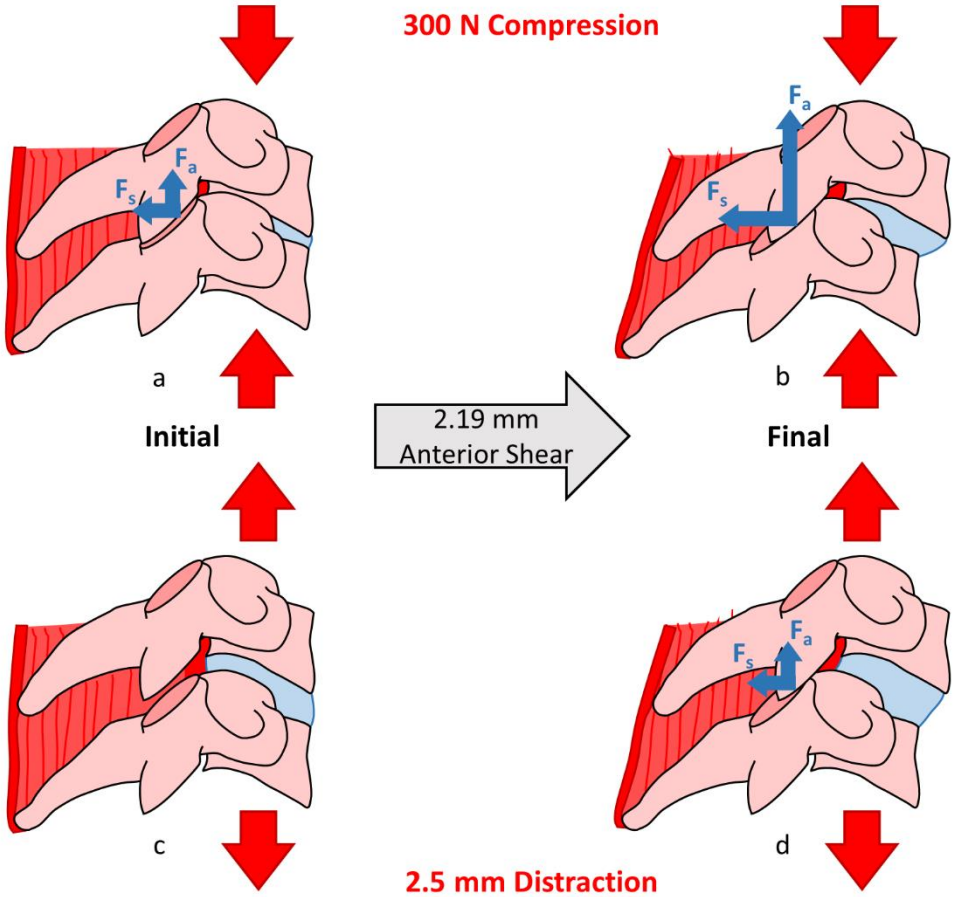

Figure 6.1: Illustrations of facet contact and proposed inter-facet loads when 300 N of axial compression (b) and 2.5 mm of axial distraction (d) are superimposed on 2.19 mm of constrained anterior shear motion. (a) Intervertebral axial compression engages the articulating facets, producing initial axial (F_a) and shear (F_s) inter-facet loads due to the inclined angle of the C6/C7 facet joints. (b) Constrained anterior shear motion further compresses the facet joint, increasing inter-facet loads. (c) Intervertebral distraction initially unloads the facet joints. (d) Constrained anterior shear motion causes only the facet tips to engage (after a low-stiffness region suggesting no inter-facet loading), producing a smaller change in F_a and F_s than for the compressed specimens. Intervertebral motions and force arrows have been exaggerated for illustration purposes.

In general, larger shear and axial loads, and shear displacements, were observed at the point of initial facet fracture for the specimens in the compressed group, compared to the distracted specimens. The difference in shear displacement is probably due to differences in the initial location of facet contact. For the compressed specimens, the initial centre of facet contact would have coincided with the approximate geometric centre of the articular facet surfaces. As the facets deflected during the anterior shear motion, the centre of facet contact likely translated towards the facet tips until the volume of articulating bone was insufficient to withstand the inter-facet loads, and subsequent fracture occurred. This mechanism of facet fracture associated with anterior shear motion is described in Chapter 3 (see Figure 3.11). For the distracted specimens,

the centre of contact upon initial facet engagement would have been closer to the facet tips (Figure 6.1d), so less shear displacement and load was required to produce a facet fracture.

6.5.2 Angular facet deflections

In Study 3, sagittal facet deflections were significantly larger when axial compression (either 50 or 300 N) was imposed on 1 mm of anterior shear motion, compared to when the specimen was distracted. Larger deflections for the compressed specimens were associated with higher surface strains, supporting the conclusion that the facets experience greater loading in this condition, compared to the distracted condition.

During supraphysiologic and traumatic anterior shear motions the compressed specimens almost always exhibited larger *non-sagittal* facet deflections than the distracted group, and this is likely due to differences in facet engagement area. The articulating plane of the C6/C7 facet joints is (on average) orientated at approximately 10° to the coronal plane, with the lateral facet 'edges' angled slightly anteriorly (Panjabi et al., 1993). Therefore, during supraphysiologic and traumatic constrained anterior shear motions it is likely that transverse deflections would occur and would be greater for the compressed specimens in which the articulating facets are fully engaged. In contrast, if the facet engagement area is lower for the distracted specimens (i.e. only the tips are in contact) then the coronal orientation of the articulating surfaces would be less likely to cause off-axis facet deflections. This may explain why, at 2.19 mm of shear, sagittal facet deflections were significantly *lower* for the *distracted* specimens despite strain magnitudes being comparable or *smaller* than the *compressed* specimens, as three-dimensional 'resultant' facet deflections would likely be similar between groups.

Sagittal facet deflections at the point of facet failure in FSUs (Study 4; average of the compressed and distracted specimens = 3.76°) was comparable with those measured for the isolated C6 specimens that were failed in the simulated anterior shear direction (Study 2; 3.43°). The similarity in sagittal deflections suggests that the point loading applied to the isolated facets in Study 2 was not substantially dissimilar to *in vivo* facet loading conditions; however, non-

sagittal deflections were substantial in Study 4 (particularly for the compressed specimens) but were negligible in Study 2. The rigid loading pins applied a point force in a constant, defined direction, causing the facets to deflect in the sagittal plane during simulated anterior shear. In contrast, the superior facets of C7 are angled by up to 11° relative to the coronal plane (Panjabi et al., 1993) and likely deflect as they engage with the inferior C6 facets. The angled loading surface likely produces non-sagittal facet deflections during traumatic anterior shear.

6.5.3 Principal and shear surface strains

The larger facet deflections observed for the compressed conditions in Studies 3 and 4 generally corresponded to higher surface strains (compared to the distracted condition). This difference was statistically significant for minimum principal and maximum shear strains at 1 mm of anterior shear, and for minimum principal strains at the supraphysiologic shear analysis point (2.19 mm). In Study 3, minimum principal strains magnitudes were approximately twice that of the maximum principal strains for the compressed groups, indicating that the facet bases were primarily experiencing compressive load in this axial condition; however, tensile principle strains were larger for the distraction tests. Minimum principal strains differed significantly between the left and right facet bases at the supraphysiologic analysis point in Study 4, making interpretation difficult. This difference may be due to anatomical asymmetry, as 'facet angle' was a significant covariate in the final LMM. Within-specimen facet angle asymmetry was 5.4±5.9° (range: 0.1 – 19.9°), and an average difference in facet height of 2.0±1.1 mm was measured. Such asymmetry of the subaxial cervical facet anatomy has previously been described (Panjabi et al., 1993). Correlation between this anatomical asymmetry and the large difference in compressive strain magnitudes is difficult to decipher.

In contrast to the sub-failure results, *maximum principal* and shear strains were generally larger for the compressed group at point of failure, and minimum principal strains were similar for the two groups (excluding one outlier in the compressed group). With the exception of one specimen (#10), the fractured facet experienced maximum principal strain magnitudes that were consistently larger than minimum principal strains. This demonstrates that the C6 inferior facet

bases experience high tensile loading during supraphysiologic anterior shear displacement and may be at risk of failure.

6.6 Limitations of the mechanical testing

In Studies 2-4, quasi-static loading was applied to isolated subaxial cervical facets, and intervertebral motions were applied to C6/C7 FSUs, at rates that are substantially lower than those estimated to occur during cervical trauma. A *minimum* global impact velocity of 3 m/s is generally thought necessary to produce clinically relevant injuries during head-impact testing of full cervical spines (McElhaney et al., 1979; Nightingale et al., 1996; Saari et al., 2013) and it is likely that *in vivo* loading rates are considerably higher than this during high-speed MVAs or falls (~6 m/s assuming same-level fall height of 1.8 m) leading to CFD (Quarrington et al., 2018b) (Chapter 2). However, dynamic head-impact testing of whole cervical spines has not produced CFD+Fx, and generally results in uncontrolled intervertebral motion and loading. The overall aim of Studies 2-4 was to obtain information about the response of individual anatomical units, specifically the inferior facets, when loaded in defined, consistent directions that are traditionally associated with CFD±Fx, and to investigate the injury mechanisms that may differentiate CFD+Fx from CFD-Fx.

6.6.1 The use of functional spinal units

Short spinal segments such as FSUs have been used in biomechanical laboratory experiments for decades (Edwards, 1998). Where full cervical spines can respond unpredictably to applied loading, due in part to anatomical variations in their many biological components, FSUs can be manipulated to simulate the intervertebral motions observed during trauma. However, the use of FSUs has its own limitations such as non-physiological boundary conditions. To reliably apply defined intervertebral motions to the FSUs in Studies 3 and 4, approximately one-third of the superior and inferior anatomy of C6 and C7, respectively, were embedded in PMMA – this included the joining superior/inferior facets of the bilateral articular pillars, and some of the spinous processes, of each vertebra.

It is likely that the non-physiologic boundary conditions in Studies 3 and 4 affected the mechanical response of the C6 posterior elements and inferior facets. Embedding the adjoining superior facet of the C6 articular pillars effectively applied a fully-constrained condition at these locations, which likely prevent some deflection of the C6 posterior elements (including the inferior facets). As such, the C6 inferior facet deflections measured in these studies are likely an *underestimate* of the deflections that occur in vivo during C6/C7 intervertebral motions. It is difficult to hypothesise how these boundary conditions may have affected the facet surface strains as this is likely influenced by the altered deflection of the posterior elements, and end-effects of the constrained anatomy. To account for the effect of these boundary conditions, repeated measures analysis was used to determine the effect of axial condition on within-specimen facet loading (in Study 3), and great care was taken to ensure that each specimen was prepared in a consistent manner. When using this data to validate subject-specific computational models of cervical FSUs, it is important to incorporate these boundary conditions.

6.6.2 Quasi-static loading rates

Quasi-static loading rates were necessary to maintain accurate control of the materials testing machines so that non-destructive load and displacement limits weren't exceeded. During non-destructive testing in Studies 2 and 3, pre-determined load and displacement limits ensured that the specimen was not unintentionally damaged. This enabled testing of each specimen in multiple directions/conditions so that within-specimen comparisons could be performed. Due to the test setup in Study 2 it was also necessary to limit the travel of the axial actuator, otherwise the loading pins would contact and damage the support apparatus after failing the specimen during the destructive tests. In Study 4, the 20 mm displacement limit ensured that a Stage 4 dislocation injury (Allen et al., 1982) was created – dislocation injuries with anterior translation greater than ~20 mm are rarely observed clinically (Allen et al., 1982), and trauma of this severity was outside the scope of this investigation. Limiting destructive anterior displacement allowed for investigation of the features of associated fractures using post-test CT with the specimen in a clinically-relevant, injured pose. To ensure that none of the aforementioned load or displacement

limits were exceeded, quasi-static displacement rates were required due to the control limitations of the Instron WaveMatrix software.

Quasi-static loading rates also ensured that adequate motion capture data (at maximum frame rate) was collected. The Optotrak motion-capture system that was used to measure facet deflections could collect no faster than 300 Hz for Study 2, and 200 Hz for Studies 3 and 4, due to the number of motion-capture markers necessary to conduct these experiments. The loading rates chosen were the maximum possible to ensure at least 100 samples per loading cycle were obtained to appropriately capture the response of the facets.

The displacement rates applied in Studies 2-4 are probably substantially slower than those observed by the complete cervical spine *in vivo*, but it is unlikely that these quasi-static rates drastically affected the mechanical response of the subaxial cervical facets. During pilot testing for Study 2, increasing displacement rate by an order of magnitude (from 0.1 to 1 mm/s) was found to have no discernible effect on the mechanical response (stiffness, surface strain, or sagittal deflection) of the inferior facets of two isolated subaxial cervical vertebrae (see Appendix C). This result is consistent with the tensile behaviour of cortical bone at strain-rates up to 1/second, and beyond this point elastic modulus increases by only a factor of two as loading rate is increased by over three orders of magnitude (1500/second) (McElhaney, 1966). It is difficult to relate purely tensile, cortical strain rates to *in vivo* facet loading, but relatively slow subaxial cervical intervertebral loading velocities are likely observed during real life trauma as the *global* loading rate is distributed across all levels of the cervical spine (Edwards, 1998). As such, the mechanical response of the facets reported in Studies 2-4 is likely similar to that which occurs in vivo. The quantitative data obtained from these experiments provide an indication of how the facets are loaded during the intervertebral motions associated with CFD, regardless of the loading rate, and will be important for validating computational models of cervical trauma.

6.7 Recommendations and future work

This thesis has identified areas of research relating to CFD that are significantly understudied. In this section, recommendations are made for future investigations into the biomechanics underlying CFD.

6.7.1 Prospective investigation of CFD

A large-cohort prospective investigation is required to further elucidate the injury mechanisms of CFD. Study 1 provides new data concerning epidemiology, injury causation, and radiographic features of DFIs, and the association of these injury features with the occurrence of SCI, but is restricted by the inherent limitations of retrospective analyses. Detailed medical information (including evidence of head contact injury, associated spinal fractures etc.) combined with engineering evidence from accident investigation reports (similar to the CIREN program) would provide crucial evidence to improve our understanding of the external loading environments that cause CFD±Fx.

Such an investigation could also provide higher fidelity information about the predictive value of radiographic analyses to assess neurological involvement. The DFI medical image analysis program developed in Study 1 (described in detail in Appendix A) could be distributed to clinicians to provide them with real-time, quantitative information regarding DFI severity, and the association of these measurements with patient outcomes (both long-term, and at admission) could be evaluated.

6.7.2 Improving the destructive anterior shear experiments

Further experimental studies of the mechanical response of the subaxial cervical facets when axial compression and distraction are superimposed on destructive anterior shear motion is required. Supraphysiologic compression/distraction loads were not applied to the specimens in Study 4 due to the limitations of the six-axis materials testing machine and to be consistent with the axial forces applied in Study 3. However, axial compressive forces as high as 4000 N (Nightingale et al., 2016) and inter-facet separations up to 8 mm (Panjabi et al., 2007) have been

calculated during cervical trauma. The injury mechanisms that distinguish CFD+Fx from CFD-Fx may be elucidated if more extreme axial loading is superimposed on traumatic, constrained anterior shear. Future experiments could supplement the constrained anterior shear testing configuration from Study 4 with an independent, horizontal actuator that applies larger axial compression and distraction loads to the specimen (Figure 5.11). This test setup would also prevent deflection of the axial actuator that occurred due to off-axis loading in Study 4.

6.7.3 Computational modelling of cervical intervertebral motion

The inability to directly visualize inter-facet engagement and the response of the facets to this loading, due to the surrounding soft-tissue, was a limitation of Study 3 and Study 4. Visualization of the bone during testing could be achieved using fluoroscopy, but this method may be limited by the low-resolution and accuracy of x-ray measurements. Alternatively, specimen-specific computational simulations of these experiments could be generated by combining high-resolution, pre-test CT images and motion capture data. Such models could be used to indirectly visualize inter-facet engagement and facet apposition/contact area, and could be used for specimen-specific finite element analysis (FEA).

Cook and Cheng (2010) used 3D anatomical models of *in vitro* testing to quantify the change in facet apposition, or "contact area ratio" (CAR), during flexion and extension mechanical testing of cadaveric *lumbar* spines. During preparation of complete lumbar segments (L1-sacrum), three fiducial markers (3 mm aluminium spheres) were rigidly fixed to each vertebral body prior to CT-scanning. Vertebrae and fiducial markers were then segmented from the CT data to generate 3D hard-tissue models. Prior to mechanical testing, the 3D co-ordinates of each fiducial marker were registered relative to the motion-capture marker-carrier attached to the corresponding vertebral body (Figure 6.2a) so that the locations of these markers could be tracked during each test. The 3D models of each vertebra could then be transformed from the CT co-ordinate system to the motion-capture co-ordinate system by co-registering the locations of the fiducial markers, resulting in 3D, specimen-specific representations of vertebral kinematics during each biomechanical test. The CAR of each facet joint was then calculated as the ratio of

the area of opposing facet surfaces that were within an "articulating distance threshold" (2 mm) of each other, to the total articular facet surface area of the joint in a "neutral" posture, at each level during global lumbar flexion-extension motion (Figure 6.2b).

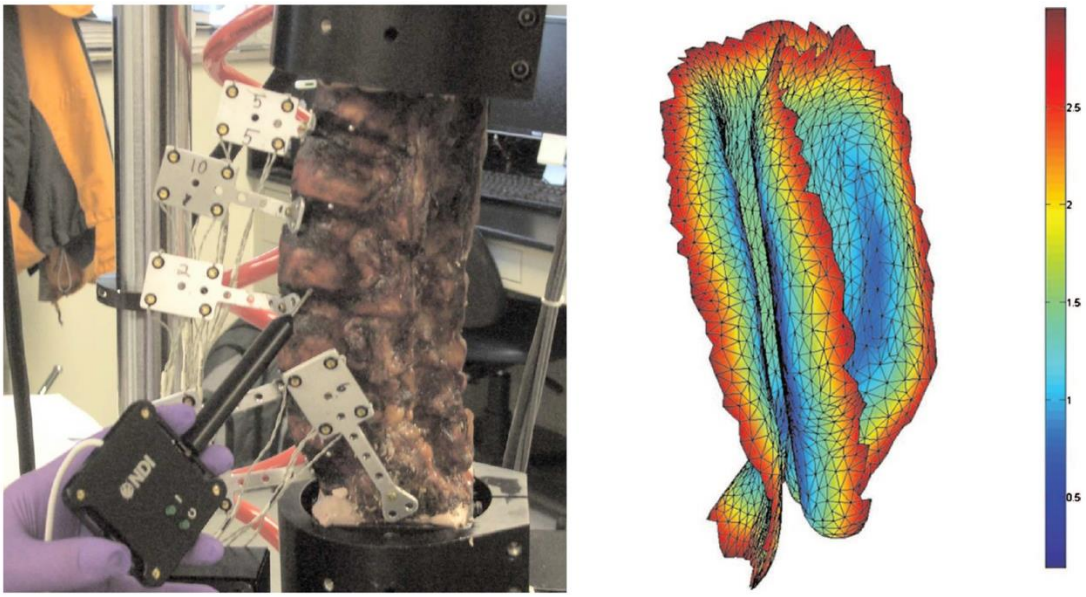

a b

Figure 6.2: (a) Digitisation of fiducial markers on a complete human cadaver lumbar spine segment. (b) Distance map for a 3D computational model of a left, L1/L2 facet joint, where hotter colours illustrate greater distance between articular facet surfaces. Image adapted from Cook and Cheng (2010).[1]

A similar investigation of facet articulation during constrained intervertebral motion may elucidate the injury mechanisms of CFD±Fx. Of particular interest is how axial separation affects facet engagement during constrained, traumatic anterior shear, as this may dictate the presence and features of facet fractures associated with CFD. Similar methods to those described by Cook and Cheng (2010) could also be employed to generate specimen-specific FEA models of cervical trauma to investigate the regions of highest stress and strain during traumatic and non-traumatic intervertebral motions. The quantitative information gained in Studies 2-4 would be important for validation of such models.

[1] Image adapted by permission from ASME: Cook, D.J. and Cheng, B.C., 2010. *Development of a model based method for investigating facet articulation*. Journal of Biomechanical Engineering **132**(6):064504.

6.7.4 Experimental production of UFD±Fx

UFD is commonly associated with SCI and more frequently presents with associated facet fracture than BFD (see Section 1.4.2 and Section 2.3), but the injury mechanisms of UFD±Fx are not well understood. Intervertebral axial rotation and lateral bending have produced UFD±Fx in cervical FSUs (Crawford et al., 2002; Nadeau et al., 2012; Roaf, 1960) and full cervical spines (Bauze and Ardran, 1978; Hodgson and Thomas, 1980; Myers et al., 1991), but these studies did not describe the loading mechanisms that distinguish UFD-Fx from UFD+Fx and did not investigate the mechanical response of the facets.

In Study 3, axial compression significantly increased facet shear surface strains (when compared to distraction) during quasi-static, constrained, non-destructive axial rotation and lateral bending motions (Figure 4.6). This suggests that reduced intervertebral axial separation increases the loading applied to the ipsilateral facet during these asymmetric motions, which may lead to UFD+Fx. Future experimental work could investigate this further by superimposing intervertebral axial compression and distraction on *supraphysiologic* axial rotation and lateral bending motions (using a methodology similar to that developed in Study 4) and measure the mechanical response of the facets using the methods described in Studies 2-4.

6.7.5 Dynamic head-impact model of CFD

A dynamic, full cervical spine, head-impact model of CFD, is required to formulate injury risk curves for CFD+Fx. The preliminary results from Study 4 demonstrate that constrained intervertebral anterior shear produces BFD+Fx in the subaxial cervical spine, when applied at quasi-static displacement rates. Nightingale *et al.* (1991) produced large intervertebral shear loads in the lower subaxial region (Nightingale et al., 2016) during *quasi-static*, axial compression testing of six full cervical spines for which head-flexion was restricted, but sagittal anterior translation was permitted (Figure 6.3) – this testing configuration reliably produced BFD-Fx. Active neck muscle replication was not performed in these experiments, which may explain why BFD+Fx did not occur.

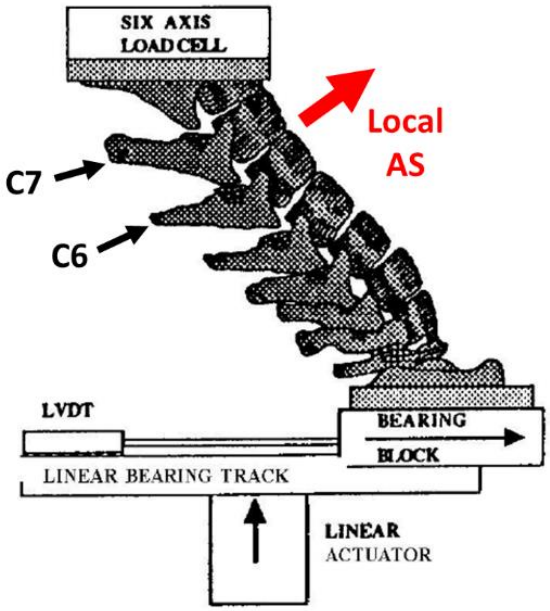

Figure 6.3: Schematic of the experimental apparatus and final cervical posture for the mechanical tests that reliably produced BFD-Fx (Nightingale et al., 1991). The local anterior shear (AS) force vector produced in the lower cervical spine is shown.[1]

Future experiments could perform similar tests at higher speed (up to 3 m/s) and include neck muscle simulation to try to produce dynamic BFD+Fx in complete cervical segments. Dynamic impact speeds may prevent the cranial region from escaping the weight of the torso, which, when combined with active neck muscle replication, would impose a larger axial compression force onto the subaxial intervertebral anterior shear motion. The results of Study 4 suggest that this loading combination will cause BFD+Fx in full cervical spines. If successful, testing parameters such as impact velocity and angle, head-constraints, spinal posture etc. could be varied to develop injury risk curves for BFD+Fx, leading to better neck injury criteria for ATDs. Further dynamic impact experiments could also investigate the role of asymmetric global loading in producing intervertebral axial rotation and lateral bending to further explore the injury mechanisms of UFD±Fx.

[1] Awaiting copyright permissions.

6.8 Contributions

This thesis has made the following novel contributions to basic science and clinical research relating to cervical spine trauma:

- In Chapter 2, the first large-cohort investigation of the epidemiology and radiographic features of DFI (including CFD), and the risk-factors for SCI in these patients, is documented. Younger adults were over-represented amongst MVAs, whilst falls contributed to a majority of DFIs sustained by older adults. The C6/C7 vertebral level was most commonly involved, and there was a similar incidence of UFDs and BFDs. UFDs more commonly presented with associated facet fracture, but this was not indicative of SCI. Dislocation, bilateral injury, reduced Glasgow Coma Scale, spinal canal occlusion and spinal cord compression were predictive of neurological deficit. The inter- and intra-observer agreement of radiographic measurements of DFI were evaluated for the first time, and were found to be highly reproducible;
- Chapter 3 presents the first study to measure the mechanical response of isolated subaxial cervical facets when loaded in directions that simulate the intervertebral motions commonly associated with BFD – anterior shear and compressive-flexion. Substantial deflections of the posterior elements, relative to the vertebral body, were observed during non-destructive and failure tests, suggesting that the subaxial vertebrae should not be assumed to act as a rigid-body during computational simulations of cervical motion. The mechanical response varied between the upper and lower regions of the cervical spine, and distinct failure mechanisms were observed for each loading direction;
- The effect of superimposed axial compression versus distraction on the mechanical behaviour of the C6 inferior facets during constrained intervertebral anterior shear, axial rotation, flexion, and lateral bending motions, was reported in Chapter 4. In general, imposed axial compression increased surface strains and facet deflections, but this was dependant on the motion direction. The significant influence of the facet capsule on facet mechanics during axial rotation was observed;

- For the first time, BFD+Fx was produced experimentally by applying 20 mm of constrained anterior shear to C6/C7 FSUs. Clinically-relevant concomitant facet fractures were created when axial compression and distraction were imposed on this motion. Axial compression generally increased shear and axial loads, shear surface strains, and coronal and transverse facet deflections at the point of facet fracture, when compared to the distracted condition.

6.9 Conclusions

Despite the devastating consequences of traumatic subaxial CFD, the mechanisms that cause this injury are significantly understudied. This lack of understanding hinders the development of improved preventative devices and better treatment methods. Traditionally, BFD is thought to result from a global flexion moment about the subaxial cervical spine, caused by axial compressive forces applied to the head with large anterior eccentricity or from inertial motion of the head during high deceleration events, while UFD is thought to have an additional axial rotation component to the injury vector. However, there is limited clinical evidence to support the proposed inertial injury mechanism, and global distractive flexion motions applied to whole cervical spines do not produce CFD. Intervertebral anterior shear motion is observed in the lower cervical spine during the experimental production of BFD, but the role of shear during cervical trauma has not been thoroughly investigated. Anterior shear has also been associated with concomitant facet fracture, but CFD+Fx had not previously been produced experimentally. This thesis presents a series of studies that improve understanding of the clinical presentation and the biomechanics of CFD.

A large-cohort investigation of DFIs admitted to a single centre over a decade was performed. Hard-copy medical records and radiographs were reviewed, and patient epidemiology and radiographic features were obtained – the association of these features with SCI was investigated. Patient epidemiology was similar to that previously reported for non-specific cervical trauma, and the C6/C7 level was most commonly affected. Facet dislocation (vs. subluxation), bilateral injury (vs. unilateral), reduced Glasgow Coma Scale (a surrogate for head-

contact injury), spinal canal occlusion, and cord compression were predictive of neurological deficit.

A series of biomechanical experiments were performed to investigate the mechanical response of the subaxial cervical facets during intervertebral motions that are thought to cause CFD. Principal and shear posterior facet surface strains, 3D deflections of the posterior elements relative to the vertebral body, and load-displacement characteristics were quantified during point-loading of isolated subaxial facets that simulated the inter-facet loading during supraphysiologic and traumatic intervertebral anterior shear and compressive-flexion motions. The same measurements were obtained for the C6 inferior facets during non-destructive, constrained anterior shear, axial rotation, flexion, and lateral bending motions of C6/C7 FSUs. These motions were imposed with 50 N (head-weight) and 300 N (neck muscle bracing) of axial compression, and 2.5 mm of axial distraction (inertial separation) to investigate their effect on facet mechanics. Finally, a method was developed to apply 20 mm of constrained anterior shear, imposed with either 300 N compression or 2.5 mm of distraction, to the same C6/C7 specimens from Study 4. The mechanical behaviour of the C6 inferior facets was measured at 2.19 mm of supraphysiologic anterior shear, and at the point of initial anatomical failure.

Anterior shear produced inferior facet fractures similar to those observed in clinical cases of CFD during both the isolated facet and FSU testing. Imposed axial compression generally increased surface strains and deflections of the inferior C6 facets, but this was dependant on test direction and did not influence the type of fractures observed during traumatic anterior shear motion. The facet capsule, and the presence of other surrounding soft-tissue structures, seemed to influence the mechanical response of the facets, especially during axial rotation. This response differed between the upper (C3-C4) and lower (C5-C7) subaxial regions and was often dependant on specimen-specific parameters such as donor demographics and vertebral geometry. It is anticipated that the information gained in this thesis will lead to improved detection of SCI associated with CFD, assist with the development and validation of computational and dynamic

experimental models of cervical trauma, and lead to improved injury prevention devices and neck injury criteria.

References

Aarabi, B., Walters, B.C., Dhall, S.S., Gelb, D.E., Hurlbert, R.J., Rozzelle, C.J., Ryken, T.C., Theodore, N., Hadley, M.N., 2013. Subaxial cervical spine injury classification systems. Neurosurgery 72 Suppl 2, 170-186.

Access Economics Pty Limited, 2009. The economic cost of spinal cord injury and traumatic brain injury in Australia. The Victorian Neurotrauma Initiative.

Allen, B.L., Jr., Ferguson, R.L., Lehmann, T.R., O'Brien, R.P., 1982. A mechanistic classification of closed, indirect fractures and dislocations of the lower cervical spine. Spine (Phila Pa 1976) 7, 1-27.

Anderst, W.J., Donaldson, W.F., 3rd, Lee, J.Y., Kang, J.D., 2015. Three-dimensional intervertebral kinematics in the healthy young adult cervical spine during dynamic functional loading. J Biomech 48, 1286-1293.

Anissipour, A.K., Agel, J., Baron, M., Magnusson, E., Bellabarba, C., Bransford, R.J., 2017. Traumatic Cervical Unilateral and Bilateral Facet Dislocations Treated With Anterior Cervical Discectomy and Fusion Has a Low Failure Rate. Global Spine J 7, 110-115.

Argenson, C., Lovet, J., Sanouiller, J.L., de Peretti, F., 1988. Traumatic rotatory displacement of the lower cervical spine. Spine (Phila Pa 1976) 13, 767-773.

Armstrong, A.J., Clark, J.M., Ho, D.T., Payne, C.J., Nolan, S., Goodes, L.M., Harvey, L.A., Marshall, R., Galea, M.P., Dunlop, S.A., 2017. Achieving assessor accuracy on the International Standards for Neurological Classification of Spinal Cord Injury. Spinal Cord.

Arnold, P.M., Brodke, D.S., Rampersaud, R., Harrop, J., Dailey, A.T., Shaffrey, C., Grauer, J., Dvorak, M.F.S., Bono, C.M., Wilsey, J.T., Lee, J.Y., Nassr, A., Vaccaro, A.R., 2009. Differences between neurosurgeons and orthopedic surgeons in classifying cervical dislocation injuries and making assessment and treatment decisions: a multicenter reliability study. The American Journal of Orthopedics 38, E156-E161.

Bahling, G.S., Bundorf, R.T., Moffatt, E.A., Orlowski, K.F., 1995. The influence of increased roof strength on belted and unbelted dummies in rollover and drop tests. J Trauma 38, 557-563.

Baker, S.P., O'Neill, B., Haddon, W., Jr., Long, W.B., 1974. The injury severity score: a method for describing patients with multiple injuries and evaluating emergency care. J Trauma 14, 187-196.

Bakkum, B., D. Cramer, G., 2013. Muscles That Influence the Spine.

Bambach, M.R., Grzebieta, R.H., McIntosh, A.S., Mattos, G.A., 2013. Cervical and thoracic spine injury from interactions with vehicle roofs in pure rollover crashes. Accid Anal Prev 50, 34-43.

Barnes, R., 1948. Paraplegia in cervical spine injuries. J Bone Joint Surg Br 30B, 234-244.

Bartlett, J.W., Frost, C., 2008. Reliability, repeatability and reproducibility: analysis of measurement errors in continuous variables. Ultrasound in Obstetrics and Gynecology 31, 466-475.

Bauze, R.J., Ardran, G.M., 1978. Experimental production of forward dislocation in the human cervical spine. J Bone Joint Surg Br 60-B, 239-245.

Beatson, T.R., 1963. Fractures and dislocations of the cervical spine. Journal of Bone and Joint Surgery 45-B, 21-35.

Bell, K.M., Yan, Y., Debski, R.E., Sowa, G.A., Kang, J.D., Tashman, S., 2016. Influence of varying compressive loading methods on physiologic motion patterns in the cervical spine. J Biomech 49, 167-172.

Beyer, C., Cabanela, M., Berquist, T., 1991. Unilateral facet dislocations and fracture-dislocations of the cervical spine. Journal of Bone & Joint Surgery, British Volume 73-B, 977-981.

Bland, J.M., Altman, D.G., 1986. Statistical methods for assessing agreement between two methods of clinical measurement. Lancet 1, 307-310.

Bland, J.M., Altman, D.G., 2003. Applying the right statistics: analyses of measurement studies. Ultrasound in Obstetrics and Gynecology 22, 85-93.

Bogduk, N., Mercer, S., 2000. Biomechanics of the cervical spine. I: Normal kinematics. Clin Biomech (Bristol, Avon) 15, 633-648.

Bono, C.M., Schoenfeld, A., Rampersaud, R., Levi, A., Grauer, J., Arnold, P., Fehlings, M., Dvorak, M., Vaccaro, A.R., 2011. Reproducibility of radiographic measurements for subaxial cervical spine trauma. Spine (Phila Pa 1976) 36, 1374-1379.

Bono, C.M., Vaccaro, A.R., Fehlings, M., Fisher, C., Dvorak, M., Ludwig, S., Harrop, J., 2006. Measurement techniques for lower cervical spine injuries: consensus statement of the Spine Trauma Study Group. Spine (Phila Pa 1976) 31, 603-609.

Brady, W.J., Moghtader, J., Cutcher, D., Exline, C., Young, J., 1999. ED use of flexion-extension cervical spine radiography in the evaluation of blunt trauma. Am J Emerg Med 17, 504-508.

Burns, S.P., Kaufman, R.P., Mack, C.D., Bulger, E., 2010. Cost of spinal cord injuries caused by rollover automobile crashes. Inj Prev 16, 74-78.

Cadoux, C.G., White, J.D., Hedberg, M.C., 1987. High-yield roentgenographic criteria for cervical spine injuries. Ann Emerg Med 16, 738-742.

Chaffee, E.E., Greisheimer, E.M., 1974. Basic physiology and anatomy, 3d ed. Lippincott, Philadelphia,.

Chakravarthy, V., Mullin, J.P., Abbott, E.E., Anderson, J., Benzel, E.C., 2014. Neurologically intact patient following bilateral facet dislocation: case report and review of literature. Ochsner J 14, 108-111.

Chancey, V.C., Nightingale, R.W., Van Ee, C.A., Knaub, K.E., Myers, B.S., 2003. Improved estimation of human neck tensile tolerance: reducing the range of reported tolerance using anthropometrically correct muscles and optimized physiologic initial conditions. Stapp Car Crash J 47, 135-153.

Chang, U.K., Kim, D.H., Lee, M.C., Willenberg, R., Kim, S.H., Lim, J., 2007. Changes in adjacent-level disc pressure and facet joint force after cervical arthroplasty compared with cervical discectomy and fusion. J Neurosurg Spine 7, 33-39.

Cholewicki, J., Panjabi, M.M., Nibu, K., Macias, M.E., 1997. Spinal ligament transducer based on a hall effect sensor. J Biomech 30, 291-293.

Choo, A.M., Liu, J., Dvorak, M., Tetzlaff, W., Oxland, T.R., 2008. Secondary pathology following contusion, dislocation, and distraction spinal cord injuries. Exp Neurol 212, 490-506.

Choo, A.M., Liu, J., Lam, C.K., Dvorak, M., Tetzlaff, W., Oxland, T.R., 2007. Contusion, dislocation, and distraction: primary hemorrhage and membrane permeability in distinct mechanisms of spinal cord injury. J Neurosurg Spine 6, 255-266.

Clark, C.R., White, A.A., 1985. Fractures of the dens. A multicenter study. The Journal of Bone & Joint Surgery 67, 1340-1348.

Clayton, J.L., Harris, M.B., Weintraub, S.L., Marr, A.B., Timmer, J., Stuke, L.E., McSwain, N.E., Duchesne, J.C., Hunt, J.P., 2012. Risk factors for cervical spine injury. Injury 43, 431-435.

Cook, D.J., Cheng, B.C., 2010. Development of a model based method for investigating facet articulation. J Biomech Eng 132, 064504.

Copes, W.S., Champion, H.R., Sacco, W.J., Lawnick, M.M., Keast, S.L., Bain, L.W., 1988. The injury severity score revisited. The Journal of Trauma 28, 69-77.

Cotler, H.B., Cotler, J.M., Alden, M.E., Sparks, G., Biggs, C.A., 1990. The medical and economic impact of closed cervical spine dislocations. Spine (Phila Pa 1976) 15, 448-452.

Crawford, N.R., Duggal, N., Chamberlain, R.H., Park, S.C., Sonntag, V.K., Dickman, C.A., 2002. Unilateral cervical facet dislocation: injury mechanism and biomechanical consequences. Spine (Phila Pa 1976) 27, 1858-1864; discussion 1864.

Cripton, P.A., 1999. Load-sharing in the human cervical spine. Queen's University, Kingston, Ontario, Canada.

Cripton, P.A., Dumas, G.A., Nolte, L.P., 2001. A minimally disruptive technique for measuring intervertebral disc pressure in vitro: application to the cervical spine. J Biomech 34, 545-549.

Cusick, J.F., Yoganandan, N., 2002. Biomechanics of the cervical spine 4: major injuries. Clin Biomech (Bristol, Avon) 17, 1-20.

Cyron, B.M., Hutton, W.C., 1978. The fatigue strength of the lumbar neural arch in spondylolysis. J Bone Joint Surg Br 60-B, 234-238.

Cyron, B.M., Hutton, W.C., Troup, J.D., 1976. Spondylolytic fractures. J Bone Joint Surg Br 58-B, 462-466.

Dailey, A.T., Shaffrey, C.I., Rampersaud, R., Lee, J., Brodke, D.S., Arnold, P., Nassr, A., Harrop, J.S., Grauer, J., Bono, C.M., Dvorak, M., Vaccaro, A., 2009. Utility of helical computed tomography in differentiating unilateral and bilateral facet dislocations. J Spinal Cord Med 32, 43-48.

Davidson, J.S., Birdsell, D.C., 1989. Cervical spine injury in patients with facial skeletal trauma. J Trauma 29, 1276-1278.

DeVivo, M., Chen, Y., Mennemeyer, S., Deutsch, A., 2011. Costs of Care Following Spinal Cord Injury. Topics in Spinal Cord Injury Rehabilitation 16, 1-9.

DiAngelo, D.J., Foley, K.T., 2004. An improved biomechanical testing protocol for evaluating spinal arthroplasty and motion preservation devices in a multilevel human cadaveric cervical model. Neurosurg Focus 17, E4.

Doran, S.E., Papadopoulos, S.M., Ducker, T.B., Lillehei, K.O., 1993. Magnetic resonance imaging documentation of coexistent traumatic locked facets of the cervical spine and disc herniation. J Neurosurg 79, 341-345.

Du, W., Wang, C., Tan, J., Shen, B., Ni, S., Zheng, Y., 2014. Management of subaxial cervical facet dislocation through anterior approach monitored by spinal cord evoked potential. Spine (Phila Pa 1976) 39, 48-52.

Duggal, N., Chamberlain, R.H., Park, S.C., Sonntag, V.K., Dickman, C.A., Crawford, N.R., 2005. Unilateral cervical facet dislocation: biomechanics of fixation. Spine (Phila Pa 1976) 30, E164-168.

Durbin, F.C., 1957. Fracture-dislocations of the cervical spine. J Bone Joint Surg Br 39-B, 23-38.

Dvorak, M.F., Fisher, C.G., Aarabi, B., Harris, M.B., Hurbert, R.J., Rampersaud, Y.R., Vaccaro, A., Harrop, J.S., Nockels, R.P., Madrazo, I.N., Schwartz, D., Kwon, B.K., Zhao, Y., Fehlings, M.G., 2007. Clinical outcomes of 90 isolated unilateral facet fractures, subluxations, and dislocations treated surgically and nonoperatively. Spine (Phila Pa 1976) 32, 3007-3013.

Ebraheim, N.A., Liu, J., Ramineni, S.K., Liu, X., Xie, J., Hartman, R.G., Goel, V.K., 2009. Morphological changes in the cervical intervertebral foramen dimensions with unilateral facet joint dislocation. Injury 40, 1157-1160.

Edwards, W.T., 1998. Principles of Cervical Spine Biomechanical Testing. Frontiers in Head and Neck Trauma, 217-231.

Eismont, F.J., Clifford, S., Goldberg, M., Green, B., 1984. Cervical sagittal spinal canal size in spine injury. Spine (Phila Pa 1976) 9, 663-666.

el-Bohy, A.A., Yang, K.H., King, A.I., 1989. Experimental verification of facet load transmission by direct measurement of facet lamina contact pressure. J Biomech 22, 931-941.

Eppinger, R., Sun, E., Kuppa, S., Saul, R., 2000. Supplement: Development of improved injury criteria for the assessment of advanced automotive restraint systems-II, NHTSA Report. NHTSA.

Eranki, V., Koul, K., Mendz, G., Dillon, D., 2016. Traumatic facet joint dislocation in Western Australia. Eur Spine J 25, 1109-1116.

Faul, F., Erdfelder, E., Lang, A.G., Buchner, A., 2007. G*Power 3: a flexible statistical power analysis program for the social, behavioral, and biomedical sciences. Behav Res Methods 39, 175-191.

Fehlings, M.G., Furlan, J.C., Massicotte, E.M., Arnold, P., Aarabi, B., Harrop, J., Anderson, D.G., Bono, C.M., Dvorak, M., Fisher, C., France, J., Hedlund, R., Madrazo, I., Nockels, R., Rampersaud, R., Rechtine, G., Vaccaro, A.R., Spine Trauma Study, G., 2006. Interobserver and intraobserver reliability of maximum canal compromise and spinal cord compression for evaluation of acute traumatic cervical spinal cord injury. Spine (Phila Pa 1976) 31, 1719-1725.

Fehlings, M.G., Rao, S.C., Tator, C.H., Skaf, G., Arnold, P., Benzel, E., Dickman, C., Cuddy, B., Green, B., Hitchon, P., Northrup, B., Sonntag, V., Wagner, F., Wilberger, J., 1999. The optimal radiologic method for assessing spinal canal compromise and cord compression in patients with cervical spinal cord injury. Part II: Results of a multicenter study. Spine (Phila Pa 1976) 24, 605-613.

Fiford, R.J., Bilston, L.E., Waite, P., Lu, J., 2004. A vertebral dislocation model of spinal cord injury in rats. J Neurotrauma 21, 451-458.

Foster, B.J., Kerrigan, J.R., Nightingale, R.W., Funk, J.R., Cormier, J.M., Bose, D., Sochor, M.R., Ridella, S.A., Ash, J.H., Crandall, J., Year Analysis of cervical spine injuries and mechanisms for CIREN rollover crashes. In 2012 International IRCOBI Conference on the Biomechanics of Injury. Dublin, Ireland.

Funk, J.R., Cormier, J.M., Manoogian, S.J., 2012. Comparison of risk factors for cervical spine, head, serious, and fatal injury in rollover crashes. Accid Anal Prev 45, 67-74.

Furlan, J.C., Fehlings, M.G., Massicotte, E.M., Aarabi, B., Vaccaro, A.R., Bono, C.M., Madrazo, I., Villanueva, C., Grauer, J.N., Mikulis, D., 2007. A quantitative and reproducible method to assess cord compression and canal stenosis after cervical spine trauma: a study of interrater and intrarater reliability. Spine (Phila Pa 1976) 32, 2083-2091.

Furlan, J.C., Kailaya-Vasan, A., Aarabi, B., Fehlings, M.G., 2011. A novel approach to quantitatively assess posttraumatic cervical spinal canal compromise and spinal cord compression: a multicenter responsiveness study. Spine (Phila Pa 1976) 36, 784-793.

Gilroy, A.M., MacPherson, B.R., Ross, L.M., Schünke, M., Schulte, E., Schumacher, U., 2012. Atlas of Anatomy. Thieme Medical Publishers, Incorporated.

Gold, M., 2015. Magnetic Resonance Imaging of Spinal Emergencies. Top Magn Reson Imaging 24, 325-330.

Goldberg, W., Mueller, C., Panacek, E., Tigges, S., Hoffman, J.R., Mower, W.R., Group, N., 2001. Distribution and patterns of blunt traumatic cervical spine injury. Ann Emerg Med 38, 17-21.

Grant, G.A., Mirza, S.K., Chapman, J.R., Winn, H.R., Newell, D.W., Jones, D.T., Grady, M.S., 1999. Risk of early closed reduction in cervical spine subluxation injuries. J Neurosurg 90, 13-18.

Gray, H., Lewis, W.H., 1918. Anatomy of the human body. Lea & Febiger, Philadelphia.

Green, T.P., Allvey, J.C., Adams, M.A., 1994. Spondylolysis. Bending of the inferior articular processes of lumbar vertebrae during simulated spinal movements. Spine (Phila Pa 1976) 19, 2683-2691.

Greenspan, L., McLellan, B.A., Greig, H., 1985. Abbreviated Injury Scale and Injury Severity Score: a scoring chart. J Trauma 25, 60-64.

Hadley, M.N., 2002. Initial closed reduction of cervical spine fracture-dislocation injuries. Neurosurgery 50, S44-S50.

Hadley, M.N., Fitzpatrick, B.C., Sonntag, V.K., Browner, C.M., 1992. Facet fracture-dislocation injuries of the cervical spine. Neurosurgery 30, 661-666.

Hakim, N.S., King, A.I., Year Static and dynamic articular facet loads. In 20th Stapp Car Crash Conference. Dearborn, MI.

Harrington, J.F., Jr., Park, M.C., 2007. Single level arthrodesis as treatment for midcervical fracture subluxation: a cohort study. J Spinal Disord Tech 20, 42-48.

Hartman, R.A., Tisherman, R.E., Wang, C., Bell, K.M., Lee, J.Y., Sowa, G.A., Kang, J.D., 2016. Mechanical role of the posterior column components in the cervical spine. Eur Spine J 25, 2129-2138.

Hasler, R.M., Exadaktylos, A.K., Bouamra, O., Benneker, L.M., Clancy, M., Sieber, R., Zimmermann, H., Lecky, F., 2012. Epidemiology and predictors of cervical spine injury in adult major trauma patients: A multicenter cohort study. Journal of Trauma and Acute Care Surgery 72, 975-981 910.1097/TA.1090b1013e31823f31825e31828e.

Hattori, S., 1981. Cervical intradiscal pressure in movements and traction of the cervical spine. Z Orthop 119, 568-569.

Hayashi, K., Yone, K., Ito, H., Yanase, M., Sakou, T., 1995. MRI findings in patients with a cervical spinal cord injury who do not show radiographic evidence of a fracture or dislocation. Paraplegia 33, 212-215.

Hedtmann, A., Steffen, R., Methfessel, J., Kolditz, D., Kramer, D., Thols, M., 1989. Measurement of human lumbar spine ligaments during loaded and unloaded motion. Spine (Phila Pa 1976) 14, 175-185.

Henriques, T., Olerud, C., Bergman, A., Jonsson, H., Jr., 2004. Distractive flexion injuries of the subaxial cervical spine treated with anterior plate alone. J Spinal Disord Tech 17, 1-7.

Herbst, B., Forrest, S., Chng, D., Sances, A., 1998. Fidelity of anthropometric test dummy necks in rollover accidents, Sixteenth International Technical Conference on the Enhanced

Safety of Vehicles (ESV), pp. 2093-2097.

Hills, M.W., Deane, S.A., 1993. Head injury and facial injury: is there an increased risk of cervical spine injury? J Trauma 34, 549-553; discussion 553-544.

Hodgson, V., Thomas, L., 1980. Mechanisms of cervical spine injury during impact to the protected head. SAE Technical Paper 801300.

Hoffman, J.R., Schriger, D.L., Mower, W., Luo, J.S., Zucker, M., 1992. Low-risk criteria for cervical-spine radiography in blunt trauma: a prospective study. Ann Emerg Med 21, 1454-1460.

Hosmer, D.W., Lemeshow, S., 2000. Applied logistic regression, 2nd ed. Wiley, New York.

Hu, J., Yang, K.H., Chou, C.C., King, A.I., 2008. A numerical investigation of factors affecting cervical spine injuries during rollover crashes. Spine (Phila Pa 1976) 33, 2529-2535.

Hu, R., Mustard, C.A., Burns, C., 1996. Epidemiology of incident spinal fracture in a complete population. Spine (Phila Pa 1976) 21, 492-499.

Huelke, D.F., Nusholtz, G.S., 1986. Cervical spine biomechanics: A review of the literature. Journal of Orthopaedic Research 4, 232-245.

Humanetics Innovative Solutions, 2014. Hybrid III 50th Male Dummy, MI, USA.

Ivancic, P.C., 2012a. Biomechanics of sports-induced axial-compression injuries of the neck. J Athl Train 47, 489-497.

Ivancic, P.C., 2012b. Head-first impact with head protrusion causes noncontiguous injuries of the cadaveric cervical spine. Clin J Sport Med 22, 390-396.

Ivancic, P.C., Pearson, A.M., Tominaga, Y., Simpson, A.K., Yue, J.J., Panjabi, M.M., 2007. Mechanism of cervical spinal cord injury during bilateral facet dislocation. Spine (Phila Pa 1976) 32, 2467-2473.

Ivancic, P.C., Pearson, A.M., Tominaga, Y., Simpson, A.K., Yue, J.J., Panjabi, M.M., 2008. Biomechanics of cervical facet dislocation. Traffic Inj Prev 9, 606-611.

Jaumard, N.V., Bauman, J.A., Weisshaar, C.L., Guarino, B.B., Welch, W.C., Winkelstein, B.A., 2011a. Contact pressure in the facet joint during sagittal bending of the cadaveric cervical spine. J Biomech Eng 133, 071004.

Jaumard, N.V., Bauman, J.A., Welch, W.C., Winkelstein, B.A., 2011b. Pressure measurement in the cervical spinal facet joint: considerations for maintaining joint anatomy and an intact capsule. Spine (Phila Pa 1976) 36, 1197-1203.

Jenkins, D.B., Hollinshead, W.H., 2009. Hollinshead's functional anatomy of the limbs and back, 9th ed. Saunders/Elsevier, St. Louis, MO.

Jennett, B., 1994. An introduction to neurosurgery / Bryan Jennett, Kenneth W. Lindsay, 5th ed. Butterworth-Heinemann, Boston.

Jones, C.F., Clarke, E.C., 2018. Engineering approaches to understanding mechanisms of spinal column injury leading to spinal cord injury. Clin Biomech (Bristol, Avon).

Kang, J.D., Figgie, M.P., Bohlman, H.H., 1994. Sagittal measurements of the cervical spine in subaxial fractures and dislocations. An analysis of two hundred and eighty-eight patients with and without neurological deficits. The Journal of Bone & Joint Surgery 76, 1617-1628.

Kato, H., Kimura, A., Sasaki, R., Kaneko, N., Takeda, M., Hagiwara, A., Ogura, S., Mizoguchi, T., Matsuoka, T., Ono, H., Matsuura, K., Matsushima, K., Kushimoto, S., Fuse, A., Nakatani, T., Iwase, M., Fudoji, J., Kasai, T., 2008. Cervical spinal cord injury without bony injury: a multicenter retrospective study of emergency and critical care centers in Japan. J Trauma 65, 373-379.

Key, A., 1975. Cervical spine dislocations with unilateral facet interlocking. Paraplegia 13, 208-215.

King, A.I., Prasad, P., Ewing, C.L., 1975. Mechanism of spinal injury due to caudocephalad accleration. Orthop Clin North Am 6, 19-31.

King Liu, Y., W. Krieger, K., Njus, G., Ueno, K., P. Connors, M., 1982. Cervical Spine Stiffness and Geometry of the Young Human Male.

Kirshblum, S.C., Burns, S.P., Biering-Sorensen, F., Donovan, W., Graves, D.E., Jha, A., Johansen, M., Jones, L., Krassioukov, A., Mulcahey, M.J., Schmidt-Read, M., Waring, W., 2011. International standards for neurological classification of spinal cord injury (revised 2011). J Spinal Cord Med 34, 535-546.

Kumaresan, S., Yoganandan, N., Pintar, F.A., Maiman, D.J., Goel, V.K., 2001. Contribution of disc degeneration to osteophyte formation in the cervical spine: a biomechanical investigation. J Orthop Res 19, 977-984.

Kwon, B.K., Fisher, C.G., Boyd, M.C., Cobb, J., Jebson, H., Noonan, V., Wing, P., Dvorak, M.F., 2007. A prospective randomized controlled trial of anterior compared with posterior stabilization for unilateral facet injuries of the cervical spine. Journal of Neurosurgery: Spine 7, 1-12.

Kwon, B.K., Vaccaro, A.R., Grauer, J.N., Fisher, C.G., Dvorak, M.F., 2006. Subaxial Cervical Spine Trauma. Journal of the American Academy of Orthopaedic Surgeons 14, 78-89.

Landis, J.R., Koch, G.G., 1977. The measurement of observer agreement for categorical data. Biometrics 33, 159-174.

Lee, A.S., MacLean, J.C., Newton, D.A., 1994. Rapid traction for reduction of cervical spine dislocations. J Bone Joint Surg Br 76, 352-356.

Lin, C.C., Lu, T.W., Wang, T.M., Hsu, C.Y., Hsu, S.J., Shih, T.F., 2014. In vivo three-dimensional intervertebral kinematics of the subaxial cervical spine during seated axial rotation and lateral bending via a fluoroscopy-to-CT registration approach. J Biomech 47, 3310-3317.

Lintner, D.M., Knight, R.Q., Cullen, J.P., 1993. The neurologic sequelae of cervical spine facet injuries. The role of canal diameter. Spine (Phila Pa 1976) 18, 725-729.

Maiman, D.J., Sances, A., Jr., Myklebust, J.B., Larson, S.J., Houterman, C., Chilbert, M., El-Ghatit, A.Z., 1983. Compression injuries of the cervical spine: a biomechanical analysis. Neurosurgery 13, 254-260.

Maletsky, L.P., Sun, J., Morton, N.A., 2007. Accuracy of an optical active-marker system to track the relative motion of rigid bodies. J Biomech 40, 682-685.

Marar, B.C., 1974. The pattern of neurological damage as an aid to the diagnosis of the mechanism in cervical-spine injuries. J Bone Joint Surg Am 56, 1648-1654.

Marino, R.J., Barros, T., Biering-Sorensen, F., Burns, S.P., Donovan, W.H., Graves, D.E., Haak, M., Hudson, L.M., Priebe, M.M., Committee, A.N.S., 2003. International standards for neurological classification of spinal cord injury. J Spinal Cord Med 26 Suppl 1, S50-56.

McElhaney, J., Snyder, R.G., States, J.D., Gabrielsen, M.A., 1979. Biomechanical Analysis of Swimming Pool Neck Injuries. SAE International.

McElhaney, J.H., 1966. Dynamic response of bone and muscle tissue. J Appl Physiol 21, 1231-1236.

McElhaney, J.H., Doherty, B.J., Paver, J.G., Myers, B.S., Gray, L., Year Combined bending and axial loading responses of the human cervical spine. In 32nd Stapp Car Crash Conference. Atlanta, GA.

MedlinePlus, 2011. Cervical vertebrae.

Mercer, S., Bogduk, N., 1999. The ligaments and annulus fibrosus of human adult cervical intervertebral discs. Spine (Phila Pa 1976) 24, 619-626.

Metzger, M.F., Faruk Senan, N.A., O'Reilly, O.M., Lotz, J.C., 2010. Minimizing errors associated with calculating the location of the helical axis for spinal motions. J Biomech 43, 2822-2829.

Miyanji, F., Furlan, J.C., Aarabi, B., Arnold, P.M., Fehlings, M.G., 2007. Acute cervical traumatic spinal cord injury: MR imaging findings correlated with neurologic outcome--prospective study with 100 consecutive patients. Radiology 243, 820-827.

Moore, K.L., Dalley, A.F., Agur, A.M.R., 2006. Clinically oriented anatomy, 5th ed. Lippincott Williams & Wilkins, Baltimore, Md.

Moroney, S.P., Schultz, A.B., Miller, J.A., Andersson, G.B., 1988. Load-displacement properties of lower cervical spine motion segments. J Biomech 21, 769-779.

Myers, B.S., McElhaney, J.H., Doherty, B.J., Paver, J.G., Gray, L., 1991. The role of torsion in cervical spine trauma. Spine (Phila Pa 1976) 16, 870-874.

Nadeau, M., McLachlin, S.D., Bailey, S.I., Gurr, K.R., Dunning, C.E., Bailey, C.S., 2012. A biomechanical assessment of soft-tissue damage in the cervical spine following a unilateral facet injury. J Bone Joint Surg Am 94, e156.

Nassr, A., Lee, J.Y., Dvorak, M.F., Harrop, J.S., Dailey, A.T., Shaffrey, C.I., Arnold, P.M., Brodke, D.S., Rampersaud, R., Grauer, J.N., Winegar, C., Vaccaro, A.R., 2008. Variations in surgical treatment of cervical facet dislocations. Spine (Phila Pa 1976) 33, E188-193.

National Highway Traffic Safety Administration, 2011. NHTSA's Biomechanics Research Plan, 2011-2015. series no.

Newell, R.S., Siegmund, G.P., Blouin, J.S., Street, J., Cripton, P.A., 2014. Cervical vertebral realignment when voluntarily adopting a protective neck posture. Spine (Phila Pa 1976) 39, E885-893.

Newton, D., England, M., Doll, H., Gardner, B.P., 2011. The case for early treatment of dislocations of the cervical spine with cord involvement sustained playing rugby. J Bone Joint Surg Br 93, 1646-1652.

NHTSA, 2005. Laboratory Test Procedure for FMVSS 208, Occupant Crash Protection. US Department of Transportation, Washington DC.

Nightingale, R.W., Doherty, B.J., Myers, B.S., McElhaney, J.H., Richardson, W.J., 1991. The influence of end condition on human cervical spine injury mechanisms, SAE Technical Paper 912915.

Nightingale, R.W., McElhaney, J.H., Richardson, W.J., Myers, B.S., 1996. Dynamic responses of the head and cervical spine to axial impact loading. J Biomech 29, 307-318.

Nightingale, R.W., Sganga, J., Cutcliffe, H., Bass, C.R., 2016. Impact responses of the cervical spine: A computational study of the effects of muscle activity, torso constraint, and pre-flexion. J Biomech 49, 558-564.

Nowitzke, A., Westaway, M., Bogduk, N., 1994. Cervical zygapophyseal joints: geometrical parameters and relationship to cervical kinematics. Clinical Biomechanics 9, 342-348.

Nyquist, G.W., Begman, P.C., King, A.I., Mertz, H.J., 1980. Correlation of field injuries and GM hybrid III dummy responses for lap-shoulder belt restraint. J Biomech Eng 102, 103-109.

O'Brien, P.J., Schweigel, J.F., Thompson, W.J., 1982. Dislocations of the lower cervical spine. J Trauma 22, 710-714.

Pal, G.P., Sherk, H.H., 1988. The vertical stability of the cervical spine. Spine (Phila Pa 1976) 13, 447-449.

Panjabi, M.M., Cholewicki, J., Nibu, K., Babat, L.B., Dvorak, J., 1998a. Simulation of whiplash trauma using whole cervical spine specimens. Spine (Phila Pa 1976) 23, 17-24.

Panjabi, M.M., Cholewicki, J., Nibu, K., Grauer, J., Vahldiek, M., 1998b. Capsular ligament stretches during in vitro whiplash simulations. J Spinal Disord 11, 227-232.

Panjabi, M.M., Duranceau, J., Goel, V., Oxland, T., Takata, K., 1991. Cervical human vertebrae. Quantitative three-dimensional anatomy of the middle and lower regions. Spine (Phila Pa 1976) 16, 861-869.

Panjabi, M.M., Oxland, T., Takata, K., Goel, V., Duranceau, J., Krag, M., 1993. Articular facets of the human spine. Quantitative three-dimensional anatomy. Spine (Phila Pa 1976) 18, 1298-1310.

Panjabi, M.M., Simpson, A.K., Ivancic, P.C., Pearson, A.M., Tominaga, Y., Yue, J.J., 2007. Cervical facet joint kinematics during bilateral facet dislocation. European Spine Journal 16, 1680-1688.

Panjabi, M.M., Summers, D.J., Pelker, R.R., Videman, T., Friedlaender, G.E., Southwick, W.O., 1986. Three-dimensional load-displacement curves due to forces on the cervical spine. J Orthop Res 4, 152-161.

Panzer, M.B., Cronin, D.S., 2009. C4–C5 segment finite element model development, validation, and load-sharing investigation. Journal of Biomechanics 42, 480-490.

Payer, M., Schmidt, M.H., 2005. Management of traumatic bilateral locked facets of the subaxial cervical spine. Contemporary Neurosurgery 27, 1-3.

Penning, L., 1960. Functioneel röntgenonderzoek bij degeneratieve en traumatische aandoeningen der laag-cervicale bewegingssegmenten.

Penning, L., Wilmink, J.T., 1987. Rotation of the cervical spine. A CT study in normal subjects. Spine (Phila Pa 1976) 12, 732-738.

Piccirilli, M., Liberati, C., Santoro, G., Santoro, A., 2013. Cervical Post-traumatic Unilateral Locked Facets: Clinical, Radiological and Surgical Remarks on a Series of 33 Patients. Journal of Spinal Disorders and Techniques.

Pintar, F., Yoganandan, N., Sances, A., Reinartz, J., Harris, G., Larson, S.J., 1989. Kinematic and anatomical analysis of the human cervical spinal column under axial loading. SAE Technical Paper 892436.

Pintar, F., Yoganandan, N., Voo, L., Cusick, J.F., Maiman, D.J., Sances, A., Year Dynamic characteristics of the human cervical spine. In 39th Stapp Car Chrash Conference. San Diego, CA.

Pintar, F.A., Voo, L.m., Yoganandan, N.A., Cho, T.h., Maiman, D.j., 1998. Mechanisms of hyperflexion cervical spine injury. Proceedings of the International Research Council on the Biomechanics of Injury conference 26, 249-260.

Pollintine, P., Przybyla, A.S., Dolan, P., Adams, M.A., 2004. Neural arch load-bearing in old and degenerated spines. J Biomech 37, 197-204.

Pospiech, J., Stolke, D., Wilke, H.J., Claes, L.E., 1999. Intradiscal pressure recordings in the cervical spine. Neurosurgery 44, 379-384; discussion 384-375.

Prasad, P., Daniel, R.P., Year A biomechanical analysis of head, neck, and torso injuries to child surrogates due to sudden torso acceleration. In 28th Stapp Car Crash Conference. Chicago IL.

Prasad, S.S., O'Malley, M., Caplan, M., Shackleford, I.M., Pydisetty, R.K., 2003. MRI measurements of the cervical spine and their correlation to Pavlov's ratio. Spine (Phila Pa 1976) 28, 1263-1268.

Przybyla, A.S., Skrzypiec, D., Pollintine, P., Dolan, P., Adams, M.A., 2007. Strength of the cervical spine in compression and bending. Spine (Phila Pa 1976) 32, 1612-1620.

Quarrington, R.D., Costi, J.J., Freeman, B.J.C., Jones, C.F., 2018a. Quantitative evaluation of facet deflection, stiffness, strain and failure load during simulated cervical spine trauma. Journal of Biomechanics 72, 116-124.

Quarrington, R.D., Jones, C.F., Tcherveniakov, P., Clark, J.M., Sandler, S.J.I., Lee, Y.C., Torabiardakani, S., Costi, J.J., Freeman, B.J.C., 2018b. Traumatic subaxial cervical facet subluxation and dislocation: epidemiology, radiographic analyses, and risk factors for spinal cord injury. Spine J 18, 387-398.

Ramnarain, A., Govender, S., 2008. Fibular allograft and anterior plating for dislocations/fractures of the cervical spine. Indian J Orthop 42, 83-86.

Rao, S.C., Fehlings, M.G., 1999. The optimal radiologic method for assessing spinal canal compromise and cord compression in patients with cervical spinal cord injury. Part I: An evidence-based analysis of the published literature. Spine (Phila Pa 1976) 24, 598-604.

Rasoulinejad, P., McLachlin, S.D., Bailey, S.I., Gurr, K.R., Bailey, C.S., Dunning, C.E., 2012. The importance of the posterior osteoligamentous complex to subaxial cervical spine stability in relation to a unilateral facet injury. Spine J 12, 590-595.

Razack, N., Green, B.A., Levi, A.D., 2000. The management of traumatic cervical bilateral facet fracture-dislocations with unicortical anterior plates. J Spinal Disord 13, 374-381.

Rickenbacher, J., Scheier, H., Wilson, R.R., Winstanley, D.P., Siegfried, J., Landolt, A.M., Wagenhäuser, F.J., Theiler, K., 2013. Applied Anatomy of the Back. Springer Berlin Heidelberg.

Riesenburger, R.I., Potluri, T., Kulkarni, N., Lavelle, W., Roguski, M., Goel, V.K., Benzel, E.C., 2012. Unilateral cervical facet dislocation: a biomechanical study of several constructs including unilateral lateral mass fixation supplemented by an interspinous cable. J Neurosurg Spine 16, 251-256.

Roaf, R., 1960. A study of the mechanics of spinal injuries. Journal of Bone and Joint Surgery 42B, 810-823.

Robertson, G., Caldwell, G., Hamill, J., Kamen, G., Whittlesey, S., 2013. Research Methods in Biomechanics, 2E. Human Kinetics.

Rorabeck, C.H., Rock, M.G., Hawkins, R.J., Bourne, R.B., 1987. Unilateral facet dislocation of the cervical spine. An analysis of the results of treatment in 26 patients. Spine (Phila Pa 1976) 12, 23-27.

Saari, A., Dennison, C.R., Zhu, Q., Nelson, T.S., Morley, P., Oxland, T.R., Cripton, P.A., Itshayek, E., 2013. Compressive follower load influences cervical spine kinematics and kinetics during simulated head-first impact in an in vitro model. J Biomech Eng 135, 111003.

Saari, A., Itshayek, E., Cripton, P.A., 2011. Cervical spinal cord deformation during simulated head-first impact injuries. J Biomech 44, 2565-2571.

Salem, W., Lenders, C., Mathieu, J., Hermanus, N., Klein, P., 2013. In vivo three-dimensional kinematics of the cervical spine during maximal axial rotation. Man Ther 18, 339-344.

Savini, R., Parisini, P., Cervellati, S., 1987. The surgical treatment of late instability of flexion-rotation injuries in the lower cervical spine. Spine (Phila Pa 1976) 12, 178-182.

Scher, A.T., 1977. Unilateral locked facet in cervical spine injuries. AJR Am J Roentgenol 129, 45-48.

Schindelin, J., Arganda-Carreras, I., Frise, E., Kaynig, V., Longair, M., Pietzsch, T., Preibisch, S., Rueden, C., Saalfeld, S., Schmid, B., Tinevez, J.-Y., White, D.J., Hartenstein, V., Eliceiri, K., Tomancak, P., Cardona, A., 2012. Fiji: an open-source platform for biological-image analysis. Nat Meth 9, 676-682.

Schmidt, H., Midderhoff, S., Adkins, K., Wilke, H.J., 2009. The effect of different design concepts in lumbar total disc arthroplasty on the range of motion, facet joint forces and instantaneous center of rotation of a L4-5 segment. Eur Spine J 18, 1695-1705.

Schnake, K.J., Schroeder, G.D., Vaccaro, A.R., Oner, C., 2017. AOSpine Classification Systems (Subaxial, Thoracolumbar). J Orthop Trauma 31 Suppl 4, S14-S23.

Schulitz, K.P., Niethard, F.U., 1980. Strain on the interarticular stress distribution. Measurements regarding the development of spondylolysis. Arch Orthop Trauma Surg 96, 197-202.

Sekhon, L.H., Fehlings, M.G., 2001. Epidemiology, demographics, and pathophysiology of acute spinal cord injury. Spine (Phila Pa 1976) 26, S2-12.

Sellin, J.N., Shaikh, K., Ryan, S.L., Brayton, A., Fulkerson, D.H., Jea, A., 2014. Clinical outcomes of the surgical treatment of isolated unilateral facet fractures, subluxations, and dislocations in the pediatric cervical spine: report of eight cases and review of the literature. Childs Nerv Syst.

Shah, J.S., Hampson, W.G., Jayson, M.I., 1978. The distribution of surface strain in the cadaveric lumbar spine. J Bone Joint Surg Br 60-B, 246-251.

Shanmuganathan, K., Mirvis, S., Levine, A., 1994. Rotational injury of cervical facets: CT analysis of fracture patterns with implications for management and neurologic outcome. AJR. American journal of roentgenology 163, 1165-1169.

Shea, M., Edwards, W.T., White, A.A., Hayes, W.C., 1991. Variations of stiffness and strength along the human cervical spine. J Biomech 24, 95-107.

Siegmund, G.P., Davis, M.B., Quinn, K.P., Hines, E., Myers, B.S., Ejima, S., Ono, K., Kamiji, K., Yasuki, T., Winkelstein, B.A., 2008. Head-turned postures increase the risk of cervical facet capsule injury during whiplash. Spine (Phila Pa 1976) 33, 1643-1649.

Siegmund, G.P., Myers, B.S., Davis, M.B., Bohnet, H.F., Winkelstein, B.A., 2001. Mechanical evidence of cervical facet capsule injury during whiplash: a cadaveric study using combined shear, compression, and extension loading. Spine (Phila Pa 1976) 26, 2095-2101.

Sim, E., Vaccaro, A.R., Berzlanovich, A., Schwarz, N., Sim, B., 2001. In vitro genesis of subaxial cervical unilateral facet dislocations through sequential soft tissue ablation. Spine (Phila Pa 1976) 26, 1317-1323.

Song, K.J., Choi, B.W., Kim, S.J., Kim, G.H., Kim, Y.S., Song, J.H., 2009. The relationship between spinal stenosis and neurological outcome in traumatic cervical spine injury: an analysis using Pavlov's ratio, spinal cord area, and spinal canal area. Clin Orthop Surg 1, 11-18.

Stathoulis, B., Govender, S., 1997. The triple wire technique for bifacet dislocation of the cervical spine. Injury 28, 123-125.

Suezawa, Y., Jacob, H.A., Bernoski, F.P., 1980. The mechanical response of the neural arch of the lumbosacral vertebra and its clinical significance. Int Orthop 4, 205-209.

Tator, C.H., 1983. Spine-spinal cord relationships in spinal cord trauma. Clin Neurosurg 30, 479-494.

Teo, E.C., Ng, H.W., 2001. Evaluation of the role of ligaments, facets and disc nucleus in lower cervical spine under compression and sagittal moments using finite element method. Med Eng Phys 23, 155-164.

Thesleff, T., Niskakangas, T., Luoto, T.M., Ohman, J., Ronkainen, A., 2015. Fatal cervical spine injuries: a Finnish nationwide register-based epidemiologic study on data from 1987 to 2010. Spine J.

Thompson, W.L., Stiell, I.G., Clement, C.M., Brison, R.J., Canadian, C.S.R.S.G., 2009. Association of injury mechanism with the risk of cervical spine fractures. CJEM 11, 14-22.

Torretti, J.A., Sengupta, D.K., 2007. Cervical spine trauma. Indian J Orthop 41, 255-267.

Tovell, A., 2018. Spinal cord injury, Australia, 2014–15. Injury research and statistics series no. 113. Canberra: AIHW.

Vaccaro, A.R., Falatyn, S.P., Flanders, A.E., Balderston, R.A., Northrup, B.E., Cotler, J.M., 1999. Magnetic resonance evaluation of the intervertebral disc, spinal ligaments, and spinal cord before and after closed traction reduction of cervical spine dislocations. Spine (Phila Pa 1976) 24, 1210-1217.

Vaccaro, A.R., Hulbert, R.J., Patel, A.A., Fisher, C., Dvorak, M., Lehman, R.A., Jr., Anderson, P., Harrop, J., Oner, F.C., Arnold, P., Fehlings, M., Hedlund, R., Madrazo, I., Rechtine, G., Aarabi, B., Shainline, M., Spine Trauma Study, G., 2007. The subaxial cervical spine injury classification system: a novel approach to recognize the importance of morphology, neurology, and integrity of the disco-ligamentous complex. Spine (Phila Pa 1976) 32, 2365-2374.

Vaccaro, A.R., Koerner, J.D., Radcliff, K.E., Oner, F.C., Reinhold, M., Schnake, K.J., Kandziora, F., Fehlings, M.G., Dvorak, M.F., Aarabi, B., Rajasekaran, S., Schroeder, G.D., Kepler, C.K., Vialle, L.R., 2016. AOSpine subaxial cervical spine injury classification system. Eur Spine J 25, 2173-2184.

Vaccaro, A.R., Madigan, L., Schweitzer, M.E., Flanders, A.E., Hilibrand, A.S., Albert, T.J., 2001. Magnetic resonance imaging analysis of soft tissue disruption after flexion-distraction injuries of the subaxial cervical spine. Spine (Phila Pa 1976) 26, 1866-1872.

van Middendorp, J.J., Cheung, I., Dalzell, K., Deverall, H., Freeman, B.J., Morris, S.A., Sandler, S.J., Williams, R., Yau, Y.H., Goss, B., 2015. Detecting Facet Joint and Lateral Mass Injuries of the Subaxial Cervical Spine in Major Trauma Patients. Asian Spine J 9, 327-337.

Van Toen, C., Melnyk, A.D., Street, J., Oxland, T.R., Cripton, P.A., 2014. The effect of lateral eccentricity on failure loads, kinematics, and canal occlusions of the cervical spine in axial loading. Journal of Biomechanics 47, 1164-1172.

Wachowski, M.M., Mansour, M., Lee, C., Ackenhausen, A., Spiering, S., Fanghanel, J., Dumont, C., Kubein-Meesenburg, D., Nagerl, H., 2009. How do spinal segments move? J Biomech 42, 2286-2293.

Wang, B., Zhu, Y., Jiao, Y., Wang, F., Liu, X., Zhu, H., Tu, G., Liang, D., 2013. A New Anterior-Posterior Surgical Approach for the Treatment of Cervical Facet Dislocations. J Spinal Disord Tech.

Wang, C.S., Chang, J.H., Chang, T.S., Chen, H.Y., Cheng, C.W., 2012. Loading effects of anterior cervical spine fusion on adjacent segments. Kaohsiung J Med Sci 28, 586-594.

Wang, M.C., Pintar, F., Yoganandan, N., Maiman, D.J., 2009. The continued burden of spine fractures after motor vehicle crashes. J Neurosurg Spine 10, 86-92.

White, A.A., Panjabi, M.M., 1990. Clinical Biomechanics of the Spine. Lippincott.

Williams, J., Jehle, D., Cottington, E., Shufflebarger, C., 1992. Head, facial, and clavicular trauma as a predictor of cervical-spine injury. Ann Emerg Med 21, 719-722.

Wilson, J.R., Vaccaro, A., Harrop, J.S., Aarabi, B., Shaffrey, C., Dvorak, M., Fisher, C., Arnold, P., Massicotte, E.M., Lewis, S., Rampersaud, R., Okonkwo, D.O., Fehlings, M.G., 2013. The impact of facet dislocation on clinical outcomes after cervical spinal cord injury: results of a multicenter North American prospective cohort study. Spine (Phila Pa 1976) 38, 97-103.

Wiseman, D.B., Bellabarba, C., Mirza, S.K., Chapman, J., 2003. Anterior versus posterior surgical treatment for traumatic cervical spine dislocation. Current Opinion in Orthopaedics 14, 174-181.

Wolf, A., Levi, L., Mirvis, S., Ragheb, J., Huhn, S., Rigamonti, D., Robinson, W.L., 1991. Operative management of bilateral facet dislocation. J Neurosurg 75, 883-890.

Wu, G., Siegler, S., Allard, P., Kirtley, C., Leardini, A., Rosenbaum, D., Whittle, M., D'Lima, D.D., Cristofolini, L., Witte, H., Schmid, O., Stokes, I., 2002. ISB recommendation on definitions of joint coordinate system of various joints for the reporting of human joint motion--part I: ankle, hip, and spine. International Society of Biomechanics. J Biomech 35, 543-548.

Wu, S.K., Kuo, L.C., Lan, H.C., Tsai, S.W., Chen, C.L., Su, F.C., 2007. The quantitative measurements of the intervertebral angulation and translation during cervical flexion and extension. Eur Spine J 16, 1435-1444.

Yang, S., Ding, W., Yang, D., Gu, T., Zhang, F., Zhang, D., Sun, Y., Ma, L., Song, Y., 2013. Epidemiology and risk factors of cervical spine injury during heating season in the patients with cervical trauma: a cross-sectional study. PLoS One 8, e78358.

Yoganandan, N., Haffner, M., Maiman, D.J., Nichols, H., Pintar, F., Jentzen, J., Weinshel, S.S., Larson, S.J., Sances, A., 1989. Epidemiology and injury biomechanics of motor vehicle related trauma to the human spine. SAE Technical Paper 892438.

Zhu, Q.A., Park, Y.B., Sjovold, S.G., Niosi, C.A., Wilson, D.C., Cripton, P.A., Oxland, T.R., 2008. Can extra-articular strains be used to measure facet contact forces in the lumbar spine? An in-vitro biomechanical study. Proc Inst Mech Eng H 222, 171-184.

Appendix A Medical image analysis program

Overview

This appendix provides a summary of the medical image analysis program (MIAP) that was developed in MATLAB (R2012a, Mathworks, Massachusetts, USA). This program was developed to assist surgeons with performing the radiographic measures of subaxial cervical spine injury severity suggested by the Spine Trauma Study Group (STSG) (Bono et al., 2006). All available medical images (radiographs, computed tomography [CT] and magnetic resonance imaging [MRI]) acquired within 24 hours of admission for the patients with distractive-flexion injuries (DFI) (Allen et al., 1982) were retrieved in DICOM format. The following de-identified image slices were prepared and exported as high-res BMP images for analysis using 'FIJI' image analysis software (1.51p, ImageJ, Maryland, USA) (Schindelin et al., 2012):

- Lateral radiograph;
- Mid-sagittal CT;
- Parasagittal CT through the mid-sagittal plane of the left and right facets; and,
- Mid-sagittal MRI.

DICOM image stacks were re-orientated using FIJI if the patient was non-anatomically aligned. CT/MRI slices were taken through the mid- or parasagittal plane of the level of injury, as suggested by the STSG. The final BMP images for each patient were stored in a database with specific folder hierarchy. The MIAP was compiled and provided, along with the database, to two spinal surgeons. Details and functionality of the MIAP are described below.

Program description

The MIAP prompts the user to identify specific anatomical features on a database of sagittal and para-sagittal cervical spine medical images from DFI patients at the RAH. Using these landmarks, measurements of anterior vertebral translation, Cobb angle, posterior tangent angle, facet apposition, spinal canal occlusion, and spinal cord compression are calculated. The user is prompted to identify anatomical landmarks at all levels of the subaxial cervical spine, so

these measures can be calculated between any two vertebrae. By default, the most ‘injured’ intervertebral level is automatically displayed and the measurement parameters for this level are exported for analysis.

Program functionality

The functionality of the MIAP is outlined below:

1) The user can create an account to start a new analysis or continue a previous analysis using the graphical user interface (GUI). They are then prompted to analyse the next undefined image, begin from the first image in the database, or choose a specific image of interest.

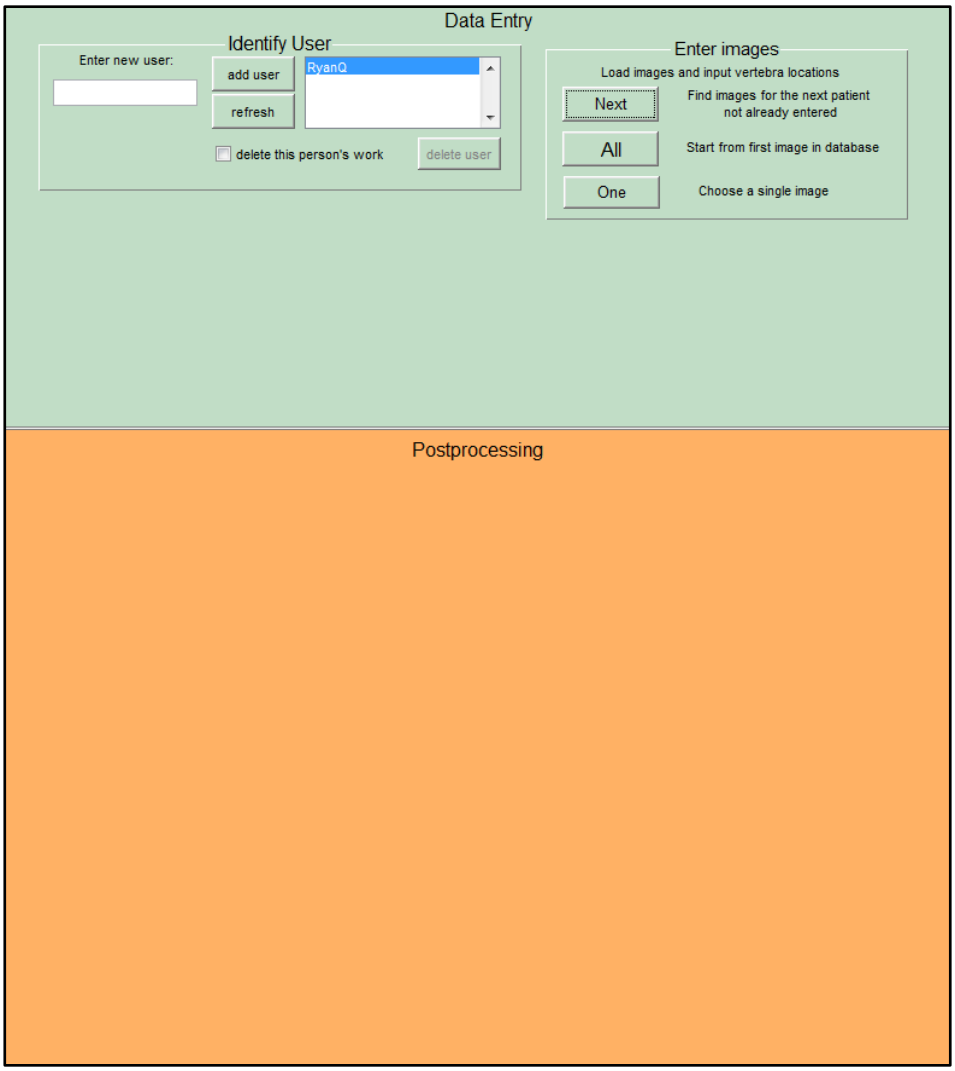

Figure A.1: The MIAP graphical user interface.

2) Sagittal images (x-ray and/or CT, if available) are loaded and the user is prompted to identify the four corners of each vertebral body (C3-T1). The user can flag if there is anything abnormal about the anatomy. For mid-sagittal CT images the user is also prompted to identify the landmarks necessary to calculate spinal canal occlusion.

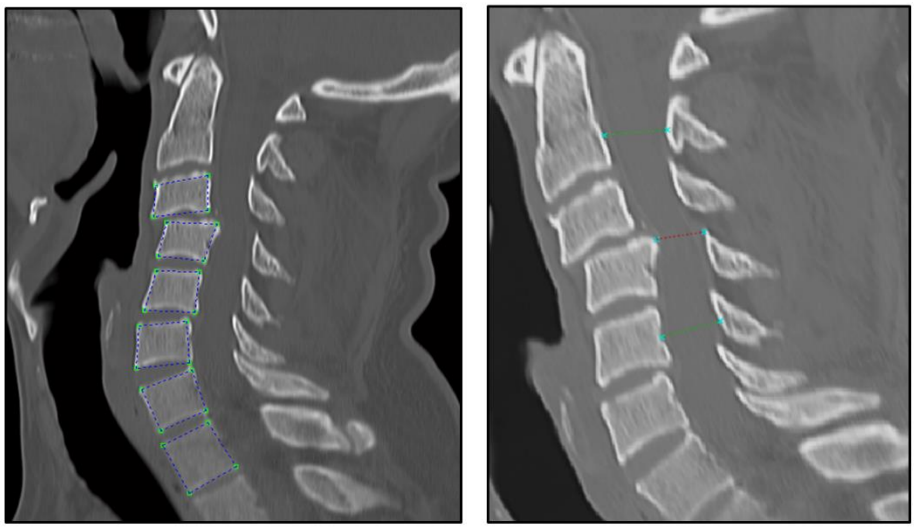

Figure A.2: Mid-sagittal CT images with anatomical landmarks identified: (a) corners of C3-T1 vertebral bodies; (b) canal space at the level of injury, and the superior and inferior uninjured levels.

3) The next available image is automatically presented to the user. For para-sagittal CT images at the level of dislocation (both left and right, through the mid-sagittal plane of facet articulation) the user is prompted to identify the anterior and posterior ends of the articular surface of the opposing facets, from which facet apposition is calculated.

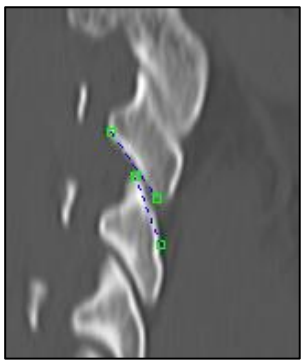

Figure A.3: Para-sagittal CT image used to calculate facet apposition.

4) Mid-sagittal MRI slices are used to measure spinal cord compression.

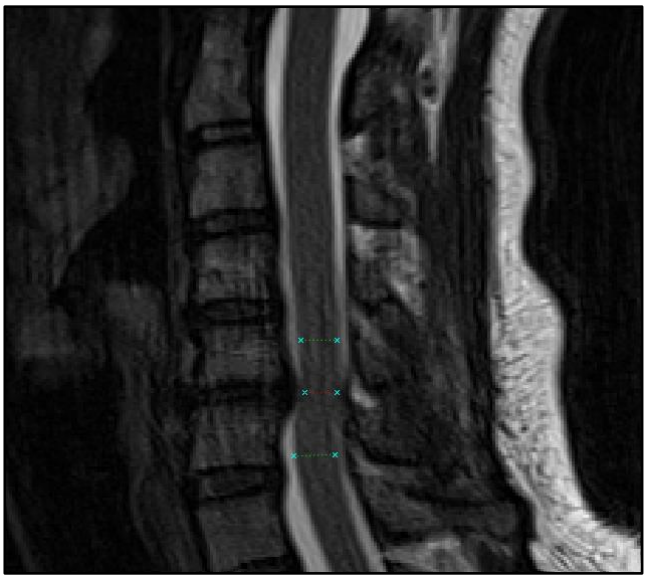

Figure A.4: Spinal cord compression landmarks identified on mid-sagittal MRI. Sagittal cord diameter at the superior and inferior uninjured levels is measured to calculate cord compression as a percentage of the normal cord diameter.

5) Using these landmarks, the radiographic measures of cervical spine injury severity suggested by the STSG are automatically calculated (Figure 2.1) and are displayed in post-processing section of the GUI.
6) The MIAP automatically displays these measures for the 'most injured' level (as defined by the magnitude of anterior vertebral translation) of the currently selected patient but can be viewed across any level for which the landmarks were defined. Super-imposed diagrams of how each measurement was calculated (specific to that image) can be generated using the "Show on image" buttons. All measurement values for the selected levels are exported by pressing the "Collate" button.
7) The co-ordinates of the landmarks are automatically saved after each click, so the MIAP can be exited at any time without losing information. The user can then re-start the MIAP and continue their analysis from the same point at a later time.

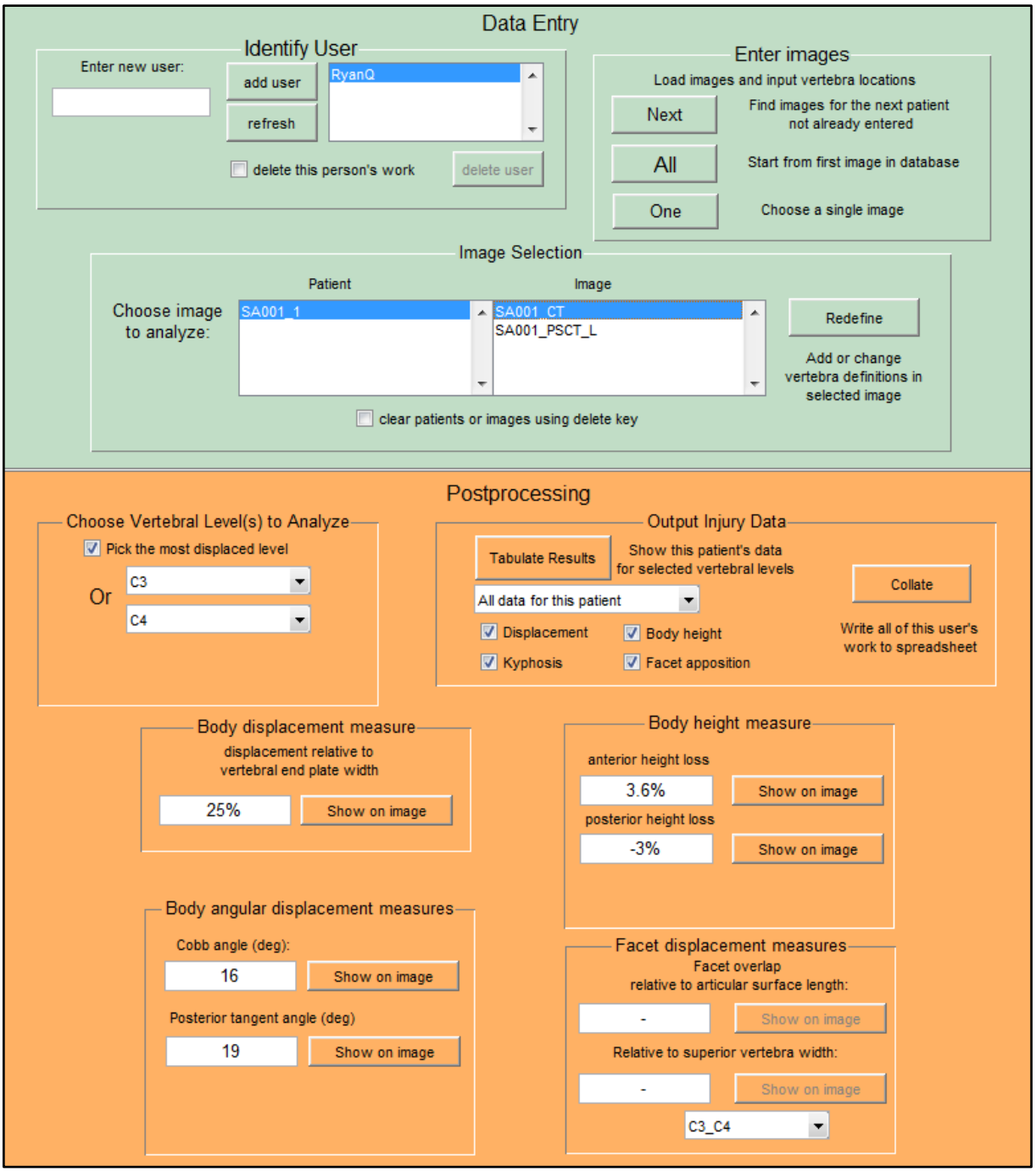

Figure A.5: Measurements calculated from the landmarks identified on a mid-sagittal CT image are displayed.

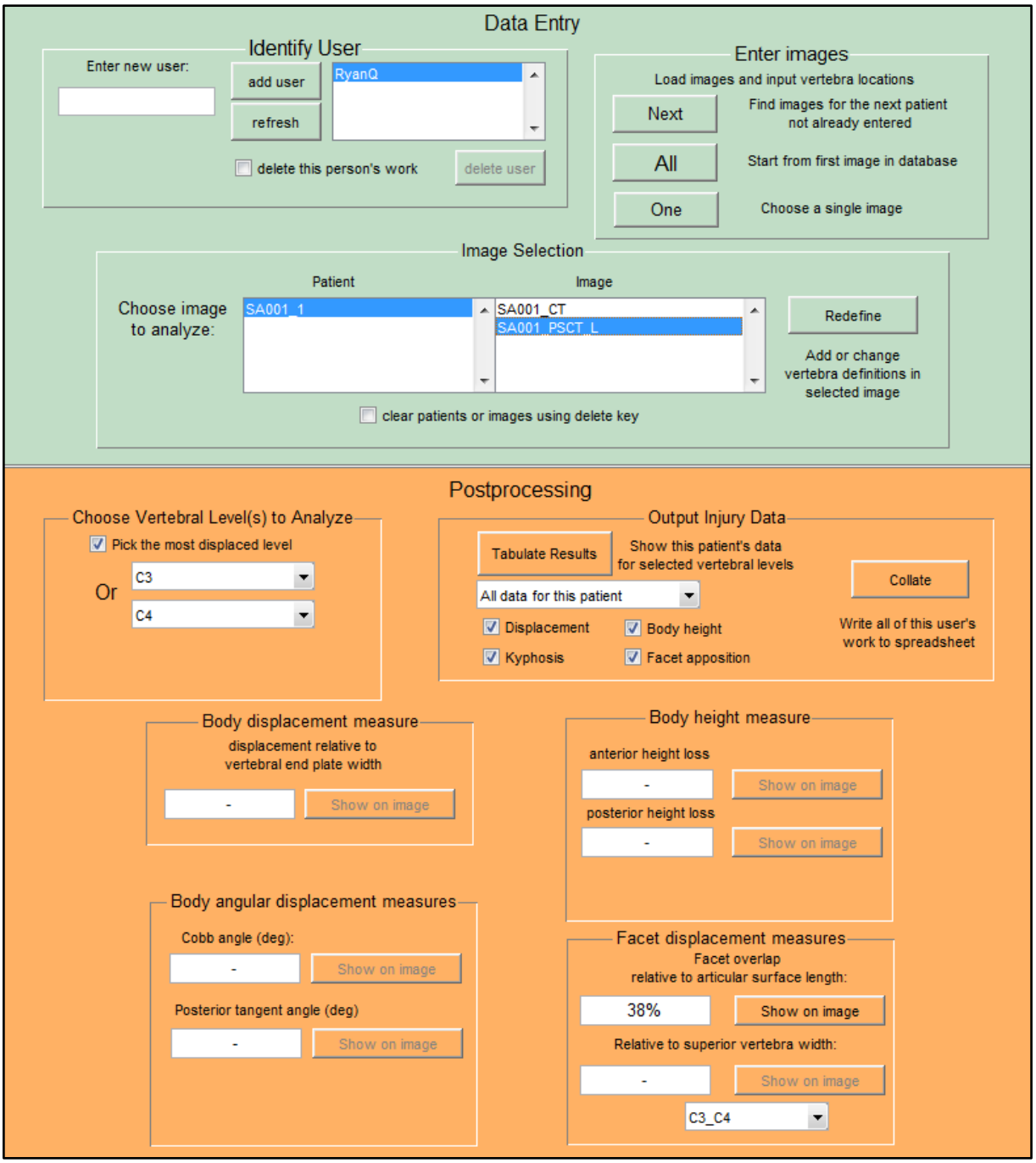

Figure A.6: Measurements calculated from the landmarks identified on a para-sagittal CT image are displayed.

Inter- and intra-observer analysis

Several weeks after completing the initial analysis, each surgeon repeated the process on images from a subset of 29 patients (11% of the DFI cohort) to investigate intra-observer repeatability (Bartlett and Frost, 2008). This subset comprised those patients with complete medical imaging (X-ray, CT and MRI) and their demographics matched the study population. Inter-observer agreement and intra-observer repeatability for radiographic measurements were

evaluated using Bland-Altman (B-A) plots and intra-class correlation coefficients (ICC) (Bartlett and Frost, 2008; Bland and Altman, 1986, 2003); absolute agreement and consistency ICC measures were obtained. The results of this analysis are provided in Section 2.3.2.

Summary

The MIAP was developed in MATLAB to provide surgeons with a simple method of quantifying DFI severity from radiographic images. The measurements were included in statistical models to investigate their association with the occurrence of concomitant SCI.

References

Allen, B.L., Jr., Ferguson, R.L., Lehmann, T.R., O'Brien, R.P., 1982. A mechanistic classification of closed, indirect fractures and dislocations of the lower cervical spine. Spine (Phila Pa 1976) 7, 1-27.

Bartlett, J.W., Frost, C., 2008. Reliability, repeatability and reproducibility: analysis of measurement errors in continuous variables. Ultrasound in Obstetrics and Gynecology 31, 466-475.

Bland, J.M., Altman, D.G., 1986. Statistical methods for assessing agreement between two methods of clinical measurement. Lancet 1, 307-310.

Bland, J.M., Altman, D.G., 2003. Applying the right statistics: analyses of measurement studies. Ultrasound in Obstetrics and Gynecology 22, 85-93.

Bono, C.M., Vaccaro, A.R., Fehlings, M., Fisher, C., Dvorak, M., Ludwig, S., Harrop, J., 2006. Measurement techniques for lower cervical spine injuries: consensus statement of the Spine Trauma Study Group. Spine (Phila Pa 1976) 31, 603-609.

Schindelin, J., Arganda-Carreras, I., Frise, E., Kaynig, V., Longair, M., Pietzsch, T., Preibisch, S., Rueden, C., Saalfeld, S., Schmid, B., Tinevez, J.-Y., White, D.J., Hartenstein, V., Eliceiri, K., Tomancak, P., Cardona, A., 2012. Fiji: an open-source platform for biological-image analysis. Nat Meth 9, 676-682.

Appendix B Optotrak Certus motion-capture system accuracy and repeatability investigation

Overview

The in-plane and out-of-plane accuracy and repeatability of the Adelaide Spinal Research Group's (ASRG) Optotrak Certus HD infrared motion-capture system (Northern Digital Inc., Ontario, Canada) was quantified to ensure that it could adequately capture the facet deflections anticipated during Studies 2-4. There was limited published data available to indicate the magnitude of facet deflections that would occur, or how this would differ between testing directions (Study 2) or axial conditions (Studies 3 and 4), but Green *et al*. reported average lumbar facet sagittal deflections of 3.25±3.07° during simulated *in vivo* flexion. Average sagittal deflections of 0.45° and 0.7° were observed at 80 N of simulated flexion and anterior shear loading, respectively, during pilot testing for Study 2 (described in Appendix C). Therefore, angular deflection accuracy of <0.1° was deemed necessary for comparisons.

Northern Digitial Inc. report positional accuracy of 0.1 mm and resolution of 0.01 mm for the Optotrak Certus HD, but (to the author's knowledge) this has not been verified experimentally by a third party. Translational and angular measurement errors as low as 0.03 mm and 0.04° have been reported during reliability analysis of the earlier Optotrak 3020 system (Maletsky et al., 2007), but a similar analysis has not been performed for the Certus HD. It is also likely that accuracy and repeatability differs between systems, so evaluation of the system that was to be used in the experiments was deemed necessary.

Methods

Optotrak rigid-body marker-carriers with three infrared-emitting diodes were rigidly fixed to a highly accurate robot arm (Katana4D, Neuronics AG, Zurich, Switzerland) and to the table on which the robot arm was mounted (Figure B.1).

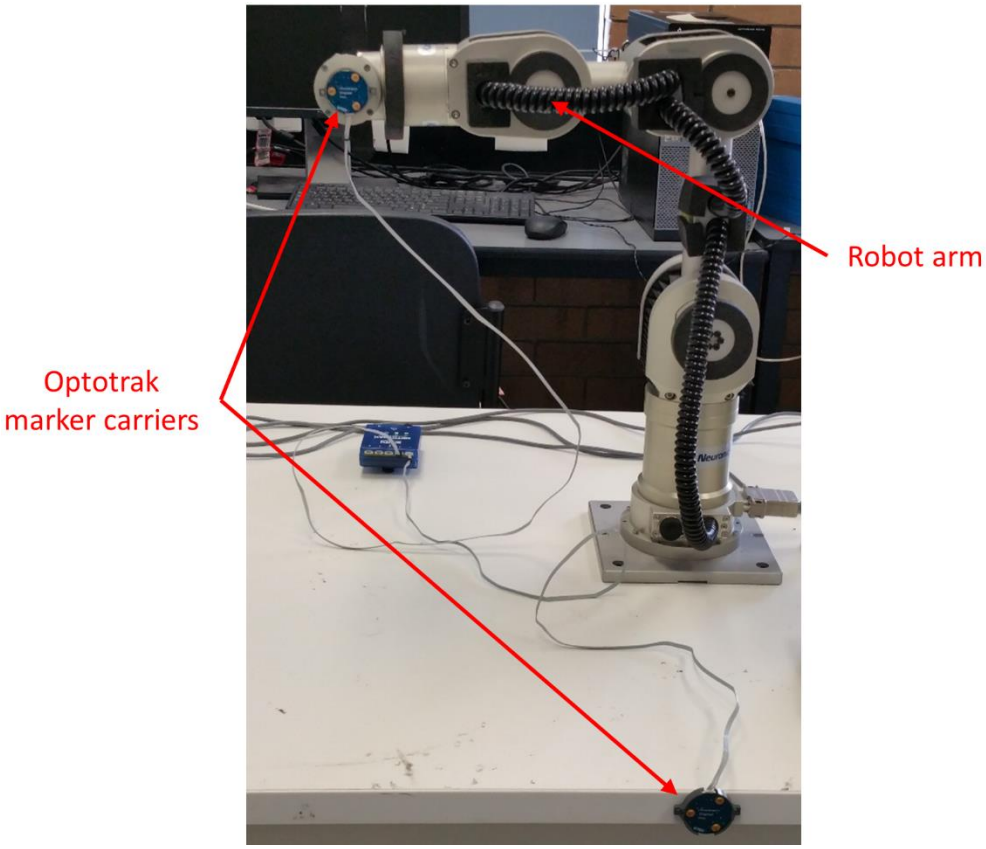

Fig B.1: Photograph of the test setup for measuring accuracy and repeatability of the Optotrak Certus HD using the Katana robot arm. Angular motion of the rigid-body marker carrier attached to the robot arm was calculated relative to the stationary marker carrier fixed to the table.

The robot arm was programmed to perform three repetitions of the following rotation motions, firstly in the plane of the Optotrak cameras and then out-of-plane:

- ±0.5° in 0.1° steps;
- ±5° in 1° steps; and,
- ±30° in 10° steps.

Each change in angular position (step) occurred over 2 s, and the robot arm held each position for 5 seconds. The Optotrak camera tower was located 2.2 m away from the robot arm (Figure B.2) so that the motion of the marker-carrier occurred within the optimum measurement distance, as specified by the manufacturer and determined by Maletsky *et al.* (2007). Motion capture data was recorded throughout each motion at 100 Hz.

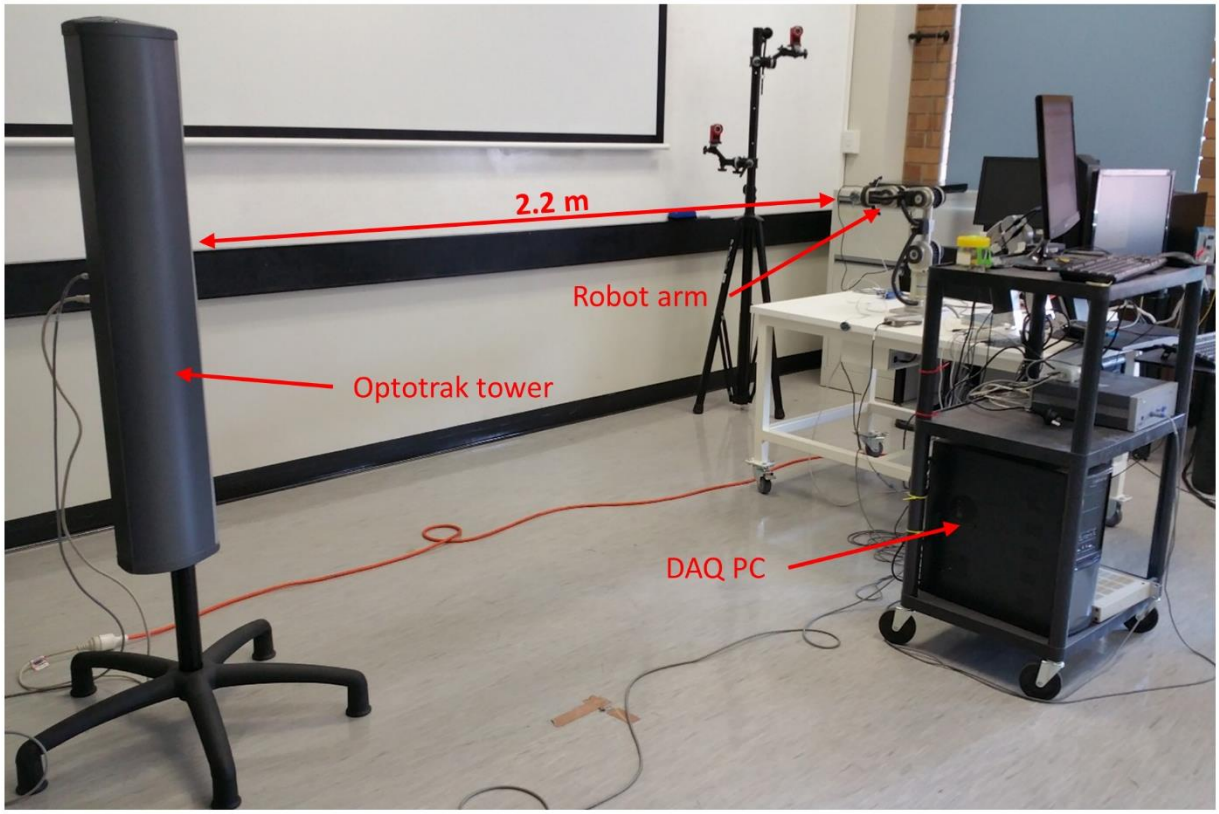

Fig B.2: The Optotrak Certus HD camera tower was position 2.2 m from the robot arm. Motion-capture position data during each motion was recorded by the data acquisition (DAQ) PC.

The change in angle of the robot arm relative to the stationary marker-carrier was calculated at each frame by solving for Euler angles using a *z-y-x* sequence (Robertson et al., 2013); raw position data used in these calculations was unfiltered. The angle at each position hold was averaged over 50 frames (0.5 seconds) for comparison with the expected values (Table B.1). For in-plane and out-of-plane motions, the mean difference between the measured and expected values gave the accuracy (bias) of the system, whilst the standard deviation of this difference gave the repeatability.

Table B.1: Expected and measured values for each step of the Optotrak accuracy and repeatability analysis.

		Expected values (deg):						Measured values (deg):				
		Test #	**Step 1**	**Step 2**	**Step 3**	**Step 4**	**Step 5**	**Step 1**	**Step 2**	**Step 3**	**Step 4**	**Step 5**
In-plane	**±0.5° at 0.1° steps**	1	-0.1	-0.2	-0.3	-0.4	-0.5	-0.106	-0.211	-0.319	-0.420	-0.528
		2	-0.1	-0.2	-0.3	-0.4	-0.5	-0.102	-0.208	-0.318	-0.420	-0.531
		3	-0.1	-0.2	-0.3	-0.4	-0.5	-0.103	-0.203	-0.319	-0.420	-0.531
		4	0.1	0.2	0.3	0.4	0.5	0.095	0.203	0.303	0.396	0.497
		5	0.1	0.2	0.3	0.4	0.5	0.099	0.204	0.305	0.399	0.492
		6	0.1	0.2	0.3	0.4	0.5	0.095	0.203	0.302	0.399	0.491
	±5° at 1° steps	7	-1	-2	-3	-4	-5	-1.002	-2.011	-2.975	-4.010	-4.985
		8	-1	-2	-3	-4	-5	-1.003	-2.009	-2.968	-4.011	-4.978
		9	-1	-2	-3	-4	-5	-0.999	-2.007	-2.968	-4.010	-4.982
		10	1	2	3	4	5	0.977	1.993	2.956	3.982	4.950
		11	1	2	3	4	5	0.978	1.995	2.957	3.984	4.952
		12	1	2	3	4	5	0.975	1.993	2.955	3.984	4.952
	±30° at 10° steps	13	-10	-20	-30			-9.997	-19.979	-29.921		
		14	-10	-20	-30			-9.992	-19.978	-29.914		
		15	-10	-20	-30			-9.993	-19.986	-29.918		
		16	10	20	30			9.956	19.966	29.935		
		17	10	20	30			9.949	19.970	29.941		
		18	10	20	30			9.954	19.975	29.942		
Out-of-plane	**±0.5° at 0.1° steps**	19	0.1	0.2	0.3	0.4	0.5	0.101	0.217	0.311	0.394	0.484
		20	0.1	0.2	0.3	0.4	0.5	0.123	0.236	0.329	0.407	0.493
		21	0.1	0.2	0.3	0.4	0.5	0.118	0.230	0.321	0.395	0.488
		22	-0.1	-0.2	-0.3	-0.4	-0.5	-0.120	-0.206	-0.283	-0.371	-0.471
		23	-0.1	-0.2	-0.3	-0.4	-0.5	-0.121	-0.209	-0.285	-0.366	-0.481
		24	-0.1	-0.2	-0.3	-0.4	-0.5	-0.121	-0.215	-0.293	-0.366	-0.483
	±5° at 1° steps	25	1	2	3	4	5	0.999	1.982	2.957	3.978	4.965
		26	1	2	3	4	5	1.008	1.981	2.956	3.993	4.963
		27	1	2	3	4	5	1.021	2.009	2.986	4.010	4.981
		28	-1	-2	-3	-4	-5	-0.973	-2.024	-2.973	-4.042	-4.986
		29	-1	-2	-3	-4	-5	-0.980	-2.032	-2.980	-4.045	-4.985
		30	-1	-2	-3	-4	-5	-0.983	-2.033	-2.977	-4.050	-4.991
	±30° at 10° steps	31	10	20	30			10.011	20.043	30.052		
		32	10	20	30			10.016	20.059	30.056		
		33	10	20	30			10.021	20.070	30.081		
		34	-10	-20	-30			-9.966	-19.962	-30.072		
		35	-10	-20	-30			-9.966	-19.958	-30.023		
		36	-10	-20	-30			-9.977	-19.978	-30.042		

Results and discussion

The ASRG Optotrak Certus HD was accurate to <0.1° for both in-plane and out-of-plane motions; the largest mean difference was 0.082° surprisingly occurring for in-plane motion (Table B.2). Optotrak repeatability better than 0.01° for all tests except out-of-plane ±30° (Table B.1). The bias of this system during ±10° step motions was slightly better than that reported for the Optotrak 3020 (0.04° vs. 0.07°) (Maletsky et al., 2007).

Table B.2: Bias and repeatability values for in-plane and out-of-plane rotational motion.

	In-plane (deg):	Out-of-plane (deg):
Bias:	0.082	0.006
Repeatability:	0.002	0.009

These results are likely an underestimate of the accuracy and repeatability of this system, as there was probably some out-of-plane motion due to camera misalignment relative to the motion of the robot arm, and uncertainty regarding the exact reliability of motion of the robot arm itself. Despite this, this investigation demonstrated that the ASRG's Optotrak Certus HD has suitable accuracy and repeatability to measure subaxial cervical facet deflections.

References

Maletsky, L.P., Sun, J., Morton, N.A., 2007. Accuracy of an optical active-marker system to track the relative motion of rigid bodies. J Biomech 40, 682-685.

Robertson, G., Caldwell, G., Hamill, J., Kamen, G., Whittlesey, S., 2013. Research Methods in Biomechanics, 2E. Human Kinetics.

Appendix C Study 2 pilot tests: the effect of loading rate and the presence of a superior adjacent vertebra on isolated subaxial cervical inferior facet mechanics

Overview

This appendix describes the pilot testing of Study 2. The aims of this pilot testing were to develop a test setup to measure the mechanical response of the subaxial cervical facets during loading that simulated anterior shear and flexion motions, and to investigate the effect of loading rate and the presence of the superior adjacent facet joint on this response. It was hypothesised that loading rate would not substantially effect the mechanical response, but resecting the adjacent facet joint would increase facet deflection and surface strains for both testing directions.

Methods

Two human cadaver subaxial cervical functional spinal units (FSUs; C2/C3 and C4/C5) were dissected from a 94 year old female donor. Specimens were prepared as described in Section 3.2.1 and were clamped by a custom support apparatus attached to a rotary table, fixed to the base of a mechanical testing machine (Instron 8874). Using the rotary table, the articular surfaces of the inferior facets of the inferior vertebra (C3 or C5) were angled relative to the actuator to simulate inter-facet loading during *in vivo* intervertebral flexion and anterior shear motion. Three cycles of uniaxial loading were applied bilaterally using 6 mm diameter loading pins, in each loading direction, and for each specimen condition (Pilot 1) or loading rate (Pilot 2). Three-dimensional angular deflections of the loaded facets, relative to the vertebral body, were measured using a motion capture system (Optotrak Certus HD, Northern Digital Inc., Ontario, Canada). Maximum and minimum principal strains at the base of the bilateral articular pillars were calculated from the output of tri-axial rosette strain gauges (FRA-1-23-1L, TML, Tokyo, Japan). Apparent facet stiffness was determined from the linear region of load-displacement data (Figure 3.6).

Pilot 1: Effect of superior adjacent facet joint

Testing was first performed on the intact C4/C5 FSU at a rate of 0.1 mm/s from 10 to 150 N, in each loading direction. The posterior elements of C4 were then removed by resecting the pedicles (Figure C.1), and testing was repeated to investigate the effect of the presence of superior adjacent facets on the mechanical response of the C5 inferior facets. The specimen was then tested to failure in the anterior shear loading direction at the same rate.

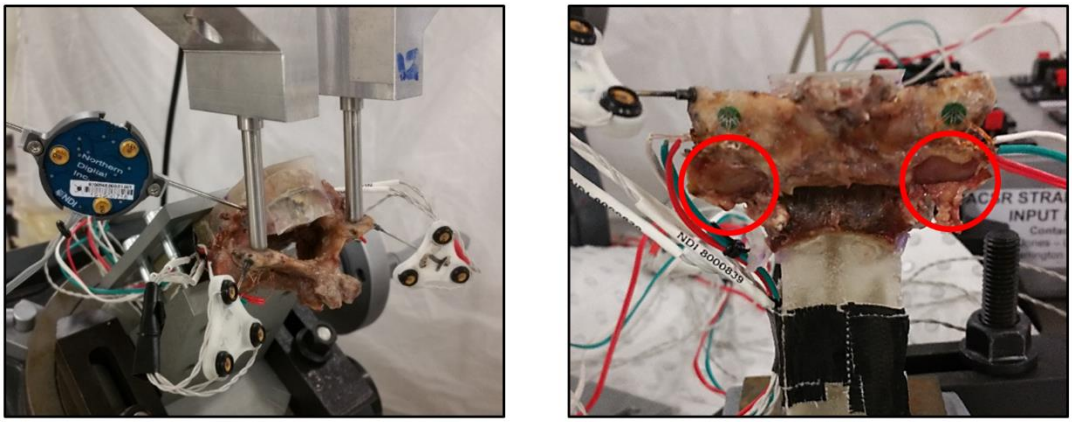

a) b)

Figure C.1: a) Photo of the C4/C5 specimen positioned for simulated flexion testing of the C5 inferior facets in Pilot 1. b) Posterior view of the specimen following resection of the posterior elements of C4. The red circles indicate the exposed superior articular facet surfaces of C5.

Pilot 2: Effect of loading rate

The C2/C3 specimen underwent three cycles of loading from 10 to 80 N at 0.1, 0.5, and 1 mm/s, in each loading direction. Destructive testing was performed in the flexion test direction at 0.1 mm/s.

Descriptive statistics

Facet deflections and surface strains at the peak load for the non-destructive and failure tests of both pilot studies were determined. Deflections were comparable for the left and right facets, so this data was pooled. SPSS v22 (IBM, Illinois, USA) was used to obtain descriptive statistics (mean±SD) for the three cycles of the non-failure test in each loading direction, and each specimen condition (Pilot 1) or loading rate (Pilot 2).

Results and discussion

Pilot 1 – Non-destructive data

Apparent facet stiffness was greater in flexion than in anterior shear, both with and without adjacent superior facets (Figure C.2). Facet deflections were only appreciable in the sagittal plane and bending up to 1.4° away from the vertebral body was observed for one specimen during anterior shear testing. Resection of the adjacent superior facets appeared to increase maximum sagittal facet deflection compared to the intact specimen, especially in anterior shear, and this corresponded with a reduction in apparent stiffness. This reduction in stiffness following resection of C4 was particularly evident for the flexion test direction, which was expected as the loading vector was orientated in the direction of the superior adjacent facet joint.

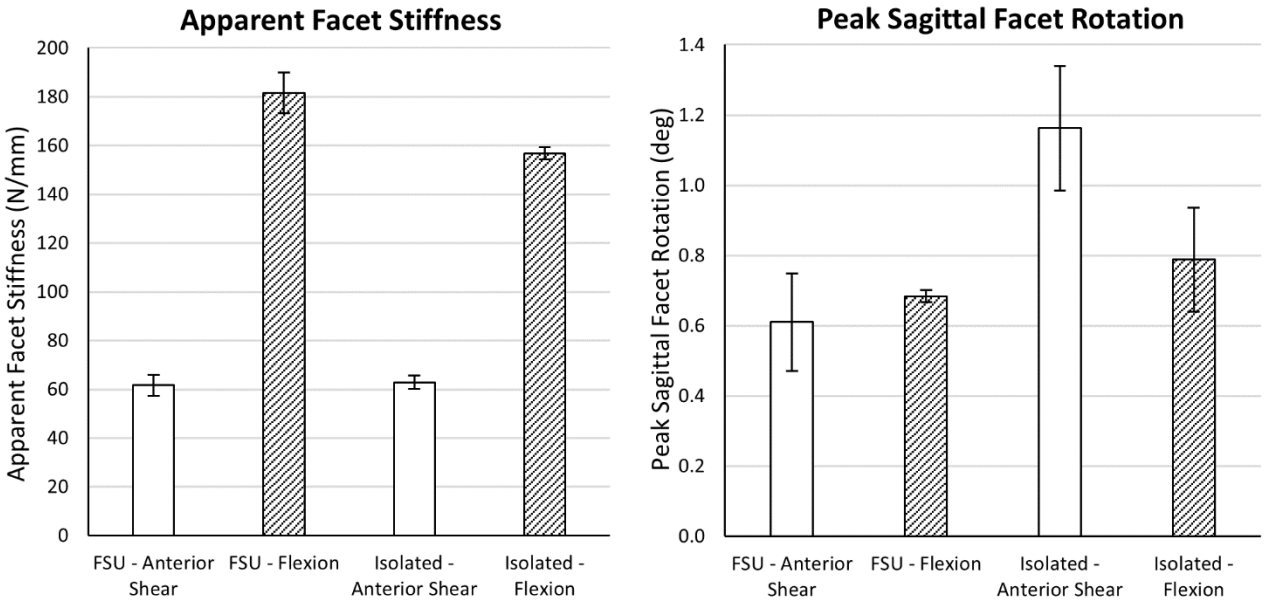

Figure C.2: Mean measured apparent facet stiffness (left) and peak sagittal facet rotation (right) for the C5 inferior facets of the C4/C5 functional spinal unit (FSU) and the isolated C5 vertebra, for each test direction during Pilot 1.

Maximum (tensile) and minimum (compressive) principal strains were generally similar for the left and right facets (Figure C.3), indicating that symmetrical loading and strain gauge placement was achieved. The base of the articular pillars were under compression during anterior shear, and in slight tension during flexion, for both the FSU and isolated conditions. Resection of the C4 posterior elements did not appear to have a substantial or consistent effect on the peak surface strains – compressive strains increased by ~20% following resection during anterior

shear, whilst a slight reduction in maximum and minimum principal strains was observed for the simulated flexion tests.

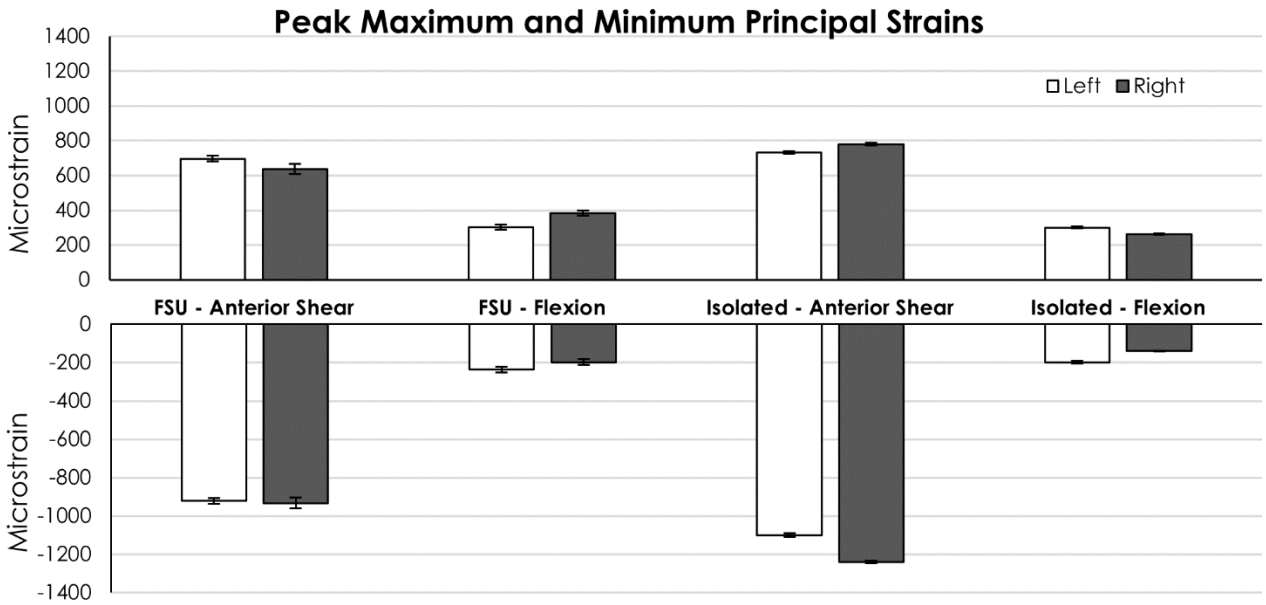

Figure C.3: Mean measured peak maximum (positive, tensile) and minimum (negative, compressive) principal strains for the left and right inferior C5 facets of the C4/C5 functional spinal unit (FSU) and the isolated C5 vertebra, for each test direction during Pilot 1.

Pilot 2 – Non-destructive data

Apparent facet stiffness values in Pilot 2 (Figure C.4) were similar to those observed for the FSU in Pilot 1 (Figure C.2). Increasing displacement rate by an order of magnitude (0.1 to 1 mm/s) increased stiffness by ~17% for the flexion tests, but a similar trend was not observed during simulated anterior shear.

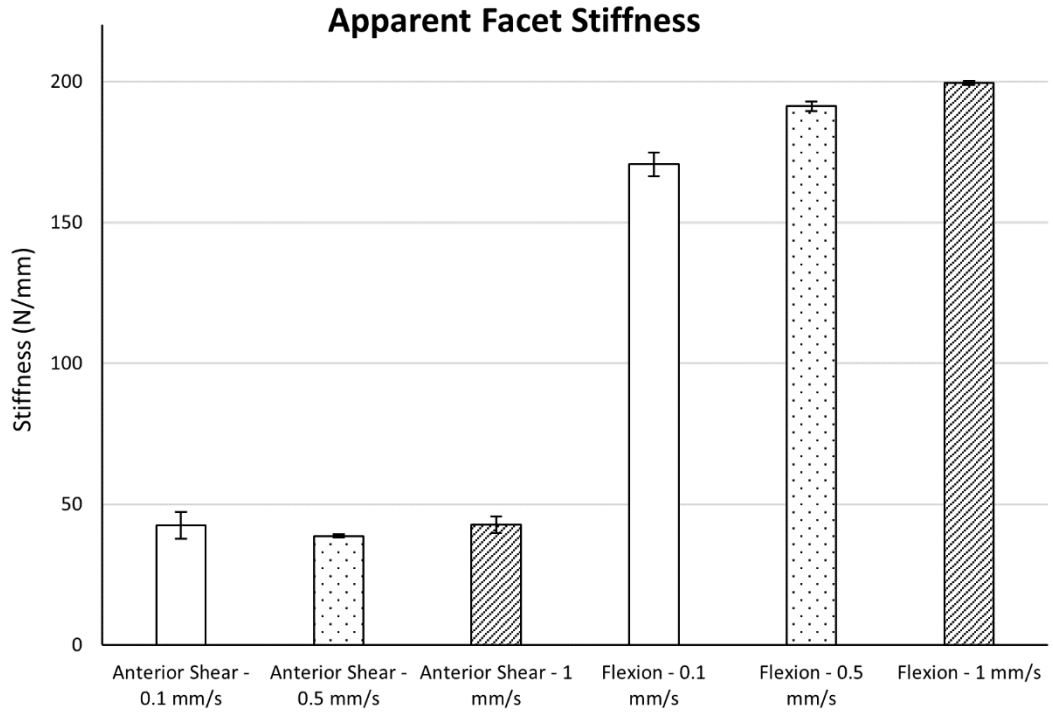

Figure C.4: Mean measured apparent facet stiffness of the C3 inferior facets for the anterior shear and flexion test directions at each loading rate during Pilot 2.

As expected, sagittal angular facet deflections were substantially lower at the 80 N peak load point in Pilot 2 (Figure C.5), compared to at 150 N in Pilot 1 (Figure C.2). Deflections were again larger for the anterior shear tests, but there was no clear effect of loading rate for either test direction.

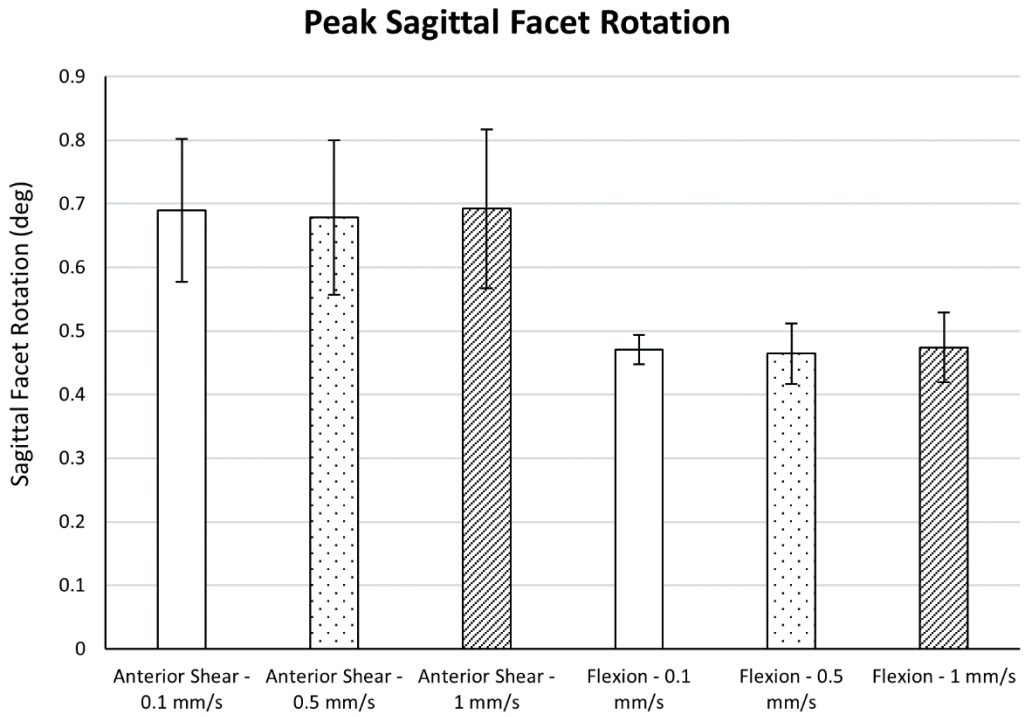

Figure C.5: Mean measured sagittal angular facet deflection of the C3 inferior facets for the anterior shear and flexion test directions at each loading rate during Pilot 2.

Asymmetry in the principal strain results was observed in Pilot 2 (Figure C.6). During the flexion tests the minimum principal strains for the left facet were in tension, while the right facet minimum principal strains were in compression (as would be expected). This unexpected result could have been caused by the loading vector of the loading pin being coincident with the location of the left strain gauge, causing the bone underneath the gauge to "bulge" radially and leading to tensile maximum *and* minimum principal strains. Therefore, the location of the strain gauge relative to the loading vector is an important consideration during instrumentation of each specimen. A slight increase in compressive strains with increasing loading rate occurred at both facet bases for the anterior shear test direction, but no such trend was observed for tensile strains, or for principal strain measurements during simulated flexion.

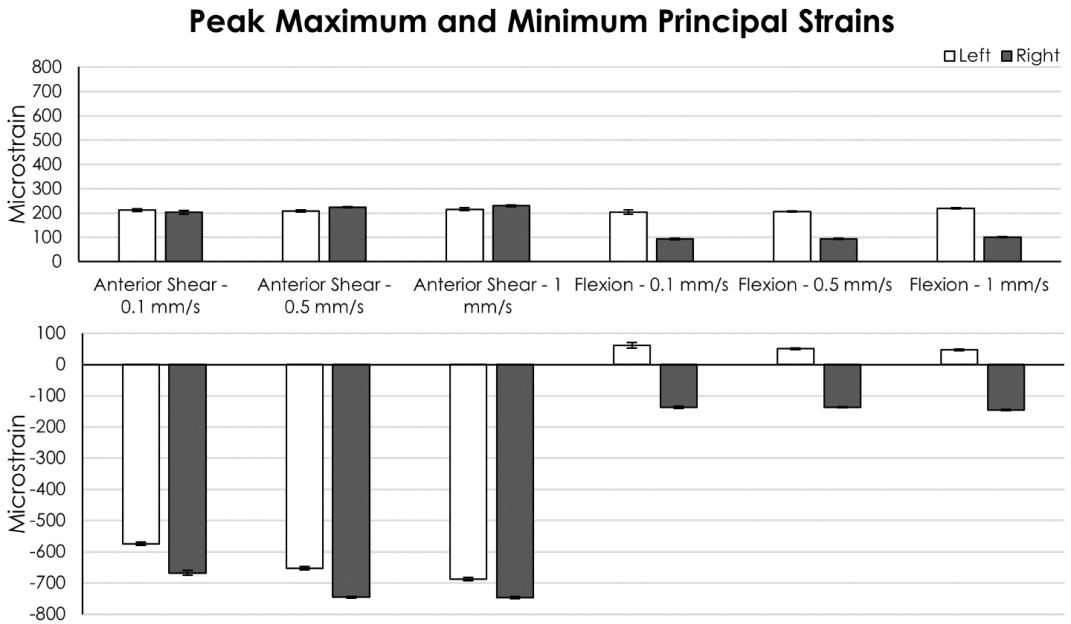

Figure C.6: Mean measured peak maximum (positive, tensile) and minimum (negative, compressive) principal strains for the left and right inferior C3 facets for the anterior shear and flexion test directions at each loading rate during Pilot 2.

Failure data

Peak failure load was higher in the simulated flexion test direction (Pilot 2, 379.4 N) than for anterior shear (Pilot 1, 202.8 N). This corresponded with distinct failure mechanisms for each loading direction – in flexion, failure occurred through the pedicles, whilst fracture through the facet tips occurred during anterior shear.

Summary

This appendix describes pilot testing that investigated the effect of loading rate and the presence of the superior adjacent facet joints on the mechanical response of subaxial cervical inferior facets during loading to simulate that experienced during intervertebral flexion and anterior shear motions. Resecting the superior adjacent facet joints reduced apparent facet stiffness, and increased sagittal deflections and compressive strain magnitudes. Increasing loading rate increased apparent stiffness during flexion, and slightly increased compressive strain magnitudes during anterior shear, but had no discernible effect on sagittal deflections in either testing direction. Peak failure load was higher for simulated flexion, and distinct failure mechanisms were observed for each test direction. These results demonstrate that a one

magnitude change in quasi-static loading rate has a marginal effect on the mechanical response of the inferior facets, and that the adjacent joints are important to consider.